

# INSPIRE

*IN situ Solar system Polar Ice Roving Explorer*

Mission Concept Study Report for the 2023 – 2032  
Planetary Science and Astrobiology Decadal Survey

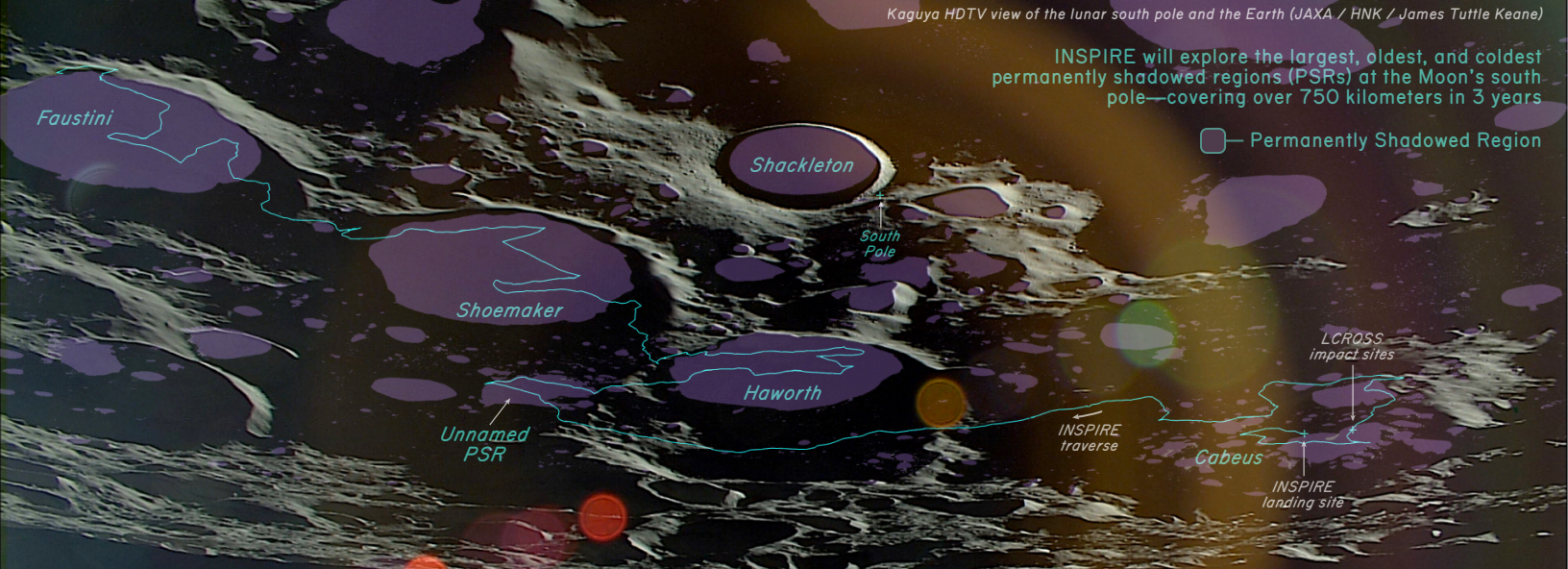
**Jennifer Heldmann**, Science Champion  
[jennifer.heldmann@nasa.gov](mailto:jennifer.heldmann@nasa.gov)

**John O. Elliott**, Study Lead  
[John.O.Elliott@jpl.nasa.gov](mailto:John.O.Elliott@jpl.nasa.gov)





INSPIRE will explore the largest, oldest, and coldest permanently shadowed regions (PSRs) at the Moon's south pole—covering over 750 kilometers in 3 years



# INSPIRE

*In Situ Solar System Polar Ice Roving Explorer*  
2023–2032 Planetary Science and Astrobiology  
Decadal Survey Mission Concept Study

## Understanding the origins, ages, and evolution of lunar volatiles is fundamental Solar System science.

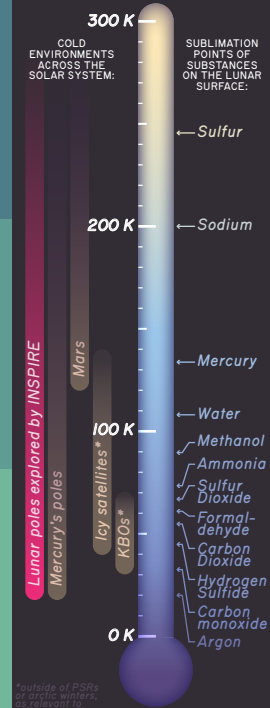
INSPIRE utilizes a long-duration rover to address the origins, ages, and evolution of Solar System volatiles on planetary bodies. INSPIRE traverses ~750 km across the Moon's south polar region within three years, capitalizing on a pre-planned traverse path and science stops as well as a high degree of rover autonomy. INSPIRE measures surface volatiles, subsurface volatiles and stratigraphy (including 2 m drill depths), exospheric volatile abundances and distributions, and local environmental conditions (surface temperatures, ion and electron fluxes, surface geomorphology) to quantitatively determine the relative contributions of volatile sources and sinks affecting the present-day distribution of volatiles on the meter scale, determine direct relationships between the environment and the presence of volatiles, and address the timing and origins of volatile deliveries.



Lunar cold traps provide an accessible, natural laboratory for analyzing volatiles found across the Solar System.

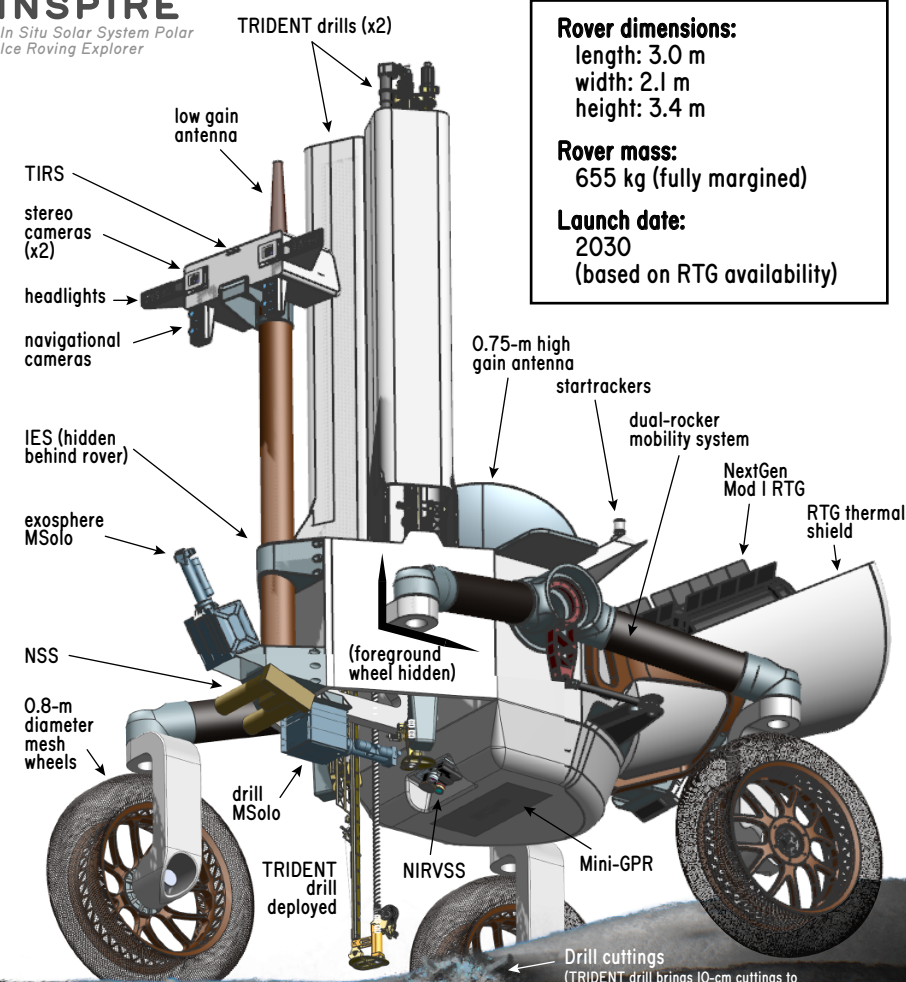
SCIENCE QUESTIONS: TESTABLE HYPOTHESES: PRIMARY OBSERVABLES:

<p>#Origins</p> <p><b>What are the origins of volatiles in the inner Solar System?</b></p>	<p><b>The dominant source of polar volatiles is...</b></p> <ul style="list-style-type: none"> <li>A. early outgassing.</li> <li>B. asteroid impacts.</li> <li>C. comet impacts.</li> <li>D. solar wind-regolith interactions.</li> <li>E. ongoing small meteoroid bombardment (including interplanetary dust, cometary dust, asteroidal dust).</li> </ul>	<p><b>Composition of volatiles</b></p>
<p>#Ages</p> <p><b>What are the timescales of volatile delivery in the inner Solar System?</b></p>	<p><b>Polar volatiles were delivered...</b></p> <ul style="list-style-type: none"> <li>A. early on (&gt;3.5 billion years ago)</li> <li>B. throughout lunar history.</li> <li>C. recently.</li> </ul>	<p><b>Distribution of volatiles</b></p>
<p>#Evolution</p> <p><b>How do volatiles evolve on Solar System airless bodies?</b></p>	<p><b>Polar volatiles...</b></p> <ul style="list-style-type: none"> <li>A. have been destroyed by solar wind sputtering.</li> <li>B. have been modified by cosmic rays.</li> <li>C. have been re-distributed by impact gardening, erasing their time-history.</li> <li>D. are distributed today as an artifact of true polar wander.</li> <li>E. are stable in zones created by thermal diffusion.</li> </ul>	<p><b>Volatile distribution, composition, and the local environment</b></p>



\*outside of PSRs or arctic winters or relevant to different bodies.





**Rover dimensions:**  
length: 3.0 m  
width: 2.1 m  
height: 3.4 m

**Rover mass:**  
655 kg (fully margined)

**Launch date:**  
2030  
(based on RTG availability)

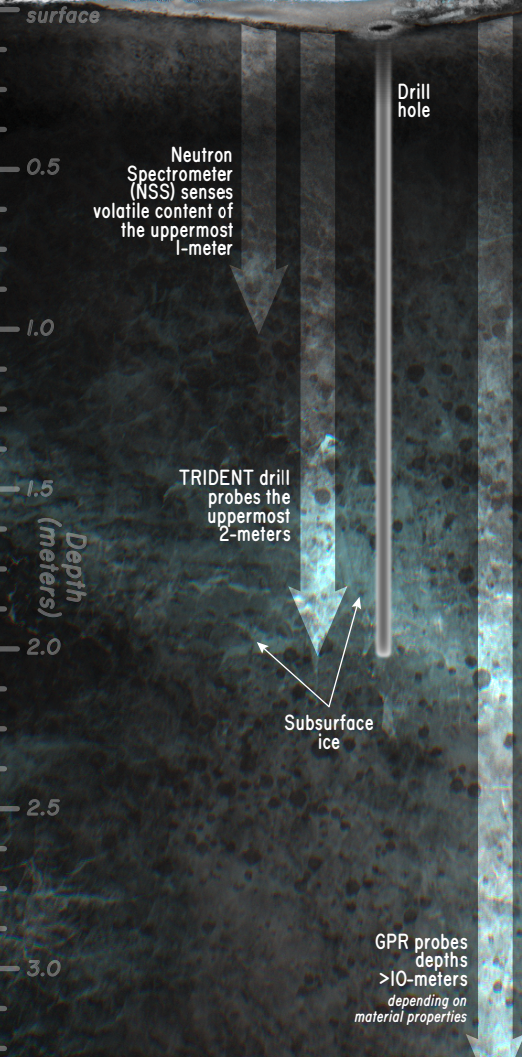
**IMPLEMENTATION HIGHLIGHTS:**

- MOBILITY**
  - Capable of operations in sunlight and permanent shadow (with headlights)
  - Highly autonomous navigation
  - Capable of traversing slopes up to 20°
  - 0.6-meter ground clearance
  - Effective drive speed: 0.23 km/hr (day), 0.16 km/hr (PSR)
- POWER**
  - Powered by a single NextGen Mod I RTG
  - Beginning of life power: ~245 W
  - Additional battery is sized to support drilling operations
- COMM**
  - 2-axis gimballed 0.75-meter S-band high-gain antenna
  - S-band omni-directional low-gain antenna
  - Conservative estimates for communications based on the expected availability of relay satellite(s) during mission timeframe
- THERMAL**
  - Ample waste heat from RTG to keep rover warm
  - Thermal loop for warming extremities (e.g., wheel motors) to limit warm-up times
  - Thermal shield around RTG limits heat flux to regolith (<6 W/m<sup>2</sup>) to limit surface volatilization

**SCIENCE INSTRUMENTS:**

INSPIRE strategically utilizes high-TRL payload elements.

- TRIDENT (x2)** (The Regolith and Ice Drill for Exploring New Terrain) for drilling 2-meters into the surface and excavating material in 10-cm bites
- Stereo Cameras (x2)** for imaging surrounding terrain and providing geologic context for drilling.
- TIRS** (Thermal Infrared Spectrometer) for measuring lunar surface temperatures, thermophysical, and geotechnical properties.
- MSolo (x2)** (Mass Spectrometer Observing Lunar Operations) for measuring volatiles released from drilling, drill cuttings, and the composition of the lunar exosphere.
- NSS** (Neutron Spectrometer System) for measuring bulk hydrogen content (including water) in the subsurface.
- NIRVSS** (Near Infrared Volatiles Spectrometer System) for imaging, and measuring composition and thermophysical properties of drill cuttings and drillhole.
- IES** (Ion Electron Spectrometer) for measuring ions and electrons in the solar wind and lunar exosphere.
- Mini-GPR** (Ground Penetrating Radar) for measuring subsurface variations in dielectric properties, including identifying deep water ice.



**INSPIRE's traverse, by the numbers:**

INSPIRE will explore five of the largest and oldest Permanently Shadowed Regions (PSRs; see front of fact sheet):

- Cabeus (including LCROSS impact sites)
- Haworth
- Shoemaker
- Faustini
- Unnamed, non-crater PSR

**62 pre-planned Science Stations, with 64 pre-planned drill holes, and 36 opportunistic drill holes selected in real time**  
(2:1 pre-planned science opportunities to reactionary science opportunities)

**Continuous measurements from NSS, IES, Mini-GPR, and TIRS during drives.**

**Nominal Traverse Distance:**  
756 km  
(rover capability: >1,000 km)

**Traverse slopes:**  
67% < 5°  
98% < 13°  
100% < 20°  
(rover capability: 20°)

**COST:**

**INSPIRE is a New Frontiers class mission.**

Phases A-D:	\$725M	\$725M
Reserves on Phases A-D:	\$362M	\$217M
RTG:	\$70M	\$70M
<b>Total Development (A-D) Costs:</b>	<b>\$1,157M</b>	<b>\$1,012M</b>
	(50% reserves)	(30% reserves)
Phases E-F:	\$149M	\$149M
Reserves on Phases E-F:	\$36M	\$21M
<b>Total Operations (E-F) Costs:</b>	<b>\$185M</b>	<b>\$170M</b>
	(25% reserves)	(15% reserves)
Launch Vehicle and CLPS Lander:	\$200M	\$200M
<small>Lunar landing provided by NASA's Commercial Lunar Payload Services (CLPS), which are anticipated to have the capability for INSPIRE delivery in this timeframe.</small>		
<b>Total Project Cost:</b>	<b>\$1,542M</b>	<b>\$1,382M</b>
	Decadal Survey mission concept study costing guidelines	traditional New Frontiers costing guidelines

**SCIENCE CHAMPION:** Jennifer L. Heldmann (NASA Ames).

**SCIENCE TEAM:** Anthony Colaprete (NASA Ames), Ariel Deutsch (NASA Ames), Masatoshi Hirabayashi (Auburn), Dana Hurley (JHUAPL), Yang Liu (JPL), James T. Keane (JPL).

**JPL STUDY LEAD:** John Elliott.

**JPL STUDY TEAM:** Deegan Aitha, Mineh Badalian, John Baker, Paul Briggs, Mark Chodas, Pam Clark, Faramaz Davirian, Martin Feather, Michael Fong, Natalie Gallegos, Ron Hall, Amy Hoffman, Richard Kim, Isabel King (Honeybee Robotics), Emily Law, Heather Lethcoe, Shan Malhotra, John Mann, Larry Matthies, Rudra Mukherjee, Charles Nainan, Hari Nayar, Issa Nesnas, Hiro Ono, Joon Park, Raul Polit-Casillas, Aaron Rodriguez, Miles Smith, Catherine Suh, Eric Sunada, Rowan Swain, Thaddaeus Voss, Kris Zacny (Honeybee Robotics), with significant participation from JPL's A-Team and Team X.



## Disclaimers/Acknowledgements

Pre-Decisional Information – For Planning and Discussion Purposes Only

The research was carried out at the Jet Propulsion Laboratory, California Institute of Technology, under a contract with the National Aeronautics and Space Administration (80NM0018D0004).

The cost information contained in this document is of a budgetary and planning nature and is intended for informational purposes only. It does not constitute a commitment on the part of JPL and/or Caltech.

© 2021. All rights reserved.



## Study Participants

### INSPIRE Science Team

Anthony Colaprete	NASA Ames Research Center
Ariel Deutsch	NPP/USRA/NASA Ames Research Center
Jennifer L. Heldmann	NASA Ames Research Center
Masatoshi Hirabayashi	Auburn University
Dana Hurley	Johns Hopkins University Applied Physics Laboratory
James T. Keane	Jet Propulsion Laboratory
Yang Liu	Jet Propulsion Laboratory

### JPL Study Team

Deegan Atha	Shan Malhotra
Mineh Badalian	John Mann
John Baker	Larry Matthies
Paul Briggs	Rudra Mukherjee
Mark Chodas	Charles Nainan
Pam Clark	Hari Nayar
Faramaz Davarian	Issa Nesnas
John Elliott	Hiro Ono
Martin Feather	Joon Park
Michael Fong	Raul Polit-Casillas
Natalie Gallegos	Aaron Rodriguez
Ron Hall	Miles Smith
Amy Hofmann	Catherine Suh
Richard Kim	Eric Sunada
Isabel King – Honeybee Robotics	Rowan Swain
Emily Law	Thaddaeus Voss
Heather Lethcoe	Kris Zacny – Honeybee Robotics

With significant additional participation from the members of JPL's A-Team and Team X.



---

# PLANETARY SCIENCE DECADAL SURVEY

## Mission Concept Study Final Report

### Table of Contents

EXECUTIVE SUMMARY.....	vi
1 SCIENTIFIC OBJECTIVES.....	1
1.1 Background: Solar System Science .....	1
1.2 Lunar Polar Volatiles .....	2
1.3 The Lunar South Pole .....	4
1.4 INSPIRE Science.....	5
2 HIGH-LEVEL MISSION CONCEPT.....	10
2.1 Concept Maturity Level (CML).....	10
2.2 Technology Maturity.....	10
2.3 Key Trades .....	12
3 TECHNICAL OVERVIEW .....	14
3.1 Instrument Payload Description.....	14
3.2 Flight System.....	17
3.2.1 Overview .....	17
3.2.2 Rover Subsystems .....	17
3.3 Concept of Operations and Mission Design.....	21
3.4 Risk List.....	25
4 DEVELOPMENT SCHEDULE AND SCHEDULE CONSTRAINTS.....	25
4.1 High-Level Mission Schedule.....	25
4.2 Technology Development Plan.....	26
4.3 Development Schedule and Constraints.....	28
5 MISSION LIFE-CYCLE COST.....	29
5.1 Costing Methodology and Basis of Estimate .....	29
5.2 Cost Estimate.....	30

## Appendices

A	ACRONYMS .....	A-1
B	SCIENCE .....	B-1
	B.1 Science Path Rationale.....	B-1
	B.1.1 The Traverse .....	B-1
	B.1.2 Science Stations .....	B-1
	B.2 Relevance to Upcoming Lunar Polar Missions.....	B-4
	B.3 Relevance to Decadal Survey Priority Science Topics .....	B-6
	B.4 Instrument Trades.....	B-10
C	JPL TEAM X REPORT.....	C-1
D	MOBILITY .....	D-1
E	AUTONOMY.....	E-1
F	AUTONOMY RELIABILITY .....	F-1
G	ESTIMATING MISSION DURATION.....	G-1
	G.1 Summary of Analysis .....	G-1
	G.2 Communication Constraints.....	G-1
	G.3 Sloped-terrain Mobility.....	G-1
	G.4 Driven Path Inefficiency (Path Tortuosity).....	G-3
	G.5 Autonomy Reliability (Fault Rates).....	G-5
	G.6 ConOps .....	G-5
	G.7 Effective Traverse Rate .....	G-6
H	DRILL.....	H-1
	H.1 Lunar Polar Volatile Rover (LPVR) Drilling System.....	H-1
	H.2 Introduction & Honeybee Heritage .....	H-2
	H.2.1 LPVR Drill .....	H-2
	H.2.2 Instrumentation .....	H-4
I	TELECOMMUNICATIONS.....	I-1
	I.1 Lunar Relay Services for the 2030s Time Period .....	I-1
	I.2 Coverage.....	I-3
	I.2.1 Emergencies.....	I-6
	I.3 Communications Link.....	I-6
	I.4 The Radio .....	I-8
	I.5 The Antenna .....	I-9
	I.6 Functional Block Diagram of the Communications System .....	I-9
J	THERMAL DESIGN .....	J-1
K	TRAVERSE PLANNING .....	K-1
L	CONFIGURATION.....	L-1
	L.1 Block Diagram.....	L-1
	L.2 Configuration.....	L-3
M	ADDITIONAL COST MODELING INFORMATION.....	M-1
	M.1 Wrap Factors.....	M-2
	M.2 SEER.....	M-2
	M.3 TruePlanning.....	M-5
	M.4 SOCM.....	M-10
	M.5 Potential Cost Savings .....	M-13



---

M.6	Costs for Alternative Mission Scenarios.....	M-13
N	SUMMARY OF LONG-RANGE LUNAR ROVER CONCEPTS FOR THE DECADAL SURVEY.....	N-1
O	REFERENCES.....	O-7
O.1	Sections 1 – 5.....	O-7
O.2	Appendices.....	O-8

## EXECUTIVE SUMMARY

Within the past decade, our understanding of volatiles on airless bodies throughout the Solar System has undergone nothing short of a revolution. Here ‘volatiles’ refers to compounds that vaporize at low temperatures but can be sequestered as ices in cold regions, such as H-, N-, C-, S-, Cl-, and F-bearing compounds. These ices are important scientific clues to determining the origins, ages, and evolution of inner Solar System volatiles including the origins of critical species such as water, carbon dioxide, and hydrogen on planet Earth. Addressing these questions will have profound implications for understanding volatile behavior and availability in the inner Solar System (including Earth), and for understanding volatile delivery and evolution on the Moon, Mercury, and Ceres, with implications for water and other volatile systems on airless bodies throughout the Solar System as well as on exoplanets. Water in particular is also key to enabling sustained human exploration beyond our home planet. Astronauts living and working on the Moon (and eventually Mars) will need to rely on in situ resource utilization (ISRU) in order to live sustainably off of local resources and reduce reliance on costly resupply missions from Earth. The quest to determine the origins, ages, and evolution of volatiles in the inner Solar System is motivated by these benefits to both science and exploration.

Since the last planetary science Decadal Survey (*Vision and Voyages for Planetary Science in the Decade 2013-2022*), our knowledge regarding Solar System volatiles has shifted from theoretical hypotheses of potential reservoirs to direct observational evidence for an unexpected, widespread, intriguingly varied, and even dynamic distribution of volatile species on airless bodies. Locales spanning the shadowed regions on our Moon, polar regions of Mercury, asteroids such as Ceres, outer planet satellites (e.g., Enceladus), and Kuiper Belt Objects as far as Pluto now demonstrably show evidence of surface, subsurface, and/or exospheric volatiles with complex histories and ongoing transport and processing. Despite this explosion of discovery, fundamental scientific questions remain regarding the sources, ages, and processes modulating volatile abundances, forms, distributions, compositions, and migration patterns on airless bodies.

To address these knowledge gaps, the INSPIRE (**IN** Situ **S**olar system **P**olar **I**ce **R**oving **E**xplorer) mission focuses on the lunar polar regions as the most accessible inventory of inner Solar System volatiles. The mission concept uses an RTG-powered, 560 kg rover that carries redundant 2-m drills and an instrument suite of spectrometers, cameras and environmental sensors. INSPIRE traverses ~750 km across the Moon’s south polar region within three years, enabled by autonomous day/night traverses along a pre-planned path marked by pre-defined Science Station stops which are determined based on existing orbital datasets. The rover is capable of driving in both sunlight and in darkness and collects science data both along the traverse as well as within targeted Science Stations. INSPIRE measures surface volatiles, subsurface volatiles and stratigraphy, exospheric volatile abundances and distributions, and local environmental conditions (e.g., surface temperatures, ion and electron fluxes, surface geomorphology) to assess the relative contributions of volatile sources and sinks affecting the present-day distribution of volatiles on the meter scale, determine direct relationships between the environment and the presence of volatiles, and establish the timing and origins of volatile deliveries. INSPIRE investigates multiple different lunar PSRs (including Cabeus, Haworth, Shoemaker, and Faustini craters) as well as seasonally shadowed regions (SSRs) where each region has unique signatures of volatiles and environmental conditions to provide a system-wide analysis of lunar polar volatiles that is not possible via remote sensing or in a single location on the Moon.

INSPIRE would provide unprecedented and transformative insight into the origin and evolution of lunar volatiles while simultaneously advancing fundamental Solar System science. INSPIRE also directly enables sustained human exploration of the Moon by providing necessary ground-based measurements not possible from orbital assets of volatile distribution, form, abundance, and composition, which are critical for developing ISRU architectures to use water ice as a resource for a sustained human presence on the Moon and beyond. The mission development cost (Phases A–D), including 50% development reserves and \$70M for the required RTG power source is \$1,157M, which is commensurate with a NASA New Frontiers mission class as stated in the Decadal Survey mission concept study ground rules. Using the more conventional costing approach typical of New Frontiers missions with 30% development reserves and including the RTG, INSPIRE has Phase A–D costs of \$1,012M.



# 1 SCIENTIFIC OBJECTIVES

## 1.1 BACKGROUND: SOLAR SYSTEM SCIENCE

Recent discoveries from theoretical modeling, laboratory analyses, remote sensing, and in situ measurements have revealed a complex story of past and present-day processes affecting volatiles on airless bodies across the Solar System. This foundational work has consequently led to more sophisticated scientific questions about origins, ages, and evolution of volatiles, which can be best addressed through in situ measurements in relevant environments.

Given that the Moon has a current obliquity of  $1.5^\circ$  from the ecliptic plane and significant topography, permanently shadowed regions (PSRs) are present at high latitudes, which are stable thermal environments for water ice and other volatiles to exist against sublimation on billion-year timescales [1-3]. Transiently shadowed regions (TSRs) are also present, exhibiting changes in shadow conditions on shorter timescales. For example, over the last decade, Diviner has measured lunar seasonally shadowed regions (SSRs), revealing that the polar cold-trapping surface area more than doubles between local summer and winter [4]. Thermal regimes dictate the temperatures at which specific volatiles are cold trapped over geologic timescales, such that colder temperatures trap more varieties of volatiles and offer a more complete record of volatile histories (Figure 1-1;[5]). The low-temperature lunar poles are analogs for small bodies (Ceres, comets, asteroids, trojans, centaurs), icy outer satellites (e.g., Europa, Enceladus), Kuiper Belt objects (e.g., Pluto), and the poles of Mercury—all targets that are also interesting due to the presence of various volatiles. Lunar cold traps provide an accessible witness plate for analyzing volatiles found across the Solar System and an opportunity to address broad-reaching and fundamental planetary science questions.

Similar to the Moon, the low obliquity and cratered polar topography of Mercury and Ceres create PSRs that are stable thermal environments for water ice and other volatiles on geologic timescales [3, 6-9]. Unlike on the Moon, ice deposits on Mercury exist as several-meters-thick, contiguous deposits [10, 11] that fill individual cold traps to the boundary of permanent shadow [6, 7], and are predicted to be composed primarily of water ice with impurities of  $<5\%$  by volume [12, 13]. While some water-ice deposits are exposed directly at the surface, other deposits at lower, warmer latitudes are covered by low-reflectance, likely organic-rich, frozen volatiles that help protect the underlying water ice against sublimation [14-16]. Examples of these dark insulating volatiles have not been observed at the lunar poles, although some reflectance data may be consistent with the presence of cold-trapped organics [17]. The similarities and differences between observed polar ice deposits on Mercury and the Moon will enable valuable comparative planetology studies to understand the processes and environments affecting the manifestations of polar deposits on these two airless bodies.

Ceres, too, is known to host polar surface volatiles, identified from spectroscopic data and images of bright deposits in PSRs [18, 19]. In contrast to the meters-thick deposits observed on Mercury, surface volatiles are interpreted to be only several microns thick [19], potentially similar to surface volatile accumulations on the Moon [20]. Interestingly, seasonal changes on Ceres are associated with variations in the amount of surface water ice, revealing an exciting active water cycle [21]. The lunar poles also exhibit large temperature changes across the seasons [4, 22], and thus studying SSRs on the

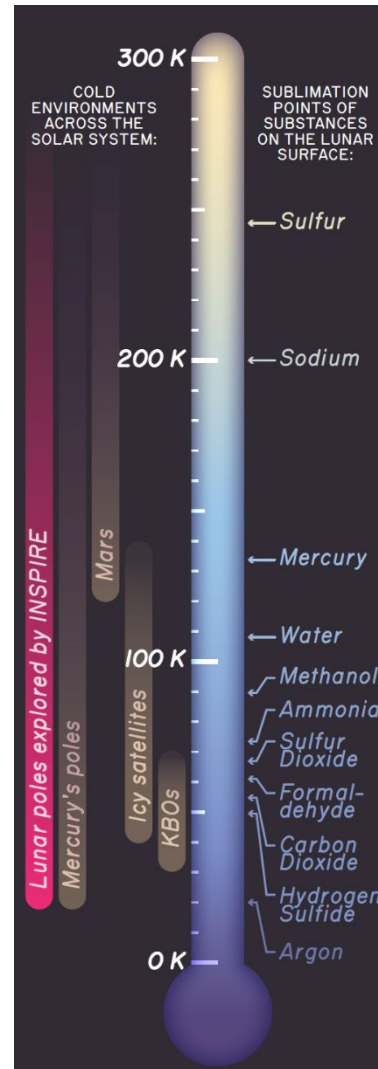


**Figure 1-1.** Volatile species as a function of thermal stability temperature (graphic courtesy James T. Keane).

Moon may provide similar insight into an active seasonal cycle of volatile migration. In addition to its seasonal cycle, Ceres also undergoes large obliquity oscillations every  $\sim 24.5$  kyr, and thus bright volatile deposits are observed only in the most persistent PSRs. The Moon is also predicted to have undergone large obliquity variations that have affected the present-day distribution of volatiles [23, 24], but models of true polar wander (TPW) predict that the Moon's current orbital spin-axis has been stable for at least  $\sim 3$  billion years, and so today's lunar cold traps have had the opportunity to accumulate volatiles over much longer geologic timescales.

The stark differences in the abundance, distribution, and purity of polar ice deposits on the Moon, Mercury, and Ceres are theorized to be largely related to differences in volatile age [25–29], and these differences raise questions about the differences in processes and rates delivering, mobilizing, modifying, and destroying volatiles across the Solar System. The Moon represents the most accessible inventory of volatiles in the inner Solar System where we can address volatile age, source fluxes, and mechanisms affecting volatile transport, modification, and loss. INSPIRE focuses on the “old and cold” lunar PSRs, which have experienced the longest volatile history on the Moon and capture a scientific history spanning billions of years, which is relevant to addressing multiple Solar System scientific objectives.

Despite numerous breakthroughs in studying volatiles on the Moon, Mercury, and Ceres over the last decade, there are still many open scientific questions regarding the volatile cycles on airless bodies. Understanding the origins and evolution of lunar volatiles is fundamental Solar System science and studying lunar polar volatiles addresses the following high priority science topics [30]:

1. Understanding the Moon's ancient water content is critical in understanding the formation and early evolution of the Earth-Moon system and inner Solar System.
2. The shadowed regions near the lunar poles hold a unique record of the delivery of water and other volatile species to the inner Solar System over the past several billion years and bear witness to processes that have shaped our local space environment.
3. Understanding the processes that control global surface hydration on the Moon is critical to understanding observations of hydration on other airless bodies, and thereby the origin and distribution of water throughout the Solar System. Comparative planetology of ice on airless bodies has important implications for the evolution of such bodies across the Solar System.
4. PSRs are among the coldest places in the Solar System, harboring a variety of volatile species, including water, hydrocarbons, and nitrogen- and sulfur-bearing compounds. The lunar polar microenvironment is a natural laboratory in which to study abiotic/prebiotic chemistry and other surface processes that may be active elsewhere in the Solar System.
5. The lunar exosphere remains our closest example of the most common class of atmosphere in the Solar System — a surface boundary exosphere. However, the density of the lunar atmosphere may have varied dramatically over time. Understanding the evolution of the lunar atmosphere has implications for our fundamental understanding of how atmospheres rise and fall, and the behavior of rarefied atmospheres across the Solar System, from the Moon and Mercury to asteroids, outer Solar System satellites, and beyond.

It is essential to address these fundamental, broad-reaching science questions in the near term. The lunar polar environment may be irrevocably altered by increased activity in the coming decade, and thus polar volatile measurements are time-critical [30, 31].

## 1.2 LUNAR POLAR VOLATILES

The Moon's PSRs (and surrounds) are the most accessible reservoir of the Solar System's volatile history—spanning billions of years. Despite recent advances in our understanding of lunar volatiles, many important questions remain, especially related to the origins, ages, and evolution of volatiles. These topics fuel exciting, heated debates in the literature that can be tested with INSPIRE. For example, the origins of lunar volatiles have been hypothesized to trace back to early lunar outgassing, asteroid delivery, comet delivery, solar wind-regolith interactions, or even recent meteoroid bombardment. It is likely that lunar PSRs have witnessed variations in volatile delivery through time, and today the relative contributions of these different potential volatile sources remain unknown.



While ancient volatiles on the Moon may seem surprising, recent work has suggested that ice may be preserved over geologic timescales during the stochastic impact process and even protected at depth from the emplacement of ejecta [25, 32, 33]. Once buried, volatiles are less sensitive to thermal processes. An old deposit that is buried by >20 cm of regolith will remain thermally stable over geologic time. Much of the lunar regolith is reworked by impact gardening and other processes, however the PSRs interrogated by INSPIRE are ancient (>3 Ga) and formed pre-TPW, so ancient ice could plausibly be buried and preserved by regolith. The present-day hydrogen distribution detected in the top 1-m of regolith (e.g., [34-40]) is consistent with at least some component potentially being a relic of volatiles from several Gyr, before TPW. Variations in the lunar spin-axis (i.e., TPW) may affect the present-day distribution of volatiles, but the extent to which volatile distribution is governed by past episodes of TPW is unknown (e.g., [23, 24]). TPW can be caused by a variety of processes (large impacts, volcanism, mass displacement of volatiles) and affects the regions of volatile stability over time. TPW, like other processes affecting the distribution of lunar volatiles, is hypothesized to occur on a variety of Solar System worlds, including the Moon, but also Earth, Mars, Ceres, Europa, Enceladus, and Pluto [41].

The highest obliquity periods are expected to have occurred early in the Moon's history (~3 Ga), and we can make predictions of where surface and near-surface ice would have been present in higher obliquity phases (e.g., [23]). This predicted ice distribution would be systematically tested with the long traverse of INSPIRE. It is likely that some of those older volatiles (~3.5–4 Ga) remain to be sampled within the top 1-m of regolith and thus INSPIRE would measure the composition and form of these materials. On the other hand, the overall abundance of volatiles on the Moon appears to be significantly less than the total expected delivery from putative sources over time [42, 43], suggesting that the Moon is inefficient at retaining volatiles. Overall, the effects and relative contributions of processes modulating volatile abundance, distribution, composition, and physical form are unknown (e.g., impact gardening, thermal environment, cosmic rays, solar wind sputtering, dielectric breakdown).

We also note that observational evidence suggests that impact gardening cannot have destroyed all records of volatiles, regardless of their age. Surficial water has been directly detected by M<sup>3</sup> (Moon Mineralogy Mapper; [20]) and indirectly by LAMP and LOLA onboard the Lunar Reconnaissance Orbiter [17, 45-47]. The LCROSS (Lunar Crater Observation and Sensing Satellite) impact into Cabeus crater revealed a plethora of sequestered volatiles including, but not limited to, H<sub>2</sub>O (gas and ice), OH, CH<sub>4</sub>, SO<sub>2</sub>, and CH<sub>4</sub> ([44], Figure 1-2). The LADEE mission observed water released from hydrated soil coincident with meteoroid impacts [48], and the GRAIL spacecraft impacts at 75°N also showed a release of endogenous volatile materials [49]. Neutron mapping indicates that there is hydrogen down to a depth up to 100 cm in the polar regions with a laterally heterogeneous signature [39]. If gardening/impact processes destroy ancient ice, it should also destroy young ice; the observed buried hydrogen may be young surficial ice that has been buried or a combination of young and old ice deposits, most consistent with the broader hydrogen maps (e.g., [23]). Either way, the fact that we observe these lunar volatiles today is evidence that gardening/impacts do not completely destroy volatile signatures.

Despite the contention, the beauty of INSPIRE is that this mission can directly test all of these competing hypotheses. For example, models of ancient ice predict different spatial distributions of water ice and other volatiles as a function of location and depth

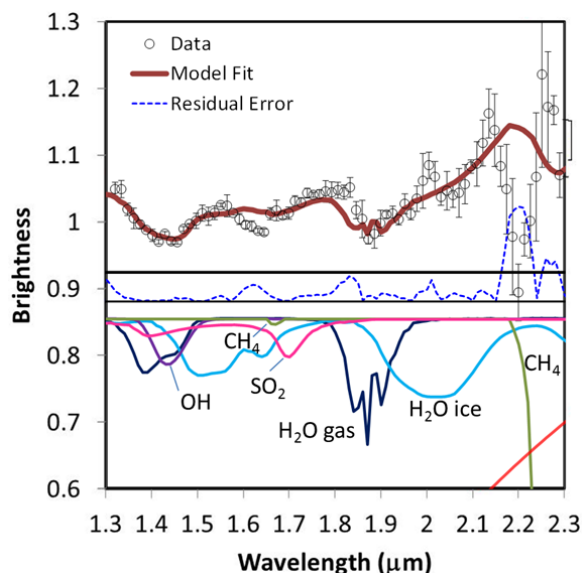


**Figure 1-2.** LCROSS near-infrared spectra showing a variety of volatile species (including water ice and vapor) in the LCROSS impact plume emanating from Cabeus crater [44].

(e.g., [23]) and different isotopic and chemical compositions, which can be directly interrogated by INSPIRE across many PSRs with different (but unexplained) ice characteristics (e.g., abundance, distribution, spectral properties, neutron signatures). In addition to isotopes, the elemental and molecular content is also indicative of origin and processes. For example, sulfur compounds are a key indicator of volcanic contributions. **At its core, INSPIRE is a mission to understand volatiles across the Solar System.**

Understanding lunar polar volatiles is also critical for enabling human exploration at the Moon through in situ resource utilization (ISRU). ISRU relies on the use of native materials as resources to enable a sustained human presence on other worlds [24, 50]. NASA’s plans to send astronauts to the south polar region of the Moon through the Artemis program is predicated on the use of water ice as a natural resource [51]. Scientific understanding of the distribution, form, abundance, and composition of lunar volatiles (including water ice) is fundamental to informing the development of ISRU architectures to support human exploration. An enhanced scientific understanding of volatiles allows for the development of predictive capabilities to inform site selection and ISRU of water ice for Artemis. The fidelity of resource characterization for ISRU hardware development cannot be achieved through remote sensing alone. Similar to terrestrial mining, ground truthing and in situ characterization is required during the resource exploration phase for the Moon [52-54].

### 1.3 THE LUNAR SOUTH POLE

INSPIRE is targeted at the lunar south pole given the abundances of observed hydrogen, the topography amenable to shadowed regions over both human (e.g., SSRs) and also geologic timescales (e.g., PSRs), the juxtaposition with sunlit terrain also bearing hydrogen, and the existing comprehensive remote sensing coverage, all of which provide a rich history of volatile evolution over time. Figure 1-3 shows a) the presence of PSRs, b) hydrogen abundance, c) temperatures <50K and <100K, d) expected locations of present-day ice thermal stability, and e) expected locations of ancient ice thermal stability. These datasets demonstrate the complexity of lunar volatiles. For example, not all PSRs have the same amounts of subsurface hydrogen. Cabeus holds the most hydrogen of any location on the Moon and Shoemaker crater also has high hydrogen content, even though Shoemaker is not the coldest PSR. Haworth crater shows the coldest PSR temperatures, yet does not have particularly high levels of hydrogen. Volatile distributions in general do not directly correlate with either present or ancient predicted ice thermal stability regimes. The reasons for these discrepancies are unknown. The diversity of the south polar region as shown here allows INSPIRE to explore multiple different past and present environmental conditions essential to understanding the history and evolution of polar volatiles, since no single location or region can address all of the high priority science questions.

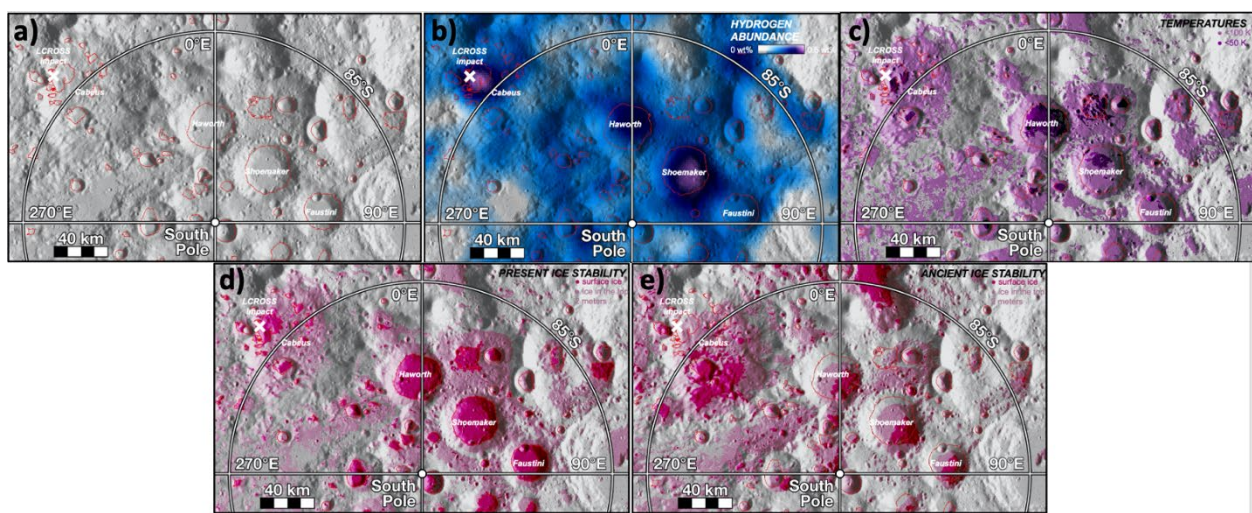


**Figure 1-3.** Maps of the lunar south polar region showing a) the presence of PSRs outlined in red, b) hydrogen abundance, c) temperatures below 50K and 100K, d) expected locations of present-day ice thermal stability, and e) expected locations of ancient ice thermal stability.



## 1.4 INSPIRE SCIENCE

INSPIRE would provide ground truth that enables application of the more extensive remote sensing data sets to system-level understanding of lunar volatiles and, by extension, provide applicability to volatiles on other airless bodies. Heterogeneity on sub-pixel scales is expected and complicates the interpretation of existing remote-sensing datasets. INSPIRE will quantify volatile heterogeneity at meter scales laterally and at decimeter scales vertically. Coupling this information with measurements of the environmental drivers, the remote-sensing data can be used to investigate trends and constrain physical driving processes affecting volatile deposits in additional PSRs and on other Solar System objects. INSPIRE will build upon NASA’s VIPER (Volatiles Investigating Polar Exploration Rover) mission, which will perform preliminary exploration of polar volatiles in 2023 but with limited capability, reduced instrumentation, and without access to the scientifically compelling “old and cold” PSRs. NASA’s Artemis program may send astronauts to the lunar poles, although their access to PSRs will be limited. Nonetheless, INSPIRE will benefit from initial data gathering and risk reduction from early missions to optimize overall operations and productivity. See Appendix B for additional information regarding feed-forward of planned lunar missions.

The INSPIRE traverse (Figure 1-4) strategically covers multiple environments at the lunar south pole to investigate the origins, ages, and evolution of polar volatiles. The traverse is designed to sample five of the largest [1] and oldest [32, 55, 56] PSRs at the surface: Cabeus, Haworth, an unnamed PSR, Shoemaker, and Faustini. Furthermore, these five PSRs are key locations for improving our understanding of the lunar volatiles. Specifically, Cabeus hosts one of the oldest PSRs [32, 55, 56] and is the location of the predicted paleopole [23]. Neutron data suggest that the highest H concentrations at the lunar poles are within Cabeus (e.g., [36, 37, 40, 57]), and this crater is also where LCROSS impacted with its spent Centaur upper stage and shepherding spacecraft, providing important in situ measurements of polar volatiles [44], which INSPIRE will be able to place into broader regional context with numerous ground measurements. Haworth is one of the coldest PSRs on the Moon [4] and thus has the potential to harbor some of the most volatile species (i.e., those stable only at hyper-low temperatures) [2]. The

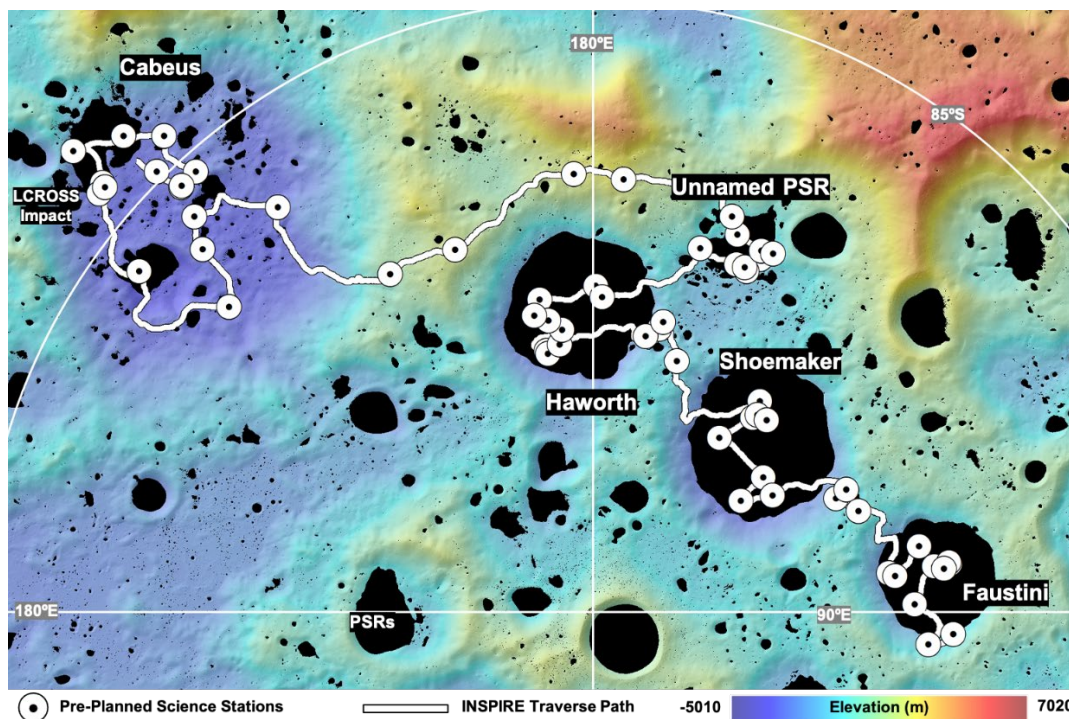


**Figure.1-4.** INSPIRE traverse plan. Landing site is within Cabeus crater (land in sunlight) and covers a traverse distance of ~750 km over ~3 years of operations. White circles indicate locations of pre-planned Science Stations.



Unnamed PSR is unique because it is not an impact crater, but rather some other topographic depression. Thus, the Unnamed PSR will provide important new information about the influence of varying topography and morphology on volatile distribution and retention. This site is also of high interest for HEO/ISRU because it may be more accessible than large, deep impact craters. Next, Shoemaker has a significantly elevated H signature (e.g., [54]), but UV and NIR spectral signatures consistent with surface hydration are suggestive of different distributions of surface frost ([20, 59]; Figure B-1). Finally, Faustini, although similarly cold to nearby Shoemaker [4], has relatively low H signatures (e.g., [54]).

INSPIRE collects science data both 1) while traversing across the south polar region, which allows for a thorough mapping and assessment of volatiles over space and the geologic time histories and 2) within targeted Science Stations where more detailed mapping and drilling operations occur. Sixty-two preselected Science Stations are included in the traverse plan (Table B-3 in Appendix B). Science Station locations are chosen for (1) testing of cold-trapping thermal environments, (2) testing the evolution of ice-stability environments, and (3) ground truthing of volatile-related orbital measurements (Table 1-1). Sixty-two Science Stations are the minimum number required to fulfill the above science site criteria within and between each of the PSRs (see Appendix B for details).

The payload is specifically tailored to address the priority INSPIRE science questions. The Science Traceability Matrix (Table 1-2) traces science questions, to competing hypotheses, primary observable(s), and relevant payload elements. The origins and ages of inner Solar System volatiles are primarily addressed by observing the composition and distribution of volatiles, respectively. These measurements are accomplished by the following instruments. The Neutron Spectrometer System (NSS) maps volumetric hydrogen in 1-m wide swaths down to 1 m depth during rover traverses. The thermal infrared spectrometer (TIRS) measures surface temperatures across 1-m wide swaths coincident with NSS using a pushbroom system to constraint the types of volatiles that can be sequestered in different locations. The first Mass Spectrometer (MSolo-drill) observes sublimation from surface volatiles as well as sublimation from subsurface samples acquired by drilling. The Near InfraRed Volatiles Spectrometer System (NIRVSS) measures the composition of surface volatiles and subsurface samples. The NIRVSS camera images drilling operations and an associated IR sensor measures the surface temperature in its field of view. The Regolith and Ice Drill for Exploring New Terrains (TRIDENT) extracts cuttings from different depths up to 2 m and deposits them on the surfaces for observations by MSolo-drill and NIRVSS. Similar to the VIPER mission, NIRVSS measures solid-phase volatile components while MSolo-drill measures sublimating vapor-phase components [61]. Figure 1-5 shows the mounting and fields of view for observing the cuttings pile provided by TRIDENT.

**Table 1-1.** Identification of INSPIRE Science Station criteria. <sup>1</sup>[4] <sup>2</sup>[23] <sup>3</sup>[20] <sup>4</sup>[46] <sup>5</sup>[58] <sup>6</sup>[44] <sup>7</sup>[59] <sup>8</sup>[60]

(1) Testing of Cold-Trapping Thermal Environments <sup>1</sup>			
Average Summer Temperature (K)			
<50	50–100	>100	<100 in winter and >100 in summer
(2) Testing the Evolution of Ice-Stability Environments <sup>2</sup>			
Surface and Subsurface Ice			
Stable today (not paleo)	Stable paleo (not today)	Stable today and paleo	
(3) Ground Truthing of Volatile-Related Orbital Measurements <sup>3–8</sup>			
Surface Ice			
No M <sup>3</sup> or LAMP ice detections	M <sup>3</sup> ice detections (but no LAMP)	LAMP ice detections (but no M <sup>3</sup> )	Both M <sup>3</sup> and LAMP ice detections
Subsurface Ice			
LCROSS		Mini-RF	
Centaur Impact	SSC Impact	Radar anomalous craters	High CPR region

The origins and ages of inner Solar System volatiles are primarily addressed by observing the composition and distribution of volatiles, respectively. These measurements are accomplished by the following instruments. The Neutron Spectrometer System (NSS) maps volumetric hydrogen in 1-m wide swaths down to 1 m depth during rover traverses. The thermal infrared spectrometer (TIRS) measures surface temperatures across 1-m wide swaths coincident with NSS using a pushbroom system to constraint the types of volatiles that can be sequestered in different locations. The first Mass Spectrometer (MSolo-drill) observes sublimation from surface volatiles as well as sublimation from subsurface samples acquired by drilling. The Near InfraRed Volatiles Spectrometer System (NIRVSS) measures the composition of surface volatiles and subsurface samples. The NIRVSS camera images drilling operations and an associated IR sensor measures the surface temperature in its field of view. The Regolith and Ice Drill for Exploring New Terrains (TRIDENT) extracts cuttings from different depths up to 2 m and deposits them on the surfaces for observations by MSolo-drill and NIRVSS. Similar to the VIPER mission, NIRVSS measures solid-phase volatile components while MSolo-drill measures sublimating vapor-phase components [61]. Figure 1-5 shows the mounting and fields of view for observing the cuttings pile provided by TRIDENT.

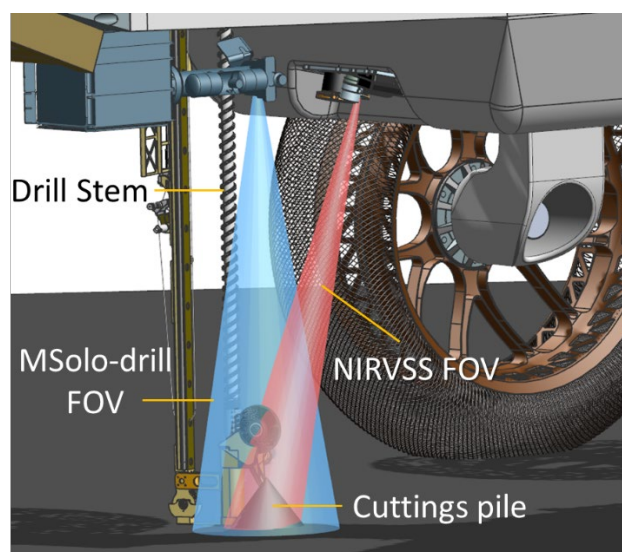


**Figure 1-5.** Placement of MSolo-drill and NIRVSS below rover provides clear view of cuttings.

The quantity and distribution of volatile species in the near-surface lunar exosphere are measured by a second Mass Spectrometer (MSolo-exosphere) dedicated to measuring exospheric volatile transport. The plasma environment, which can affect the movement of volatile species, is assessed by the Ion Electron Sensor (IES), which measures local ion and electron fluxes. The subsurface stratigraphy is measured for context purposes using the mini-GPR (ground penetrating radar) to potentially identify subsurface layering of ice and/or rock. Additional details can be found in §3.1.

While based on VIPER’s TRIDENT 1 m drill, INSPIRE employs a 2 m version to potentially provide an extra ~billion years of history based on the lunar overturn gardening rate [24] and greatly enhance science return as discussed in Appendix B.

### Science Traceability

INSPIRE is designed to assess the origins, ages, and subsequent evolution of lunar polar volatiles. Specific measurements for addressing these scientific questions are outlined below with testable hypotheses as shown in Table 1-2.

**#Origins.** There are five sources that have been hypothesized to have contributed to volatiles in the inner Solar System, which would be tested by INSPIRE. For the following discussion,  $\delta$  notion is defined as  $\delta^{H/E} \text{‰} = [(^{H/E}/^{L/E})_{\text{sample}} / (^{H/E}/^{L/E})_{\text{VSMOW}} - 1] * 1000$ , E is element (O, D),  $^H\text{E}$  is D,  $^{18}\text{O}$ , or  $^{17}\text{O}$ , and  $^L\text{E}$  is H or  $^{16}\text{O}$ .

**Volcanic outgassing.** Early lunar volcanic outgassing has been proposed as a potential source of volatiles now trapped in lunar polar regions [42, 62-65]. Observations of the lunar surface indicate that volcanic features are often associated with anomalously high water contents [20, 66]. Volcanic volatiles mostly composed of C, H and S species as measured in Apollo 15 and Apollo 17 volcanic glasses [67-70]. Needham and Kring (2017) [64] estimated that 90-100% of these dissolved volatiles are lost to the volcanic gas. Thermochemical models of lunar volcanic gas showed that C-H-S will exist as CO, H<sub>2</sub> and S<sub>2</sub> (e.g., Fegley 1991, Renggli et al. 2017). If lunar volcanic gas contained sufficient pressure, COS, H<sub>2</sub>S and a small amount of H<sub>2</sub>O may be present in the gas (Renggli et al. 2017). When these species condense, the S:C ratios are expected to be high since CO and H<sub>2</sub> are not as condensable as S species.

INSPIRE will measure C-H-S species in ice deposits to identify previous volcanic outgassing events that can be preserved in the volatile record. Because lunar volcanism largely ceased by ~3 Gyr [71], any cold-trapped volcanic volatiles would be relatively ancient. Given their time-exposure to the lunar bombardment environment [25], volatiles from volcanic sources would be expected to be heterogeneously mixed within the regolith [64].

**Asteroid impacts.** Asteroids can also deliver volatiles to the lunar surface (e.g., [42, 73, 74]). The influence of asteroid impacts on volatile inventories will be addressed via isotopic measurements. Asteroids are parent bodies for meteorites, where distinct isotope characteristics of water can be inferred.

Oxygen isotopes of primordial water on asteroids is inferred from chondrites. Correlations of  $\delta^{17}\text{O}$  and  $\delta^{18}\text{O}$  between anhydrous minerals, matrix, and bulk CM chondrites hint a primordial water reservoir that is rich in  $^{17}\text{O}$  and  $^{18}\text{O}$  [75], which was modeled to be  $35 \pm 9 \text{‰}$  and  $55 \pm 13 \text{‰}$ , respectively [76]. Similar correlations in an ungrouped chondrite suggested the primordial water is more enriched in  $^{17}\text{O}$  and  $^{18}\text{O}$  (both  $\delta^{17}\text{O}$  and  $\delta^{18}\text{O}$  at  $180 \pm 13 \text{‰}$ , [77]). Therefore, we expect polar ice with significant contribution of asteroid water would have measurable  $^{17}\text{O}$  and  $^{18}\text{O}$  enrichment.

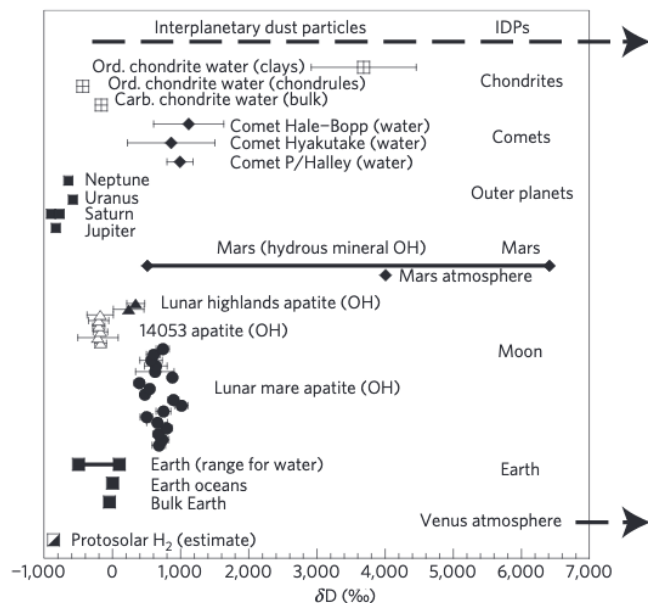


Figure 1-6.  $\delta\text{D}$  plot for the Solar System (from [72]).

Hydrogen isotopes of water in carbonaceous chondrites likely lie between terrestrial water and that of protosolar H (Figure 1-6, [78]), which also covers the range inferred for the lunar mantle [69].  $\delta D$  values of water in ordinary chondrite are enriched, similar to comets (Figure 1-6, [78]). Therefore,  $\delta D$  value alone would not be sufficient to distinguish between volcanic and asteroid sources. Oxygen isotopes will assist the identification of asteroid source in addition to C/H ratios.

*Comet impacts.* Comets have also been proposed to explain much of the volatiles sensed at the lunar poles today (e.g., [74, 81-83]), and it has even been proposed that a single comet (or water-rich asteroid) may explain all the surface ice observed on Mercury today [84]. An elevated D/H ratio of ice could be consistent with a cometary origin [72, 85] as well as other sources. However, comets have a unique signature of multiple volatile compounds (Table 1-3), and thus INSPIRE will assess the abundances of these compounds relative to water to distinguish between comet and asteroid sources. A cometary source would also imply a heterogeneous distribution of volatiles mixed with regolith over time as cometary delivery would occur early in the Moon's history. The physical form of the ices could include larger blocks and/or layers which could form a temporary atmosphere generated on the Moon from the impact event.

*Solar wind.* Interactions between the solar wind and regolith can create water on the lunar surface. Specifically, the solar wind implants H atoms in mineral surfaces on defects of atomic lattices, where they bind strongly to their positions (e.g., [86]). In O-bearing targets, these protons can react with O atoms and form OH groups [87]. Mineral surfaces can become saturated with OH and H<sub>2</sub>O can form from this process as well (e.g., [88, 89]). Models predict that the solar wind would produce a homogeneous and diffuse surface layer on grains, which can be measured by INSPIRE instruments. The solar-wind-H-bearing species can then be released, mobilized, and transported to the poles [90]. This process is hypothesized to be responsible for much of the dynamic OH/H<sub>2</sub>O signal observed by multiple spacecraft [66, 91-93]. Solar wind is highly depleted in D (D/H < 10<sup>-7</sup>,  $\delta D \approx -1000\%$ ). The transport process of solar wind from lower latitudes to polar regions will certainly fractionate D from H. After depositing in cold traps, cosmic-rays may further alter the D/H values. However, lack of S or C in the ice will likely support solar wind origin.

*Ongoing meteoroid bombardment.* Finally, meteoroid bombardment can continuously deliver volatiles to the lunar surface [94-97] and this process would result in an amount of deuterium inconsistent with solar wind levels. The composition of sequestered volatiles would be similar to the composition of volatiles being delivered currently through ongoing bombardment, and an increase in exosphere abundances would occur during meteoroid streams.

**#Ages.** INSPIRE will constrain the relative ages of lunar volatile deposits by measuring volatile form and distribution and correlating with past and present environmental conditions. Ancient deposits (~3.5-4 Ga) would have a spatial distribution consistent with paleo ice stability regimes, which likely changed from paleo to present-day due to true polar wander [23]. This lateral distribution should be interrogated over large (10s-100s km) length scales to compare paleo and modern ice stability regions. A vertical distribution to 2 m depth is needed to determine the form and distribution of volatiles in uniquely paleo and uniquely present-day ice stability regions. Accessing material at 2 m depths provides an improved chance to sample this ancient ice. An ongoing contribution to volatile deposits over geologic timescales would follow changing ice stability locations and present a wider spatial distribution as an admixture between paleo and present-day ice stability zones. Discrete delivery events may also be preserved as layers and/or ice blocks within the subsurface. If lunar polar volatiles are recent deposits, surface frosts would be replenished and correlated with deeper ice distributions. The spatial distribution of volatile deposits would favor present-day stability regimes and be dominated by signatures from solar wind and ongoing meteoroid bombardment processes.

**#Evolution.** Ice deposits likely experience some degree of modification post-emplacement, which can occur by several different processes and compound the attempt to discern the origins and ages.

**Table 1-3.** Abundances of major molecules in comets (from [79, 80]).

Compound	Abundance relative to H <sub>2</sub> O (%)
CO	<1-40
CO <sub>2</sub>	2-20
H <sub>2</sub> S	0.1-1.6
NH <sub>3</sub>	0.1-2
CH <sub>4</sub>	0.1-0.5
C <sub>2</sub> H <sub>6</sub>	0.2-2
CH <sub>3</sub> OH	0.9-7



Table 1-2. Science Traceability Matrix.

Science Question	Hypothesis	Measurement Prediction	Objective	Observables	Instrument 1	Instrument 2	Instrument 3	Instrument 4	Instrument 5	Instrument 6	Instrument 7	Instrument 8
What are the origins of volatiles in the inner Solar System? (#Origins)	Early lunar volcanic outgassing was a source of volatiles	CO, H <sub>2</sub> , H <sub>2</sub> S, COS, and S <sub>2</sub> are main volatile constituents indicating volcanic outgassing sources. Elevated S:C ratio compared to cometary abundances. Volatiles are mixed over depth with higher concentrations in older regions; Heterogeneous distribution of volatiles mixed with regolith.	Determine the abundance and distribution of lunar volatiles including water by measuring sulfur-bearing molecules, isotopic ratios, carbon-based molecules, and D/H ratios. Use volatile distributions (lateral and vertical) and the physical form of volatiles to distinguish between sources.	Sulfur-bearing molecules. Certain compounds and concentrations in ppm. Fraction of sulfur and relative abundance. Measure volatile concentration variations with depth, spectroscopic reflectance of the surface.	MSolo-drill, MSolo-exosphere	NIRVSS	NSS	Vis Imager	TRIDENT			
	The source of lunar polar volatiles was asteroid impacts.	Mix of constituents with isotopic ratios consistent with asteroids. Enrichment of both <sup>17</sup> O and <sup>18</sup> O, D/H of 10 <sup>-4</sup> to 10 <sup>-7</sup> or ~3x10 <sup>-4</sup>		Isotopic ratio of (1) <sup>18</sup> /17/ <sup>16</sup> O (2) D/H in water								
	The source of lunar polar volatiles was comet impacts.	Presence of complex molecule and carbon bearing constituents (complex organics) consistent with cometary compounds; Relative abundance compared to water of (1) CO (2) CO <sub>2</sub> (3) H <sub>2</sub> S (4) NH <sub>3</sub> (5) CH <sub>4</sub> (6) C <sub>2</sub> H <sub>6</sub> (7) CH <sub>3</sub> OH as consistent with cometary ratios. Large D/H values (2-4 x 10 <sup>-4</sup> ). Heterogeneous distribution of volatiles mixed with regolith; Physical form can include some ice chunks and/or layers (can be derived via ices condensed from temporary atmosphere generated on the Moon from the impact event).		Isotopic ratio of D/H. Relative abundance with respect to water of (1) CO (2) CO <sub>2</sub> (3) H <sub>2</sub> S (4) NH <sub>3</sub> (5) CH <sub>4</sub> (6) C <sub>2</sub> H <sub>6</sub> (7) CH <sub>3</sub> OH. Physical form of volatile components.								
	Solar wind interaction is a source of lunar volatiles	D/H ratio in water would be similar to solar abundance, e.g., very low (D/H < 10 <sup>-7</sup> ); Homogeneous and diffuse distribution on grain surfaces; Physical form is implanted OH and coated on grains.		Isotopic ratio of D/H in water; physical form and distribution of OH.								
	Ongoing small meteoroid bombardment (incl. IDPs, cometary dust, asteroidal dust) is the source of lunar volatiles	Composition of sequestered volatiles are similar to composition of volatiles being delivered currently; amount of deuterium in H <sub>2</sub> O is not consistent with solar wind D/H. Increased exosphere abundances during meteoroid streams; detect changes in the exospheric content during strong meteoroid streams to determine whether this is a significant ongoing factor.		Isotopic ratio of H <sub>2</sub> O in the exosphere. Spatial distribution (lateral and vertical) of volatile components; Exospheric volatiles during meteoroid events.								
What are the timescales of volatile delivery in the inner Solar System? (#Ages)	Lunar polar volatiles are ancient.	Exosphere composition matches surface compositions; Spatial distribution correlates with paleo ice stability regions.	Determine the age of lunar volatiles by measuring the form and distribution and comparing with past and present-day environmental conditions.	Exosphere composition; lateral distribution of volatiles over large (10s km+) length scales to compare with paleo ice stability regions; vertical distribution to 2 m depth to determine form and distribution of volatiles. Map present-day frosts.	MSolo-drill, MSolo-exosphere	NIRVSS	NSS	Vis Imager	TIRS	IES	TRIDENT	
	Lunar volatiles have been delivered throughout lunar history.	Ice blocks and/or layers exist in the subsurface through discrete delivery events; Volatile distributions span multiple ice stability regimes over geologic time.										
	Lunar volatiles are recent deposits.	Surface frosts are replenished and frost occurrences are correlated with ice distributions at depth; Subsurface distributions are not correlated with paleo ice stability regions; volatile distributions are consistent with present-day temperature regimes; Evidence of solar wind & ongoing meteoroid volatile deposition primarily in regions of present-day temperature stability regimes for volatiles.										
How do volatiles evolve on Solar System airless bodies? (#Evolution)	Solar wind sputtering has destroyed all evidence of ancient polar volatiles.	Surface volatile distribution is correlated with solar wind ion flux; surface abundance is anti-correlated with ion flux.	Determine how lunar volatiles have evolved over time by measuring the distribution of volatiles and correlating with environmental factors and geological context.	Ion flux and abundance of volatiles primarily water. Solar protons and electrons; Ions and electrons from few eV to 10s of keV.	MSolo-drill, MSolo-exosphere	NIRVSS	NSS	Vis Imager	TIRS	IES	TRIDENT	mini-GPR
	Impact gardening has re-distributed volatiles to erase the time-history.	Minimal variance in vertical distribution from place-to-place; Small lateral correlation on meter scales; Existence of protected deposits under thin ejecta blankets.		Depth distribution with 10 cm resolution down to 2 m depth. Vertical distribution in a number of locations with very close spacing (m scale). Examine thin ejecta blankets.								
	Cosmic rays have destroyed the surface manifestation of ices.	Volatile distribution has no correlation with solar wind flux; Existence of cosmic-ray induced chemistry products.		Ion flux and abundance of volatiles primarily water. Solar protons and electrons. Examine for cosmic-ray induced chemistry products.								
	The present day distribution of volatiles is an artifact of true polar wander.	Spatial distribution correlates with ancient polar position; volatile abundance correlates with theoretical predictions of ancient cold trap locations and predicted migration of cold trap locations over time.		Lateral and vertical distribution of volatiles in presumed modern and ancient ice. Measure similar regions of different age ice (same temperature, conditions, but different age) at depth (surface to 2 m). Measure water abundance, isotopes at depth.								
	Thermal diffusion creates zones where volatiles can be stable.	The distribution of volatiles with depth are correlated with subsurface temperature; subsurface enhancements are found at ice pumping depths. Process occurs where mean surface temperature is below 105 K and the peak surface temperature is above 120 K.		Surface and subsurface temperature below 20 cm to 2 m deep and water abundance. Also porosity and other geotechnical aspects. Distinguish between physical state of ice.								

INSPIRE will constrain these processes by measuring the distribution of volatiles and correlating with present-day environmental factors and geological context to infer their past effects.

*Solar wind sputtering.* The flux of solar wind into PSRs varies across different PSRs and within different areas in a single PSR due to potential shielding, electric fields that can deflect electrons and not protons, etc. Here we will correlate surface frost occurrences with the ion-electron flux and measure fluxes that are lower than the typical solar wind (order of <10% of typical solar wind flux) to understand the effects of solar wind sputtering on surface-frost deposits due to the presence and abundance of solar protons and electrons.

*Impact gardening.* Impact gardening is an ongoing process altering the lunar regolith [25]. Remote sensing data suggests heterogeneity of surface and subsurface volatile deposits, however, the vertical variations in volatile signatures should be minimal if deposits have been completely reworked by impact gardening with small lateral correlations on meter scales. Thermally protected volatile deposits are possible under thin ejecta blankets on order of 20 cm or greater in thickness, which protects the deposits from further micrometeorite gardening and/or destruction since deposition. By directly measuring subsurface ice stratigraphies, INSPIRE will constrain the impact models since gardening is a prime driver affecting the depth and lateral distribution of ices in cold regions, especially where thermal diffusion is minimal.

*Cosmic rays.* If cosmic rays have altered the surface ice deposits, cosmic ray induced chemistry products should be present. These products include isotopic changes and species such as C<sub>2</sub>H<sub>6</sub>, CH<sub>3</sub>OH, HCOOH, and CH<sub>4</sub> [98]. The older the ice deposits are, the more abundant the cosmic-ray products are. In this case, the volatile deposits would not be correlated with solar wind flux but would correlate with the age of the deposits.

*True Polar Wander.* True polar wander theorizes that the lunar polar axis has shifted over time, which alters the thermal stability regions for volatile deposits [23]. This hypothesis is tested by mapping the lateral and vertical distribution of volatile deposits and comparing this distribution with paleo and present-day ice stability regimes over 10-100s km lateral length scales and 2 m vertical depths.

*Thermal diffusion.* Under suitable temperature conditions, water molecules can migrate into the lunar subsurface driven by day-night temperature cycles and subsequent “ice pumping” [99]. This process would lead to higher ice concentrations at depth compared with the surface and could occur where the mean surface temperature is below 105 K and the peak surface temperature is above 120 K [99].

## 2 HIGH-LEVEL MISSION CONCEPT

### 2.1 CONCEPT MATURITY LEVEL (CML)

The INSPIRE concept as presented in this study is at CML 4, per the definitions presented in the PMCS ground rules. The rover concept was defined at the assembly level and was estimated for mass, power, data volume, link rate, and cost by Team X using JPL’s institutionally endorsed design and cost tools. Following this an in-depth configuration, design and operations refinement effort was conducted by the study team.

### 2.2 TECHNOLOGY MATURITY

The INSPIRE rover design benefits from significant prior art, robust engineering processes and design practices, and a large body of knowledge generated in developing and successfully operating Mars rovers over the last two decades. INSPIRE leverages experience from past and current lunar rovers (Apollo LRV, Lunokhod, Yutu) and builds on current lunar development activities including the VIPER lunar rover, as well as significant advances in capabilities from other space and terrestrial applications. As is the case with any new mission concept, the INSPIRE rover will need specific engineering developments and the application of key technologies.

**Lunar Dust Environment:** Lunar dust is a potential hazard with unique challenges posed by abrasive particles, electrostatic charging of surfaces, and differential charging effects over the day/night cycle. Our current understanding of lunar dust challenges for rovers is built on experience gained from past lunar surface missions and is informed by continuing technology efforts [100] as well as current plans for the upcoming commercial (CLPS) lander and VIPER rover missions. While engineering

development activities and validation to mitigate dust remain and are planned for, especially for the long-distance traverse, there are no new technologies that are anticipated beyond what has been employed by prior missions (including Mars) and those being addressed by the upcoming VIPER rover. The VIPER mission will provide much information on the success of current mitigating techniques and identify any further improvements needed. Given that dust deposition in the lunar environment primarily results from the interactions of the wheels with terrain the system is designed to keep all dust-sensitive surfaces well above height of the wheels to minimize dust accumulation at INSPIRE’s low mobility speed (average <0.2 km/hour). The slow mobility together with frequent hourly stops minimize any wheel triboelectric charging and enhances charge dissipation. Instruments are kept as far off the regolith as possible during vehicle driving. Further, drilling operations will be conducted over long durations with slow drill motions to minimize lofting dust. Pauses between active drilling segments will also reduce dust. In addition, NIRVSS has sapphire windows covering the optics, which are durable to dust with low dust adhesion as demonstrated in chamber testing. Dust transmission loss is also included in SNR calculations, and calibration targets are used for the camera with each drill deployment. MSolo uses a cross-beam aperture such that dust cannot impact the filaments and the thermal shroud around the drills also serves to contain dust from the rover’s body and/or instruments.

**Science Instruments:** The INSPIRE mission objectives are met through the use of a comprehensive suite of in situ instruments, most of which are flight proven or in advanced phases of development. The NIRVSS, MSolo, and NSS instruments are copies of instruments baselined to fly on the VIPER mission in 2023 and will also be flown as payloads on several of the first CLPS missions as early as 2021. In addition, a 1-m version of the TRIDENT drill will fly to the Moon on the PRIME-1 mission in 2022 and VIPER in 2023. The IES is directly based on the IES flown on the Rosetta mission and the TIRS instrument is based on the instrument currently being prepared for flight on the PREFIRE mission, with heritage from the Mars Climate Sounder on MRO and Diviner on LRO. The science cameras have heritage with MSSS ECAM MSL and LRO imaging systems. The NIRVSS, MSolo, and NSS instruments are employed on INSPIRE in the same configurations they will be used on VIPER. While standard engineering will be needed to adapt the remaining instruments to the INSPIRE mission, none of them require new technologies. Only the mini-GPR will require additional development to mature it to TRL 6, as detailed in §4.2. Table 2-1 summarizes the current TRL and heritage of the instruments on INSPIRE.

**Mobility System:** INSPIRE is a four-wheel-drive, all-wheel-steered vehicle with a dual rocker suspension. The dual rocker design has proven effective for all NASA’s Mars rovers. INSPIRE’s 0.8 m compliant wheels are similar in both size and design to the LRV mesh wheels. NASA Glenn Research Center has conducted a detailed design, development, and testing campaign (currently at TRL 6 for Mars environment) that improved this design to extend durability and traversability (rocks and craters). Further maturation of the wheel design and materials for the lunar environment for this mission will be needed (see Appendix D). Actuator technology is adequately mature from martian and lunar missions.

**Avionics:** The rover flight compute element and avionics for the vision system and motor control are based on current engineering developments at JPL (currently on-track to achieve TRL 5 by September of 2021), and whose specifications would encompass the needs of this mission. Other avionics (e.g., instrument interface, battery and power management, radio) have flight heritage and are not new technology. The rover sensor suite uses flight-proven cameras, optics, IMUs, and sun sensors.

**Autonomy:** Based on the trade described in the next section, the INSPIRE rover requires, in the nominal case, reliable day/night autonomous surface navigation with intermittent ground oversight and human-directed actions in off-nominal cases. Autonomous operations comprise perception, hazard assessment, pose estimation, and global localization, and system health and resources management. Autonomous daytime navigation leverages flight-operational capabilities from MER and MSL,

**Table 2-1. Instrument Heritage Table.**

Instrument Name	Abbrev.	Current TRL	Flight Maturation/Heritage
Near IR Spectrometer	NIRVSS	6	VIPER NIRVSS
Mass Spectrometer	MSolo	6	VIPER Msolo
Neutron Spectrometer	NSS	6	VIPER NSS
Ion Electron Sensor	IES	6	Rosetta IES
Thermal IR Spectrometer	TIRS	6	PREFIRE TIRS
Science cameras	SC	6	MSL, LRO
Ground Penetrating Radar	Mini-GPR	4	Needs development



which have been further advanced for faster traverse on the Perseverance rover [101, 102]. Lunar night perception, hazard assessment, pose estimation, and day/night global localization, and their integration into a reliable self-aware and self-directed autonomous system are necessary technologies to be developed, adapted, and matured as described in §4.2. Unlike Mars though, the availability of continuous, low-latency communications (nominally 4 hours every 24 hours at high bandwidth or 9 hours every 12 hours for emergencies) allows ground operators to more rapidly interrogate, diagnose, and respond to faults that cannot be resolved by the rover’s autonomous system.

**Drill System:** The INSPIRE 2-m drill system is based on the Honeybee Robotics TRIDENT 1-m drill, slated to fly on the PRIME-1 mission in 2022 and the VIPER mission in 2023. A number of subsystems such as the rails, the brushing station, and the auger will not need any further technology maturation. Extending the drill’s stroke from 1 m to 2 m is an engineering development. However, certain subsystems will require further development to extend the life from 50 m to 200 m (the specification for the INSPIRE mission is one hundred, 2 m holes, providing 36% margin for each drill against the minimum science requirement of 64 holes). Subsystems that would need further development and life testing will include the percussion mechanism, actuators, cable/pulley, brush, and the drill bit. Operations for deeper drilling will need to be matured (see Appendix H).

**Thermal Subsystem:** The INSPIRE thermal design relies on a two-phase, mechanically pumped, fluid loop system that has been under development at JPL with industry partners starting in 2015 at TRL 3. On January 11, 2021, the JPL Office of the Chief Technologist conducted an assessment and determined that it is on schedule to achieve TRL 5 by the end of FY 2021 when the integrated system will be tested in a relevant environment.

## 2.3 KEY TRADES

### Mobility

Table 2-2 captures INSPIRE’s key mobility requirements and expected terrain characteristics. INSPIRE will be driving ~70% of the distance at night and/or in PSR. Average night and PSR driving is slower than day driving (Table 2-2) because the viewing horizon is limited by onboard lighting, requiring additional stops with long camera exposures.

For the mobility trade, key drivers are robustness and durability, long-traverse distance, energy efficiency, low power, and the ability to traverse expected terrain. The terrain is relatively flat with 67% of the route at less than 5° in slope and 91% at less than 10° (see Appendix D, Table D-2).

Mobility designs with different wheel/steering configurations, suspension (passively compliant or actuated) [103], and wheel types and sizes, leveraging Apollo wheel-design data (see Appendix D) were examined based on these requirements. Table 2-3 summarizes the mobility configuration trades, selection, and rationale for this mission. The selected architecture is four-wheel drive, all-wheel steering with a passive, dual-rocker suspension that balances the weight of the vehicle among its four wheels. The wheels are large for better traction and narrow to reduce mass. Compliant wheel rims improve traction and reduce wear [104].

The choice of the dual-rocker suspension was primarily driven by the need to accommodate the drill system at the front of the vehicle for visibility and maneuverability for positioning with respect to drill locations. This requirement drove the INSPIRE vehicle suspension design to adopt a side-mounted dual rocker mechanism design that wraps around the vehicle chassis. The dual-rocker design has heritage from the successful Mars rover as it was part of their rocker-bogie suspension. For

**Table 2-2. Key Mobility Requirements and Constraints.**

	Requirements		Comments
	Rover	Nominal Distance	756 km
Actual Distance		1,140 km	Accounts for terrain tortuosity based on martian and lunar simulations and science site mapping (10% of 300 m x 300 m)
Max wheel speed		1 km/hr	Mechanical speed (or 28 cm/s)
Ave traverse rate (day)		0.23 km/hr	Incl. eng. stops for localization and comm
Ave traverse rate (night)		0.16 km/hr	Also incl. long-exposure imaging, localization and comm
Environ.	Characteristics		Comments
	Surface properties	Regolith	Largely ubiquitous
	Max slope	16°	Based on 5–10 m/pixel DEMs

INSPIRE, the rocker differential that connects the left and right sides of the mechanism uses the same design as the Mars Curiosity and Perseverance rovers, but is mounted below the vehicle chassis to accommodate the top-mounted lunar rover radiator. This differential was placed toward the back of the chassis to minimize impact on ground clearance. This change did not add a significant penalty in mass nor volume of the vehicle. In addition to opening up the front of the rover for accommodating the drills, the dual rocker suspension halves the tilt that the vehicle chassis experiences when traversing over wheel-surmountable terrain features.

### Autonomy/Localization

For the autonomy trade, key constraints that drive the viability of the operation modes, listed in Table 2-4, include: (1) the visibility and availability of the orbiting communication relay satellite, (2) the bandwidth and latency of the end-to-end communication link between the rover and ground, (3) the cadence of rover motions (day/night traverse and Science Stops) and (4) the nominal workday ground operations schedule following the initial phase of surface operations (this is a soft constraint with cost implications that can be adjusted, in particular, for handling off-nominal situations).

Unlike Intrepid, INSPIRE will conduct a significant portion of its traverse operations in the dark during the night or in PSRs. To identify the required level of autonomy, we examined trades ranging from ground-based *human control*, similar to the joystick operations of the Lunokhod rover, to *onboard-decide* (autonomous control) for mobility and system management. Table 2-4 summarizes the autonomy-related trades. Throughput analyses based on sensors dataflow, onboard computation performance, and communication bandwidths showed that this mission has to rely on the *onboard-decide* mode for a significant portion of its nominal operations and on the *human-decide* mode for handling contingencies. Furthermore, after the first two weeks of 24/7, the project transitions to a normal workday schedule, where both traverse and science operations would inevitably fall outside the work-day schedule. Therefore, a significant portion has to be conducted through autonomous operations (*onboard-decide*).

Key capabilities needed for autonomous surface operations include: day/night navigation (hazards assessment, motion planning, and hazard avoidance), pose estimation (dead-reckoning), and global localization (determining the vehicle’s location relative to orbital maps). Heritage navigation and pose estimation would be leveraged from the Mars rovers, but these rovers use ground-based global localization. Night navigation requires development and maturation to assess the ability to perceive all hazards with artificial myopic lighting. Optical, radiometric, or hybrid techniques can be used for onboard global localization but require further investigation to assess accuracy based on the number of available relay orbiters and the quality of the orbital maps and surface images using lighting at night. Similar to the Mars rovers, INSPIRE would have to update its global localization every ~300 m. Given the ground-operations schedule and communication constraints, onboard global localization becomes necessary to meet the traverse rate and distances. Optical techniques would image unique surface features, such as craters or boulders and map them to lower-resolution orbital images to correct for drift in the rover’s pose estimation (dead reckoning). Periodic stops every 300 m for global localization at night would be necessary to maintain an error of < 10 m relative to the orbital maps. Since INSPIRE will be covering greater distance at night than Intrepid, global localization at night would have to rely

**Table 2-3. Mobility Trades, Selection, and Rationale.**

	Key Trades	Selection	Rationale
Type	Wheeled vs. tracked	<b>Wheeled</b>	Lower mass, larger ground clearance and lower risk of rocks entrapment
Configuration	<u>Drive + steering wheels:</u> 3-wheel (1 steering) 4- and 6-wheel config (see App. D)	<b>4-wheel (4-steering)</b>	Adequate stability (low tip-over risk) and best maneuverability at lower mass and power; resilient to single-steering failure.
	<u>Suspension:</u> Active vs. passive vs. spring-loaded	<b>Passive</b>	Balanced weight on wheels,
	Dual-sided rocker vs. single-sided rocker	<b>Dual-sided rocker</b>	To accommodate the drill and reduce chassis tilt over rockier/undulating terrain than single rocker in the polar region.
Wheels	<u>Diameter:</u> Large vs. small Narrow vs. wide (large: ~1½ x MSL) (narrow: ½ x MSL)	<b>Large Narrow</b>	Superior traction, energy efficient, enhanced obstacle traversal; fewer rotations and terrain contacts for longer life.
	Rigid vs. compliant	<b>Compliant</b>	Improved mobility in soft regolith and over rocks, improved wear resistance
Gravity	Lunar rover to operate under Earth gravity vs. only lunar gravity	<b>Earth-gravity rover</b>	Enables end-to-end testing of rover in different terrains without complex gravity off-loading aids

rely on longer exposures of illuminated images to increase the perception horizon. Alternatively, radiometric techniques would use the known ephemerides of the orbiting satellite(s) for Doppler ranging and time-of-flight measurements to localize the rover. Depending on the precision of the inputs, the estimated localization accuracy may range between 5–15 meters. But because of the uncertainty associated with the number and availability of orbital assets at the time of the mission, an optical-based approach was baselined for this mission.

### Power

The INSPIRE mission concept is predicated on having a rover that is capable of extended operations in lunar PSRs. Such a requirement led the team to an early decision to adopt a radioisotope power system (RPS) in the baseline design. Use of RPS allows the rover to operate independent of solar illumination, enabling exploration of the old, cold regions of PSRs that are the focus of this mission.

Choices of RPS for the INSPIRE design are detailed in the study Groundrules. These include Mod-0, Mod-1 and Mod-2 Next Gen RTGs, as well as the Dynamic Radioisotope Power System (DRPS).

With a beginning of life (BOL) output power of 293 W and a mass of 56 kg, the Mod-0 Next Gen RTG is an attractive choice, however the limited availability of this model (only one will be produced) led the team to evaluate other options to ensure a viable design. The Mod 2 Next Gen RTG promises significant performance improvement, but its later predicted availability date (2034) might unnecessarily delay the implementation of the mission. While the DRPS falls into the right range of power as well and would actually have the advantage of rejecting less waste heat to the local environment, concerns regarding the significantly increased mass of this option led the team to baseline the Mod-1 Next Gen RTG as the optimal choice. The Mod-1 RTG has a BOL power output of 245 W, a power level that readily meets the mission needs as shown in Table 3-4.

It should be noted that the type of RPS is somewhat flexible for the INSPIRE design. While the Mod-1 RTG has been baselined, the Mod-0 or Mod-2 RTGs would be a drop-in replacement that would have no impact on system mass or design and would provide increased power for the mission. The DRPS could also be readily accommodated with a slight mass increase, but also a resultant benefit in power.

**Table 2-4. Autonomy-related Trades, Selection, and Rationale.**

	Key Trades	Selection	Rationale
Operation Modes	Human control: operators joystick every action Human decide: ground computers assess w/ humans deciding on actions Ground compute: computers assess and decide w/ limited async human oversight Onboard decide: onboard computer controls w/ limited async human oversight	Main: Onboard decide  Backup: Human decide	Visibility and availability of the relay orbiter (nominal 4 hours every 24 hours) and the need to drive for hundreds of hours during lunar day and night (Earth day/night) using daytime operations left the <i>onboard-decide</i> mode as the only viable option for nominal operations to meet traverse rate. Slower operations can use <i>human-decide</i> mode.
	<u>Exteroceptive</u> Cameras (stereo) vs. LIDARs (flash, spinning) Star tracker Sun sensor	Stereo cameras w/ Lighting + Sun sensor + Star tracker	Lower power and mass; mature capability; wide field-of-view.
Sensors	Perception Sensor Mounting <u>Front only vs. front/rear perception</u> <u>Body mounted vs. articulated</u> <u>mast mounted</u>	Front/rear perception Articulated front + body-mounted back	Bi-directional driving allows retracting the rover from entrapments  Primary forward driving direction requires situational-awareness of a wide area for path planning
	<u>Proprioceptive</u> Inertial Resolvers, encoders, hall effect Motor currents	IMU + hall-effect (all) + resolvers (steer only) + current	IMU complement visual odometry for low textured terrains, provides vehicle tilt; hall-effect sensors and resolvers are more reliable than encoders at high temperatures.
Compute	<u>Main Processor:</u> LEON3 (dual-core) / Sphinx LEON4 (quad-core) / Sabertooth	LEON 4 Sabertooth	Quadruple compute and more I/O
	<u>Aux Processor:</u> Virtex 5	Virtex 5	Mars 2020 heritage

## 3 TECHNICAL OVERVIEW

### 3.1 INSTRUMENT PAYLOAD DESCRIPTION

The INSPIRE science payload consists of eight elements (7 distinct instruments; 2 copies of the same mass spectrometer), the data from which will together enable discernment among competing hypotheses regarding the dominant source, the timeline for delivery, and the evolution of lunar polar volatiles. Technical details for each instrument can be found in Table 3-1 and mounting is shown in Figure 3-1.



The payload represents a mature suite as discussed in §2.2; instrument summaries follow.

**NIRVSS:** The Near-Infrared Volatile Spectrometer System is a multi-component instrument consisting of two modified commercial point spectrometers—one short-wave (SW) and one long-wave (LW)—that measure over wavelength ranges of 1300–2500 nm and 2200–4000 nm, respectively. Both spectrometers sample at a minimum of 1 nm intervals, with spectral resolutions of <20 nm (SW) and <50 nm (LW) [105, 106]. Additional NIRVSS components include: a 4-megapixel CMOS sensor that uses multiple LEDs for context imaging over 348–940 nm; a Longwave Calibration Sensor with four thermopiles and wavelength filters covering 6–25, 10, 14, and 18 μm to measure IR flux and surface temperature down to ~100 K; a dual-filament tungsten IR lamp filtered to transmit from ~1500–5000 nm for even, calibrated illumination of the surface [105, 106]. Together, these components enable measurements of lunar surface and subsurface composition (including volatile abundances from drill cuttings), morphology, and thermophysical properties as well as drillhole imaging from NIRVSS’s position mounted under the rover.

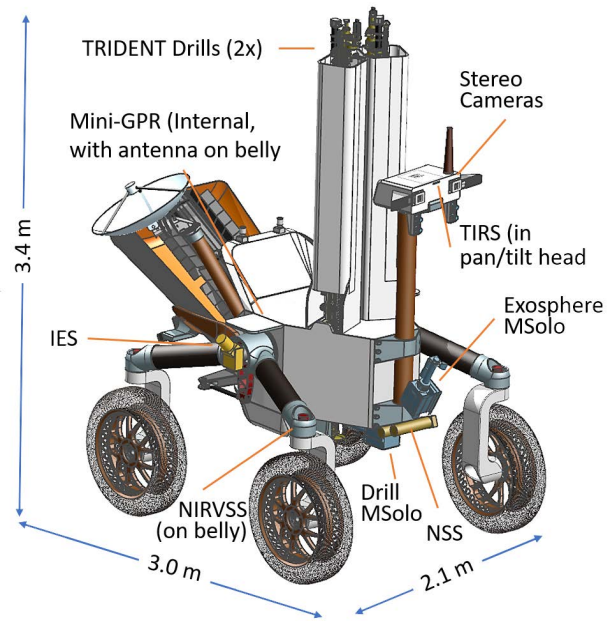


Figure 3-1. Rover with instrument accommodation.

**NSS:** The Neutron Spectrometer System consists of two gas-proportional counters containing

Table 3-1. INSPIRE Instrument Suite. Power and mass estimates are from high TRL instruments (§2.2).

Instrument	NIRVSS	NSS	MSolo	IES	Mini-GPR	TIRS	Cameras
Size/dimensions (cm)	18 × 18 × 9 + 23 × 13 × 15	21 × 32 × 7	15 × 20 × 46	7.5 φ × 10 + 14 × 12 × 6	10 × 10 × 20	~0.003 m <sup>3</sup>	19 × 16 × 20 2 units
CBE* Mass (kg)	3.6	1.9	6	1.04	3	3	1.8
Mass contingency (%)	10	10	10	10	30	30	10
Mass with contingency (kg)	3.96	2.09	6.6	1.1	3.9	3.9	2.0
Average power (W, CBE*)	30	2	35	1.85	5	6 (8.5 pk.)	16 (12 idle)
Average power cont. (%)	10	10	10	10	30	30	10
Average power w/ cont. (W)	33	2.2	38.5	2.03	6.5	7.8 (11 pk.)	18, 13 idle
Average science data rate <sup>A</sup> (kbps, CBE)	115 (drive), 145 drilling/imaging	0.85	15 driving, 30 all else	4	25	12	12 × 3 bands × 2 meas. = 72
Average science data rate <sup>A</sup> contingency (%)	10	10	10	10	30	30	10
Average science data rate <sup>A</sup> with contingency (kbps)	126.5	0.935	16.5 driving, 33 all else	4.4	32.5	15.6	79.2
Fields of View (deg)	NIR cone 8, cus- tomizable; vis im- ager square 38 di- agonal; IR imager cone 35, customi- zable, toward nadir, .3 cm at 1 m	Uncollimated (effectively 180 degree down- ward, upward blocked by rover)	18 for two aper- tures: Sky- ward, toward drill hole	90 × 360, an- gular res 5 × 5 solar wind sector, other- wise 5 × 22.5 electrons, 5 × 45 ions	Nadir (30 de- gree beam width)	Forward (ram) 14.4, IFOV 1.3	90 (wide) (.034 × .046 pixels)
Pointing requirements (knowledge, deg)	10% control	10% control	10% control	10% control	10% of control	<0.15	0.03
Pointing requirements (control, deg)	0.1	Normal to ground +/- 10	1 (assuming 1 cm at 50 cm)	1	w/in 15 from vertical	<0.2	0.3
Pointing requirements (stability, deg/s)	0.05	5	0.5	0.05	7.5	0.1	0.15

\*CBE = Current Best Estimate. <sup>A</sup>Instrument data rate defined as science data rate prior to on-board processing

pressurized  $^3\text{He}$  to detect the cosmic-ray-generated thermal and epithermal neutron flux emanating from the lunar surface. One channel covers an energy range spanning thermal ( $<1$  eV) through epithermal neutrons (1–1000 eV), while the second channel is limited to only epithermal neutrons [107]. Epithermal neutron measurements enable the determination of bulk water-equivalent hydrogen (WEH) abundance down to 0.5 weight percent [108] with absolute accuracy of 5–10% [108] and uncertainty of  $<0.1\%$  [109]. The difference between the two channels’ measurements facilitates estimation of hydrogen-rich volatile burial depths down to  $\sim 1$  meter [107]. The NSS will be mounted on the rover body.

**MSolo:** The Mass Spectrometer Observing Lunar Operations is a modified version of the commercial, off-the-shelf Inficon Transpector® quadrupole mass spectrometer [107]. MSolo is designed for detection and quantification of low molecular weight volatiles in the lunar environment and operates over a mass range of 2–100 amu with 1 amu mass resolution [108, 109]. Two MSolo units will be deployed in different locations on the rover: The first, mounted on the underside of the rover, will be used to measure the composition of volatiles on the lunar surface as well as those released from the subsurface during drilling and from the cuttings pile. The second MSolo unit is mounted at the base of the camera mast and will be used to measure composition of the lunar exosphere.

**IES:** The Ion and Electron Sensor, initially flown as part of the Rosetta Plasma Consortium (RPC), consists of two electrostatic plasma analyzers—one for ions and one for electrons—that are arranged in a ‘top-hat’ geometry such that the two electrostatic analyzers share a common aperture. The RPC-IES was designed to obtain three-dimensional ion and electron distributions over the energy range 1 eV/e to 22 keV/e with 4% energy resolution and 128 s temporal resolution [110]. RPC-IES was used to measure both the solar wind and the pickup ions created via interaction of the solar wind with gas evolved from the nucleus of comet 67P [111]. On INSPIRE, the IES will be mounted adjacent to the rover deck to perform ongoing measurements of the energy and angular distribution of impinging ions—including the solar wind—and electrons along the rover route in order to provide the basis for understanding the role of charged particles in lunar volatile origin, distribution, and evolution.

**Mini-GPR:** The miniature Ground Penetrating Radar consists of a compact Ka-band radar transmitter with compact dual Ka-band deployable transmitter/receiver antennas. The instrument technology draws from recent advances in miniaturization of radar instruments and electronics for CubeSat missions RainCube [112, 113] and COVE [114]. With  $\geq 10$  cm vertical resolution, the mini-GPR measures subsurface variations in dielectric constant as a function of return time; from these data, the percentage of subsurface water ice down to a detection limit of  $\sim 0.1\%$  can be derived. The mini-GPR will be mounted on the underside of the rover; its measurements will enable an independent derivation of subsurface ice distributions, which can be compared to the results from NSS, and provide a subsurface context for volatile measurements by NIRVSS and MSolo.

**TIRS:** The miniature Thermal InfraRed Spectrometer for INSPIRE is a 64-channel, high-resolution mid- and far-infrared imaging spectrometer based on those currently being developed for NASA’s PREFIRE CubeSat mission. The two PREFIRE TIRS are themselves based on technology previously flown as part of the Mars Climate sounder on MRO [115]. TIRS measures over a wavelength range from 5–54 microns with 0.86 micron spectral resolution and an expected radiometric performance better than 1.5 K (at 300 K) for all channels [116]. TIRS will be mounted on the INSPIRE mast and used to measure lunar surface temperatures along the rover route and at INSPIRE drilling sites.

**Cameras:** The cameras for INSPIRE are modified from the OSIRIS-REx TAGCAMS suite, a Malin Space Science Systems ECAM-C50 imaging system. The cameras consist of a 5-megapixel image sensor discretized into a  $2592 \times 1944$  pixel CMOS detector with RGB Bayer Pattern color filter array coupled to a wide field of view lens; each camera head interfaces via SpaceWire to an onboard digital video recorder

**Table 3-2. Summary MEL.**

Subsystem	Mass (kg)		
	CBE	Cont.	MEV
Instruments	26.4	15%	30.2
C&DH	13.2	13%	14.9
Telecom	20.2	19%	23.9
GNC	7.5	11%	8.3
Power	81.7	29%	105.5
Thermal	31.9	30%	41.4
Structures	83.2	22%	101.2
Drill System	58.0	20%	69.6
Mobility	111.9	21%	135.3
Harness	24.1	30%	31.3
<b>Rover Total</b>	<b>457.8</b>	<b>23%</b>	<b>561.5</b>
Lander Allocation (MPV) <sup>1</sup>			655
<b>Margin (MPV-CBE)/MPV</b>			<b>30%</b>

<sup>1</sup>Allocation represents minimum capability of lander to meet 30% mass margin

(DVR) [117]. Two modified ECAM-C50 cameras mounted on the INSPIRE mast with a pan/tilt mechanism provide stereo imaging of the lunar landscape surrounding the rover; images can be used for visual navigation, hazard detection, and contextualization of drilling sites.

### 3.2 FLIGHT SYSTEM

#### 3.2.1 OVERVIEW

The INSPIRE rover design began with the long-range rover concept developed for the earlier Intrepid PMCS. Intrepid laid the groundwork for an autonomous, long-range long-distance rover and the INSPIRE team was able to take advantage of many of the subsystem developments performed for that design to provide a solid foundation for a rover capable of a similarly high-performance mission in the PSR environment. A comparison of Decadal rover designs is presented in Appendix N.

System mass and power modes are shown in Tables 3-2 and 3-3. The rover launch mass maximum expected value (MEV) is 562 kg. Carrying the suggested 30% margin results in a requirement that the CLPS lander capability be at least 655 kg, which should be within the range of medium class cargo landers expected to be available in the mission time frame. Power output of the Mod-1 RTG provides robust margins in most power modes through end of mission. The driving power mode occurs during drilling stops with all instruments active. The battery is sized for this mode and will see <60% depth of discharge through end of mission. Rover characteristics are summarized in Table 3-4 and an overview of the rover configuration is shown in Figure 3-2.

#### 3.2.2 ROVER SUBSYSTEMS

Subsystem elements for INSPIRE were derived from the design of the original Intrepid rover concept using proven, heritage designs as well as product lines currently in late stages of development.

##### Mobility

The mobility system is designed for the expected terrain along the planned route (see Appendix D, Table D-2). The route is designed to maintain slope angles that do not exceed 16°, which are expected to be traversed at rates shown in Appendix G, Table G-8. The mobility system uses a four-wheel drive, all-wheel steering configuration with a passive dual-sided rocker suspension. Two rocker mechanisms pivot on the left and right sides of the vehicle. The two sides are connected to each other by a differential mechanism that kinematically couples them under the vehicle chassis so the motion on one side causes the opposite motion on the other side. The rover is designed to drive in either direction supported by front and back stereo cameras. With all-wheel

Table 3-3. Power Modes.

Subsystem	Power Modes				
	Traverse Night/PSR (W)	Traverse Day (W)	Drilling Stop (W)	Stop w/ Telecom (W)	Charge (Safe) (W)
Instruments	17	17	116	0	0
GNC	22	20	15	15	15
C&DH	29	29	13	23	1
Power	11	11	11	10	10
Mobility	45	53	0	0	0
Drill System	0	0	93	0	0
Telecom	10	10	31	31	10
Thermal	3	3	3	3	3
<b>Rover total</b>	<b>137</b>	<b>143</b>	<b>283</b>	<b>83</b>	<b>39</b>
Contingency	59	62	122	35	17
<b>MEV Power</b>	<b>196</b>	<b>205</b>	<b>405</b>	<b>118</b>	<b>56</b>
Avail. Power <sup>1</sup>	217	217	217	217	217
<b>Margin<sup>2</sup></b>	<b>37%</b>	<b>34%</b>	<b>-30%</b>	<b>62%</b>	<b>82%</b>

<sup>1</sup>Represents EOM power from RTG

<sup>2</sup>Drilling mode is augmented with battery

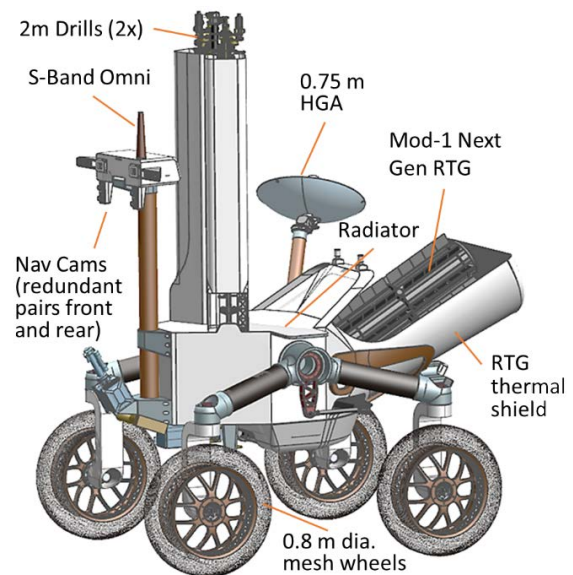


Figure 3-2. INSPIRE rover overview.



**Table 3-4. INSPIRE Rover Characteristics.**

Flight System Element Parameters	Value/Summary, Units
<b>General</b>	
Design Life	36 months
<b>Structure</b>	
Structures material	Aluminum and composite
# of deployed structures	2 (Drills)
<b>Mobility/Articulation</b>	
Control method	4-wheel drive, 4-wheel steer
Control reference	Stellar, terrain recognition
Slope capability	20 degrees
Max/ave ops drive speed	0.36/0.23 km/hr
# of articulated structures	14 (8 mobility, 2 pan/tilt mast, 2 axis HGA, 2 drills)
<b>Thermal Control</b>	
Type of thermal control used	Heat pipes/radiators/RHUs/thermal switches/pumped loop
<b>Command &amp; Data Handling</b>	
Housekeeping data rate	2 kbps
Data storage capacity	128,000 Mbits
Max. storage record rate	700 kbps
Max. storage playback rate	700 kbps
<b>Power</b>	
Expected power generation at Beginning of Life (BOL) and End of Mission (EOM)	RTG: 245 W BOL, 217 W EOM
Average power consumption	205 W (MEV, day drive mode)
Battery type	Li-ion
Battery storage capacity	100 amp-hr

wheel steering, the rover can also drive sideways at different angles. The rover has >0.6 m ground clearance and large-diameter compliant wheels to improve rock traversal, traction on regolith, and energy efficiency [104, 118, 119]. The 0.8 m-diameter wheels use a mesh structure, similar to the LRV, to traverse rocks that are less than 30 cm in height and drive through smaller craters not apparent in orbital data (<5 m in diameter with slopes below 10°).

### Drilling System

INSPIRE carries two redundant 2-m drills developed by Honeybee Robotics. INSPIRE extends TRIDENT to achieve the required 2-m depth. The two drills are mounted in such a way as to produce a pile of cuttings for observation by MSolo and NIRVSS in the same location. The rover design is such that if either of the drill were to get stuck, they can be detached from the rover via hold-release mechanisms, and the rover can use its 4-wheel steering capability to drive away from the drill (Fig. L-8, L-9 in Appendix L).

TRIDENT is a rotary-percussive drill which enables it to cut into icy material that could be as hard as rock. The drill consists of several major subsystems: a rotary-percussive drill head for providing percussion and rotation to the drill string, a deployment stage for deploying the drill to the surface, a feed stage for advancing the drill string up to 2 m into the subsurface, a drill string for drilling and sampling, and a brushing station for passively depositing material onto the surface (see details of drill design in Appendix H). The drill includes dedicated motor driver electronics. Operation of the drill is illustrated in Figure 3-3. To reduce thermal

risks, risk of getting stuck, reduce drilling power, and provide stratigraphic information, the drill will capture samples in 10 cm “bites”, bringing up 10 cm worth of material at a time to the surface.

### Autonomous Surface Operations

The overall science objective of the mission is to visit specified target sites along a pre-planned path. Due to limited communication windows (4.5 hours every 12 hours based on 50% availability of the orbital communication asset), an Earth-based operations schedule (8 hour shift/5 days per week), and the required traverse distances and science observations, these activities must be executed autonomously and reliably with ground oversight to monitor progress during the shifts, re-adjust the plan, and support fault

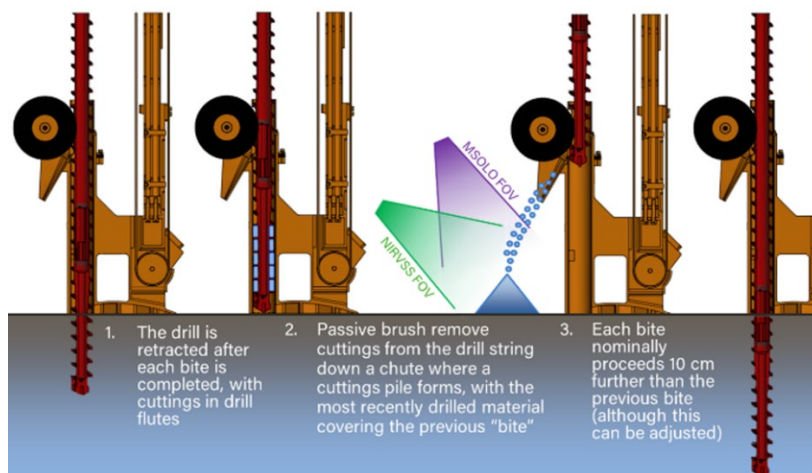


**Figure 3-3. Operation of the TRIDENT Drill.**

handling (for more details, see Table 3-5 and Appendix E, Table E-2). The science and drill operations are described separately in the previous section.

The rover’s sensors, avionics, and software are designed to support onboard autonomous operations with ground oversight. The rover has two redundant stereo camera pairs (Mars 2020 EECAM) mounted on a pan-tilt mast and a second redundant pair mounted on the rear of the rover, making bidirectional driving fully redundant. With a height of 1.5 m above the ground, dust covers for the cameras were deemed unnecessary. All engineering cameras have 90° field-of-view lenses and a ~25-cm baseline to enable bi-directional surface navigation without mast articulation. Short exposures (~10 – 20 ms) allow imaging-while-driving during the lunar daytime (similar to the Perseverance rover). At night, INSPIRE will use high-intensity LED lights to image the terrain frequently while driving. It will stop for longer exposures and multiple panoramic images every 10–15 m in order to reconstruct a 3D model of its environment and plan its next steps. The rover uses an Adcole pyramid-type coarse Sun sensor, a star tracker and redundant heritage LN200 IMUs or equivalent for navigation purposes.

In nominal situations, autonomous operations use vision-based waypoint navigation that respects keep-in and keep-out zones to reach targets of interest. Resources and activities are managed onboard and monitored by the system-health manager (fault protection), which has to detect and identify all faults/failures but only respond to a subset. For off-nominal situations that cannot be handled onboard, operations fall back on ground-in-the-loop control. Table 3-5 summarizes the onboard and ground needed for functions for autonomous operations.

### Command & Data Handling (C&DH)

The INSPIRE rover’s C&DH subsystem consists of three assemblies: a compute element, an instrument interface and a motor controller. All are JPL-designed and have heritage traceable to flight units. A block diagram of the C&DH system is shown in Appendix L (Figure L-1).

The compute element is built around redundant GR740, Quad-core LEON4 processor boards, redundant power supplies and a fault management unit that facilitates timer, sleep functions, and swap-over between the processor boards. Redundant navigation interface boards are connected to the processors to implement the specific interfaces required for the INSPIRE architecture. The redundant instrument interface units are built around the GR712 Dual-core LEON 3 processor and control and collect data from the science instruments. The motor controllers were developed for the Europa Lander and built using the same processing board as the instrument interface. These control the mobility, mast, and HGA. Each motor control board can control three motors, but only one motor at a time, so the current configuration supports ten simultaneous motor operations.

The Flight Software (FSW) for the compute element is direct heritage from JPL’s Psyche FSW product with modifications from the Mars 2020 rover software. The FSW heritage includes not only the flight code, but also the software development and management processes required for a class B flight software deliverable. Over 99% of the inherited flight software is written in the C programming language. The remainder is written in assembly to cover niche areas in SUROM and operating system routines. The basic FSW architectural principles have remained the same for years with successful architectural reuse across MSL, M2020 and Psyche missions.

**Table 3-5. Onboard and ground activities.**

Onboard and Ground Functions	
Onboard Rover	While driving
	Surface navigation (stereo imaging, 3D mapping, hazard assessment (rocks, craters), path planning, path following)
	Dead reckoning pose estimation (visual/inertial/wheel odometry ego-motion estimation)
	While stopped
	Global localization (Sun/Earth sensing, crater detection from rover and registration with orbital imagery)
	Positioning, drilling and retracting the drill
	Analyses of drill cuttings
	Both
	Reliable operations (mean-distance between faults > 6 km)
	System health management (monitoring devices and activities, assessing health, limited diagnosing and response)
Activity and resource planning, scheduling and execution	
Ground	Ops: 24 hours / 7 days a week (first 2 weeks)
	75% coverage and continuous oversight
	Checkouts and shakedown of remaining bugs
	Rapid fault response (min 1-hour turn around)
	Ops: 8 hour shift / 5 days per week (remaining 3 years)
Ground-based monitoring and health assessment	
On-call fault diagnosis and response	

The FSW for the motor controller and instrument interface units is built from the F<sup>7</sup> (F Prime) programming language developed at JPL to facilitate software development for embedded applications. A C++ framework for basic features such as message queues, threading and OS abstraction, and an evolving collection of generic components for commands, memory management and event logging are supported by a suite of tools for testing. F<sup>7</sup> is deployed in Mars Helicopter, Lunar Flashlight and Near-Earth Asteroid Scout and has flown on the ASTERIA CubeSat.

## Telecom

For INSPIRE, direct communication with Earth will not be possible for most of the mission. For this reason, a relay satellite will be used to meet the mission's telecommunications requirements. The Lunar Communications Pathfinder relay network by Surrey Satellite Technology Limited (SSTL), a UK commercial company with ties to the European Space Agency (ESA), has been baselined as the relay service provider. The trade that resulted in this choice is detailed in Appendix I. Pathfinder is on track to be the first spacecraft in orbit around the Moon to commercially offer communication services to lunar assets starting in 2024. Analyses of relay visibility, coverage statistics and link throughput indicate that Pathfinder can support the requirements of the mission, as detailed in Appendix I. The rover telecommunications subsystem supports all mission uplink and downlink requirements using S-band frequencies and components. A 75-cm directional antenna with tracking capability and 22.5 dBi gain combined with a 5 W power amplifier supports the 2 Mbps data rate of Pathfinder with 3 dB margin; it also supports a commanding (receive) rate of 128 kbps with 3-dB margin. A JPL product, the UST-Lite radio, is chosen to support the required data rates. This radio is a lighter variant of JPL-built UST transponder. One version of UST, a Ka-band modulator called KaM, is slated to fly on the NISAR Earth Orbiting mission in 2022, and, currently, the KaM flight units are being integrated into the spacecraft. UST-Lite is presently under development at JPL with a mass of 1 kg and 14 W power consumption when engaged in simultaneous reception and transmission. For emergencies and safe mode, a low-gain 3-dBi antenna supports a transmit data rate of 128 bps, and a commanding rate of 22 kbps. This low-gain antenna does not need to track the relay. The radio protocol for communicating with the relay is a CCSDS standard known as Proximity-1. This standard will allow the radio to communicate with other relay systems as they become available. It is expected that, by the time of the launch of the mission, additional lunar relay satellites will be available to provide a backup to Pathfinder. For the sake of redundancy, two radios and two 5 W SSPAs are provided.

## Power

The Mod-1 Next Gen RTG coupled with a 100 A-hr Li-Ion battery provides sufficient power for all operating modes at end of mission per Table 3-3. The battery is sized to support modes requiring more instantaneous power than the RTG can provide (e.g. drilling) while maintaining a DoD of <60%. The design includes three power control modules to support the ~245 W capability at beginning of life (BOL) as well as providing the battery charge/discharge control interface.

Power electronics are based on a SmallSat avionics architecture currently in development at JPL. This includes RTG power control functionality as well as power distribution for loads and pyro events. This distribution functionality has a fault tolerant control interface to C&DH. Further, switches can be placed in parallel to mitigate stuck open faults, or in series to mitigate stuck on faults.

## Thermal

The INSPIRE thermal design is driven by two primary requirements: 1) maintain a high degree of operability while in PSRs and also while exposed to the Sun at latitudes as low as 85° with rover tilts up to 15°; and 2) limit imposed lunar surface heat fluxes to <6 W/m<sup>2</sup> while in PSRs to preclude volatile sublimation in the sample area. The limit of 6 W/m<sup>2</sup> is based on a simple instantaneous temperature calculation of the power required to raise a 50 K surface above 112 K, the stability temperature of water ice (Figure 1-1). Note that a high degree of operability is defined as minimal flight rules that would otherwise restrict rover orientations and drive paths due to thermal considerations as well as minimal warm-up delays for actuator turn-on, both of which could consume considerable time and/or energy that adversely impacts overall science data gathering capability. The surface heat flux limit is significant to the thermal control of the Mod-1 RTG, which outputs up to 3600 W<sub>th</sub> of waste heat.



The required shielding around the RTG works against the need to maintain the RTG fin root temperature to below its maximum allowable of 260 °C.

To satisfy these requirements, INSPIRE employs a “hot-blooded” rover design where a pumped fluid loop is able to exploit the abundance of waste heat from the RTG to maintain a hot-biased thermal design that is relatively insensitive to warm electronics box (WEB) heat leaks, maintains actuators at minimum turn-on temperatures, and actively removes heat from the RTG to allow adequate shielding to meet the surface heat flux requirement that would otherwise cause too much radiative blockage to maintain fin root temperatures.

A two-phase pumped fluid loop is utilized with water as the working fluid. Saturation temperatures are set at 100 °C which limits system pressures to about 1 atm. The high latent heat capacity of water allows flow rates as low as 20 mL/min (< 1 W pumping power assuming 2% mechanical efficiency) while reclaiming up to 700 W<sub>th</sub> off of the RTG. The high-quality heat at 100 °C enables passive heat conduction across joints to maintain minimum actuator temperatures of > -55 °C without the need for fluid slip rings. The internal WEB temperatures are maintained with minimal fluid tube exposure within it for adequate warming via radiation. WEB temperatures are regulated by a passive system using heat switches attached to the radiator via flexible thermal straps. A detailed description including block diagrams of the active and passive thermal control systems is provided in Appendix J.

## Structures

The structure configuration employs a lightweight approach using a combination of carbon fiber composite struts, aluminum brackets, and aluminum honeycomb panels. These materials are compatible with all radiation and thermal conditions during the traverse. Details of structural design and rover configuration are presented in Appendix L.

The rover incorporates a honeycomb chassis, as well as metal fixtures using aluminum metal sheet bending techniques for instruments and cameras. The chassis provides mechanical attachments as well as space for the thermal system and attachment points for interface with the lander. The rocker system is made of large-diameter hollowed composite rods and metal fittings. The rest of the rocker mechanisms, as well as the attachment to the chassis are made of machined aluminum parts. The radiator is mounted on top of the chassis and all electronics are placed on a horizontal plate accessible from the bottom to facilitate integration and thermal performance.

## 3.3 CONCEPT OF OPERATIONS AND MISSION DESIGN

The INSPIRE mission explores the history of lunar volatiles by traversing through multiple PSRs and sunlit areas of interest near the lunar South Pole. The mission will explore the horizontal and vertical extent of volatiles by taking measurements of the exosphere, surface, and sub-surface. To accomplish its mission, the rover will traverse a nominal 756-km (1,140 km estimated actual distance) over the course of three years, including one year of margin.

The INSPIRE concept of operations can be divided into four phases: (1) Launch, Cruise, and Landing; (2) Checkout; (3) Traverse, and (4) Science Stations as shown in Figure 3-4. After landing on the Moon and completing checkout of all subsystems and instruments, the bulk of the mission involves traversing between Science Stations and performing detailed measurements and drilling at each Science Station.

### Launch, Cruise, and Landing Phase

In the Launch, Cruise, and Landing Phase, the rover launches from Earth, cruises to the Moon, and lands on the lunar surface while attached to a CLPS (Commercial Lunar Payload Services) lander. The rover is in an idle state during this phase while all critical functions are performed by the CLPS lander.

### Checkout Phase

In the Checkout phase, the rover checks out its systems after landing. Instruments are checked out, launch

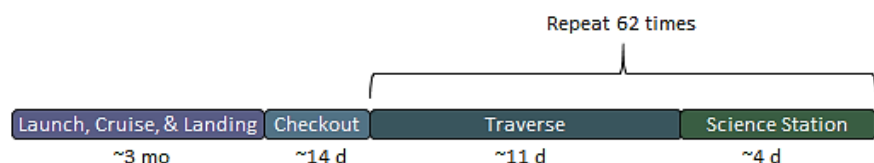
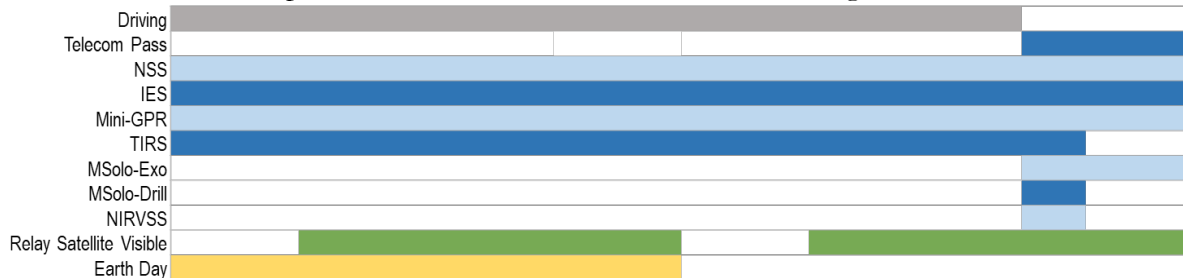


Figure 3-4. The INSPIRE mission phases and durations.

locks are released, and the rover disembarks from the CLPS lander onto the lunar surface.

### Traverse Phase

In the Traverse phase, the rover drives across the south polar terrain towards its next Science Station while collecting science data along a pre-planned path. The Traverse phase follows a 24-hr cadence in which the rover drives for 20-hrs while collecting science data and then stops for 4-hrs to take additional science measurements and communicate through the relay satellite. This cadence enables frequent communication with Earth while avoiding excessive cycling of instrument filaments and time lost to instrument warmup. An overview of the cadence is shown in Figure 3-5.



**Figure 3-5.** Operations timeline for the 24-hr Traverse Phase cycle.

For the first 20-hrs out of the 24-hr cycle, the rover drives across the lunar surface with NSS, IES, Mini-GPR, and TIRS taking continuous measurements. The rover stops every 300-m for 10-min to perform localization imaging. If the rover is driving during lunar night or through a PSR, then it also stops every 10-m for 1-min to perform navigation imaging. The rover’s headlights provide momentary illumination when nighttime or PSR imaging is needed. The maximum speed of the rover is limited to 10-cm/sec to provide an adequate SNR for the NSS. For the next 1.5-hrs, the rover turns on both MSolo instruments and NIRVSS (NSS, IES, Mini-GPR, and TIRS remain on) and communicates through the relay satellite. Finally, for the last 2.5-hrs out of the 24-hr cycle, the rover turns off MSolo- drill, NIRVSS, and TIRS, leaving the other instruments on, while continuing to communicate through the relay satellite. The data volume collected by each instrument over the 24-cycle is shown in Table 3-6. The rover covers ground at an average rate of 230 m/hr over this 24-hr cycle when in sunlight. Driving at night and in PSRs is slower due to the frequent navigation stops with the rover covering ground at an average rate of 157 m/hr.

**Table 3-6.** INSPIRE Traverse phase observations.

Instrument	Data Collected
NIRVSS	783 Mbit (stationary)
NSS	61 Mbit (moving) 12 Mbit (stationary)
MSolo-exo	432 Mbit (stationary)
MSolo-drill	162 Mbit (stationary)
IES	288 Mbit (moving) 58 Mbit (stationary)
Mini-GPR	1800 Mbit (moving) 360 Mbit (stationary)
TIRS	864 Mbit (moving) 65 Mbit (stationary)

### Traverse Plan

The INSPIRE traverse enables interrogation of terrain that broadly addresses the stated science objectives and enables targeted measurements at predetermined Science Stations to more deeply address the science hypotheses while remaining within the traverse capability of the rover. The traverse was planned using LOLA 5- and 10-m DEMs. LRO NAC DEMs of higher resolution were also constructed for some portions of the traverse in order to verify that the path based on the 5- and 10-m DEMs remained valid at higher spatial resolution (2 - 4-m). Details on traverse planning can be found in Appendix K.

The traverse path enables collection of key data along the path itself and visits pre-planned Science Stations that enable more targeted data collection. The Science Stations were chosen based on the criteria described in Table 1-1. The only location constraints on the traverse path are the Science Station locations. The path between the Science Stations is relatively flexible since the science conducted between Station is gained by traversing broad regions and the Stations themselves are hundreds of meters across. The rover’s onboard autonomy and the Operations Team will work together to identify the optimal path between Science Stations. INSPIRE carries ~50% margin on its mission duration in order to account for unforeseen hazards that may cause replanning of the traverse.

## Science Station Phase

In the Science Station phase, the rover performs a detailed investigation of a region of scientific interest. There are three types of Science Stations: Normal, Super, and Lite. Over the course of the mission, the rover performs 60 Normal Science Stations, 1 Super Science Station, and 1 Lite Science Station. Locations of the Normal, Lite, and Super Science Stations are pre-identified, with Stations located both inside and outside of PSRs. The rover also has the capability for an additional 36 Opportunistic Drill Sites that can be inserted into the mission plan based on the data that the rover collects while on the Moon (See Appendix B.1.2 for the Opportunistic Drill Site selection criteria). Opportunistic Drill Sites can be located within pre-defined Science Stations or along the traverse path.

Upon arriving at the location of a Normal Science Station, the rover turns on all of its instruments except the Science Camera and maps the 300 m × 300 m Science Station in a raster pattern that covers 10% of its area. This degree of coverage has been shown via Monte Carlo modeling to provide sufficient coverage to robustly determine the lateral and vertical distribution of volatiles [120]. Ten percent areal coverage is baselined assuming a 1 m swath width of NSS measurements and results in a 3.5 km traverse. After the collected data are downlinked, the Science Team uses these data to select the optimal drill location (see Appendix B for drill site selection drivers). The rover drives to the drill site and performs a drilling activity with all instruments on, except the Science Camera. Drilling is performed while in real-time communication to permit expeditious resolution of any anomalies. Figure 3-6 shows a timeline of operations during a Normal Science Station.

The Super and Lite Science Stations are located at the impact sites of the LCROSS Centaur and LCROSS Shepherding Spacecraft respectively. Super Science Station operations are the same as those for a Normal Science Station except that the rover performs drilling in two locations on opposite sides of the Centaur impact crater. The second drilling activity is only 12 hrs long as a subsurface temperature measurement is only collected by TRIDENT at the first drill site. Lite Science Station operations are the same as Super Science Station operations except that the Science Station area is smaller due to the smaller impact crater created by the Shepherding Spacecraft and so the rover only needs to drive ~250 m to characterize the Station and identify the best location for both drill sites, nominally on opposite sides of the impact crater.

### Drill Operations

The TRIDENT drill follows a repeating pattern of operations in order to drill 2-m into the lunar subsurface. First, the rover locks its wheels and NIRVSS acquires imaging of the drill site. The drill is then deployed and preloaded against the lunar surface and a set of initial measurements are obtained. NIRVSS acquires additional images of the location where the drill cuttings pile will be located on the lunar surface. NIRVSS and MSolo-drill acquire background volatile measurements. Both MSolo-drill and NIRVSS are mounted on the rover underside such that both instruments' fields of view are focused on the location of the cuttings pile produced by either drill system (see Figure 1-5). TRIDENT then initiates drilling with a first cut of 10 cm into the surface. The drill is then retracted from the drill hole and material is brushed from the drill's auger onto the lunar surface. Measurements of the cuttings (subsurface samples) are collected by MSolo-drill and NIRVSS and then the drill is placed back in the drill hole. The cycle of drilling 10-cm into the subsurface, bringing the collected material to the surface, and taking measurements is repeated until the drill has reached the required depth. At most drill sites,

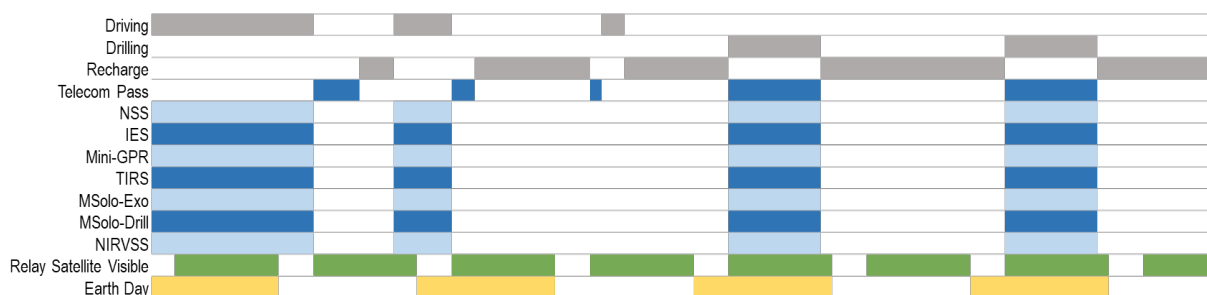


Figure 3-6. Ops timeline during a Normal Science Station. Other types of Science Stations follow a similar cadence.



after completing drilling, the drill is left in the hole for ~3-hrs in order to measure the temperature and thermal conductivity of the subsurface with its integrated heater and RTDs. The subsurface thermal measurements complement the surface temperature measurements from TIRS and are used to understand the observed volatile sequestration which is primarily governed by temperature (Figure 1-1). After thermal measurements are complete, the drill is removed from the drill hole and final images of the hole are collected by NIRVSS.

### Telecom Strategy

Communication with the rover occurs only through a relay satellite orbiting the Moon. Uplink and downlink strategies differ from phase to phase, depending on the goals of each phase. The telecom strategy assumes an average duration of visibility between the rover and the relay satellite of 9 hours and an average of 2 visibility periods per Earth day but an availability of 50% post the Checkout Phase as this may not be the only asset being serviced (see Appendix I for more information).

During the Launch, Cruise, and Landing phase, communications occur through the CLPS lander. During the Checkout phase, communications initially occur through the CLPS lander until reliable communication between the rover and the relay satellite can be established. Communication windows while attached to the CLPS lander are set by the CLPS provider. Once the rover separates from the lander, it communicates with Earth whenever the relay satellite is visible for the remainder of the Checkout phase. The CLPS lander is assumed to not need significant communications through the relay satellite after the rover has been successfully delivered to the Moon’s surface.

During the Traverse phase, the rover communicates with Earth through the relay satellite for 4-hrs each Earth day. This contact duration provides >300% margin over the daily data volume that is collected during the Traverse phase.

During the Science Station phase, communication is performed frequently in order to maximize the time that the operations teams have to make decisions about where to drill and how to resolve anomalies. Up to 6 hrs of downlink via the relay satellite each Earth day provides >100% margin on the data that is collected during a Science Station. Drilling is performed in real-time and so all drill operations are designed to be performed in ≤8-hr segments to ensure that the relay satellite is always in view of the rover when drilling.

### Operations Strategy

Rover operations are commanded from JPL with co-located Science and Engineering Teams. A nominal plan is up-linked to the rover that contains the science and engineering activities. The rover can autonomously alter its path and its operations to avoid obstacles or take advantage of benign terrain. Telemetry is continuously recorded and stored onboard the rover until the next downlink opportunity. Anomalies are handled hierarchically: onboard the rover if possible and only through ground intervention when necessary. Rapid response to faults is enabled by on-call personnel on the ground who can rapidly evaluate the rover’s state and restore nominal operations quickly using real-time interactions. Some challenging terrains may require the operations team to take over control of the rover. Because the rover can be interrogated and controlled in near real-time as long as the relay link is available, the expectation is that the rover would be able to traverse more difficult terrain relatively quickly as compared to Mars rovers .

**Table 3-7.** INSPIRE communication between the rover and the Relay Satellite during surface mission phases. Communication periods during the Launch, Cruise, and Landing phase are determined by the CLPS provider.

Downlink Information	Checkout	Traverse	Science Station
Number of Contacts per Week	14	7	~5
Downlink Contact Duration, hr	9	4	~8
Number of Weeks for Mission Phase, weeks	2	~56	~46
Downlink Frequency Band	S		
Telemetry Data Rate(s), kbps	HGA: 2000, LGA: 22		
Total Daily Data Volume, (MB/day)	165	632	1595
Uplink Information	Checkout	Traverse	Science Station
Number of Uplinks per Day	2	1	~1
Uplink Contact Duration, hr	9	4	~8
Uplink Frequency Band	S		
Telecommand Data Rate(s), kbps	HGA: 128, LGA: 1.2		

The Science and Engineering Teams operate largely in parallel with the Science Team establishing long term goals and traverse paths while the engineering team focuses on monitoring the rover’s progress. The two teams work together during real-time operations such as driving through challenging terrain or drilling in order to make sure that rover remains safe and healthy and accomplishes its science goals. The ~12-hr orbital period of the relay satellite enables communications passes to be scheduled on a daily basis at times that are convenient to the operations teams. Operations in the vicinity of the CLPS lander are closely coordinated with the CLPS provider in order to ensure the safety of both vehicles. Uplink and downlink telecom characteristics are summarized in Table 3-7.

### 3.4 RISK LIST

The INSPIRE concept takes a conservative approach to engineering, mission planning and operations, informed by experience from past lunar and Mars missions. New technology is limited and the operating environment and traverse is well defined. Significant risks identified by the team are shown in Table 3-8.

**Table 3-8.** INSPIRE’s adoption of existing technologies and proven instrument designs facilitates a high-performance mission with manageable risks.

Risk	C*	L*	Mitigation
Mod-1 Next Gen RTG not available in time for launch	3	2	Design could use Mod-0 Next Gen RTG or DRPS, if available, with minimal impact to mission Design could be adapted to use MMRTG with significant impact to mission duration required to meet baseline science objectives Mission opportunity is not time-critical and could accommodate some slip in Next Gen schedule
Accommodation of lunar dust environment requires additional qualification and design changes to ensure reliable operation for the span of the mission	3	2	Seal all exposed joints: Use three-stage seal derived from Mars rovers. Raise sensitive surfaces and instruments: all unprotected sensitive surfaces such as optical/thermal surfaces are mounted higher than the wheels to mitigate the effect of dust and debris. Place instruments at least 60 cm above regolith. Perform testing of drilling system with variety of regolith simulants to characterize dust migration Account for dust in performance analysis and design: all thermal analyses assume a mono-layer of dust at all times
Reliability of autonomous operations cannot be made sufficiently high during lunar day and night to ensure execution of mission within allotted time	2	2	Mature and integrate all required autonomous capabilities in unison on a prototype rover with same mobility, drilling, sensors, and avionics leveraging flight-relevant components (h/w and s/w) Develop high-fidelity simulation models of night/PSR driving informed by data from VIPER night/PSR operations for situational awareness, navigation, localization and instrument placements. Conduct extensive field-testing complemented with a validated simulation to collect adequate statistics for characterizing the long-distance traverse, manipulation, and system-level performance. Adjust the plan and functions that have to occur autonomously onboard vs. with ground assistance and plan for increased ground engagement for functions that have lowest autonomous reliable performance. Include significant margin and flexibility in the mission plan to allow for anomaly resolution in operations
Rover encounters lunar terrain with unexpected trafficability features	2	2	Rover mobility test plan will encompass worst case terrain types Mobility system designed with multiple ways to detect mobility problems and back out of hazardous areas Timeline includes margin for alternate route planning should hazardous terrains be encountered on planned path
Drilling system gets stuck or experiences unforeseen wear	3	2	Drill design rated for minimum 200 m total drilling in lunar environment providing 36% margin over minimum science requirement of 64 two-meter holes Fully redundant drill systems are included in the design Rover design incorporates ability to jettison either drill in event of unrecoverable failure

\* C=Consequences; L=Likelihood, in accordance with the NASA 5x5 Table. Consequence and Likelihood criteria defined per SOMA Cost Threat Matrix (ref. Discovery 2014 Transition Briefing, 3/3/2017). Consequence criteria (C): cost impact to complete Phases A-D: 1=Very Minimal (<\$10M). 2=Minimal (\$10-20M). 3=Limited (\$20-40M). 4=Moderate (\$40-80M). 5=Significant (\$80-\$120M). 6=Very Significant (>\$120M). Likelihood criteria (L): % probability of occurrence; 1=Unlikely (<10%). 2=Possible (10-30%). 3=Likely (30-60%). 4=Very Likely (60-75%). 5=Almost Certain (>75%).

## 4 DEVELOPMENT SCHEDULE AND SCHEDULE CONSTRAINTS

### 4.1 HIGH-LEVEL MISSION SCHEDULE

Figure 4-1 presents a feasible full mission schedule for INSPIRE. The mission complexity falls in the range of a New Frontiers-class development. The reference schedules used for this study were derived from the JPL mission schedule database, informed by recent rover developments, past sample return

mission concepts, and the unique schedule features associated with the use of radioisotope power systems.

The INSPIRE mission has a direct analog to rover-specific aspects of MER/MSL/2020. Overall mission architecture is simplified through use of the CLPS provider for cruise and landing. The mobility range for INSPIRE is significantly beyond that of previous rover missions, and that is reflected

in the number of field tests and component life tests planned to begin early in the development cycle.

The INSPIRE mission has a direct analog to rover-specific aspects of MER/MSL/2020. Overall mission architecture is simplified through use of the CLPS provider for cruise and landing. The mobility range for INSPIRE is significantly beyond that of previous rover missions, and that is reflected in the number of field tests and component life tests planned to begin early in the development cycle.

No major schedule drivers or long-lead items need to be addressed beyond the proposed schedule. Table 4-1 provides key phase durations for the project. Since the mission is targeted as a New Frontiers competed mission, all instruments and instrument providers are selected during proposal preparation and the schedule need not accommodate a competitive Instrument AO.

**Table 4-1. Key Phase Duration Table.**

Project Phase	Duration (Months)
Phase A – Conceptual Design	14
Phase B – Preliminary Design	15
Phase C – Detailed Design	22
Phase D – Integration & Test	23
Phase E – Primary Mission Operations	38
Phase F – Extended Mission Operations	6
Start of Phase B to PDR	8
Start of Phase B to CDR	23
Start of Phase B to Delivery of Instrument #1-7	37
Start of Phase B to Delivery of Flight Element #1	54
System Level Integration & Test	17
Project Total Funded Schedule Reserve	6 (120 days)
Total Development Time Phase B - D	61

## 4.2 TECHNOLOGY DEVELOPMENT PLAN

As identified in §2, several technologies need to be matured to higher technology readiness levels, one of which is reliable integrated autonomous rover operations.

Autonomous surface operations leverage several Mars-heritage autonomous functions but need to Inspire Plan (B/C/D 61 mo)

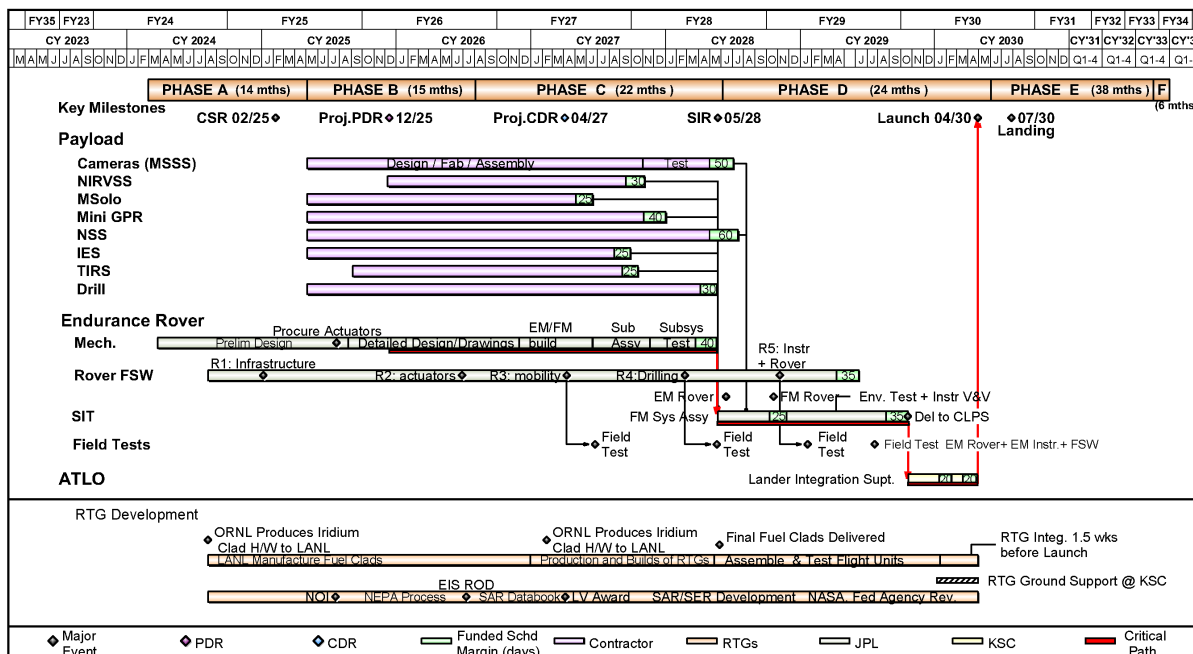


**Figure 4-1. Notional High-Level Schedule Assuming a 2030 Launch.**



provide integrated perception, navigation, global localization, and system management for long distances with high reliability, especially when there is little or no natural illumination. Such operations could fall during the lunar day or night and may not coincide with the ground operations schedule nor the available communication link, which drives the need for autonomy. System management includes onboard activity planning and resource/health management, relying only on the strategic science plan but without daily tactical planning, as neither ground-operations schedule nor mission timeline allow for a daily ground-based tactical planning cycle. However, the 62 science stops are planned to frequently engage ground operators, which include drill site selection, incremental drilling operations, and handling drilling contingencies.

The autonomous surface operations needs to provide this integrated functionality at a higher reliability than the Mars rovers whose activities are planned every sol (Martian day). The performance metric needed for INSPIRE to complete its mission is a combination of mean-distance-between-faults and fault-recovery response time. With an intermittent communication link and accounting for an Earth-based operations schedule, a preliminary model incorporating fault frequency and recovery times provide insight into the reliability performance metrics needed for this mission. Parametric data for this model was based on fault rates and response times of prior Mars missions adjusted for the cadence of lunar communication. A Monte-Carlo statistical analysis indicated that for minor faults, INSPIRE needs a mean distance-between-faults of  $> 6$  km with an average response time of 3 hours (a conservative estimate for the expected lunar communication scenario, albeit, at times, at lower rate) and for major faults a mean distance-between-faults of 16 km with an average response time of 7 hours (see more details in Appendix F, Autonomy Reliability). This level of reliability for autonomous operations would allow INSPIRE to complete its baseline science in a manner consistent with the current concept of operations and within the planned two-year period, leaving one year of unallocated margin. The baseline current plan within the two-year period includes a percentage of ground-in-the-loop driving for the most challenging terrain with up to 25% of ground-in-the-loop driving at a rate similar to VIPER of 1 cm/s for the highest slopes of  $15^{\circ}$ – $16^{\circ}$ .

Ground-operation tools, matured for Mars rovers, are expected to have the needed functionality to support the rapid response. The plan is to adapt and integrate flight-matured autonomous functions that include surface navigation (Mars 2020: 3D perception, hazard assessment, motion planning, visual/wheel/inertial odometry), and activity/resource planning (Mars 2020), with system health management and global localization into an autonomous system and deploy it in simulation and on a prototype rover with relevant sensing, mobility, controls, and compute avionics. Night driving would be critical for the INSPIRE mission as more than 70% of the total distance would be driven at night on in PSR since 50% of the planned route is currently in PSRs. Unlike Intrepid's limited night driving (1–2 km per lunar night), INSPIRE is covering a total of 650 km at night or in PSRs. Both day and night driving require frequent (every  $\sim 300$  m) global localization to keep the rover on the planned route. Initial maturation of the integrated autonomy capabilities for long-duration, long-distance, night driving and fault recovery can be demonstrated in simulation (*e.g.*, the Mars 2020 rover simulation used for autonomous navigation) as well as on existing rover prototypes. To validate the required INSPIRE performance, a combination of flight-relevant rover prototype and validated high-fidelity INSPIRE simulation would be necessary. The use of the relevant prototype in relevant environments to validate the simulation is similar to the approach adopted by the Mars 2020 mission for entry, descent and landing and for autonomous rover traverse. Table 4-2 provides a development plan for a focused technology program, which is similar to the multi-year programs that preceded MER, MSL and Mars 2020. Trends to reduce mean-distance-between-faults have been well-documented for the autonomous vehicle industry [121], which similarly, complemented on-road testing on relevant hardware with high-fidelity simulations.

The mini-GPR design relies on well understood technology but will use new versions of components from existing product lines. As the current TRL is at 4, the mini-GPR instrument would have to be fabricated and flight qualified for operations on the Moon. This will include design and qualification of the instrument electronics, packaging, antenna, and electrical interface design and software development. This process is expected to take 3 years. NASA has instrument development programs

**Table 4-2. Technology Development Plan.**

Justification (completed activities)	Maturation Plan (work to go)	Duration	ROM Cost
<b>Reliable Integrated Autonomous Operations</b>			
INSPIRE needs integrated and reliable autonomous operations for traverse, localization, and system management.  Preliminary models long-traverse indicate that Intrepid requires the following mean-distance-between-faults (MDBF) with fault-recovery response time (RT): MDBF > 6 km w/ Ave RT < 3 hours MDBF > 16 km w/ Ave RT < 7 hours (see Appendix F, Autonomy Reliability)	<b>Phase I: Pre-Phase A (FY21–24) (feasibility assessment)</b> <b>Integrated autonomy framework:</b> set up framework for integration of all functions <b>Function adaptation:</b> adapt/update Perseverance rover autonomy functions (surface navigation (perception, hazard assessment, pose estimation, path planning, mobility), thermal, power and comm modeling, activity planning, and system health into framework that enables the rover to execute without ground ops the full cycle of driving, localization, comm, science measurements, and resumption of driving <b>Night navigation:</b> develop from TRL 3 to 6 Investigate further trades for night perception (LIDAR vs. stereo), assess quality of night stereo (near-range and mid-range) for short and long exposures; for stationary and for imaging while driving; assess hazards based on night perception. Develop capability, mature, and test <b>Fallback:</b> reduce percent of night driving to available ground-in-the-loop rates and extend mission duration (60% rate of night driving would use up all the margin but fit within 3 years).	<b>4 years</b> 2 years 3 years  3 years	<b>\$7.0 M</b> \$2.0 M \$2.0 M  \$1.5M
	<b>Day global localization:</b> develop from TRL 3 to 6; funded by NASA STMD GCD ('21–24); <b>Fallback:</b> use ground-based localization techniques used in current Mars missions every 2.5 km.	3 years 2 years	Funded \$1M
	<b>Night global localization:</b> investigate trades for optical, radiometric, and hybrid techniques for global localization. Develop capability, mature, and test <b>Fallback:</b> use ground-based localization techniques used in current Mars missions every 10 km.	1 year <b>4 years</b>	\$0.5 M <b>\$8.6 M</b>
	<b>Demonstration:</b> demonstrate integrated functions in existing simulation or on existing rover prototype <b>Phase II: Pre-Phase A (FY23–FY26) (reliability assessment)</b> <b>Rover prototype:</b> develop prototype rover with similar mechanical configuration, sensing, and avionics (compute elements, camera interface and motor controls).	3 years  1 year	\$3.5 M  \$0.8 M
	<b>SW Bench top:</b> set up equivalent bench top system for software/autonomy development <b>Simulation:</b> increase fidelity of simulation and validate against field campaigns <b>MOS/GDS:</b> mature MOS/GDS tools to support rapid anomaly identification and resolution	3 years 2 years 2 years	\$2.3 M \$1.0 M \$1.0 M
	<b>Validation campaigns:</b> conduct 10s of km of autonomous full-cycle driving and science ops to collect statistics to mature integrated capabilities and validate simulation; fully characterize reliability; inform hw changes in time <b>Fallback:</b> extend mission duration to accommodate the achievable reliability performance metrics	2 years	\$1.0 M

(e.g. PICASSO and MatISSE) that can be exercised for the flight qualification for TRL 6. We also propose a phase A activity for any residual activities to get to TRL 6 prior to PDR.

### 4.3 DEVELOPMENT SCHEDULE AND CONSTRAINTS

The development schedule including Phases C and D is shown in Figure 4-1. The schedule represents a relatively straightforward completion of design and transition to integration and test (I&T) through launch operations for a rover of this type. Instrument development is complete for all instruments prior to start of Phase D. The critical path runs through the rover mechanical system, which is necessary to begin I&T. Rover field tests to validate mobility and autonomy continue throughout these phases and feed into FSW builds. The RTG development line is representative of the typical activities associated with an MMRTG mission and may need to be revisited should there be any changes associated with use of the NextGen RTG.

Note that the schedule is tied to a launch date in April of 2030, representing an early opportunity for execution of this mission given the timing of advanced RPS development. It should be noted that the INSPIRE mission schedule is flexible and can be adapted to any CLPS payload opportunity in this timeframe.

## 5 MISSION LIFE-CYCLE COST

### 5.1 COSTING METHODOLOGY AND BASIS OF ESTIMATE

INSPIRE developed its cost estimate using JPL’s cost estimation process for early formulation. The INSPIRE team initiates this process by describing the project in a technical data package (TDP) containing the science requirements, technical design, instrument design, and project schedule. An initial estimate is generated using JPL Institutional Cost Models (ICM) in a focused Team X session that allows the INSPIRE team to perform subsequent design-to-cost trades.

This study of the INSPIRE mission generated a cost estimate for a lunar rover that will explore the shadowed regions of the Moon and perform occasional drilling operations to examine sub-surface materials. The JPL Team X has estimated the lifecycle cost for the INSPIRE concept to be \$1,542M FY25, as detailed in Table 5-1. The estimate is organized by NASA’s standard Work Breakdown Structure (WBS).

Team X estimates are generally model-based, and generated from a series of instrument and mission-level studies. The costs presented in this report are ROM estimates and do not constitute an implementation or cost commitment. It is possible that each estimate could range from as much as 20% higher to 10% lower. The costs presented are based on Pre-Phase A design information, which is subject to change.

The payload elements were estimated using the NICM System Tool for in situ instruments which relies on mass and power. The rover was estimated assuming an in-house build.

Flight software was assessed based on analogy to the MSL and Mars2020 rover missions. One key difference and a significant cost driver is that the INSPIRE rover will require a high degree of autonomy to drive day and night for long distances without ground in the loop.

The RTG is based on the NextGen Mod 1 RTG. The \$70M cost is derived from the “Groundrules For Mission Concept Studies in Support of Planetary Decadal Survey”, Appendix A, Nov. 2019.

Planetary Protection was assumed for this mission and is accounted for under WBS 02.

As required by NASA for this study, Reserves were applied at 50% for Phase A-D development (excluding LV) and 25% for Phase E operations (excluding tracking costs).

The LV value of \$200M is based on the expected delivery cost for a medium class CLPS lander as estimated by the NASA CLPS Program Office. Cost includes delivery to the lunar surface at the targeted landing site.

As another step to validate these costs, JPL’s business organization evaluated the INSPIRE mission using parametric models supplemented with analogies and wrap factors based on historical data. The cost model used include SEER and TruePlanning for Phase B-D, and SOCM for Phase E. Launch system and Phase E tracking costs were a passthrough from the Team X estimate. Phase A costs were assumed to be \$5M based on the value of the Phase A cost from a pre-release draft of the NF 5 AO. The details for each of the cost model estimates is provided in Appendix M.

Table 5-1 shows the mission cost breakdown for the JPL Team X cost estimate, as well as the average from the cost model estimates. The bottom line total

**Table 5-1. JPL Team X and cost model estimates for INSPIRE (FY25\$M).**

WBS Element	Team X	Cost Models
<b>Phase A-D Development Cost</b>		
Phase A Concept Study	Incl. below	5.0
01/02/03 PM/PSE/SMA	89.4	91.8
04 Science	37.9	19.0
05 Payload	84.3	94.9
06 Flight System	475.9	442.4
07 Mission Ops System	32.6	26.2
09 Ground Data System	33.4	27.4
10 Project System I&T	41.3	59.3
<b>Total Dev. w/o Reserves</b>	<b>794.7</b>	<b>766.0</b>
Development Reserves (50%)	362.4	348.0
<b>Total A-D Development Cost</b>	<b>1,157.1</b>	<b>1,114.0</b>
<b>Phase E-F Operations Cost</b>		
01/02 PM/PSE	5.3	1.8
04 Science	63.3	67.3
07 Mission Ops System	53.3	55.3
09 Ground Data System	27.3	22.7
<b>Total Ops w/o Reserves</b>	<b>149.1</b>	<b>147.1</b>
Operations Reserves (25%)	35.6	35.1
<b>Total E-F Operations Cost</b>	<b>184.8</b>	<b>182.2</b>
08 Launch System	200.0	200.0
<b>Total Cost</b>	<b>1,541.9</b>	<b>1,496.2</b>



costs for Team X and the cost models differ by 3% (see Appendix M). The flight system cost (WBS 06) shows the greatest numeric difference between the two estimates (\$33M) with the cost model being lower. One factor that contributes to this difference is the flight software. SEER and TruePlanning can model software based on lines of code. Since this information was not available in Pre-Phase A, a factor was applied to the hardware costs based on a historical average. Because of INSPIRE’s requirement for autonomous driving, this is not well represented by historical data and is possibly underestimated in the cost model results.

WBS 10 has a large percentage difference (44%) with the cost model estimate higher than Team X. This is especially observable with the TruePlanning estimate. A possible explanation is that Team X carries the cost for a mechanical integration testbed and the driving tests for the mobility system as part of WBS 06 whereas TruePlanning captures this under WBS 10. Because of this mapping difference, it is better to compare WBS 06 and 10 together, which makes the delta 3%.

## 5.2 COST ESTIMATE

The INSPIRE team has adopted the Team X cost as the more conservative estimate. To create a mission cost funding profile, historical missions were analyzed to define representative profiles by phase. The analogous mission set includes the MER and MSL rovers, and a selection of completed Discover and New Frontiers missions. The normalized percentage spreads were then used to phase the Team X estimate over the duration of 60 months for Phase B-D development and similarly for the 3 year duration for Phase E. The base year profile was then escalated to real year dollars using the JPL Composite Inflation Index.

Table 5-2 shows the total mission cost funding profile for INSPIRE. It reflects a Phase A start date of March 2024 and a launch date of April 2030.

**Table 5-2. Total Mission Cost Funding Profile for INSPIRE. (FY costs<sup>1</sup> in Real Year Dollars, Totals in Real Year and FY25 Dollars)**

Item	FY24	FY25	FY26	FY27	FY28	FY29	FY30	FY31	FY32	FY33	FY34	Total (RY\$M)	Total (FY25\$M)	
<b>Cost</b>														
Phase A Concept Study	2.1	2.9	-	-	-	-	-	-	-	-	-	4.9	5.0	
Technology Development	-	-	-	-	-	-	-	-	-	-	-	-	-	
Phase B-D Development <sup>2</sup>	-	62.3	212.7	269.2	164.9	91.3	37.4	-	-	-	-	837.8	789.7	
Phase B-D Reserves	-	28.6	97.6	123.5	75.7	41.9	17.1	-	-	-	-	384.4	362.4	
Total A-D Development Cost	2.1	93.7	310.3	392.8	240.6	133.2	54.5	-	-	-	-	1,227.2	1,157.1	
Launch services	-	-	34.3	35.2	36.2	37.3	38.3	39.4	-	-	-	220.8	200.0	
Phase E Science	-	-	-	-	-	-	12.4	20.7	21.3	21.9	-	76.3	63.3	
Other Phase E Cost	-	-	-	-	-	-	16.8	28.1	28.9	29.7	-	103.5	85.9	
Phase E Reserves	-	-	-	-	-	-	7.0	11.7	12.0	12.3	-	43.0	35.6	
Total Phase E Cost	-	-	-	-	-	-	36.1	60.4	62.2	64.0	-	222.7	184.8	
Education/Outreach	-	-	-	-	-	-	-	-	-	-	-	-	-	
Other (specify)	-	-	-	-	-	-	-	-	-	-	-	-	-	
<b>Total Cost</b>	<b>2.1</b>	<b>93.7</b>	<b>344.6</b>	<b>428.0</b>	<b>276.8</b>	<b>170.5</b>	<b>128.9</b>	<b>99.9</b>	<b>62.2</b>	<b>64.0</b>	<b>-</b>	<b>1,670.6</b>	<b>1,541.9</b>	
												<b>Total Mission Cost</b>	<b>1,670.6</b>	<b>1,541.9</b>

<sup>1</sup> Costs should include all costs including any fee

<sup>2</sup> MSI&T - Mission System Integration and Test and preparation for operations included

## A ACRONYMS

AAS	American Astronomical Society
ACS	Attitude Control System
AO	Announcement of Opportunity
APL	Applied Physics Lab
ArcGIS	Geographic Information System
ASTERIA	Arcsecond Space Telescope Enabling Research in Astrophysics
AV	Autonomous Vehicle
BIRCHES	Broadband InfraRed Compact High Resolution Exploration Spectrometer
BOL	Beginning of Life
C&DH	Command & Data Handling
C <sub>2</sub> H <sub>6</sub>	Ethane
CA	California
CBE	Current Best Estimate
CCD	Charge-Coupled Device
CCHP	Constant Conductance Heat Pipes
CCSDS	Consultive Committee for Space Data Systems
CDR	Critical Design Review
CFA	Cumulative Fractional Area
CH <sub>3</sub> OH	Methanol
CH <sub>4</sub>	Methane
CLPS	Commercial Lunar Payload Services
CM	Carbonaceous Chondrites
CML	Concept Maturity Level
CMOS	Complementary Metal Oxide Semiconductor
CNI	Comm Navigation and Identification
CO	Carbon Monoxide
CO <sub>2</sub>	Carbon Dioxide
COVE	CubeSat On-board processing Validation Experiment
CPR	Circular Polarization Ratio
CR	Carbonaceous Chondrites (Renazzo)
CTE	Coefficient of Thermal Expansion
D/H	Deuterium Hydrogen
DALI	Development and Advancement of Lunar Instrumentation
DARPA	Defense Advanced Research Projects Agency
dBW	Decibel Watt
DEM	Digital Elevation Map
DoD	Depth of Discharge
DOF	Degrees of Freedom
DRPS	Dynamic Radioisotope Power System
DSN	Deep Space Network
DTE	Direct-to-Earth
DTM	Digital Terrain Map
DVR	Digital Video Recorder

---

ECAM	Electronic Camera
EDL	Entry, Descent, and Land
EE	Electronic Engineering
EECAM	Enhanced Engineering Camera
EIRP	Effective/Equivalent, Isotropically Radiated Power
EM	Electromagnetic
EO-1	Earth Observing-1
EOM	End of Mission
EOS	Earth Observing System
ESA	European Space Agency
FAQ	Frequently Asked Questions
FOV	Field of View
FPGA	Field Programmable Gate Array
FSW	Flight Software
FWHM	Full Width at Half Maximum
FY	Fiscal Year
G/T	Gain-to-Noise Temperature
GDS	Ground Data Systems
GN&C/GNC	Guidance, Navigation, and Control
GPHS	General Purpose Heat Source
GPR	Ground Penetrating Radar
GRAIL	Gravity Recovery and Interior Laboratory
GRC	Glenn Research Center
H <sub>2</sub>	Hydrogen
H <sub>2</sub> O	Water
H <sub>2</sub> S	Hydrogen Sulfide
HGA	High-Gain Antenna
HST	Hubble-Space Telescope
I/F	Interface
I/O	Input/Output
I&T	Integration & Test
ICM	Institutional Cost Models
ICRA	International Conference on Robotics and Automation
IDP	Interplanetary Dust Particles
IEEE	Institute of Electrical and Electronics Engineers
IES	Ion and Electron Sensor/Spectrometer
IM	Intuitive Machines
IMU	Inertial Measurement Unit
INSPIRE	In Situ Solar System Polar Ice Roving Explorer
IR	Infrared
ISRU	In Situ Resource Utilization
JPL	Jet Propulsion Laboratory
KaM	Ka band Modulator
KBO	Kuiper Belt Objects



---

KOZ/KIZ	Keep Out Zone/Keep In Zone
LADEE	Lunar Atmosphere and Dust Environment Explorer
LAMP	Lyman Alpha Mapping Project
LCMS	Lunar CubeSat Mass Spectrometer
LCROSS	Lunar Crater Observation and Sensing Satellite
LED	Light-emitting Diode
LGA	Low-Gain Antenna
LIDAR	Light Detection and Ranging
LOLA	Lunar Orbiter Laser Altimeter
LPSC	Lunar and Planetary Science Conference
LPVR	Lunar Polar Volatile Rover
LRO	Laser Altimeter LOLA
LRV	Lunar Roving Vehicle
LSSM	Local Scientific Survey Module
LV	Launch Vehicle
LW	Long Wave
M2020	Mars 2020
M3	Moon Mineralogy Mapper
MatISSE	Maturation of Instruments for Solar System
MDBF	Mean Distance Between Faults
MEL	Master Equipment List
MER	Mars Exploration Rover
MEV	Maximum Expected Value
MIMU	Miniature Inertial Measurement Unit
Mini-RF	Miniature Radio-Frequency
MLI	Multi-layer Insulation
MMRTG	Multi-Mission Radioisotope Thermoelectric Generator
MOS	Mission Operations System
MOU	Memorandum of Understanding
MPV	Maximum Possible Value
MPV-CBE	Maximum Possible Value Current Best Estimate
MRO	Mars Reconnaissance Orbiter
MSI&T	Mission System Integration and Test
MSL	Mars Science Laboratory
MTBF	Mean Recovery Time Between Faults
MTBF	Mean Time Between Faults
MUX	Multiplexer
N/A	Not Applicable
NAC	Narrow Angle Camera
NASA	National Aeronautics and Space Administration
NEN	Near Earth Network
NH3	Ammonia
NICM	NASA Instrument Cost Model
NIR	Near-Infrared

---

NIRVSS	Near Infrared Volatile Spectrometer System
NISAR	NASA-ISRO Synthetic Aperture Radar mission
NRHO	Near Rectilinear Halo Orbit
NSS	Neutron Spectrometer System
OCC	Oort Cloud Comets
OH	Hydroxide
OH/H <sub>2</sub> O	Hydroxide/Water
OHP	Oscillating Heat Pipe
OS	Operating System
OSIRIS	Origins Spectral Interpretation Resource Identification Security
PBC	Power Block Controller
PCB	Printed Circuit Board
PDR	Preliminary Design Review
PI	Principal Investigator
PICASSO	Planetary Instrument Concepts for the Advancement of Solar System Observations
PM/PSE	Project/Program Manager Project System Engineer
PMCS	Planetary Mission Concept Study
PREFIRE	Polar Radiant Energy in the Far InfraRed Experiment
PRIME-1	Polar Resources Ice Mining Experiment-1
Prox-1	Proximity-1
PRT	Platinum Resistance Thermometers
PSR	Permanently Shadowed Regions
QIT	Quadrupole Ion Trap
QIT-MS	Quadrupole Ion Trap-Mass Spectrometer
RAD	Radiation
RBG	Red, Blue, Green
RF	Radio Frequency
RGB	Red, Green, Blue
RHU	Radioisotope Heater Unit
RIMFAX	Radar Imager for Mars Subsurface Experiment
ROM	Rough Order of Magnitude
RP	Resource Prospector
RPC	Rosetta Plasma Consortium
RPC-IES	Rosetta Plasma Consortium-Ion and Electron Sensor
RPS	Radioisotope Power System
RT	Response Time
RTD	Resistance Temperature Detector
RTG	Radioisotope Thermoelectric Generator
RY	Real Year
S/C	Spacecraft
S <sub>2</sub>	Sulfide
SAR	Synthetic Aperture Radar
SC	Science Cameras
SEER	System Evaluation and Estimate of Resources

---

SEER-H	System Evaluation and Estimate of Resources-Hardware
SELENE	Selenological and Engineering Explorer
SfM	Structure from Motion
SNR	Signal-to-Noise Ratio
SO <sub>2</sub>	Sulfur Dioxide
SOCM	Space Operations Cost Model
SOMA	Science Office for Mission Assessments
SPACE	Space and Astronautics Forum and Exposition
SPIE	Society of Photo-Optical Instrumentation Engineers
SS	Sun Sensor
SSC	Shepherding Spacecraft
SSPA	Solid State RF Power Amplifier
SSR	Seasonally Shadowed Regions
SSTL	Surrey Satellite Technology Limited
STIM	Smart Transducer Interface Module
STM	Science Traceability Matrix
SUROM	Start-Up Read Only Memory
SW	Short Wave
TAGCAMS	Touch and Go Camera System
TBC	To Be Confirmed
TBD	To Be Determined
TBR	To Be Refined
TDP	Technical Data Package
TIRS	Thermal Infrared Spectrometer
TPW	True Polar Wander
TRCTL	Terrain Adaptive Wheel Speed Control
TRIDENT	The Regolith and Ice Drill for Exploring New Terrains
TRL	Technology Readiness Level
TSR	Transiently Shadowed Regions
TVAC	Thermal Vacuum Chamber
UHF	Ultra-High Frequency
UK	United Kingdom
UST	Universal Space Transponder
UV	Ultraviolet
UV/IR	Ultraviolet/Infrared
VIPER	Volatiles Investigating Polar Exploration Rover
VO	Visual Odometry
W/K	Watts/Kelvin
W/m <sup>2</sup>	Watt Per Square Meter
WBS	Work Breakdown Structure
WEB	Warm Electronics Box
WEH	Water Equivalent Hydrogen
WES	Waterways Experiment Station
WFOV	Wide Field of View



## B SCIENCE

### B.1 SCIENCE PATH RATIONALE

#### B.1.1 THE TRAVERSE

The INSPIRE traverse (Fig. 1-4) is designed to systematically sample multiple environments at the lunar south pole to investigate the origin, age, and evolution of polar volatiles. The traverse covers ~750 km in distance, connecting 62 pre-planned Science Stations (B.2.2) that are selected to critically test the multiple science hypotheses presented in the INSPIRE STM (Table 1-1). Addressing these hypotheses requires in situ analyses of volatiles and cold-trapping environments over multiple length scales. Thus, the traverse path is optimized to study the local heterogeneity of volatiles and cold-trapping environments at sub-orbital scales (~meters), at larger scales (~50-100s of meters) for critical ground-truthing and valid calibration of the multiple remote sensing datasets currently used to characterize surface/near-surface volatiles and their environments, and at even larger scales (>100s of meters) to study the possible effects of on volatile accumulation and retention.

The traverse is designed to sample five of the largest old and cold permanently shadowed regions (PSRs) at the surface (Cabeus, Haworth, an unnamed PSR, Shoemaker, and Faustini) as well as the scientifically important terrain between these shadowed regions. These PSRs are ideal to study processes affecting volatile delivery, modification, retention, and loss over the last ~4 Gyr because these locations exhibit variation in the abundance of water sensed at the surface [1-3] and subsurface [4-10], variation in the estimated age of cold traps [11-13], and variation in the history of ice-stability conditions predicted by models of changes in the lunar spin axis [14]. These five sites are also ideal locations to study the more recent and even ongoing flux of lunar volatiles (e.g., [15-20]) because they host various seasonally shadowed regions (SSRs). SSRs are regions where temperatures are cold enough for water ice to accumulate during local winter, but are too warm (>112 K) for water ice to be stable against sublimation during the summer (e.g., [21, 22]). Sampling of SSRs would provide new and important information about the ongoing activity and transport of volatiles (e.g., [21-23]).

Overall, the traverse (Fig. 1-4) covers ~750 km across the surface in order to analyze volatiles and cold-trapping environments at multiple length scales, while connecting the various INSPIRE Science Stations designed for additional science activities (§1.2). This distance across PSRs is of high scientific value because the rover will traverse across the present-day and predicted paleo ice stability regions, while also interrogating each of these PSRs based on their intrinsic scientific merit. The traverse is designed to provide a safe path between the Science Stations (B.2.2), which are selected to test the scientific hypotheses presented in the INSPIRE STM (Table 1-1). Appendix K provides specific details on the criteria and limitations guiding the traverse path design. INSPIRE's long traverse (~750 km) was designed from the outset to address the full range of possible transformative science investigations at the Moon's poles—far above and beyond what is possible with VIPER and exploration by Artemis astronauts (as currently envisaged). By utilizing the long-range rover architecture developed for Intrepid and Endurance (which were designed to traverse >1,700 km), INSPIRE is more than capable of exploring the entire lunar south pole, and therefore, substantially shortened traverses were not considered in substantial detail. It is possible that a shorter traverse may exist that could address preponderance of INSPIRE's science objectives. A future study or proposal would need to evaluate the traverse in more detail.

#### B.1.2 SCIENCE STATIONS

Science Station operations are designed to include both detailed mapping and subsurface drilling. Each of INSPIRE's two TRIDENT drills is conservatively designed for 100 2-m holes. To ensure full redundancy of TRIDENT, science planning only assumes the use of one drill (100 2-m drill holes). Science Stations are selected based on fulfilling criteria outlined to address the INSPIRE science questions (Ref Table 1-1; Table B-3). The traverse therefore includes 64 pre-planned drill holes at 62 pre-planned Science Stations (each of the LCROSS impact sites will be drilled twice; Table B-3). The remaining 36 drill holes are reserved for opportunistic drilling locations which will be determined real-

time during ground operations by the Science Team in response to INSPIRE measurements. For example, the Science Team may elect to perform another drilling operation (1) elsewhere in the Science Station in response to unexpected sub-surface measurements or observations, (2) elsewhere in the Science Station when multiple science variables are present for further investigation (e.g., the location is both a present-day hyper-cold trap and also a past ice stability zone), (3) within a few meters of another drilling to measure lateral variations at meter scales, or (4) in areas of local heterogeneity (e.g., perform one drilling within a patch of surface frost and another nearby drill site outside the surface frost coverage in order to assess effects of surface frost on subsurface volatile content). The 36 opportunistic sites will not be unused and can always be allocated between the pre-planned Science Stations, thus providing additional critical ground-truthing within each station. This hybrid approach of coupling pre-planned science with opportunistic and reactionary science is modelled after the science operation strategy for VIPER drilling [24]. The allocation of  $\sim 1/3$  of INSPIRE drill sites to opportunistic locations highlights the excitement of exploring this dynamic terrain and adaptability of the INSPIRE mission.

Like the traverse path, the 62 pre-planned Science Stations along it are strategically selected to probe the INSPIRE Science Questions presented in the STM (Table 1-1). As detailed in the following sections, these Science Stations are designed for a broad sampling of cold-trapping thermal environments (spanning temperatures between  $<30$  K and  $>200$  K), past and present ice-stability regions (spanning paleo and present-day ice stability zones predicted for the last  $\sim 4$  Gyr; [14]), and locations linked to key orbital observations of surface/near-surface volatiles (spanning locations both with positive and negative ice detections by multiple instruments, and also targeting locations where instrument data do not agree).

### Testing of Cold-Trapping Thermal Environments

Temperature is a primary factor controlling the distribution of volatiles [2, 14, 24-26], modulating the rates of volatile diffusion and sublimation [27, 28]. From remotely-sensed data, putative water-ice detections are largely constrained to surfaces with temperatures  $<112$  K, but there are still many questions related to how the speciation and concentration of volatiles vary as a function of temperature [1-3]. Furthermore, while large polar cold traps (like the large five PSRs guiding the INSPIRE traverse) are typically thought of as being stable thermal environments for water ice on billion-year timescales [24, 25], the seasonal temperature changes could have a profound effect on the sequestration and retention of volatiles, with cold-trapping surface area more than doubling between summer and winter [22]. This dynamic thermal environment, which has been measured over the last decade by Diviner [22], suggests that temperature may be actively driving the transport of volatiles today, offering a unique opportunity for INSPIRE to quantify the present-day volatile cycle as the rover traverses through multiple lunar seasons.

The INSPIRE traverse covers a wide range of local temperatures to study the thermal environment of the lunar poles and understand its control over volatile presence, abundance, mobility, and distribution. The 62 pre-planned Science Stations thus cover a wide sampling of temperatures, broken into four groups: hyper-cold traps ( $<50$  K), stable cold traps (50-100 K), warmer environments ( $>100$  K), and seasonal cold traps ( $<100$  K in winter but  $>100$  in summer). Importantly, temperature measurements acquired by INSPIRE (§3.1) will significantly improve our understanding of the lunar surface thermal environment, as our current understanding relies on temperatures measured from orbit that have a low pixel resolution of  $\sim 240$  m [22]. Therefore, INSPIRE will significantly improve the known state-of-the-art.

### Testing the Evolution of Ice-Stability Environments

In addition to today's thermal environment, the past thermal environments of the Moon are predicted to have a control on the distribution of lunar surface water. Sampling of multiple surface and subsurface ice stability regions will provide an important test of this hypothesis. Thus, where possible in each of the five PSRs, pre-planned Science Stations are selected to sample regions where surface ice and

subsurface ice are predicted to be stable (1) today but not early on when the Moon was on the paleo-axis predicted by [14], (2) early on but not today, and (3) both today and early on (Table B-2).

### Ground-Truthing of Volatile-Related Orbital Measurements

Water ice has been sensed on the surface of the lunar poles using various IR and UV spectroscopic techniques [1-3]. While these different datasets are broadly consistent in the spatial distribution of their detections and correlations with low-temperature cold traps [25], there are some differences in the spatial distribution of the detections that have yet to be explained. For example, ice exposures were identified in many locations across the floor of Shoemaker crater on the basis of diagnostic overtone and combination mode vibrations for H<sub>2</sub>O ice in NIR spectral data acquired by the M<sup>3</sup> instrument [3], but there are far fewer putative ice exposures identified from the ratios of reflected UV radiation (consistent with both H<sub>2</sub>O and OH) measured by the LAMP instrument [2] (Fig. B-1). Furthermore, variations in these remotely-sensed signals (which range in spatial resolutions between 240 and 256 mpp) imply different concentrations of water ice [2, 3]. Strategically sampling locations on the ground is essential for ground-truthing these datasets so that (1) the processes driving the distribution and local spatial heterogeneity of the ice can be more fully understood, (2) volatiles concentrations can be measured and tied to the broader orbital datasets from the M<sup>3</sup> and LAMP instruments, and (3) differences in positive/negative ice detections by different instruments can be understood and applied to broader orbital datasets. Therefore, the pre-planned Science Stations target surfaces that (1) lack putative ice detections in both M<sup>3</sup> [3] and LAMP [2] data, (2) have positive ice detections in M<sup>3</sup> data but not in LAMP data, (3) have ice detections in LAMP data but not in M<sup>3</sup> data, and (4) have ice detections in both M<sup>3</sup> and LAMP data. As discussed in §1.2.4, these four groups are targeted in all of the major thermal environments (<50, 50-100, and 100 K), although some combinations are not possible (e.g., both M<sup>3</sup> and LAMP ice detections at temperatures > 100 K).

In addition to surface water ice, subsurface water is also present on the Moon. For example, water, along with various other volatiles, has been detected in the LCROSS plume (e.g., [30]). Additionally, anomalous radar signatures are suggestive of local patches of icy materials in some locations across the poles (e.g., [31, 32]). However, different instruments (Mini-SAR, Chandrayaan-1 vs. Mini-RF, Lunar Reconnaissance Orbiter) have observed variations in the strength and location of radar signals, and thus various hypotheses exist related to the concentration and location of ice associated with radar anomalous locations. INSPIRE will measure volatile abundance and form at various radar anomalous sites to provide the critical ground-truthing required to better understand the existing database of polar data. To accomplish this, INSPIRE will drill at sites where subsurface volatiles have been detected at the LCROSS impact sites [30] and where subsurface volatiles are predicted to be present from radar analyses [31, 32]. As described in the Concept of Operations and Mission Design (§3.3), two drill sites are planned for the impact sites of the LCROSS Centaur and the shepherding spacecraft, for a total of four drill sites at these locations.

### Selection of Pre-Planned Science Stations

Combining the key science targets discussed above, the INSPIRE traverse path includes 62 pre-planned Science Stations, distributed across the five large PSR targets: 17 in Cabeus, 12 in Haworth, 9 in the unnamed PSR, 10 in Shoemaker, 10 in Faustini, and 6 along-traverse (Fig. 1-4; Table B-3). The 6 stations along-traverse are included to target thermal environments that are not accessible within all of the 5 large PSRs, specifically SSRs and warmer surfaces with temperatures >100 K. The full array of pre-planned Science Stations is presented in Table B-3.

### Ancient Lunar Volatiles

Some researchers suggest that a substantial fraction of lunar polar volatiles are ancient, where here “ancient” does not imply “primordial” but refers to ~3.5–4 Ga ages corresponding to large outgassing events, large impact events, and the ages of the permanently shadowed host craters [3, 12, 14, 33-35]. Other research favors more recent or ongoing volatile deposition by micrometeoroid bombardment and/or in situ interactions between the solar wind and regolith [15-20]. This debate has been fueled



by various theoretical models, spacecraft observations, comparisons with Mercury [36-38], and even new analyses of returned lunar samples [39-45]. In this context, potential volatile sources cover a broad temporal history, including volcanism and early lunar outgassing, comet and/or asteroid delivery, and solar wind production. INSPIRE is designed to significantly constrain this history and test hypotheses of volatile emplacement and retention.

The scientific design of INSPIRE makes this mission very complimentary to missions such as comet sample return for studying ancient volatiles of the Solar System. Regarding the Moon, the lunar poles are an accessible witness plate to the bombardment of Solar System, and effectively an admixture of different sources that have been modified by lunar processes (e.g., impact gardening, UV photolysis, solar wind sputtering). Then there are also comets (and other small bodies) which are one of the possible sources for those volatiles, which have also been modified by cometary processes (e.g., thermal alteration) and uncertain dynamical histories. INSPIRE would explore and characterize that accessible witness plate, while a comet sample return mission would explore and characterize one accessible object from a class of sources. Ultimately, results from both types of missions are biased in some way by processes that have shaped their targets since the dawn of the Solar System. In this case, INSPIRE exploits the accessible and informative volatile reservoir of the Moon.

### Drill Depth

We note that the TRIDENT 2 m drill is based on the TRIDENT 1 m heritage drill flying on NASA's CLPS (Commercial Lunar Payload Services) 19C mission and on NASA's VIPER (Volatiles Investigating Polar Exploration Rover) mission. INSPIRE requires the deeper 2 m drill for multiple science reasons. First, a 2 m depth into the lunar subsurface likely allows access to older materials. Depth is a first-order proxy for age where an additional 1 m in depth can provide an extra  $\sim 1$  billion years in history based on the lunar overturn gardening rate [36]. Second, the INSPIRE Science Station selections also utilize a 2 m drill depth because to interrogate paleo vs present-day ice stability regions, the 2 m depth was needed in order to find zones that are exclusively paleo or present-day stability zones which are not overlapping. Third, the LCROSS impact of the Centaur rocket upper stage created an impact crater in Cabeus that is  $\sim 3$ -5 m deep while the smaller LCROSS Shepherding Spacecraft created a slightly shallower impact crater, and so having a 2 m drill depth allows INSPIRE to more robustly characterize these impact sites in the only ground truthed regions of known polar volatiles on the Moon at depths coincident with expected LCROSS excavation depths.

## B.2 RELEVANCE TO UPCOMING LUNAR POLAR MISSIONS

At the time of this writing, we are potentially on the cusp of an exciting new era of lunar exploration with multiple robotic and human missions planned for the lunar south polar region. Here we review these planned missions to the lunar polar regions and discuss the capabilities of each to address Decadal Survey-level science goals. INSPIRE will benefit from these early lunar polar missions which are more limited in scope and capability but will inform science and reduce operations and technology risks for INSPIRE. Much as NASA's Mars Program has effectively built increased technical capability and science knowledge by building on previous mission experiences (e.g., the Mars rover progression of Pathfinder, Mars Exploration Rovers, Curiosity, Perseverance), the lunar program would benefit from a similar strategy. Ultimately, **INSPIRE will conduct *transformative new science* while also building on past missions.**

NASA's CLPS (Commercial Lunar Payload Services) and Artemis program are planning to send robotic and human missions to the lunar south polar region, respectively. Table B-1 shows these missions along with key science and operations information for CLPS, Artemis, and INSPIRE. We also note that NIRVSS, MSolo and NSS will also be flying to the Moon on the CLPS Astrobotic mission to Lacus Mortis. Although not a polar landing site, this flight mission will also provide valuable science, technology, and operations lessons relevant for INSPIRE.

**Table B-1.** Comparison of anticipated NASA missions to the lunar south polar region within the coming decade.

		PRIME-1	CLPS 19C	VIPER	Artemis	INSPIRE
<b>Science and Science Stations</b>	Surface Temp 110-225 K	One sunlit site	Sunlit		TBD, limited range	The Holy Grail
	Surface Temp 50-100 K					
	Surface Temp < 50K					
	LAMP ice detection			Some Volatiles		
	M3 ice detection					
	LCROSS impact site					
	Present + paleo ice stability (surface)					
Present + paleo ice stability (subsurface)						
		PRIME-1	CLPS 19C	VIPER	Artemis	INSPIRE
<b>Mission Characteristics</b>	Launch Date	2022	2022	2023	2024	2030
	Mission Purpose	Technology	Science/Technology	Science/Exploration	Exploration	Science
	NASA Division	STMD	SMD (ESSIO)	SMD (ESSIO, PSD)	HEOMD	SMD (PSD)
	Landing Site	south pole	south pole	south pole	south pole	south pole
	Mission Duration	??	10 days	100 days	days-weeks	3 years
	Traverse Distance	stationary	.5 km	20 km	TBD	~750km
	Number of Instruments	1	4	3	TBD	9
	Number of drills	1 (1m depth)	1 (.3-.4m depth)	1 (1m depth)	TBD	2 (2m depth)
	Cost (A-D)	?	?	\$433M (incl E-F)	\$XXB	\$1.1B
	Risk Class	D	D	D	A	B
	Lander	CLPS	CLPS	CLPS	SpaceX	CLPS
	Communications	direct-to-Earth	direct-to-Earth	direct-to-Earth	unknown	Relay
	PSR Ops Time	0 hrs	0 hrs	~8 hours	~hours	~years
Drill Sites	1	1 (arm)	40	unknown	100+	
Power Source	solar	solar	solar	unknown	RPS	

The planned NASA south polar landed missions are as follows:

*PRIME-1 (Polar Resource Ice Mining Experiment-1).* PRIME-1 will land and operate at one sunlit site near the lunar south pole. The stationary nature precludes PRIME-1 from interrogating PSRs, but the PRIME-1 payload includes a 1 m TRIDENT drill and MSolo instrument which will reduce risk for INSPIRE and provide valuable conops and science interpretation information.

*CLPS 19C:* The CLPS 19C mission is manifested aboard a Masten Space Systems lander to operate in a sunlit location near the lunar south pole. This mission also won't investigate PSRs or other areas of identified INSPIRE science interest as outlined in Table B-1, but will fly multiple INSPIRE instruments (NIRVSS and MSolo from a stationary lander and NSS on the small Moon Ranger rover) to reduce risk, gain operational expertise, and inform INSPIRE science through volatile studies in sunlit polar locations.

*VIPER (Volatiles Investigating Polar Exploration Rover):* NASA's VIPER mission will interrogate both sunlit regions and PSRs to provide valuable in situ information regarding lunar polar volatiles. VIPER has a shorter mission duration (~100 days) and traverse distance (10-20 km) compared to INSPIRE but is flying several payload elements (TRIDENT 1 m drill, NSS, NIRVSS, MSolo) also included in the INSPIRE concept. VIPER will not reach the "old and cold" PSRs of the INSPIRE traverse but VIPER will provide valuable information to inform INSPIRE science and operations.

*Artemis.* NASA's Artemis program aims to send humans to the south polar region of the Moon. Architectural details are TBD, although we assume the astronaut crew will initially have limited mobility and limited ability to collect data within PSRs which reduces the ability to address Decadal Survey level volatiles science which requires extended access to the oldest and coldest PSR locations on the Moon.

### B.3 RELEVANCE TO DECADAL SURVEY PRIORITY SCIENCE TOPICS

The National Academies Decadal Survey on Planetary Science and Astrobiology 2023-2032 has identified twelve priority topics to address Solar System science over the next decade. The INSPIRE mission provides relevant scientific contributions to a preponderance of these high priority science topics as outlined in Table B-2.

**Table B-2.** High priority Decadal Survey science addressed by the INSPIRE mission.

Decadal Survey Priority Science Topics	INSPIRE Relevance	Supporting Rationale
Evolution of the Protoplanetary Disk	Contributing	Record of ancient volatiles available within protoplanetary disk for lunar & inner Solar System planet formation: INSPIRE would identify water and other volatiles delivered by cometary impacts on the Moon, providing information regarding the compositions in their wider population including Kuiper Belt Objects (KBOs) and Oort Cloud Comets (OCCs), thus constraining the chemical and physical structures inside of the protoplanetary disk.
Accretion in the outer Solar System	Contributing	Comparative planetology of processes affecting ice & hydration on airless bodies relative to the origin & distribution of ices on bodies across the Solar System: INSPIRE would measure hydrogen isotopes, which would generalize the contrasts of accreted chemicals between icy small bodies (KBOs and OCCs) (high D/H) and gas giants (low D/H).
Origin of Earth and Inner Solar System Bodies	Critical	Constrain origin of volatile species, including terrestrial ancient water content, to understand formation of Earth and inner Solar System bodies: INSPIRE would measure relevant isotopes and volatile species to determine origin of volatile delivery in the inner Solar System.
Impacts and Dynamics	Critical	Constrain the effects of impacts and gardening on volatiles distributions, regolith mixing & overturn. INSPIRE would measure isotopes and D/H ratios which would constrain whether exogenous water driven by comet and/or asteroid impacts are a dominant source of the current water ice distribution on the Moon. INSPIRE would determine the lateral and vertical distribution of water ice, which would quantify impact-driven material mixing processes.
Solid body interiors and surfaces	Critical	Characterization of surface & subsurface volatile components. INSPIRE would measure the form, abundance, and distribution of volatile species which would constrain the distribution and behavior of ices on and within the Moon.
Solid body atmospheres, exospheres, magnetospheres, and climate evolution	Critical	Evolution of lunar atmosphere rise & fall, behavior of rarefied atmosphere affecting habitable conditions. INSPIRE would measure gas species in the lunar exosphere which would constrain how the exosphere is developed and whether water molecules from non-PSRs are cold trapped in PSRs.
Giant Planet Structure and Evolution	None	
Circumplanetary Systems	Critical	Present-day ice distributions records the history of early lunar interior geophysics. INSPIRE would measure volatile distributions to compare with predictions of ice stability regions both before and after the formation of the low-density anomaly beneath the Procellarum region that is hypothesized to have caused true polar wander and constrain the magnitude and timescale of the rotational excitation and tidal dissipation.
Insights from Terrestrial Life	None	
Dynamic Habitability	Contributing	Evolution of lunar atmosphere rise & fall, behavior of rarefied atmosphere affecting habitable conditions. INSPIRE would characterize the current state and behavior of the lunar exosphere to constrain how exospheric processes affect the evolution of molecular components relevant to developing habitable conditions over lunar history.
Search for Life Elsewhere	Contributing	Record of volatile and organic delivery to solid surface. The cold lunar regions allow the study of abiotic/prebiotic chemistry and related surface processes that are active throughout the Solar System. INSPIRE would measure organic species which would constrain how abiotic/prebiotic chemical evolution is supported and/or constrained by the Moon's geochemical and environmental contexts.
Exoplanets	Contributing	Understanding of volatile components (indigenous vs exogenous) for airless bodies. INSPIRE's investigations would be an analog for quantifying the volatile delivery cycles and environments supporting volatiles on exoplanets and exomoons. The lunar environment is relevant for exoplanets as surface boundary exospheres are the most common type of atmosphere in the Solar System.

**Table B-3.** INSPIRE Pre-Planned Science Stations.

Location (°S, °E)	Cold-Trapping Thermal Environments				Evolution of Ice-Stability Environments				Ground-Truthing			
	Surface T <50 K	Surface T 50-100 K	Surface T >100 K	SSR	Present-day surface ice stable	Paleo surface ice stable	Present-day sub- surface ice stable	Paleo subsurface ice stable	LAMP ice detection	M <sup>3</sup> ice de- tection	LCROSS impact	Radar anomalous
<b>Cabeus (N=15)</b>												
84.77, -41.85	X				X	X						
84.72, -48.82	X				X	X			X			
85.37, -52.91	X				X	X				X		
84.94, -44.57		X					X	X				
84.33, -48.30		X			X			X	X			
84.54, -44.45		X			X			X		X		
85.42, -45.07		X					X	X	X	X		X
85.17, -43.91			X				X	X				
85.16, -41.86			X			X	X		X			
85.82, -37.70				X			X	X				
85.66, -46.91				X		X	X					X
85.17, -43.83				X			X	X				X
86.13, -49.80	X					X	X					X
84.68, -48.71 (x2 drill sites)			X		X			X			X	
84.72, -49.61 (x2 drill sites)		X			X	X					X	
<b>Haworth (N=12)</b>												
87.60, -8.23	X				X	X						
87.41, -9.23	X				X			X	X			
87.33, 0.91	X				X			X		X		
87.42, 2.14	X				X	X			X	X		
87.80, -6.61		X			X			X				
87.68, -5.75		X			X			X	X			
87.86, -9.34		X			X			X		X		
87.83, -9.53		X			X			X	X	X		
87.70, 11.25		X				X		X				
87.55, 14.07		X					X					
87.62, 13.67		X					X	X				
87.53, -10.77	X				X	X						X
<b>Unnamed PSR (N=9)</b>												
86.56, 19.71	X				X			X				
86.67, 21.01	X				X			X	X			



**Table B-3.** INSPIRE Pre-Planned Science Stations.

Location (°S, °E)	Cold-Trapping Thermal Environments				Evolution of Ice-Stability Environments				Ground-Truthing			
	Surface T <50 K	Surface T 50-100 K	Surface T >100 K	SSR	Present-day surface ice stable	Paleo surface ice stable	Present-day sub- surface ice stable	Paleo subsurface ice stable	LAMP ice detection	M <sup>3</sup> ice de- tection	LCROSS impact	Radar anomalous
86.91, 22.75	X				X			X		X		
86.73, 25.31	X				X			X	X	X		
86.69, 21.27		X			X			X				
86.91, 24.11		X			X			X	X			
86.93, 24.61		X			X			X		X		
86.89, 16.76		X			X			X	X	X		
86.71, 27.01	X					X	X					
<b>Shoemaker (N=10)</b>												
87.79, 38.76	X				X			X				
87.87, 42.56	X				X			X	X			
87.93, 39.75	X				X			X		X		
88.21, 52.07		X			X			X				
88.47, 53.49		X			X			X	X			
88.23, 36.51		X			X			X		X		
88.23, 57.39		X			X	X			X	X		
87.79, 65.13		X				X	X					
87.68, 64.37		X					X	X				
87.88, 40.18	X				X		X					X
<b>Faustini (N=10)</b>												
87.09, 82.99	X				X	X						
87.04, 82.09	X				X	X			X			
87.03, 82.37	X				X	X				X		
87.35, 88.64		X			X			X				
87.49, 83.23		X			X			X	X			
87.16, 82.39		X			X			X		X		
87.54, 82.53		X			X			X	X	X		
87.03, 93.47		X				X	X					
87.03, 94.13		X					X	X				
87.26, 78.62	X				X			X				X
<b>Traverse (N=6)</b>												
86.78, 30.67			X				X	X				
86.45, 4.36			X				X	X				
86.41, -2.22				X			X	X				

**Table B-3.** INSPIRE Pre-Planned Science Stations.

Location (°S, °E)	Cold-Trapping Thermal Environments				Evolution of Ice-Stability Environments				Ground-Truthing			
	Surface T <50 K	Surface T 50-100 K	Surface T >100 K	SSR	Present-day surface ice stable	Paleo surface ice stable	Present-day sub- surface ice stable	Paleo subsurface ice stable	LAMP ice detection	M <sup>3</sup> ice de- tection	LCROSS impact	Radar anomalous
86.83, -20.46				X	X			X				
87.66, 69.34				X			X	X				
87.83, 18.96				X			X	X				

## B.4 INSTRUMENT TRADES

During the study period, the team considered several instrument trades before converging on the payload presented in Section 3. For completeness and to support continued investment in flight-instrument technology development, we include those trade options here, noting that, in each case, standard engineering modifications (e.g., to achieve acceptable TRL for the lunar environment as in the GPR) and/or additions (e.g., inclusion of a context camera and thermal radiometer for the IR spectrometer) to the instruments described below would be required for inclusion as an element of the INSPIRE payload.

### **Mass Spectrometer: Lunar CubeSat Mass Spectrometer (LCMS) for Lunar Exosphere Investigations**

Currently TRL 5 for the lunar environment, the LCMS is being advanced to TRL 6 (by 2022) under DALI funding at the Jet Propulsion Laboratory. The LCMS is designed to identify and quantify exosphere species with abundances  $\geq 10$  molecules/cm<sup>3</sup>. The instrument consists of a separable quadrupole ion trap (QIT) mass sensor and electronics unit, enabling accommodation of the QIT sensor on a mast or arm, and draws heritage from the QIT-MS flown on the International Space Station from 2010–2012 and 2019–present. LCMS performance requirements include a mass range of 1–140 Da, mass resolution ( $m/\Delta m$ , FWHM) of 200, sensitivity of 30 cps, dynamic range of  $10^5$ , and target species partial pressure of  $\leq 1\text{E-}14$  Torr. Current best estimates for mass, power, and volume are 7 kg, 30 W, and 6500 cm<sup>3</sup>, respectively. [46]

### **Infrared Spectrometer: Broadband InfraRed Compact High-resolution Exploration Spectrometer (BIRCHES)**

BIRCHES is a compact broadband (1–4 micron) point spectrometer utilizing a compact HgCdTe focal plan array that has been developed by Goddard Spaceflight Center for determining the composition and distribution of volatiles in the lunar regolith. BIRCHES is set to fly on *Lunar Ice Cube*, a deep-space cubesat mission to be launched on ARTEMIS I. BIRCHES employs a linear variable bandpass filter to achieve a resolution of 10 nm within the 3-micron region, which will enable discrimination of various spectral features characteristic of hydroxyl bands and molecular H<sub>2</sub>O in different matrices and physical states (e.g., bound, adsorbed). Mass, power, and volume of the instrument (including the cryocooler) are 3 kg, 15–20 W, and 2000 cm<sup>3</sup>, respectively. [47]

### **Ground-Penetrating Radar: Radar Imager for Mars Subsurface Experiment (RIMFAX)**

RIMFAX is a ground-penetrating radar payload element aboard the Mars 2020 mission's *Perseverance* rover and thus is TRL 9 for the martian environment. The RIMFAX antenna is mounted on the rover deck ~60 cm above the martian surface. RIMFAX operates over a frequency range of 150–1200 MHz; scanning over the full bandwidth enables imaging from the surface down to a depth of ~10 m into the subsurface with a vertical resolution of < 20 cm. RIMFAX is designed to map out subsurface structure as well as geologic composition. RIMFAX measurements will be taken when the rover is stationary as well as at ~10 cm intervals while the rover is in motion—conops comparable to those considered for INSPIRE. Mass, power and volume of the instrument are 3 kg, 5–10 W, and ~1300 cm<sup>3</sup>, respectively.

---

## C JPL TEAM X REPORT

This appendix provides the Executive Summary and Systems Engineering sections from the INSPIRE (formerly called Lunar Polar Volatiles Rover) Team X Study Report. Note that rover detailed design activities by the INSPIRE team continued following this study, resulting in values for some parameters (e.g., total mass, power modes, etc.) being slightly different from those in the body of the report.





## **Lunar Polar Volatiles Rover**

**Customers: John Elliott and Jenn Heldmann**

**Facilitator: Alfred Nash**

**Session Dates: 23-March-2021 to 25-March-2021**

**Study ID: 375**



## Data Use Policy



- The information and data contained in this document may include restricted information considered JPL/Caltech Proprietary, Proposal Sensitive, Third-party Proprietary, and/or Export Controlled. This document has not been reviewed for export control. It may not be distributed to, or accessed by, foreign persons.
- The data contained in this document may not be modified in any way.
- Distribution of this document is constrained by the terms specified in the footer on each page of the report.

## Team X Participants



- Alex Austin – Systems
- Benjamin Donitz – DSE
- Ron Hall – Power
- David Hansen – Telecom
- Karla Hawkinson – Administration
- William Jones-Wilson – ACS
- Roger Klemm – CDS
- Melora Larson – Instruments
- Alfred Nash – Facilitator
- Mieszko Salamon – Mechanical
- Bill Smythe – Science
- Sherry Stukes – Cost
- Eric Sunada – Thermal
- Mason Takidin – Cost
- Ban Tieu – SVIT
- Greg Welz – Ground Systems
- Clayton Williams – Software

## Table of Contents



1. Executive Summary
2. Systems
3. Science
4. Instruments
5. Mission Design
6. Configuration
7. Mechanical
8. ACS
9. Power
10. Thermal
11. CDS
12. Telecom
13. Ground Systems
14. Software
15. Planetary Protection
16. Risk
17. Cost



# Executive Summary

Author: Alfred Nash  
Email: [Alfred.E.Nash@JPL.NASA.Gov](mailto:Alfred.E.Nash@JPL.NASA.Gov)  
Phone: 818-458-0501



REVIEW DRAFT: 5/14/2021 12:05 PM

# Executive Summary

## Study Overview



- Goals
- To assess, and as necessary complete, the design, and estimate the cost, of a lunar rover concept being studied by the planetary decadal survey.
- Objectives
  - From a customer supplied MEL, PEL, and pass through costs, Team-X shall assess the design, and estimate the cost of all the work comprising the total mission.

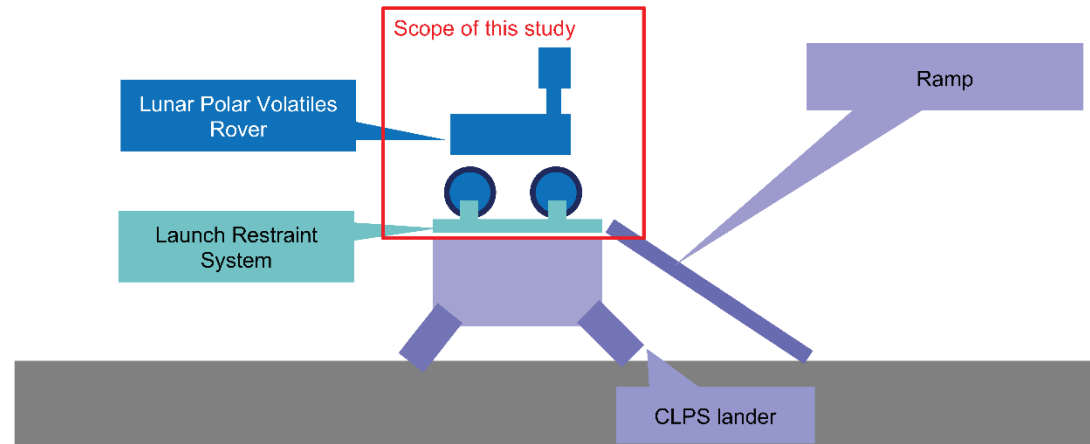


# Executive Summary

## Mission Architecture and Assumptions



- Team X costed the **Lunar Polar Volatiles Rover**
  - A design (MEL and configuration) was supplied by the customer; image at lower right
- The cost and mass also includes a **Launch Restraint System** (to hold the rover during flight, and to release it)
- The rover will be delivered by a **Commercial Lunar Payload Service (CLPS) lander**
  - CLPS delivery was treated only as a pass-through launch cost in our WBS
  - The target mass allocation was 500 kg, though if this were broken, Team X was asked to report the final required mass allocation
  - The lander was assumed to provide a **Ramp** to get to the surface





REVIEW DRAFT: 5/14/2021 12:05 PM

# Executive Summary

## Mission Architecture and Assumptions – Concept of Operations while Driving



Assumed telecom orbiter provides telecom relay



When driving, the rover follows a repetitive set of power modes which occur nominally on a 24 hour cycle

- Each day has a designated 4 hour telecom pass with the relay orbiter
- The amount of time spent driving versus recharging is driven by how often the instruments are used while driving. Team X assessed 2 scenarios:
  - Instruments on 100% of the time while driving
  - Instruments on at designated rover stops every 10 meters (40 seconds out of every 140 seconds – 29% duty cycle)

1. Rover drives for 7.5 hours (instruments 100% duty cycle) to 15.8 hours (instruments 29% duty cycle)

2. Rover stops driving and has a 4 hour telecom pass with the relay orbiter

3. Rover recharges battery for 12.5 hours (instruments 100% duty cycle) to 4.2 hours (instruments 29% duty cycle)



Driving is a series of 100 second traverses that covers 10 meters, followed by a 40 seconds pause





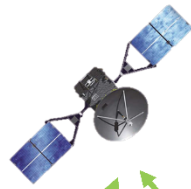


# Executive Summary

## Mission Architecture and Assumptions – Concept of Operations while Drilling



Assumed telecom orbiter provides telecom relay



The rover occasionally performs a drilling operation using one of the two drills mounted to the side of the rover (2 meter drill depth)

- The drilling operation takes a total of 8 hours and includes a number of drill starts and stops, increasing depth by 10 cm increments.
- The science instruments are all active during drilling.
- Telecom is assumed to be active during drilling.
- Once drilling is complete, the rover performs an additional 1 hour of telecom and then must recharge the battery for a total of 22.2 hours before undertaking a new drilling operation.

1. Rover performs a drilling operation over 8 hours, which consists of a number of stop and starts of the drill (average drill power is 93 W)



2. Rover stops drilling and has a 1 hour telecom pass with the relay orbiter



3. Rover recharges battery for 22.2 hours





REVIEW DRAFT: 5/14/2021 12:05 PM

# Executive Summary

## Technical Findings



Mass Fraction	Mass (kg)	Subsys Cont. %	CBE+ Cont. (kg)	Mode 1 Power (W) Cruise - on lander	Mode 2 Power (W) Sunlit Driving + Science	Mode 3 Power (W) PSR Driving + Science	Mode 4 Power (W) PSR Stationary + Drilling Science	Mode 5 Power (W) PSR Stationary + Telecom	Mode 6 Power (W) PSR Recharge	Mode 7 Power (W) PSR Driving (29% Duty Cycle)	
<b>Payload on this Element</b>											
Instruments	5%	24.8	17%	28.9	0	106	118	118	13	13	43
<b>Payload Total</b>	5%	24.8	17%	28.9	0	106	118	118	13	13	43
<b>Spacecraft Bus</b>											
Attitude Control	2%	7.7	10%	8.5	0	23	23	13	17	0	23
Command & Data	3%	13.2	13%	14.9	7	29	29	13	23	1	29
Power	18%	81.7	30%	105.8	10	11	11	11	10	10	10
Structures & Mechanisms	60%	276.9	30%	359.9	0	43	43	93	0	0	43
Cabling	5%	24.1	30%	31.3							
Telecom	3%	14.2	14%	16.2	10	10	10	35	35	10	10
Thermal	4%	20.1	29%	25.8	3	3	3	3	3	3	3
<b>Bus Total</b>		437.8	28%	562.4	30	119	119	168	88	24	118
<b>Spacecraft Total (Dry): CBE &amp; MEV</b>											
		462.6	28%	591.3	30	225	237	286	101	38	162
Subsystem Heritage Contingency	28%	128.7			0	0	0	0	0	0	0
System Contingency	15%	70.3			13	97	102	123	44	16	70
Total Contingency <small>(Include Contingency?)</small>	43%	198.9									
<b>Spacecraft with Contingency:</b>		662			43	321	339	409	145	54	231
<b>Launch Mass</b>		662									
<b>CLPS Lander Capability Required</b>		662									
<b>CLPS Lander Margin</b>		0.0									
<b>Dry Mass Allocation: MPV</b>		662									
JPL Design Principles Margin		199.0	30%	(MPV - CBE)/MPV							
NASA Margin		70.3	12%	(MPV - MEV)/MEV							

### Mass and Contingency Summary

<b>Payload Mass CBE</b>	<b>24.8 kg</b>
<b>Rover Mass CBE</b>	<b>437.8 kg</b>
<b>Rover &amp; Payload Subsystem Contingency</b>	<b>128.7 kg</b>
<b>Rover &amp; Payload CBE + Contingency</b>	<b>591.3 kg</b>
<b>Additional Systems Contingency</b>	<b>70.3 kg</b>
<b>Rover &amp; Payload Mass MEV</b>	<b>661.6 kg</b>

**Total dry mass contingency = 43% (per JPL Design Principles)**

With this design, a total CLPS lander payload mass allocation of 662 kg would be required to provide for 30% JPL Design Principles Margin (which is equivalent to the 30% Margin required in the study ground rules)



REVIEW DRAFT: 5/14/2021 12:05 PM

# Executive Summary

## Programmatic Findings



COST SUMMARY (FY2025 \$M)	Team X Estimate		
	CBE	Res.	PBE
<b>Project Cost</b>	<b>\$1031.9 M</b>	<b>41%</b>	<b>\$1450.9 M</b>
MM RTG	\$70.0 M	0%	\$70.0 M
<b>Project Cost (w/o LV)</b>	<b>\$961.9 M</b>	<b>44%</b>	<b>\$1380.9 M</b>
<b>Development Cost</b>	<b>\$724.7 M</b>	<b>50%</b>	<b>\$1087.1 M</b>
Phase A	\$7.2 M	50%	\$10.9 M
Phase B	\$65.2 M	50%	\$97.8 M
Phase C/D	\$652.3 M	50%	\$978.4 M
<b>Operations Cost</b>	<b>\$237.2 M</b>	<b>24%</b>	<b>\$293.8 M</b>

- All costs in FY2025 \$M
- Reserves Posture: 50% Phase A-D, 25% Phase E-F
- Total development cost + RTG cost estimated as **\$1,157 M FY25**
- Total project cost + CLPS Lander (assumed \$200M) estimated as **\$1,651 M FY25**
- See the cost report for more details

## Executive Summary

### Conclusions, Risks, and Recommendations



- The rover design closed at 662 kg margined launch mass, which is over the 500kg “safe” allocation
  - There may however be other CLPS landers which are capable of higher payload masses
- The customer MEL CBE mass of 428.9 kg is 33.7 kg less than the Team X CBE mass of 462.6 kg. The principle drivers for the mass growth are:
  - 16 kg battery mass upper to provide power for the drilling operation
  - 9 kg balance/ballast mass upper, which was not included in the customer MEL
  - 9 kg other structures upper, which was calculated by the Team X tools
- The development cost (Phase A-D), without Launch (CLPS), but including the RTG (\$70M) and with 50% reserves, comes to \$1,157 M FY25, making this a “\$1.1B class mission”.
- As the concept matures, further consideration should be given to the concept of operations, including which instruments are active at what times to optimize science return and driving distance.



# Systems Report

Author: Alex Austin  
Email: [alexander.austin@jpl.nasa.gov](mailto:alexander.austin@jpl.nasa.gov)  
Phone: (626) 714-8341



REVIEW DRAFT: 5/14/2021 12:05 PM

# Systems

## Study Overview



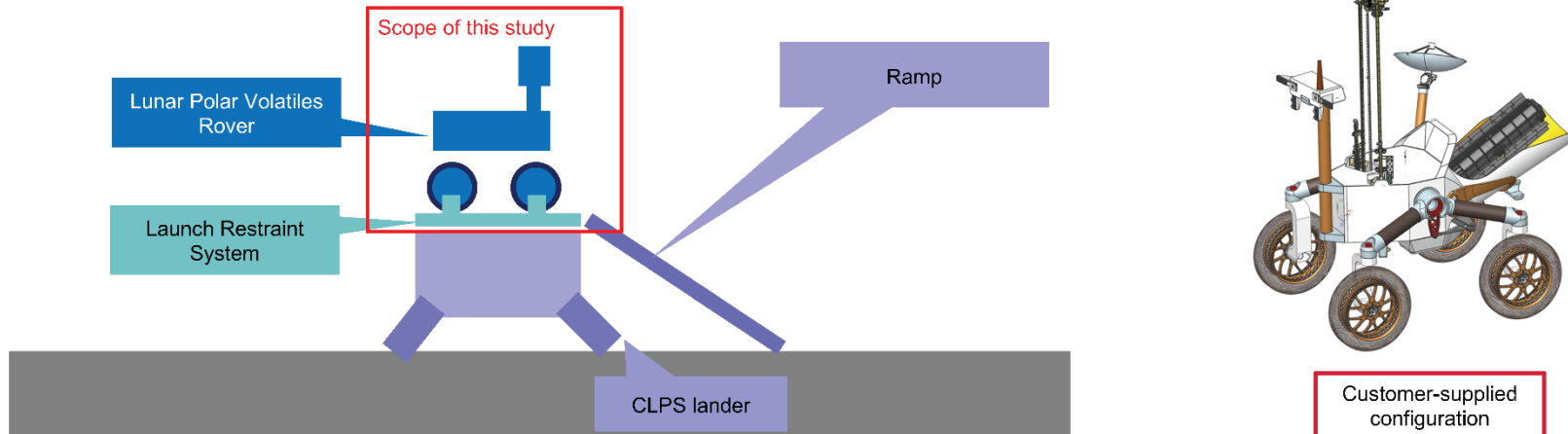
- The goal of this study was to design and cost a rover that would explore permanently shadowed regions (PSRs) of the Moon. The study is funded by NASA as part of the Planetary Science Decadal Survey process.
- The study focused only on the **rover design**, though the entire mission architecture also involves a lander for delivery (assumed as part of NASA's CLPS program) and a telecom relay orbiter (assumed already in place and not part of the rover project).
- The rover has a suite of instruments for exploring lunar volatiles, including two 2 meter drills.
- Customer Inputs
  - Rover design and MEL
  - Instrument payload parameters
  - CLPS Lander delivery cost assumption of \$200M
  - Assumed telecom relay orbiter capabilities
- Team X Outputs
  - Project-level cost (and WBS)
  - Team X design (primarily customer-supplied design, with minor modifications)



# Systems Architecture



- Team X costed the **Lunar Polar Volatiles Rover**
  - A design (MEL and configuration) was supplied by the customer; image at lower right
- The cost and mass also includes a **Launch Restraint System** (to hold the rover during flight, and to release it)
- The rover will be delivered by a **Commercial Lunar Payload Service (CLPS) lander**
  - CLPS delivery was treated only as a pass-through launch cost in our WBS
  - The target mass allocation was 500 kg, though if this were broken, Team X was asked to report the final required mass allocation
  - The lander was assumed to provide a **Ramp** to get to the surface

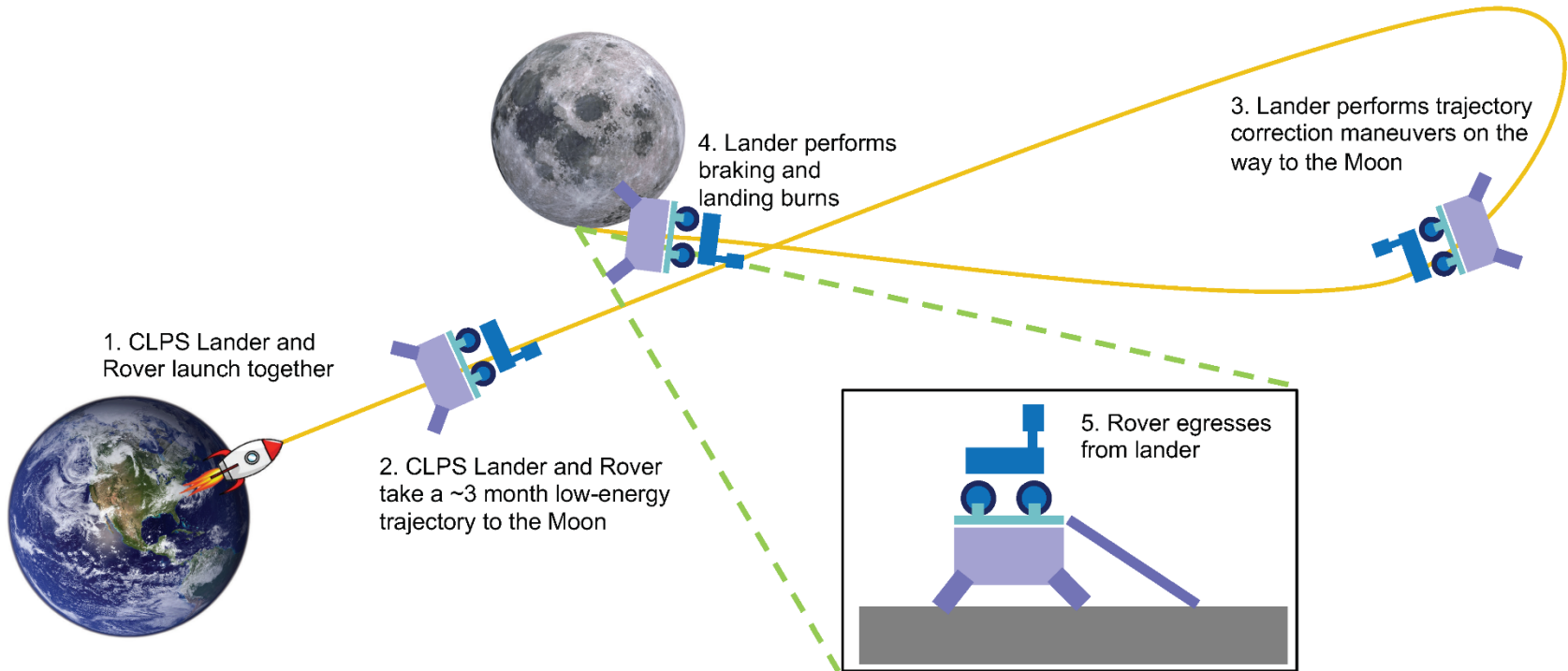




REVIEW DRAFT: 5/14/2021 12:05 PM

# Systems

## Concept of Operations – Launch to Landing





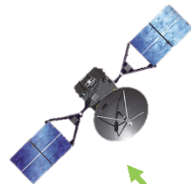


# Systems

## Concept of Operations – Driving



Assumed telecom orbiter provides telecom relay



When driving, the rover follows a repetitive set of power modes which occur nominally on a 24 hour cycle

- Each day has a designated 4 hour telecom pass with the relay orbiter
- The amount of time spent driving versus recharging is driven by how often the instruments are used while driving. Team X assessed 2 scenarios:
  - Instruments on 100% of the time while driving
  - Instruments on at designated rover stops every 10 meters (40 seconds out of every 140 seconds – 29% duty cycle)

1. Rover drives for 7.5 hours (instruments 100% duty cycle) to 15.8 hours (instruments 29% duty cycle)

2. Rover stops driving and has a 4 hour telecom pass with the relay orbiter

3. Rover recharges battery for 12.5 hours (instruments 100% duty cycle) to 4.2 hours (instruments 29% duty cycle)



Driving is a series of 100 second traverses that covers 10 meters, followed by a 40 seconds pause



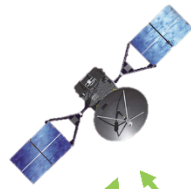


# Systems

## Concept of Operations – Drilling



Assumed telecom orbiter provides telecom relay



The rover occasionally performs a drilling operation using one of the two drills mounted to the side of the rover (2 meter drill depth)

- The drilling operation takes a total of 8 hours and includes a number of drill starts and stops, increasing depth by 10 cm increments.
- The science instruments are all active during drilling.
- Telecom is assumed to be active during drilling.
- Once drilling is complete, the rover performs an additional 1 hour of telecom and then must recharge the battery for a total of 11.3 hours before undertaking a new drilling operation.

1. Rover performs a drilling operation over 8 hours, which consists of a number of stop and starts of the drill (average drill power is 93 W)



2. Rover stops drilling and has a 1 hour telecom pass with the relay orbiter



3. Rover recharges battery for 11.3 hours



# Systems

## Design Assumptions



- Much of the design was taken from the customer MEL, though Team X used internal models to check the design for feasibility and made some modifications (see conclusions slide for a comparison).
- The rover is Class B risk posture, dual string redundancy
- Baseline mission duration is 5.25 years (3 months cruise and 5 years science operations)
- The rover is delivered to the lunar surface by a CLPS lander. Team X performed no design work or costing for the launch and delivery system.
- The telecom relay assumptions were provided by the customer. Team X performed no design work or costing for a telecom relay asset.
- The rover is assumed to be built at JPL for cost estimating purposes.



# Systems

## System Guidelines



Team X Study Guidelines	
Lunar Polar Volatiles Rover 2021-03 Rover	
<i>Project - Study</i>	
Customer	John Elliott
Study Lead	Al Nash
Study Type	Lunar Study
Report Type	PPT Report
<i>Project - Mission</i>	
Mission	Lunar Polar Volatiles Rover 2021-03
Target Body	Moon
Science	Characterization of volatiles in PSRs
Launch Date	30-Apr-30
Mission Duration	5 years on surface and 3 months cruise
Mission Risk Class	B
Technology Cutoff	2026
Minimum TRL at End of Phase B	6 TBR
Planetary Protection	Outbound: II, Inbound: N/A
Flight System Development Mode	In-House
<i>Project - Architecture</i>	
Rover	on CLPS Lander
CLPS Lander	on Launch Vehicle
Launch Vehicle	Delivered by CLPS Lander
Trajectory	Low energy transfer to the Moon
Lander Capability, kg	500 kg
Tracking Network	DSN
Contingency Method	Apply Total System-Level

Spacecraft	
Spacecraft	Rover
Instruments	NIRVSS, NSS ,Msolo, IES, Mini-GPR,TIRs, Camera Pair- Malin ECAMs, Camera DVR
Redundancy	Dual (Cold)
Heritage	MSL, M2020, MER
Radiation Total Dose	28.35 krad behind 100 mil. of Aluminum, with an RDM of 2 added.
P/L Mass CBE, kg	24.8 kg Payload CBE
P/L Power CBE, W	118 W
<i>Project - Cost and Schedule</i>	
Cost Target	\$1.1B
Mission Cost Category	Large - e.g. New Frontiers
FY\$ (year)	2025
Include Phase A cost estimate?	Yes
Phase A Start	March 2024
Phase A Duration (months)	14
Phase B Duration (months)	15
Phase C/D Duration (months)	45
Review Dates	PDR - August 2026, CDR - July 2027, ARR - June 2028
Phase E Duration (months)	62
Phase F Duration (months)	6





# Systems

## Power Modes



- Operating on repeating 24 hour cycles, the power system allows for drive times between 7.5 hours (instruments 100% duty cycle) to 15.8 hours (instruments 29% duty cycle) per day.
- The battery sizing is driven by the drilling scenario, not by driving. One 8 hour drill cycle must be followed by a 11.3 hour recharge period.

Mode Name	Cruise - on lander	Sunlit Driving + Science (100% Duty Cycle)	PSR Driving + Science (100% Duty Cycle)	Stationary + Drilling Science	Stationary + Telecom	Recharge	PSR Driving + Science (29% Duty Cycle)
<b>Payload Power Summary</b>	• None	• NIRVSS • NSS • Msolo (Qty. 2) • IES • Mini-GPR • TIRS	• NIRVSS • NSS • Msolo (Qty. 2) • IES • Mini-GPR • TIRS	• Drill • NIRVSS • NSS • Msolo (Qty. 2) • IES • Mini-GPR • TIRS	• None	• None	• <b>Instruments duty cycled 29%</b> • NIRVSS • NSS • Msolo (Qty. 2) • IES • Mini-GPR • TIRS
<b>Rover Power Summary</b>	• Avionics • Telecom receive	• Avionics • Telecom receive • IMU, Nav Cameras, Star Trackers • Drive Actuators	• Avionics • Telecom receive • IMU, Nav Cameras, Star Trackers, Illuminator • Drive Actuators	• Avionics • Telecom transmit & receive • IMU, Illuminator	• Avionics • Telecom transmit & receive • IMU, Star Trackers, Illuminator	• Avionics • Telecom receive	• Avionics • Telecom receive • IMU, Nav Cameras, Star Trackers, Illuminator • Drive Actuators
<b>MEV Power Requirement</b>	43 W	321 W	339 W	409 W	145 W	54 W	231 W

# Systems

## Design Summary



- **Instruments**
  - NIRVSS (Near IR Spectrometer)
  - NSS (Neutron Spectrometer)
  - Msolo (Mass Spectrometer) (2x)
  - IES (Ion Electron Spectrometer)
  - Mini-GPR (Ground Penetrating Radar)
  - TIRs (Thermal Imager)
  - Stereo Camera
- **CDS**
  - Sabertooth dual-string avionics
  - Motor controllers
  - Dual-string instrument handlers
  - 16 Gbytes on-board storage
- **Ground Systems**
  - Communication through orbital relay asset
  - Baseline one 4-hour pass per 24 hour cycle
- **Telecom**
  - 0.75-m S-band HGA on 2-axis gimbal for link to relay orbiter
  - S-band omnidirectional LGA for safe mode to relay orbiter
  - Dual-string UST-Lite transponders & 5 W S-band SSPAs
- **ACS**
  - IMUs, Star Trackers, Nav Cameras, Illuminator
- **Structures**
  - Primary Structure Mass MEV= 75.9 kg
  - Secondary Structure Mass MEV = 7.3 kg
  - Mobility Structures + Mechanisms Mass MEV = 140.9 kg
  - TRIDENT Drill (2x) MEV = 67.6 kg
  - Other Mechanisms
    - HGA gimbals = 7.8 kg MEV
- **Thermal**
  - Active pumped two-phase fluid loop
  - Five RHUs to maintain instrument survival temperatures
- **Power**
  - One NextGen Mod 1 RTG
  - 100 Ah battery sized to support drilling scenario
  - Power electronics leveraging recent R&TD



REVIEW DRAFT: 5/14/2021 12:05 PM

# Systems Summary Sheet



Mass Fraction	Mass (kg)	Subsys Cont. %	CBE+ Cont. (kg)	Mode 1 Power (W) Cruise - on lander	Mode 2 Power (W) Sunlit Driving + Science	Mode 3 Power (W) PSR Driving + Science	Mode 4 Power (W) PSR Stationary + Drilling Science	Mode 5 Power (W) PSR Stationary + Telecom	Mode 6 Power (W) PSR Recharge	Mode 7 Power (W) PSR Driving (29% Duty Cycle)	
<b>Payload on this Element</b>											
Instruments	5%	24.8	17%	28.9	0	106	118	118	13	13	43
<b>Payload Total</b>	5%	<b>24.8</b>	17%	<b>28.9</b>	0	<b>106</b>	<b>118</b>	<b>118</b>	<b>13</b>	<b>13</b>	<b>43</b>
<b>Spacecraft Bus</b>											
Attitude Control	2%	7.7	10%	8.5	0	23	23	13	17	0	23
Command & Data	3%	13.2	13%	14.9	7	29	29	13	23	1	29
Power	18%	81.7	30%	105.8	10	11	11	11	10	10	10
Structures & Mechanisms	60%	276.9	30%	359.9	0	43	43	93	0	0	43
Cabling	5%	24.1	30%	31.3							
Telecom	3%	14.2	14%	16.2	10	10	10	35	35	10	10
Thermal	4%	20.1	29%	25.8	3	3	3	3	3	3	3
<b>Bus Total</b>		<b>437.8</b>	28%	<b>562.4</b>	30	119	119	168	88	24	118
<b>Spacecraft Total (Dry): CBE &amp; MEV</b>											
		<b>462.6</b>	28%	<b>591.3</b>	30	225	237	286	101	38	162
Subsystem Heritage Contingency	28%	128.7			0	0	0	0	0	0	0
System Contingency	15%	70.3			13	97	102	123	44	16	70
Total Contingency <input type="checkbox"/> Include Contingency?	43%	198.9									
<b>Spacecraft with Contingency:</b>		<b>662</b>			<b>43</b>	<b>321</b>	<b>339</b>	<b>409</b>	<b>145</b>	<b>54</b>	<b>231</b>
Launch Mass		662									
CLPS Lander Capability Required		662									
CLPS Lander Margin		0.0									
Dry Mass Allocation: MPV		662									
JPL Design Principles Margin		199.0	30%	(MPV - CBE)/MPV							
NASA Margin		70.3	12%	(MPV - MEV)/MEV							

## Mass and Contingency Summary

<b>Payload Mass CBE</b>	<b>24.8 kg</b>
<b>Rover Mass CBE</b>	<b>437.8 kg</b>
<b>Rover &amp; Payload Subsystem Contingency</b>	<b>128.7 kg</b>
<b>Rover &amp; Payload CBE + Contingency</b>	<b>591.3 kg</b>
<b>Additional Systems Contingency</b>	<b>70.3 kg</b>
<b>Rover &amp; Payload Mass MEV</b>	<b>661.6 kg</b>

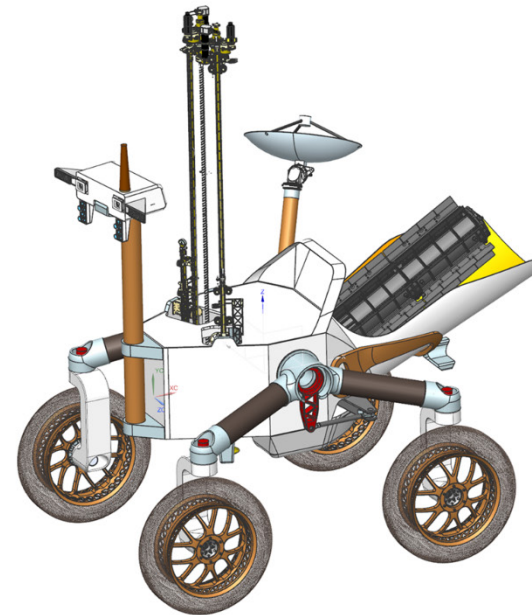
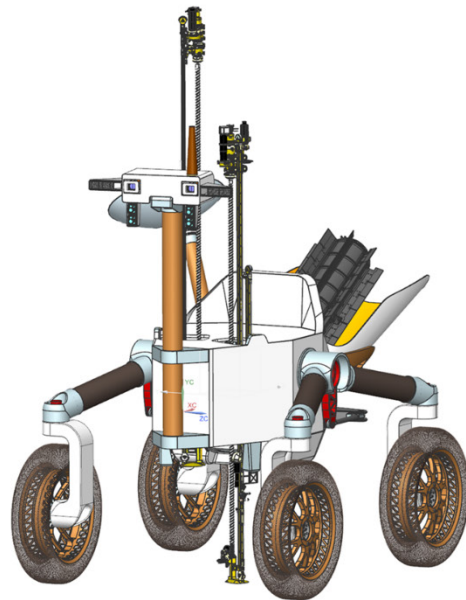
**Total dry mass contingency = 43% (per JPL Design Principles)**

With this design, a total CLPS lander payload mass allocation of 662 kg would be required to provide for 30% JPL Design Principles Margin (which is equivalent to the 30% Margin required in the study ground rules)



# Systems

## Configuration – Customer Provided



375

JPL/Caltech Proprietary, for JPL internal release only by Lunar Polar Volatiles Rover, JPL customer team lead John Elliott

24

REVIEW DRAFT: 5/14/2021 12:05 PM





# Systems

## Cost Summary



COST SUMMARY (FY2025 \$M)	Team X Estimate		
	CBE	Res.	PBE
<b>Project Cost Excluding Launch Vehicle</b>	<b>\$1031.9 M</b>	<b>41%</b>	<b>\$1450.9 M</b>
Next-Gen RTG	\$70.0 M	0%	\$70.0 M
<b>Project Cost (w/o RTG)</b>	<b>\$961.9 M</b>	<b>44%</b>	<b>\$1380.9 M</b>
<b>Development Cost</b>	<b>\$724.7 M</b>	<b>50%</b>	<b>\$1087.1 M</b>
Phase A	\$7.2 M	50%	\$10.9 M
Phase B	\$65.2 M	50%	\$97.8 M
Phase C/D	\$652.3 M	50%	\$978.4 M
<b>Operations Cost</b>	<b>\$237.2 M</b>	<b>24%</b>	<b>\$293.8 M</b>

- All costs in FY2025 \$M
- Reserves Posture: 50% Phase A-D, 25% Phase E-F
- Total development cost + RTG cost estimated as **\$1,157 M FY25**
- Total project cost + CLPS Lander (assumed \$200M) estimated as **\$1,651 M FY25**
- See the cost report for more details

# Systems

## Margin and Contingency Guidelines



- To ensure compliance with JPL's Design Principles (v8), we asserted a 30% JPL Dry Mass Margin on launch mass
  - JPL Dry Mass Margin =  $(\text{Dry Capability} - \text{CBE Dry Mass}) / (\text{Dry Capability})$ 
    - Dry Capability = Launch Allocation – Propellant Mass (in this case propellant mass was zero)
    - In the case of this study, the Launch Allocation was allowed to “float” such that the design converged with 30% JPL Dry Mass Margin
  - 30% JPL Dry Mass Margin corresponds to a 43% increase over the CBE dry mass
    - Margined Dry Mass =  $1.43 * \text{CBE Dry Mass}$
  - **The final Margined Wet Mass of 662kg is what would be required as a CLPS payload allocation, to allow for 30% JPL Dry Mass Margin**
- NASA Margin was also calculated and is shown in mass tables; however, it did not drive the design
  - NASA Dry Mass Margin =  $(\text{Dry Capability} - \text{MEV Dry Mass}) / (\text{MEV Dry Mass})$
- Payload power values were also assigned 30% JPL Margin (43% over CBE) for the purposes of sizing
- For the purposes of the Decadal Study, the 30% JPL Margin appears to be equivalent to the required 30% Margin listed in the Ground Rules, page 3:
  - Margin = Max Possible Resource Value – Proposed Resource Value
  - Margin (%) =  $(\text{Margin} / \text{Max Possible Resource Value}) * 100$

# Systems

## Conclusions, Risks, and Recommendations



- The rover design closed at 662 kg margined launch mass, which is over the 500kg target allocation
  - This defines the minimum payload capability required of the CLPS lander for this mission
- The customer MEL CBE mass of 428.9 kg is 33.7 kg less than the Team X CBE mass of 462.6 kg. The principle drivers for the mass growth are:
  - 16 kg battery mass upper to provide power for the drilling operation
  - 9 kg balance/ballast mass upper, which was not included in the customer MEL
  - 9 kg other structures upper, which was calculated by the Team X tools
- The development cost (Phase A-D), without Launch (CLPS), but including the RTG (\$70M) and with 50% reserves, comes to \$1,157 M FY25, making this a “\$1.1B class mission”.
- As the concept matures, further consideration should be given to the concept of operations, including which instruments are active at what times to optimize science return and driving distance.

## D MOBILITY

**Requirements:** We examined mobility trades for the requirements described in Table D-1. While terrain information at the scale of the mobility system is not available for the planned route, it can be inferred from available data and current knowledge of lunar surface formation process. This information includes data from the Apollo missions, full coverage of orbital imagery at 0.5 – 2 m resolution at different incidence angles from the Lunar Reconnaissance Orbiter Narrow Angle Camera (LRO NAC), derived high-resolution digital-elevation map (DEM) at 5–10 m scale, 7 m/pixel DEM from Chang-E, lower-resolution DEM from Kaguya Terrain Camera at 60 m scale for the entire path, thermal imaging from Diviner on LRO, and HST (Hubble-Space Telescope) UV and RBG imagery of the lunar surface. For the mobility trades, we drew on mobility and navigation expertise from the lunar (Apollo) and martian surface missions. Table D-2 shows the terrain types along the rover’s route.

Based on test data from the Apollo program, mobility on 15°–20° is possible in lunar simulants [48], which exceeds the maximum slope required for INSPIRE. However, for angles exceeding 15°, slip would likely exceed 30%.

**Mobility configuration:** Based on the key requirements of distance, speed, and anticipated terrain properties (topography, regolith properties) (Table D-2), we examined vehicle designs with different wheel/steering configurations (skid-steered, Ackermann-steered, and omni-directional) and with different suspension types (passively and actively articulated). We note we do not know the terra-mechanical properties of PSR regions, which will get informed by the upcoming VIPER. For now, consider the following: surface processes for regolith formation on the Moon are largely the same, which result isotropic meteorite impact. Variation among Apollo and Surveyor sites no greater than within a single site. The Moon does not and never had liquid water.

Largely, the Moon has no exposed bedrock due to absence of wind. However, PSR regions could have potential differences: (a) the grain sizes could be different from those at the Apollo sites due to the lack of thermal cycling and, hence cracking; (b) as far as we know, there is no volcanism near the poles and hence there will be no large-scale pyro deposits; and (c) the electrostatic properties may differ from equatorial regions. Further, we do not know

**Table D-1. Mobility Requirements.**

Requirement		Comments
Nominal Distance	756 km	Based 5–10 m/pixel DEM
Actual Distance	1,140 km	Accounting for terrain tortuosity
Max wheel speed	1 km/hr	Mechanical speed (or 28 cm/s)
Ave traverse rate (day)	0.23 km/hr	Incl. eng. stops for localization and comm
Ave traverse rate (night)	0.16 km/hr	Also incl. long-exposure imaging, localization and comm
Max slope	16°	Based 5–10 m/pixel DEM
Nominal regolith (largely ubiquitous)	Fine Coarse	30%: 40–100 μm angular fines 70%: mm – cm regolith
Worst terrain	Interior crater walls	
Nominal sinkage	2 – 5 cm	In regolith
Crater distribution	10% 20%	Diameter: 5 m < φ < 35 m Diameter: φ < 5 m
Small crater slopes	7° – 8°	Depth = 0.17 φ (diameter) at formation w/ rapid degradation
Rock distribution (area coverage)	1% 10%	Most of the traverse route Around crater rims
Obstacle height	±0.25 m	Max traversable ± obstacle

**Table D-2. Terrain Characteristics on INSPIRE Traverse.**

Direction	Slope Range	INSPIRE Route % of Path	% Skid or Slip (estimate)	Likely Rock Abundance		Source
				< 1 m	> 1 m	
Downslope	$-15^\circ \leq \alpha < -13^\circ$	0.4%	–15%	Medium	2– 15%	DTM 5–10 m/pixel
	$-13^\circ \leq \alpha < -10^\circ$	3.5%	–12%	Medium-low	2– 15%	
	$-10^\circ \leq \alpha < -5^\circ$	11.8%	–9%	Low	< 2%	
	$-5^\circ \leq \alpha < 0^\circ$	<b>33.7%</b>	–4%	Low	< 2%	
Upslope	$0^\circ \leq \alpha < 5^\circ$	<b>32.2%</b>	8%	Low	< 2%	DTM 5–10 m/pixel
	$5^\circ \leq \alpha < 10^\circ$	12.3%	17%	Low	< 2%	
	$10^\circ \leq \alpha < 13^\circ$	3.5%	25%	Medium-low	2– 15%	
	$13^\circ \leq \alpha < 15^\circ$	1.3%	30%	Medium	2– 15%	
	$15^\circ \leq \alpha < 16^\circ$	0.3%	40%	Medium	2– 15%	



the morphology at 1–10 m scale and we do not know the compaction of the regolith from the lack of thermal cycling.

Figure D-1 shows examples of different mobility wheel configurations and suspensions with examples from both flight and research rovers [49].

Table D-3 captures the pros and cons of skid-steered vehicles that have four or more wheels, where none of the wheels can steer. Figure D-2 shows an example of how a skid-steered vehicle that is amenable to walking out of entrapments. With an articulated suspension, the vehicle can lean forward and then use its link suspension to flip one wheel a time clockwise to overcome a difficult terrain. Wheels with walking abilities can be made smaller and lighter since the rover can walk out of areas of higher sinkage.

A variant of skid-steered and partially-steered vehicles is one with toe-in steering. In this configuration, the steerable wheels can toe in to allow the vehicle to rotate around a point at the center of the non-steerable wheels (Figure D-3). The advantage of toe-in steering is that it does not require a clear sweep volume for the motion of the steerable wheels, yet it allows turns-in-place without the slip experienced by skid-steered vehicles. Table D-4 captures the pros and cons of this configuration.

Table D-5 looks at the trades of partially-steered vehicles. One of the key benefits of this configuration is that it can drive along arcs. Partially steered vehicles allow the use of large



**Figure D-2.** Four-wheeled skid vehicle with active suspension (amenable to walking)

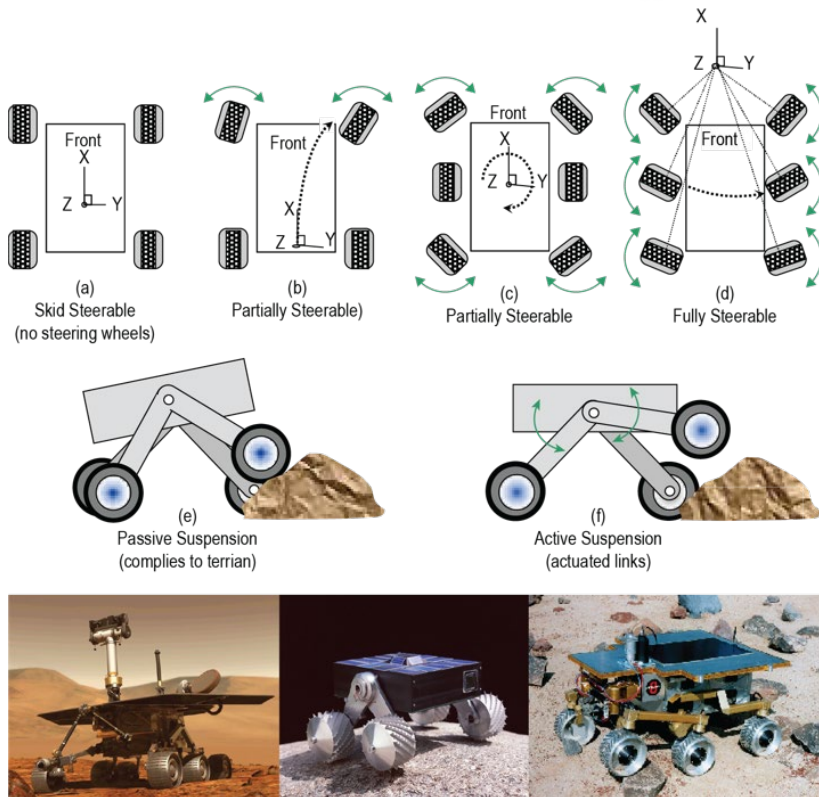


**Figure D-1.** Examples of different mobility configurations (drive wheels and steering) (top), active vs. passive suspension (middle), and examples from flight and research rovers (bottom). MER is a six-wheel-drive, four-wheel steering with passive suspension (bottom left), Nanorover is a four-wheel drive skid-steered vehicle with active suspension (bottom middle), and Rocky 8 is a six-wheel drive, six-wheel steering with passive suspension (bottom right).

**Table D-3.** Skid (no steering) pros and cons.

Pros	Cons
<ul style="list-style-type: none"> <li>• Has fewer actuators (no steering actuators)</li> <li>• Is amenable to larger wheels (no sweeping volume needed for steering)</li> <li>• Is not susceptible to steering failure</li> <li>• Is amenable to walking</li> <li>• Can steer and drive simultaneously (by differentially driving each side)</li> </ul>	<ul style="list-style-type: none"> <li>• Cannot position vehicle predictably (but may be able to use control to compensate)</li> <li>• Experiences high sinkage during turn-in-place</li> <li>• Slides downslope when turning</li> <li>• Turning is friction dependent</li> <li>• Uses more power (may be negligible)</li> <li>• Turning is sensitive to small terrain variation. Cannot turn with rocks adjacent to wheels (i.e., cannot steer wheels to roll over adjacent rocks)</li> <li>• Experiences higher wheel wear from turning</li> <li>• Has stability concerns if front/back wheels are closely placed*</li> <li>• Experiences high loads on frame (not quantified yet)*</li> </ul>

\* There is disagreement among subject-matter experts about these cons.

wheels for the non-steered wheels, which have the advantage of improved trafficability over rocky and loose terrains and without loss of maneuverability (Figure D-4). Table D-6 captures the trades associated with the configuration of large non-steerable wheels and smaller steerable wheels. Figure D-5 shows a prototype that preceded the LRV with larger non-steerable front wheels.

Vehicles with all-wheel drive, whether four-wheeled, or six-wheeled and so on, are capable of omni-directional driving, also known as crabbing. This additional maneuverability that comes at a cost of additional actuation offers functional redundancy and can handle a loss of a single steering wheel. The Spirit rover's maneuverability was impacted when the steering wheel froze at a fixed angle.

In all-wheel-steering vehicles, one can overcome such constraint by orienting the vehicle along the direction of the failed steering angle and then drive. Figure D-6 shows two examples of all-wheel steered vehicles with different suspensions. Table D-7 outlines the trade related to all-wheel (omni-directional) vehicles. Figure D-7 depicts a six-wheel drive vehicle with all-wheel steering, which is capable of arc-crabbing by rotating the vehicle around any single point in the plane it drives on. Table D-8 examines the trades associated with six-wheel omni-directional vehicles, such as the Rock 8 rover shown in Figure D-1.

**Wheel design:** We also examined wheel types and sizes (stiff vs. compliant, small vs. large), leveraging Apollo wheel-design data (Table D-11) [50-52]. Tracked vehicles were excluded from the trade due to their low-ground clearance, large mass, and high risks associated with rock entrapment in the tracks of lighter versions.

Larger wheel diameters with narrower widths were favored over smaller wider wheels because of their superior traverse performance (traction, energy efficiency, and obstacle traversal) [53]. Larger wheels have lower coefficient of rolling resistance and a larger contact area for the same wheel width, offering improved traction. When compared to a rigid wheel, compliant wheels have better performance in wear resistance and soft-regolith mobility and slightly better performance in rock traverses.

Larger wheels, however, require large sweep volumes to support vehicle suspension and steering motions, which impact vehicle design. However, for long traverses, large wheels undergo fewer actuator rotations, which extends their lifetime and reduces wheel wear.

**Rover selection:** Considering the traverse requirements (distance/speed) and the anticipated terrain properties (slopes, crater abundance, regolith, and other hazards) (Table D-2), designs with fewer

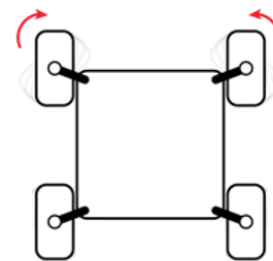


**Figure D-3.** Four-wheeled skid-steered vehicle with toe-in steering.

**Table D-4.** Skid with toe-in steering pros and cons.

Pros	Cons
<ul style="list-style-type: none"> <li>• Is amenable to using large wheels for better traversal</li> <li>• Enables turn-in-place for predictable pointing</li> <li>• Eliminates many cons of skid-steered vehicles</li> </ul>	<ul style="list-style-type: none"> <li>• Does not offer more benefit over same design with full front-wheel steering</li> <li>• Increased number of actuators compared to skid while remaining a skid vehicle</li> <li>• Risks steering failure</li> <li>• Slides downslope when turning (unless you turn in place)</li> </ul>

**Table D-5.** Partial steering pros and cons.

Pros	Cons
<ul style="list-style-type: none"> <li>• Improves maneuverability (allows arc drives) – all wheels moving in the rolling direction</li> <li>• Improves directionality for driving on slopes</li> <li>• Requires only partial steering</li> <li>• Steering fails gracefully to skid steer</li> </ul>	<ul style="list-style-type: none"> <li>• Requires more actuation than and complexity than skid-steered vehicles to support steering</li> <li>• Needs large sweep volume for steering</li> <li>• Is less amenable to large wheels (requires a large sweep volume that moves with the suspension)</li> </ul>

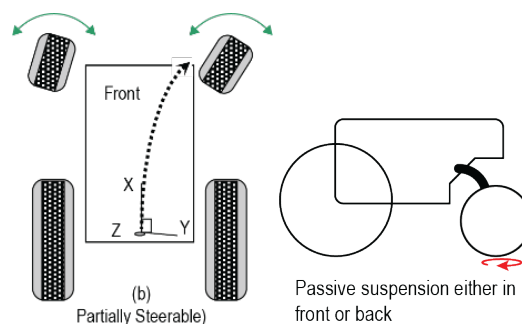


**Figure D-4.** Partially steerable vehicles with different sized wheels.

**Table D-6. Partially steered: race car/tractor pros and cons.**

Pros	Cons
<ul style="list-style-type: none"> <li>Improves back-wheel rock traversal (rough terrain)</li> <li>Can house rear actuators inside thermally controlled electronics box</li> <li>Is volumetrically compact</li> <li>Improves maneuverability over skid; provides directionality for driving on slopes</li> <li>Has fewer actuators than fully-steerable</li> <li>Fails gracefully to skid steer</li> <li>Could be more energy efficient with larger wheels (requires further analysis)</li> </ul>	<ul style="list-style-type: none"> <li>Has higher cost due to different front/rear actuator gear-train types</li> <li>Has more actuation and complexity than skid</li> <li>Needs large sweep volume for front steering</li> <li>Has some drawbacks to being asymmetric:                             <ul style="list-style-type: none"> <li>Uneven performance for bi-directional mobility</li> <li>Could lead to higher structural mass</li> <li>May be more susceptible to tip over when compared to using equal-size wheels</li> </ul> </li> </ul>



**Figure D-5.** An example of a lunar rover prototype with different sized front and rear wheels: the Local Scientific Survey Module (LSSM) developed in 1965 by Brown Engineering (NASA).

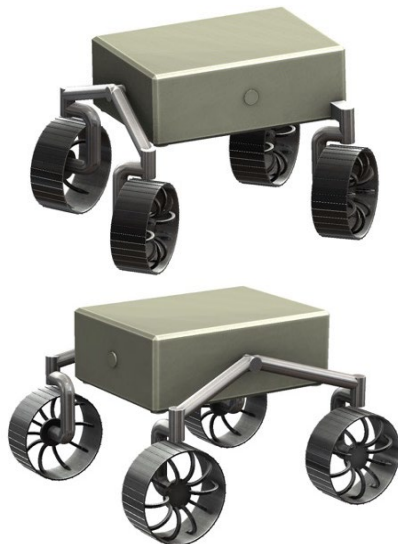


**Figure D-6.** Examples of a four-wheel drive, all-wheel steering vehicle with front rocker (top) and a side rocker (bottom).

wheels offers several advantages. They have: (1) enhanced maneuverability with fewer steering actuators, (2) lower mass with less complex mechanisms, and (3) lower power and higher energy efficiency compared to rovers with more wheels.

As such, a four-wheeled design with all-wheel steering was favored over six-wheel designs. Among the four-wheeled vehicles with large narrow wheels, three designs emerged as contenders for the baseline: (1) a four-wheeled vehicle with one-sided toe-in steering, (2) a four-wheeled vehicle with one-sided full-range steering, and (3) a four-wheeled vehicle with two-sided full-range steering. Each of these configurations offer non-skid steering for improved heading control and non-skid driving, which is necessary for maneuvering on rocky crater rim slopes and for pointing and placing instrument on targets. The first two options allow for even larger wheel diameters and fewer actuators since the wheels on one side do not steer. However, option (3) with its all-wheel drive, all-wheel steering is selected for the baseline because it affords some steering redundancy and has improved maneuverability for negotiating terrains around crater rim. The vehicle is designed to drive and steering in either directions. With all wheel steering, the rover can also drive sideways at different angles. Descoptes reduce the design to option (2).

A four-wheeled vehicles requires only a single passive degree-of-freedom to ensure that all wheels remain in contact with the terrain and support equal weight on each wheel. While a three-wheeled vehicle conforms to the terrain without any suspension, it is less stable, risking tip over. INSPIRE's suspension uses a dual-sided rocker with a single passive degree of freedom.

**Table D-7. Crabbing (full steering, omni-directional, four-wheels) pros and cons.**

Pros	Cons
<ul style="list-style-type: none"> <li>Allows fine positioning</li> <li>Can tolerate a single steering failure with minimal impact on mobility</li> <li>Allows changing drive direction on steep slopes</li> <li>Has improved maneuverability for getting out of trouble (out of a rut if rover slides into it)</li> </ul>	<ul style="list-style-type: none"> <li>Is not amenable to very large wheels</li> <li>Steering sweeps large volumes</li> <li>Has more actuation than partially steerable</li> <li>Forces either a higher center of gravity to accommodate the large wheels or forces the wheels out to accommodate the sweep volume for steering.</li> </ul>



The two rocker mechanisms that pivot on the left and right sides of the vehicle are connected to each other by a differential mechanism that kinematically couples them under the vehicle chassis, resulting in a single passive degree-of-freedom suspension. With this mechanism, a motion on one rocker (one side of the vehicle) causes the opposite motion on the other side. The dual rockers were selected over a single front rocker, like the one chosen for the Intrepid rover, primarily to accommodate INSPIRE’s redundant drills and instruments, which are mounted on or near the front side of the rover. The dual-sided rocker has the benefit of minimizing the side-to-side rolling when traversing rocky or undulated terrain, compared to a single rocker design. However, that benefit comes at a cost of a slight increase (<10%) in the mass of the mobility subsystem.

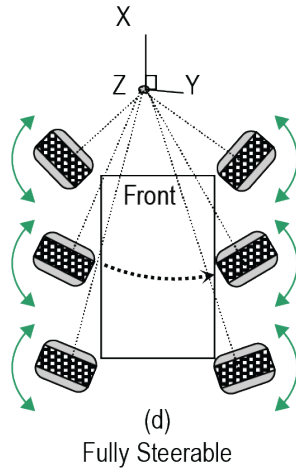


Figure D-7. Figure caption.

The baseline uses large-diameter compliant wheels to improve rock traversal, traction on regolith, and energy efficiency [50, 52, 53]. The 0.8 m-diameter wheels use a mesh structure, similar to the LRV, to traverse rocks that are less than 0.3 m in height and drive through smaller craters not apparent in orbital data (<5 m in diameter with slopes below 10°). The vehicle is designed with a ground clearance of > 0.6 m.

The drive wheels use magnetic detent in lieu of brakes to reduce power draw and increase robustness to failures. Steering wheels do use brakes nor detent to minimize power draw and maintain smooth steering motions. The rover is designed to drive in either direction supported by front and back stereo cameras.

Table D-8. Crabbing (full steering, six wheels) pros and cons.

Pros	Cons
<ul style="list-style-type: none"> <li>Additional drive wheels allow improved traction on steep, rocky, and fine regolith terrains</li> <li>Allows fine positioning for arm placement</li> <li>Can tolerate a single steering failure with minimal impact on mobility</li> <li>Allows changing drive direction on steep slopes</li> <li>Has improved maneuverability for getting out of trouble (out of a rut if rover slides into it)</li> </ul>	<ul style="list-style-type: none"> <li>Is not amenable to large wheels</li> <li>Requires more complex suspension design (larger mass)</li> <li>Steering sweeps large volumes</li> <li>Has more actuation than partially steerable</li> <li>Forces either a higher center of gravity for large wheels or forces the wheels out to accommodate sweep volume for steering.</li> </ul>

Table D-9. Wheel design.

Pros	Cons
<b>Wheel diameter (large vs. small)</b>	
<ul style="list-style-type: none"> <li>Larger contact length and area for same width (key)</li> <li>Lower coefficient of rolling resistance</li> <li>Lower wheel contact angle</li> </ul>	<ul style="list-style-type: none"> <li>Large steerable wheels sweep large volumes (larger accommodations)</li> <li>Large wheels are harder to turn</li> </ul>
<b>Wheel width (narrow vs. wide)</b>	
<ul style="list-style-type: none"> <li>Lower mass with lower impact on mobility performance</li> </ul>	<ul style="list-style-type: none"> <li>Lower ground pressure, but that is no longer a good metric to use</li> </ul>
<b>Grouser (stiff vs. compliant)</b>	
Third order effect	
<b>Further requires analyses</b>	
Quantifying impact of wheel diameter/width on power, energy, thermal, wear, and mass for long lunar traverses	

Table D-10. Summary of mobility trades, selection, and rationale.

	Key Trades	Selection	Rationale
Type	Wheeled vs. tracked	<b>Wheeled</b>	Lower mass, larger ground clearance and lower risk of rocks entrapment
Configuration	<u>Drive + steering wheels:</u> 3-wheel (1 steering) 4-wheel (0 steering) 4-wheel (2 steering) 4-wheel (4 steering) 6-wheel (4 steering) 6-wheel (6 steering)	<b>4-wheel (4-steering)</b>	Adequate stability (low tip-over risk) and best maneuverability at lower mass and power; resilient to single-steering failure.
	<u>Suspension:</u> Active vs. passive vs. spring-loaded	<b>Passive</b>	Balanced weight on wheels, lower mass and volume in rover body, fewer failure modes, adequate for expected terrain difficulty and rock traversal. Dual-sided rocker to accommodate sampling.
Wheels	Dual-sided rocker vs. single-sided rocker	<b>Dual-sided rocker</b>	
	<u>Diameter:</u> Large vs. small <u>Narrow vs. wide</u> (large: ~1½ x MSL) (narrow: ½ x MSL) <u>Rigid vs. compliant</u>	<b>Large Narrow</b>  <b>Compliant</b>	Superior traction, energy efficient, enhanced obstacle traversal; fewer rotations and terrain contacts for longer life.  Improved mobility in soft regolith and over rocks, improved wear resistance










informed by subject matter experts that drew from prior analyses, designs, implementations, and lessons learned.

Figure D-10 rolls up a comparison of the aforementioned trades and maps them to flight and research rovers.

Number of wheels Suspension		Four								Six				Comparative Criteria
		Passive				Active				Passive		Active		
		Skid Steered	Toe-in Steered	One-sided Steered	All-wheel Steered	Skid Steered	Toe-in Steered	One-sided Steered	All-wheel Steered	Partial Steered	All-wheel steering	Partial Steered	All-wheel steering	
Design	# of actuators	4	6+	6	8	6	8+	8	10+	10+	12	14+	18+	<div style="display: flex; flex-direction: column; gap: 5px;"> <div><span style="color: green;">■</span> Most favorable</div> <div><span style="color: orange;">■</span> Moderately favorable</div> <div><span style="color: red;">■</span> Least favorable</div> </div>
	Is amenable to large wheels													
	Generates high loads on mechanisms													
	Complexity													
Failure	Benefits from asymmetric wheels													
	Robust to steering failure	N/A				N/A								
Maneuvering	Wheel wear from turning													
	Handling turns (sinkage)													
	Handling turns (w/ rocks, topo on the side)													
	Handling longitudinal slopes													
	Handling lateral slopes													
	Omni directional mobility (crabs)													
	Controlability and positioning													
	Amenable to walking (e.g., out of high sink areas)													
Examples	Complexity of control algorithms													
	Examples of current flight or research rovers	ATRV Jr*		Apollo-LRV+	<b>INSPIRE†</b>	Scarab	Lunokhod		VIPER Robosimian	MER Curiosity‡	Athena	ExoMars ATHLETE		

**Figure D-10.** Summary of the mobility trades for INSPIRE mobility systems, which would traverse shy of a thousand kilometers across relatively benign polar lunar terrain. Bold in the examples are flight rovers while non-bold are research rovers; +LRV uses spring in lieu of passive suspension; † includes Intrepid and Endurance; ‡ includes Perseverance, Yutu, Yutu-2.

**Table D-11.** The Development of a Moon Rover [51].

Criteria	Relative Value Factors								
		Rigid Wheel	Pneumatic Tire	Wire Mesh Tire	Metal-elastic Tires		Elliptical Wheel	Hemi-spherical Tire	Hubless Wheel
Mechanical Reliability	15	90.0	67.5	75.0	70.5	70.5	25.5	60.0	28.5
Weight	14	92.0	46.2	121.8	35.0	63.0	14.0	81.2	7.0
Soft Ground Performance*	14	53.0	101.5	101.5	121.1	121.1	114.8	116.4	121.1
Obstacle Performance**	10	68.0	74.0	74.0	64.0	64.0	68.0	74.0	64.0
Steerability	6	43.8	34.8	34.8	12.0	12.0	24.6	39.6	12.0
Ride Comfort	13	ZERO	104.0	117.0	39.0	65.0	78.0	26.0	39.0
Stability	8	64.0	56.0	56.0	22.4	45.6	34.4	56.0	22.4
Wear Resistance	8	24.0	12.0	42.0	48.0	48.0	48.0	42.0	48.0
Environment Compatibility	6	48.0	ZERO	36.0	42.0	42.0	36.0	36.0	18.0
Development Risk & Cost	6	64.0	8.0	48.0	48.0	48.0	24.0	32.0	16.0
Total	100	Eliminated	Eliminated	706.0	502.0	579.0	467.0	553.0	376.0

\*Includes Slopes and Slip.

\*\*Includes vertical obstacles and crevasses.

## E AUTONOMY

### Summary of Driving Requirements

To characterize the volatiles on the surface and within the shallow subsurface across the identified permanently shadowed regions, the rover has to traverse over 900 km and conduct its science operations in less than four years. For this pre-planned route, 70% of the driving has to occur in darkness either during the lunar night or in the PSRs. At each of the 62 Science Stations, the rover maps 10% of a 300 m × 300 m area to identify the desired drilling site. Given the limited number of Science Stations, the 16-hour science-intensive drilling operation can be executed with ground in the loop across two ground shifts to assess the science and guide the drilling process. To identify the appropriate operations mode and the necessary degree of autonomy for the traverse, we examined trades that ranged from ground-based human control to onboard autonomous driving.

### Summary of Constraints

Key constraints that determine the viability of the operations modes include: (1) the visibility and availability of lunar relay orbiter and associated ground stations, (2) the uplink and downlink bandwidth and latency of the communication infrastructure from the lunar rover to the ground operations center, (3) the cadence of rover motions (traverse and instrument placement) throughout the lunar day and night, and (4) the nominal operations schedule. The baseline communication system through the lunar orbital asset has a downlink bandwidth of 2 Mb/s when the rover is idle and 1 Mb/s when the rover is driving and an uplink bandwidth of 128 kb/s for both. The visibility of the communication orbiter is 9 hours every 12 hours and its availability is assumed to be at 50%, resulting in a communication window of 4.5 hours every 12 hours. The availability is based on assuming that this mission would not be the only one supported by the orbital asset but is one that would secure 50% of the time on that orbiting asset. The round-trip latency was estimated at 60 seconds given the multiple communication hops and the overhead for moving the telemetry through.

### Operations Trades

To identify the required level of autonomy, we examined trades from ground-based human control, similar to the joystick operations of the Lunokhod rover back in the 1970s, to onboard autonomous control for mobility, instrument placement and system management. The trades are summarized in Table E-1.

Figure E-1 and Table E-2 summarize the required operations and operational constraints in a lunar day and night for two representative examples. Sustained *human control* under the communication latency induces fatigue [54] and was deemed too cognitively taxing and not viable for the four-year operations period. *Human decide* and *ground compute* modes were also not viable because they are unable to meet even the average traverse. Table E-2 estimates the throughput based on sensors' dataflow, onboard computation performance, and communication bandwidths. Leveraging ground-based computing infrastructure (*ground compute*) to supplement the onboard computing does not offer an advantage due to the communication availability and bandwidth. As a result, this mission has to rely on *onboard decide* for a significant portion of its nominal operations and on the *human decide* for off-nominal operations that cannot be handled by the onboard system. Percentages of ground-in-the-loop driving that were used in calculating mission duration are captured in Table G-9. These percentages were based on terrain slopes, where driving on higher slopes are more likely to engage ground operators.

As shown in Figure E-1, after mission operations transition to an Earth-based schedule, traverse would inevitably fall outside the nominal operations schedule. Therefore, a significant portion mobility has to be conducted through autonomous operations.

As shown in Figure E-1, after mission operations transition to an Earth-based schedule, traverse would inevitably fall outside the nominal operations schedule. Therefore, a significant portion mobility has to be conducted through autonomous operations.

Special accommodations would be necessary for the drilling operations to align with Earth-day shifts. The drilling operations have significant ground engagement<sup>1</sup> when compared to mobility.

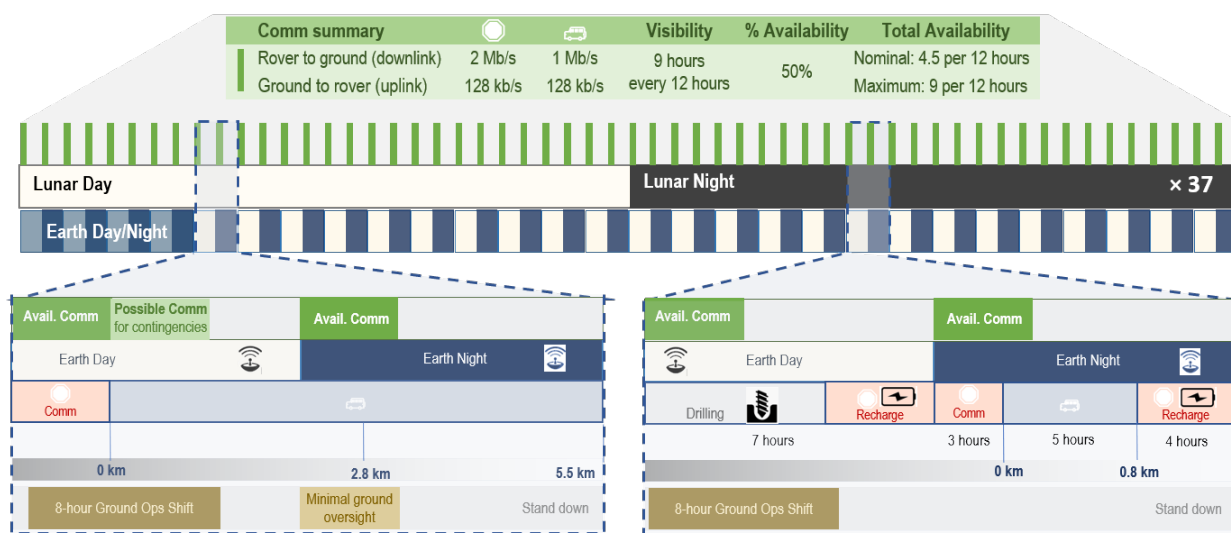
### Autonomy Requirements

Table E-3 captures the required capabilities for INSPIRE’s autonomous operations, which encompass surface navigation and system management. Autonomous navigation includes perception, hazards assessment, path planning, relative pose estimation, and global localization. While the maximum mechanical speed of the rover is 1 km/hour, the maximum operational speed during the traverse will be at 0.36 km/hour, which is constrained by the neutron spectrometer measurements. Portions of the route that enter and exit the large craters, such as Faustini and Shoemaker, may not be constrained by instrument measurements as the rover may not be acquiring measurements while entering and exiting these large craters.

For autonomous and ground-assisted navigation, the rover would have to perceive its surrounding environment during the day and at night (or in PSRs) with a horizon of at least 10–15 meters. Perception for day driving and near-horizon night driving (0–5 m) can be achieved while the rover is moving. However, depending on the sensing modality, long-range night driving may necessitate stops for long exposures of the sensors. The maximum day/night traverse rates capture the rover

**Table E-1. Operations modes and trades.**

Mode	Downlink	Ground	Uplink
<b>Human control</b>	Stereo imagery and rover telemetry	<b>Human</b> assesses and controls rover, arm, and instruments	Actions for every step
<i>Sustained human control was deemed too cognitively taxing and not viable to sustain for the four-year operations (24/7).</i>			
<b>Human decide</b>	Stereo imagery and rover telemetry	<b>Ground computer</b> assesses and generates actions. <b>Extensive synchronous human selection/oversight.</b>	Actions for every step
<b>Ground compute</b>	Stereo imagery and rover telemetry	<b>Ground computer</b> assesses and generates actions autonomously. <b>Limited asynchronous human oversight.</b>	Actions for every step
<i>Human decide and ground compute modes were also not viable because they are unable to meet even the average traverse. Leveraging ground-based computing infrastructure (ground compute) to supplement the onboard computing does not offer an advantage due to the communication availability and bandwidth.</i>			
<b>Onboard decide</b>	Thumbnail imagery and rover telemetry	<b>Onboard computer</b> assesses and generates actions autonomously. <b>Limited asynchronous human oversight.</b>	Route plan and goals
<i>Onboard decide was the only viable option for nominal operations. Contingencies and off-nominal operations can leverage ground-based human decide option.</i>			



**Figure E-1. Examples of operations from a lunar day and night across an Earth day that shows drive and drilling operations with communication constraints and operations shifts.**

<sup>1</sup> During sampling operations that only occur during the lunar day, the science team would be engaged in all key drill-related decisions: site selection, incremental drilling, measurements of cutting, repeated drilling.



**Table E-2.** Assessing viability of ground-based compute mode.

Mode	Time for human confirmation (s)	Distance between onboard images (m)	Distance between images sent to ground (m)	Image Resolution (pixels)	Traverse Rate (m/hour)		Required Traverse Rate (m/hour)		
					Possible (comm visible)	Possible (comm not visible)	Daytime	Nighttime	
<b>Nominal Comm Window:</b> 4.5 hours per 12-hour period					<b>Downlink Rate:</b> 📶 2 Mb/s 🚗 1 Mb/s				
Ground Compute	60	1.7–2.3	10-m drive steps	1280×960	208	0	Effective 600	Effective 300	
				640×480	219	0			
Onboard decide	N/A	1.7-2.3	continuous drive	128×96 thumbnails	1,018	1,018	Max 900		
<b>Backup Comm Window:</b> when nominal comm not visible					<b>Downlink rate:</b> 📶 200 kb/s 🚗 100 kb/s				
Ground Compute	60	1.7-2.3	10-m drive steps	1280×960	119	0	Effective 600	Effective 300	
				640×480	183	0			
Onboard decide	N/A	1.7-2.3	continuous drive	128×96 thumbnails	1,018	1,018	Max 900		

speed between engineering stops, while the average traverse rate include engineering stops for long-exposure night imaging (every 10 m) and localization (every 300 m). Estimated traverse rates on different slopes are captured in the detailed traverse analysis described in Appendix G.

Throughout, the rover has to plan and manage its shared resources and monitor its health while executing its day/night traverses. The long-traverse path necessitates a level of reliability in autonomous surface navigation to complete the mission within the targeted duration. To keep the mission duration within the margined four years, the rover would have to demonstrate a level of reliability that can meet specific mean-distance-between-faults and mean-time-to-recover. The performance metrics for autonomous surface navigation are summarized in Table 4-2 based on the analysis described in Appendix F.

### Sensor Trades, Selection, and Placement

Sensors selection and placement are critical to establish situational awareness for operating the rover. Sensors are selected and mounted on the rover to support both autonomous and ground-assisted operations, simplify operations, provide adequate sensing coverage with minimal articulation of the mast, and offer robustness through functional of physical redundancy (see Redundancy Section).

Tables E-4 and E-5 examine the perception trades of passive (cameras) and active imaging (LIDAR). Stereo cameras in the visible range are selected over LIDAR options (both spinning and flash) and Near-Infrared cameras for traverse and arm operations. Despite their superior 3D range and being agnostic to sun angle and shadows, LIDARs require higher power, have limited resolution in, at least, one dimension (vertical for spinning), and are currently at a lower TRL for lunar surface applications than cameras. Lunar regolith tend to be more reflective in the near infrared but NIR

**Table E-3.** Autonomy Requirements.

	Requirement	Description
Surface navigation	Effective Rate	0.36 km/hour max during daytime; 0.23 km/hour max during nighttime
	Hazard assessment	Detection and avoidance for all hazards that include: terrain topography (positive: untraversable rocks, negative: deep depressions or craters), lateral slip toward a terrain hazard, sink hazards in soft terrain
	Path planning	Route path around hazards
	Pose estimation	Estimation of delta motion of the rover
	Global localization	Registration of rover position relative to orbital maps
System	Health management	Continuously monitor the health of the hardware and software components
	Resource management	Plan and schedule activities based on intent and available resources

**Table E-4. Active imaging pros and cons.**

Pros	Cons
<b>LIDARs</b>	
High range	High power
High accuracy at range	Low TRL for lunar environment
Works at night	Higher cost
Data can be used for science	Laser life
Agnostic to shadow	Localization accuracy
Agnostic to sun angle	Dust accumulation on optics
Could filter out dust (like snow from blizzard in terrestrial apps)	Motion distortion
<b>Spinning LIDAR</b>	
360° coverage (no mast articulation)	Low vertical resolution Moving parts
<b>Flash LIDAR</b>	
	Small FOV (50° –60°)

**Table E-5. Passive imaging pros and cons.**

Pros	Cons
<b>Stereo vision</b>	
Low power	Texture dependent
No moving parts	Limited range (especially with night imaging)
High heritage (TRL9 hw/sw)	Dependent on incident/phase angles
High-density point cloud	Lens distortion for WFOV lenses
Intensity + 3D data	Requires calibration
Data can be used for science	Requires large computation and memory for stereo
Dust tolerant (quantified by MS <sup>3</sup> )	Motion smear/blur at higher speeds
Functional redundancy (SfM)	

**Table E-6. Internal sensing. Limited options for low-mass, low-power, reliable long-duration Class B IMUs.**

	Power	Mass	Rationale
MIMU	22 W ave 32 W max	4.5 kg*	High mass and power compared to other options. Used on M2020 EDL; baselined for Mars Sample Return Ascent Vehicle
LN200**	15 W	0.6 kg	Has reliability problems; will be discontinued
ASTERIX 120	6 W × 3	6.5 kg	Large mass
Siru	43 W max	5.5 kg	High cost; used for classified work
SmallSat IMUs	1.5 W ave 2 W max	0.06 kg	Not available in Class B (e.g. STIM300)
Accels only			Allows recovery of rover tilt, but without gyros, rover loses ability to accurately control its heading.

tem. The stereo cameras on both sides of the rover improve situational awareness and enable bi-directional rover driver. The redundant stereo pairs on each rover side preserve functional through a fully redundant pair for both driving directions.

cameras are usually less optimal overall. The plan is to select a visible-range camera that has the best NIR response among that class of cameras.

Redundant high-resolution stereo-camera pairs with 90° field-of-view lenses and a ~25-cm baseline are mounted on either end of the rover to accommodate driving in either direction. These parameters are based on relevant analysis that was conducted for the Perseverance rover to improve rover perception when compared to its predecessors. The wide field of view allows rover navigation without the need to articulate and point the mast during nominal traverses. At the maximum traverse rate, short exposures (~10–20 ms) allow imaging-while-driving during the lunar daytime. At night, the rover flashes its LED lights for short-exposure imaging while driving (1.7–2.3 m/image) and stops its drive every 10 m for long and multiple-exposure imaging with enough time to allow mast slew for mini-panoramas (imaging the sides of the rover in addition to the front). Approaching and placing instruments on regolith and rocks at night would use the same capabilities as those during the daytime, supported by rover-based lights.

With the cameras mounted at ~1.5 m off the ground, articulated covers for the camera lenses are not necessary.

Table E-6 captures the trade for inertial sensors, which are used for pose (position and attitude) estimation of the rover. Selection favored low mass and power options.

In addition to the perception and inertial sensors, all actuators use hall-effect sensors in lieu of encoders to estimate and control wheel/joint motions. Hall-effect sensors are more tolerant to higher temperatures experienced by components outside the thermally managed electronics box. In addition to these relative-position sensors, the steering and arm joints use resolvers on the joint outputs for absolute positioning. Torques on the wheels and arm are inferred from the motor winding currents and is sufficient since the arm does not require contact for instrument placement.

## Redundancy

The INSPIRE rover features numerous physical and functional redundancy ensuring a robust sys-

In addition to these physical redundancy of the two front and two rear stereo cameras, 3D information can also be generated using functional redundancy from a single camera using structure-from-motion.

The compute elements, motor controllers, and IMU are also redundant. For pose estimation, the rover uses both visual odometry as well as wheel and inertial dead reckoning, providing some overlap sensing modalities.

## Autonomy Functions

**Surface Navigation:** The MER and Curiosity rovers have enhanced their mobility with autonomous navigation [55]. INSPIRE's autonomous surface navigation leverages flight-operational capabilities from both missions, which have been further advanced for faster traverse on the Perseverance rover. These capabilities have been developed for daytime only operations. INSPIRE would have to adapt and addressing technology gaps associated with night/PSR driving, pose estimation, and localization. It will also have to increase the performance of autonomous day/night operations.

Based on the trade described in the next section, the INSPIRE rover requires, in the nominal case, reliable autonomous day and night surface navigation with intermittent ground oversight in nominal cases and human-directed actions in off-nominal cases that cannot be addressed onboard. The Perseverance rover transitioned autonomous navigation from an enhancing capability to an enabling one, resulting in increased performance. Terrestrial autonomous driving, which was boosted through DARPA's off-road and urban challenges [56, 57], similarly increased in performance (mean-distance between faults) through focused and sustained industrial investment. Similarly, INSPIRE would need a focused technology investment to mature the integrated functions to a higher degree of performance as discussed in §4.2. Unlike Mars though, for off-nominal situations that cannot be resolved by the onboard system, the relatively low-latency communications (60 seconds roundtrip) and the 75% visibility of the communication orbiter (assuming 100% available for off-nominal situations), allow ground operators to more rapidly interrogate, diagnose, and respond to faults or failures. A fault is a physical or logical cause, which explains a failure. A failure is the unacceptable performance of an intended function.

**Global localization:** Global localization requires knowledge of rover position relative to a global reference frame, which is coupled with knowledge of heading. Heading knowledge also serves antenna pointing, but this is not a driver with the relatively wide antenna beams; therefore, heading knowledge requirements and trades were assessed as part of meeting position knowledge requirements.

Position knowledge error will likely be on the order of a few meters per 1,000 m of traverse in order to see science targets identified from orbital maps in the rover imagery. However, tighter requirements derive from rover hazard avoidance processes. Rover navigation follows routes designated with orbital imagery and must respect human-specified keep-in and keep-out zones, which keep the rover safely away from navigation hazards that are visible from orbit. In case of PSRs, only low-resolution DEMs are available on the order of 5–10 m/pixel. Upcoming missions, such as Lunar FlashLight and ShadowCam, are expected to generate higher resolution images of PSRs (but not DEMs) (ShadowCam is expected to produce images at 1.7 m/pixel). The most frequent hazards on the Moon are craters; absolute position knowledge on the order of the smallest crater reliably detectable from orbit (5 m diameter in lit areas and TBD m in PSRs) is required at all times to respect these zones.

Potential sources of absolute position knowledge include radiometric sensing from lunar relay orbiter if they are equipped with such capability, co-registration of digital elevation maps (DEMs) created onboard the rover to DEMs created from orbit, recognizing and co-registering skyline landmarks, and recognizing crater landmarks near the rover. In between absolute position corrections, relative position updates are possible from wheel odometry, visual odometry, and an inertial measurement unit (IMU). Potential sources of absolute heading knowledge include sensing directions to the sun, the Earth, and stars; relative heading updates are possible from an IMU and from wheel and visual odometry.

Since INSPIRE will be traversing distances during both the lunar day and night, both sun sensors (e.g., Adcole pyramid-type coarse sun sensor) and star trackers are used for correcting absolute heading during the day and night respectively. It is possible to only rely on star tracker for both day and night heading corrections. A typical star tracker would operate with the sun within  $26^\circ$  of boresight and  $18^\circ$  of Earth. It is possible to operate a star tracker with decreased accuracy with the Earth in the FOV. The Sun exclusion angle can also be made smaller with bigger baffles. By pointing the redundant star trackers in different directions (or changing the rover's heading), it is possible to avoid the Sun in at least one of the sensors at all times. Since the rover's absolute heading would not be adequately known, it is not possible to always avoid the sun in the star tracker's FOV. However, having the sun in a star tracker's FOV would not damage the sensor.

To correct for absolute position, in addition to the necessary aforementioned absolute heading correction, surface landmarks detected from the rover stereo cameras are be matched with orbital maps to correct dead reckoning errors from relative updates of wheel odometry, visual odometry, and the IMU. Example of landmark detection is detecting  $\sim 10$  m diameter craters, which appear every  $\sim 100$  m along the route.

**System-level autonomy:** The long traverse requires a level of reliability that exceeds that of prior Mars missions. It also requires both day and night operations. System health, shared resource and activities are managed using an onboard autonomous system that can plan activities based on intent from the ground, available onboard resources, and the health of the components of the systems. Critical to the operations of the INSPIRE rover is the system integration of several functional elements into an autonomous system and the maturation of all its constituents to achieve the necessary overall reliability for this long-distance mission. Over the years, both space and terrestrial applications have incrementally increased their level of autonomy. Fault protection is integrated with the system manager to handle both nominal and off-nominal conditions through the same control-flow. Robustness of performance both at the function and system levels for a range of uncertainties is critical to successfully meet the objectives of the mission. Similar to autonomous mobility, system management (resource/activity planning and system-health management) leverage decades of technology development and demonstrations on terrestrial prototypes [2008 CLARAty]. Aspects of these capabilities have also been or will soon be demonstrated in flight [Mars2020 Simple Planner].



## F AUTONOMY RELIABILITY

To assess the required autonomous traverse performance for long-distance lunar roving for INSPIRE, Endurance, and Intrepid, we studied data from past Mars rovers (the MER rovers and Curiosity) and created a simulation to investigate the effect of drive interruptions on planned the planned traverse. While the conditions that triggered drive interruptions for these past, largely non-autonomous drives, would be different from those anticipated for INSPIRE, the analysis remains valuable in that it represents mobility interruptions of a rover traversing a route planned in orbital imagery, a surface vehicle traversing a planetary surface with uncertainties in the terra-mechanical properties, perception from rover-mounted stereo cameras, and a mobility control system designed for a Class B mission. INSPIRE’s autonomous traverse would exhibit a different set of interruptions related to limitations of perception with LEDs at night, limitations due to lower orbital resolutions in PSRs, and limitations of the algorithms themselves, but in the absence of that information, we examine the cadence profile and impact of interruption recovery on the mission timeline.

**Past Mars rovers:** We analyzed faults that resulted in an incomplete traverse of the Curiosity rover, which has been operating on Mars since August 2012. This reports Curiosity drove a total of 21,318.5 meters during its first seven years, in 738 drives ranging in length from 2.6 centimeters to 142.5 meters. Of those, 622 completed successfully, 26 were halted by time (the end of the driving day occurred before it could cover the over-ambitiously set planned distance), 25 were not allowed to start due to rover conditions (e.g., the robotic arm had not been stowed at the end of the preceding science), and the remaining 65 were interrupted during driving for the reasons shown in Figure F-1. Each such interruption terminated the rover’s drive, requiring operators on Earth to diagnose the situation and develop a plan to resume driving on the next sol (Mars day) that a drive was requested.

We are interested in similar interruptions to INSPIRE’s autonomous driving, those requiring operator intervention. However, the majority of the time Curiosity was not being driven completely autonomously. Instead, operators planned the route the rover would drive over the next Sol (or sometimes several Sols), and estimated the terrain conditions (e.g., slope) it would experience. When Curiosity then followed this route, any conditions causing exceedances of the rover’s self-monitoring (e.g., tilt) would interrupt the drive, after which Curiosity made no attempt to autonomously recover. Since operators were predicting terrain conditions from already returned camera images, accurate estimation at longer distances was challenging, and the primary cause of drive interruptions.

We also looked history of the two MER rovers to see the trend in software anomalies due to all causes (not just those triggered by driving). The data shows that *within a few months of operation, the frequency of anomalies drops by an order of magnitude.*

### Simulating drive interruptions:

INSPIRE’s science plan calls for approximately 26 unmarginated lunar days and nights of activities. A typical day involves a long autonomous drive (~20 hours) followed by a four-hour telecom/charging period. The rover drives significant distances during both the lunar day and night, with 70% of the route distance covered at night or in a PSR. The distance between stops varies since the effective traverse rate is based on the time of the day (day/night), the terrain slope and direction (upslope vs. downslope), the hazard density, and the engineering stops that are needed for localization and for long-exposure imaging to the visible horizon at night.

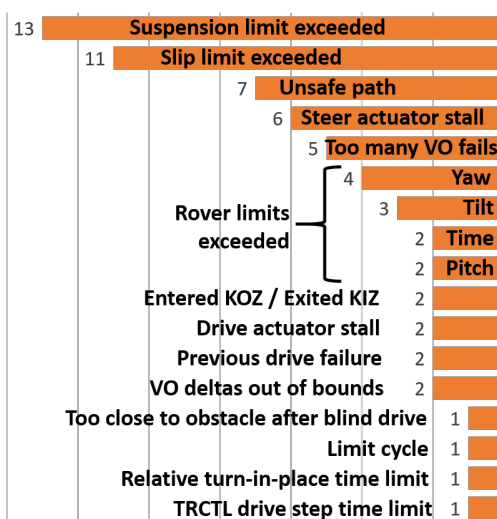


**Figure F-1.** Causes of interruptions to Curiosity’s drives. KOZ/KIZ = Keep Out/In Zone; TRCTL = Terrain-adaptive wheel speed control; VO = Visual Odometry.

The INSPIRE rover is designed to autonomously drive between locations, *i.e.*, without guidance from operators back on Earth. As it does so, INSPIRE’s driving software continually checks for anomalous conditions, its response to which is to: cease movement; transmit data at the earliest opportunity on its condition and surroundings to Earth; and rely on the operators to analyze the situation and direct INSPIRE’s actions necessary to recover and resume driving. Such interruptions consume time, and depending on how frequent they are and how long it takes the operators to direct recovery, the lunar day’s schedule may not be attainable. We simulated interruptions and their effects on this schedule based on two key parameters, as follows:

*Interruption rate:* we used a distance-dependent rate of interruptions, characterized by the mean distance between interruptions. Figure F-2 plots the distribution of interruption distances (in km) from a sample of 10,000, based on a mean of 10 km.

*Recovery time:* we used an exponential distribution of recovery times, with a minimum of one hour, characterized by the mean recovery time. Figure F-3 plots the distribution of recovery times (in hours) for a sample of 10,000 based on a mean of 5 hours.

The simulation mimics an entire mission based on the detailed science plan’s daytime drives (distances and speeds) and science stops (minimum stop times). In each Monte Carlo run of the simulation, drive interruptions occur as drawn from the interruption distribution, incurring a delay whose length is the time drawn from the recovery distribution. Inability to get to a daytime stop with night driving hours counts as a “failed” lunar day, requiring an extra lunar day to be spent getting there, after which the mission continues. The outcome of a Monte Carlo simulation run is the count of such “failed” lunar days.

The science planners had recognized that some of the lunar days have ambitious schedules, and indicated in the detailed science plan a few instances where science stops could be skipped if behind schedule, and where there would be flexibility to carry out a night stop short of its planned location. The simulation takes these into account. It is plausible that further refinement of the science plan will occur based on understanding of the remaining most challenging lunar days.

Figure F-4 shows results of simulation runs for combinations of mean recovery time and mean distance between interruptions. Each small dot and number to its right reports the result of 10,000 Monte Carlo simulation runs. The number indicates that over the Monte Carlo runs, 90% of them had no more than this many “failed” lunar days. Blue lines connect points of zero “failed” lunar days, red lines connect points of three, and green lines connect points of six. These results show, for example, that to have zero “failed” lunar days 90% of the time could be achieved

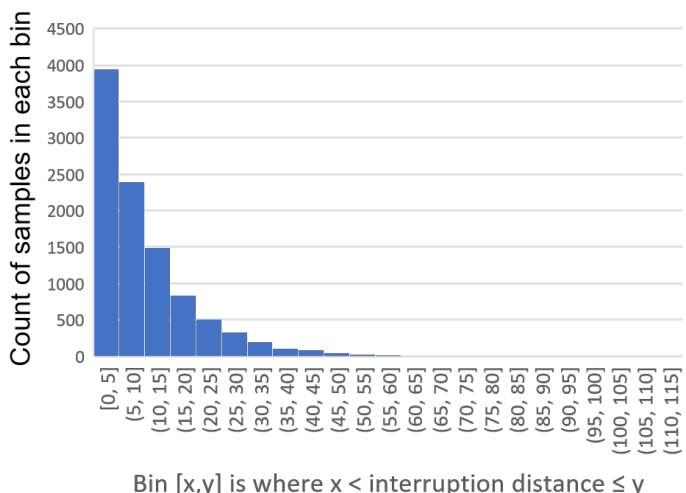


Figure F-2. The distribution of interruption distances.

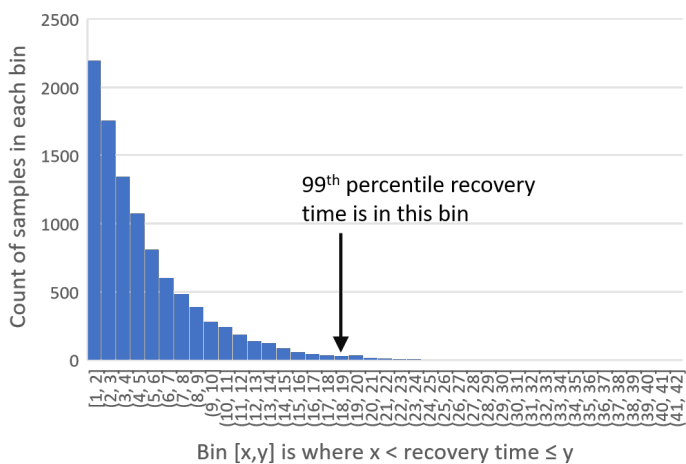


Figure F-3. The distribution of recovery times.

with a mean interruption distance of 4 km and mean recovery time of 2 hours, or 8 km and 4 hours, etc.

**Conclusions:**

It is challenging to extrapolate the experience of Curiosity’s driving on Mars to lunar driving needs. Curiosity has been predominantly directed by ground controllers identifying a path forward between waypoints 10s of meters apart for the rover to then follow. Interruptions to Curiosity’s drives have occurred due to mismatches between the controllers’ predictions of ground characteristics, based on camera images taken from only where the drive starts, and the actual terrain conditions experienced. This is obviously limited by the view ahead, the fidelity of which diminishes over distance. In contrast, INSPIRE’s long drives will be done by having the rover itself direct its path forward based on repeatedly taking images of the upcoming terrain, enabling it to accurately assess those terrain conditions and directing itself accordingly. As long as safety limits are adhered to, such as avoiding overly steep slopes and high boulders, INSPIRE should not be subject to Curiosity’s kinds of drive interruptions.

Nevertheless, mid-drive interruptions to INSPIRE’s progress may occur from time to time (e.g., from sensory glitches, hardware transients, or software bugs). When INSPIRE itself is not able to resolve the problem and resume progress, it will need to call home for ground operators’ help. We developed a simulation to explore the consequences of such interruptions on fulfilling the mission science plan’s driving needs. Its results suggest the following:

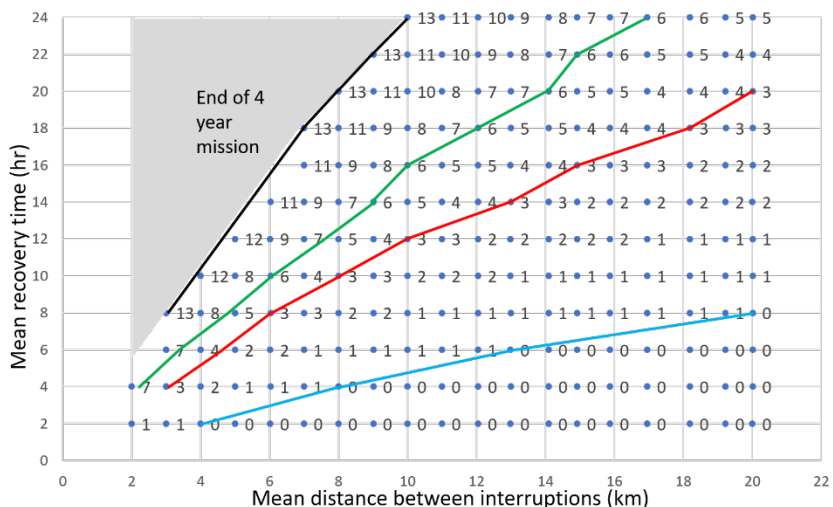


**Figure F-4.** “Failed” lunar days for recover x interruption combinations.

**Table F-1.** Effect of recovery time on mission duration based on a 3-year mission duration model.

Mission duration beyond 3 years	Allowable mean recovery time between faults (MTBF) for a given mean distance between faults (MDBF) (points from Figure F-4)					
	MDBF km	MTBF hours	MDBF km	MTBF hours	MDBF km	MTBF hours
0 months	4	2	6	3	16	7
3 months	4	5	6	8	16	16.8
6 months	4	7	6	10	16	23
13 months	4	10.5	6	15.5	16	36

For example, a middle-of-the-road goal could be to allow the mission to continue six months beyond its initial three years. To achieve this, Figure F-4 shows if drive interruptions can be expected to occur on average no more than every 8 km, then the mean recovery time must be held to no more than 10 hours.

A final note: these results may be slightly pessimistic. The simulation has incorporated only an initial attempt at identifying flexibility in the science schedule. It also does not consider the phenomenon seen on Mars rovers of “teething” troubles being found and eliminated early in the mission.

## G ESTIMATING MISSION DURATION

### G.1 SUMMARY OF ANALYSIS

This appendix captures a first order-analysis of known potential factors that could impact the traverse rate during the day and night based on the planned route to estimate an overall mission duration. Several of these factors are informed by prior applicable experience of driving on the Moon and Mars.

Based on this analysis, the nominal 756 km route planned using 5–10 m/pixel DEM would have an actual distance closer to 916 km to account for rover path tortuosity. Tortuosity results from driving around local hazards that cannot be adequately resolved from orbital images, taking a zig-zagged path upslope or downslope to minimize slip or skid respectively in lieu of the most direct route, or back-tracking when the rover encounters an unsurmountable terrain. The planned rover route is constrained to less than 15° given the uncertainty of the route’s terra-mechanical properties, in particular, in PSRs. Around 70% of the route distance driven will occur in darkness either during the lunar night or in PSRs. Night/dark traverses will necessarily be slower than day traverses because of the limited viewing horizon that has to rely on rover-based illumination of the terrain, which impacts the distance traversed at night.

An estimate of the total mission hours are based on traverse rates at different times of the day/night, the anticipated terrain difficulty, the estimated percentage of ground-in-the-loop take over of the vehicle’s mobility due to terrain difficulty, the frequency of faults and associated recovery times, and the estimated duration needed for science operations. With a capability for both day and night driving, INSPIRE’s mission duration is estimated at two full years with an additional year of unallocated margin at 50% given the uncertainty of the terrain in the PSR regions. To complete this mission within this duration, the average daytime traverse rate would have to be at 0.23 km/hour (which accounts for engineering science stops of 10 minutes every 300 m for global localization and 4 hours stops every 24 hours for communication and recharging; the average nighttime traverse rate would have to be at 0.16 m/hour to also account for additional stops of 1 minute every 10 m for long-exposure imaging.

Below, we summarize the key drivers that impact mission durations: (1) communication constraints, (2) mobility on sloped terrain and associated skid/slip, (3) estimated path tortuosity (or path inefficiency), and the (4) reliability of autonomous surface operations.

### G.2 COMMUNICATION CONSTRAINTS





The following assumptions and constraints are derived from the communications requirements described in Appendix I.

#### Assumptions:

- The lunar relay orbiter can talk to rover and ground simultaneously
- The initial ground antenna will have visibility of the orbiter 8 hours every 24 hours
- With increase in distributed antennae, visibility of orbiter will increase to full coverage over time

Table G-1 summarizes the communication constraints:

**Table G-1.** Summary of communication constraints.

	Communication	Mode	Latency (minutes)	LGA Rate		HGA Rate		Visibility (geometry)			Availability (other users)		
								%	Min (hours)	Max (hours)	Period (hours)	%	Ave Duration per period
Inspire	Rover to Ground (downlink)	Nominal	1	22 kb/s	22 kb/s	2 Mb/s	1 Mb/s	76%	9	9	12	50%	4.5
		Max	1440			100%	9.0						
	Ground to rover (uplink)	Nominal	1			128 kb/s	128 kb/s					50%	4.5
		Max	1440			100%	9.0						

### G.3 SLOPED-TERRAIN MOBILITY

The traverse rate is impacted by the terra-mechanical properties, the terrain slope angle, and the distribution of hazards. Surface processes on the Moon are largely the same since (1) the main regolith



forming process is isotropic meteorite impact, (2) the Moon has no liquid water (neither at present nor in the past), and (3) the Moon largely has no exposed bedrock due to the absence of wind. Based on prior lunar-surface missions, it was found that variations among Apollo and Surveyor sites were no greater than variations found within a single site. Below, we attempt to estimate traverse rate based on knowledge we have of the lunar terra-mechanical properties.

Having said that, there are potential differences that may occur in PSRs. The grain sizes may be different than other regions due to the absence of thermal cycling and hence cracking. The electrostatic properties of the regolith may be different from other regions. The absence of large-scale pyro deposits (no volcanism near poles) as well as the impact of volatiles in these regions could impact the cohesion of the regolith. The morphology of the terrain at the rover scale (1–10 m) is not known and neither is the compaction due to the lack of thermal cycling. Therefore, when estimating total mission duration, there are a few caveats we have to keep in mind.

**Caveats**

- The terra-mechanical properties are *not fully known in PSRs*. The agglutinates in the polar regions would vary depending on impact history.
- The interaction of the warm wheel on ice-cold regolith with a composition of 1–10% wt. water abundance has not yet been adequately characterized.
- Lunar regolith has angular particles when compared to sand used for martian/terrestrial testing; hence, slip/skid estimates are adjusted from analyses done for Mars rovers to account for that [58]. When testing with lunar simulant, it is critical to keep in mind that the knee in the slip/slope curve is dependent on the simulant type [59].

Based on the *Lunar Sourcebook* [60], the wheel-slip on the lunar surface was measured to be between only 2–3%, which allowed for reasonably accurate navigation by dead-reckoning. However, slip is very *non-linear*. We estimated the skid (downward slip) and slip (upwards) of a four-wheel vehicle in lunar regolith based on experimental results provided by [53, 58, 59, 61], tests conducted in support of the Mars Sample Return fetch rover studies, and inputs from subject matter experts.

**Table G-2.** Estimates of skid/slip vs. slope for lunar regolith.

Slope Direction	Angle	% Slip	Comments
Downslope	-25° – -20°	-40% – -26%	Skid (based on Ding's paper below)
Downslope	-20° – -18°	-26% – -20%	Skid
Downslope	-18° – -15°	-20% – -15%	Skid
Downslope	-15° – -13°	-15% – -12%	Skid
Downslope	-13° – -10°	-12% – -9%	Skid
Downslope	-10° – -5°	-9% – -4%	Skid
Flat	-5° – 0°	-4% – -3%	
Flat	0° – 5°	3% – 8%	2–3% on lunar surface (Lunar sourcebook p 524)
Upslope	5° – 10°	8% – 17%	Slip
Upslope	10° – 13°	17% – 25%	Slip
Upslope	13° – 15°	25% – 30%	Slip
Upslope	15° – 18°	30% – 60%	Slip
Upslope	18° – 20°	60% – 80%	Untraversable
Upslope	20° – 25°	80% – 100%	Untraversable

### Slip/Skid vs. Slope

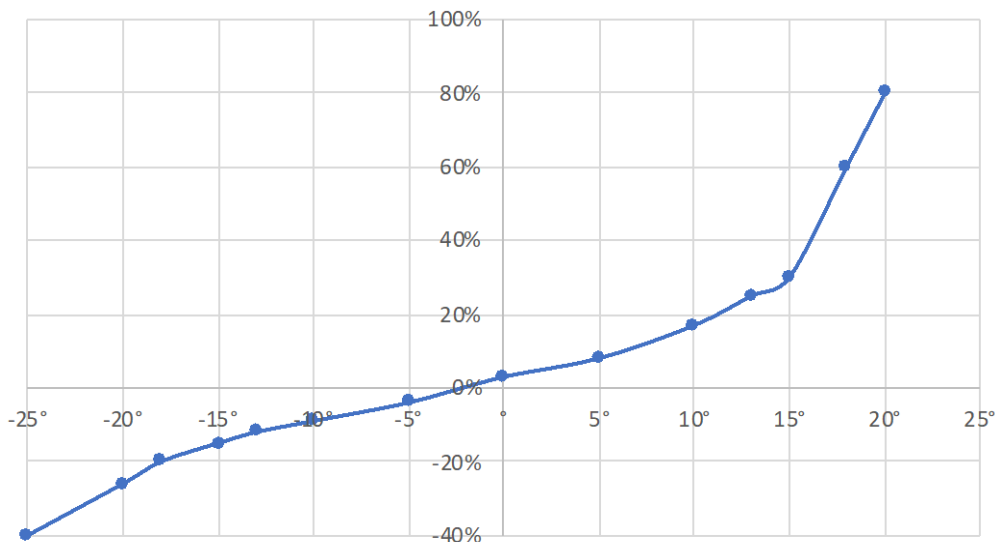


Figure G-1. Estimates of skid/slip vs. slope for lunar regolith.

## G.4 DRIVEN PATH INEFFICIENCY (PATH TORTUOSITY)

The nominal path defined for INSPIRE was based on an iterative A\* path planning algorithm that connected waypoints identified by the science team using mobility constraints of finding short routes on slopes below 16° in angle. The algorithm operated on a digital elevation map (DEM) of 5–10 m/pixel resolution. Path inefficiency captures the increase in the traverse path based on the actual route the rover is likely to take to account for terrain topography at the scale of the rover to avoid hazards. As such the driven path inefficiency, which accounts for actual rover driven path, is given by the following equation:

$$\eta_{driven} = \frac{L_{driven} - L_{straight}}{L_{straight}} \times 100$$

The commanded path inefficiency is the difference between the commanded path based on rover images and the straight-line path to a given waypoint.

$$\eta_{commanded} = \frac{L_{commanded} - L_{straight}}{L_{straight}} \times 100$$

There are several factors that impact path inefficiencies (tortuosity). These include:

- **Orbital map resolution.** Paths planned at lower resolution DEMs would increase in length at when planned at higher resolution or when driven, as the actual path would need to avoid hazards such as craters and rocks that are not resolved in the path planned at lower resolution.
- **Wheel diameter/ground clearance.** Rovers with larger wheels and larger ground clearance can drive over smaller rocks and through small craters that have to be avoided by rovers with small wheels. *E.g.*, tortuosity for VIPER rover would be higher than that of the INSPIRE rover.
- **Perception horizon.** Rovers with a limited visible horizon (*e.g.*, rovers that use lights when driving at night) would be more myopic than ones that drive in daylight. Limited horizon results in planning shorter paths, which would increase path inefficiency. *E.g.*, rovers with limited perception horizon may end up driving up to craters and then circumnavigating them to avoid driving through them

rather than being able to see these craters and avoid them from a farther distance. Other factors such as navigation camera height and terrain topography impact this as well.

- **Slip.** Slip impacts “commanded path inefficiency.” This is a concern in high-slip areas where the progress the rover makes is not always in the direction it was commanded. As a result, the rover ends up meandering more to traverse a path. This is the case of a rover climbing a slope at a lateral angle and keeps slipping a downhill. The rover then has to correct for that slip. If the rover is doing all this onboard, then the tortuosity due to side slip will be less than if ground is in the loop because of the minimum step size for every ground-in-the-loop command.

We leveraged information from subject matter experts, data from simulation of the VIPER rover mission, and that from the Mars rover missions to estimate path tortuosity for INSPIRE.

**Perseverance Simulation Data**

*Benign Terrains:* (CFA: 7%, slope < 15 deg)  
 Driven path tortuosity: **3%** (requirement < 15%)  
 % paths driven with < 15% tortuosity: **98%**

*Complex Terrains (sim results):* (CFA: 15%, slope < 20 deg)  
 Driven path tortuosity: **16%** (requirement < 35%)  
 % paths driven with < 15% tortuosity: **90%**

CFA: cumulative fractional area, a metric for rock distribution

*Caveats:*

- The above are simulation results
- Simulates Mars terrain with mainly rock hazards and not small crater hazards; the latter occupy a larger area

**VIPER Simulation Data**

The tortuosity factor for the VIPER rover have large variability

Path tortuosity for VIPER was estimated to range from 1–3x (or 50% to 200% path inefficiency). The analysis was based on a 1 m DEM upscaled to 4 cm using crater and rock abundance profiles. Actual traverses driven on that simulated terrain ranged from 1.3 - 1.5x longer, which is typical of highland terrains.

*Caveats:*

- The above are simulation results
- The tortuosity is impacted by the diameter of the wheels and the suspension mechanism

Based on the above estimates, Table G-3 summarizes relatively conservative estimates of path tortuosity that was assumed in the mission duration analysis for the INSPIRE mission.

**Table G-3.** Estimated tortuosity for different slope ranges.

Slope Range	Comments	% Nominal Inefficiency	Nominal Tortuosity Factor
0°–5°	Double MoonTrek estimate	15%	<b>1.15</b>
5°–10°		25%	<b>1.25</b>
10°–13°		50%	<b>1.50</b>
13°–15°		75%	<b>1.75</b>
15°–18°	More hazards	150%	<b>2.50</b>
18°–20°	Incl. zig-zag motion	200%	<b>3.00</b>

## G.5 AUTONOMY RELIABILITY (FAULT RATES)

Based on the autonomy reliability analysis presented in Appendix F, below we summarize the average fault rates and average recovery times for minor and major faults. This is based on a preliminary analysis of faults from the Mars rovers that are adjusted for significantly shorter and more frequent ground-in-the-loop lunar communication cycles.

### Definitions

- **MDBF:** mean distance between faults
- **MTBF:** mean time between faults
- **Minor fault:** a fault that can be rapidly fixed without requiring convening a larger multi-discipline team of domain experts. Examples include faults that can be adjusted by changing a parameter by the operations team.
- **Major fault:** a fault that would require assembling a team of experts, conducting some analysis, and generating a plan to resolve the fault

For INSPIRE, faults would occur on the rover or on the relay orbiter. The tables below summarize the average fault rates and average and maximum recovery times that the system would have to meet in order to complete the mission within the planned three-year duration.

**Table G-4.** Rover-based fault rate and recovery times requirement based on distance traversed.

	Fault type	MDBF		Ave Recovery Duration		Max Recovery Duration		Recovery Strategy
		Value	Unit	Value	Unit	Value	Unit	
Rover	Minor fault	6	km	3	hours	24	hours	Ground operators diagnose fault in near real-time
	Major fault	16	km	7	hours	72	hours	

**Table G-5.** Lunar Relay Orbiter estimated fault frequency.

	Fault type	MTBF		Ave Recovery Time		Max Recovery Time		Recovery Strategy
		Value	Unit	Value	Unit	Value	Unit	
Orbiter	Relay fault	3	Months	1	day	2	day	Multiple relays would ensure continuity

## G.6 CONOPS

During the concept of operations, the rover alternates between fast traverses (max 0.36 km/hr) and stops. Stops are required for science and engineering purposes. During the lunar day and night, the rover stops every 300 m for up to 10 minutes to image its surroundings and correct its global position and heading. At night the rover would have to make additional stops every 10 m for one minute to acquire long exposure images in front and to the side of the rover to plan its path. Night traverses include imaging while driving (short exposure and hence short-horizon imaging) as well as long-exposure imaging where the rover has come to a complete halt. Table G-6 summarizes the rover stops. Table G-7 summarizes durations needed to map the Science Stations as well as conduct the drilling.

**Table G-6.** INSPIRE's science and engineering stops.

Rover stops	Lunar Time	Stop Every	Stop Duration (min)	Reason	Comments
	Both	300 m	10.0 mins	Localization	Dead-reckoning error of ~2% of distance travelled. Error tolerance 6 m.
For mobility	Night+ PSR	10 m	1.0 mins	Imaging for navigation (long exposure ~1 sec)	Assumes two extra wedges (-90° – +90° @12 s for slewing the mast for each 90°. The Curiosity rover uses ~36 s to slew and 4 seconds for stabilization).
For comm	Both	12 hrs	2 hrs	2 Mb/s of rover-to-Earth may not be enough to download 5 Gb/day+ pictures	Data volume: 5 Gb/day (does not incl pictures)
For science	See ConOps Tab				



**Table G-7.** INSPIRE’s science stops. Additional driving to map an 10% of a 300 m x 300 m area (top) and drilling operations (bottom).

Science Stops	# of Stops			Distance per Stop	Additional Driving			
	non-PSR	PSR	Total		Day Drive		Night/PSR Drive	
					Total Duration	Duration w/ comm	Total Duration	Duration w/ comm
Normal science stops	25	35	60	3.534 km	320 hrs	384 hrs	657 hrs	788 hrs
Super science stops	0	1	1	3.534 km	0 hrs	0 hrs	19 hrs	23 hrs
Lite science stops	0	1	1	0.25 km	0 hrs	0 hrs	1 hrs	2 hrs
Unplanned science stops	0	36	36	0.25 km	0 hrs	0 hrs	48 hrs	57 hrs
<b>Total Science</b>	<b>25</b>	<b>73</b>	<b>98</b>		<b>320 hrs</b>	<b>384 hrs</b>	<b>724 hrs</b>	<b>869 hrs</b>

Science Stops	# of Stops			# of drill sites per Stop	Duration per site	Drilling Information				Total Hours
	non-PSR	PSR	Total			Day Drilling		Night/PSR Drilling		
						Total Duration	Duration w/ charging	Total Duration	Duration w/ charging	
Normal science stops	25	35	60	1	16 hrs	400 hrs	1,632 hrs	560 hrs	2,285 hrs	5,089 hrs
Super science stops	0	1	1	2	28 hrs	0 hrs	0 hrs	28 hrs	114 hrs	137 hrs
Lite science stops	0	1	1	2	28 hrs	0 hrs	0 hrs	28 hrs	114 hrs	116 hrs
Unplanned science stops	0	36	36	1	16 hrs	0 hrs	0 hrs	576 hrs	2,350 hrs	2,407 hrs
<b>Total Science</b>	<b>25</b>	<b>73</b>	<b>98</b>			<b>400 hrs</b>	<b>1,632 hrs</b>	<b>1,192 hrs</b>	<b>4,863 hrs</b>	<b>7,749 hrs</b>

operations at these Science Stations. Note that the science planning at these science stops occur in parallel to the mapping and drilling operations.

### G.7 EFFECTIVE TRAVERSE RATE

While the rover is capable of a 1 km/hour mechanical drive speed, several factors impact the rover driving speed. These include the terrain topography (slope and hazard distribution), the perception horizon, the time of the day, the engineering rover stops, the path tortuosity, instrument measurements, and the anticipated percentage of the hand-over of control from the onboard autonomous system to the ground operations team when the terrain is too difficult for the onboard autonomous system. Below is a summary of the day/night traverse rates for different portions of the path. Note in Tables G-8 and G-9, the 67% of the path is on flat terrain with slopes less than ±5°. Note that for downslope (> -5°) traversal, a 40% speed reduction was assumed to maintain a maximum speed of below 360 m/hr, which is required by the GPR instrument.

**Table G-8.** INSPIRE’s traverse rates for the 756 km nominal route.

Type	Slope Information			Traverse Rates (m/hr)					
	Slope Angle*	% of Path	Skid/Slip	w/ Slip/Skid		+ w/localz		+ comm stops	
				Day Rate	Night Rate**	Day Rate	Night Rate**	Day Rate	Night Rate**
Down-slope	-18°	0.0%	-20%	270	186	235	169	196	141
	-15°	0.5%	-15%	254	179	223	162	186	135
	-13°	3.5%	-12%	245	174	216	159	180	132
	-10°	11.8%	-9%	237	170	210	155	175	129
	-5°	33.7%	-4%	375	231	310	205	259	170
Upslope	5°	33.2%	8%	333	214	281	191	234	160
	10°	12.3%	17%	308	203	263	183	219	152
	13°	3.5%	25%	288	195	248	176	207	146
	15°	1.3%	30%	277	189	240	171	200	143
	16°	0.3%	40%	257	180	225	164	188	136
	<b>Total</b>	<b>100.0%</b>			<b>327</b>	<b>211</b>	<b>276</b>	<b>188</b>	<b>230</b>
* negative slope is downslope						232			
** night/PSR rate includes imaging stops									

Table G-8 shows the rover's speeds as a function of the slope. The daytime traverse rates account for slip (slower rate) and skid (downslope slip that increases the rate). They also take into account the 10 minute stops every 300 m for localization as well as the 4 hours stops every 20 hours for communication and charging. The night rates account for the additional one-minute stops every 10 m for the additional long-exposure imaging.

Because the rover stops more frequently at night, the effective traverse rate at night is lower than during the day. However, since day driving in PSR is effectively driving in the dark, a higher total percentage of the distance is, in fact, traversed in the dark at the slower rate. To estimate the actual distance driven in the dark, we use the derivation below.

$d_d$ : day drive distance

$d_n$ : night drive distance

$d$ : total drive distance

$t_d$ : day drive time

$t_n$ : night drive time

$t$ : total drive time

$$t = t_d + t_n$$

$$f_n = \frac{t_n}{t}$$

$$d_n = v_n t_n = v_n f_n t$$

$$d = d_d + d_n = v_d(1 - f_n)t + v_n f_n t$$

$$\frac{d_d}{d} = \frac{v_d(1 - f_n)}{v_n f_n + v_d(1 - f_n)}$$

$$\frac{d_n}{d} = \frac{v_n f_n}{v_n f_n + v_d(1 - f_n)}$$

*For the total distance*

$\xi$ : fraction of path in PSR

$$D = d + d_{PSR} = d + \xi D$$

$$d = (1 - \xi)D$$

$$\frac{d_d}{D} = \frac{v_d(1 - f_n)(1 - \xi)}{v_n f_n + v_d(1 - f_n)}$$

$$\frac{d_{n+PSR}}{D} = \frac{v_n f_n}{v_n f_n + v_d(1 - f_n)} (1 - \xi)D + \xi D$$

$$\frac{d_{n+PSR}}{D} = \frac{v_n f_n}{v_n f_n + v_d(1 - f_n)} (1 - \xi) + \xi$$

Table G-9 shows the percentage of the route that are traversed for each slope during the day and during the night/dark (PSR). On average, it shows that 70.8% of the total route is traversed at night

**Table G-9.** INSPIRE’s distance percentages and ground-in-the-loop engagement.

Type	Slope Information			Path Information				Ground in the loop Driving	
	Slope Angle*	% of Path	Skid/Slip	Inefficiency (tortuosity)	Path Length (km)	Day& % Distance	Night/PSR % Distance	Likely to Engage (L, M, H)	% Path with Ground Drive
Down-slope	-18°	0.0%	-20%	100%	0	29.1%	70.9%	M	25%
	-15°	0.5%	-15%	75%	7	28.9%	71.1%	M	20%
	-13°	3.5%	-12%	50%	40	28.8%	71.2%	ML	15%
	-10°	11.8%	-9%	25%	112	28.7%	71.3%	L	10%
	-5°	33.7%	-4%	15%	293	30.1%	69.9%	LL	0%
Upslope	5°	33.2%	8%	15%	288	29.7%	70.3%	LL	0%
	10°	12.3%	17%	25%	116	29.5%	70.5%	L	10%
	13°	3.5%	25%	50%	40	29.3%	70.7%	ML	15%
	15°	1.3%	30%	75%	17	29.2%	70.8%	M	20%
	16°	0.3%	40%	100%	4	28.9%	71.1%	M	25%
<b>Total</b>		<b>100.0%</b>		<b>21%</b>	<b>916</b>	<b>29.2%</b>	<b>70.8%</b>		
* negative slope is downslope				& Reduced by allocation for day-only sampling					
** night/PSR rate includes imaging stops									

or in PSRs. It also shows that the actual route will be closer to 916 km based on the nominal 756 km, which accounts for the terrain tortuosity of Table G-3. The last column of Table G-9 estimates the percentage of the route that will be driving by ground operators because they are too difficult for the onboard autonomous system to handle. The expectation is that flatter terrains would likely not engage ground operators, but higher sloped entrances and exists to the larger craters (Faustini and Shoemaker) may engage ground-in-the-loop driving for up to 25% of the path. However, the percentages of the path that have these higher slopes are much smaller.

Table G-10 shows the corresponding durations for traversing the different slopes at different times of the day, accounting for the slow ground-in-the-loop engagements. A total of 6,230 hours would be needed to traverse an actual path of 916 km, which includes 1,473 of day driving and 4,756 of night/PSR driving, when account for ground-in-the-loop driving and communication stops (but excluding science stops)

**Table G-10.** INSPIRE’s drive durations for the route.

Type	Slope Information			Durations (hours)					
	Slope Angle*	% of Path	Skid/Slip	Nominal Drive		Drive w/ ground in the loop		Drive w/ gil+comm	
				Day Duration	Duration	Day Duration	Night Duration	Day Duration	Duration
Down-slope	-18°	0.0%	-20%	0	0	0	0	0	0
	-15°	0.5%	-15%	9	29	18	50	19	54
	-13°	3.5%	-12%	53	179	93	270	102	301
	-10°	11.8%	-9%	153	512	227	682	254	774
	-5°	33.7%	-4%	284	1000	284	1000	341	1200
Upslope	5°	33.2%	8%	305	1058	305	1058	366	1269
	10°	12.3%	17%	131	449	213	632	236	713
	13°	3.5%	25%	47	161	89	254	97	281
	15°	1.3%	30%	20	69	43	120	46	131
	16°	0.3%	40%	5	16	11	31	12	34
<b>Total</b>		<b>100.0%</b>		<b>1,006</b>	<b>3,472</b>	<b>1,282</b>	<b>4,096</b>	<b>1,473</b>	<b>4,756</b>
* negative slope is downslope				<b>4,478</b>		<b>5,378</b>		<b>6,230</b>	
** night/PSR rate includes imaging stops									

In addition to the time spent for traversing (with engineering stops) and science operations, there is additional time that will be spent for charging after the drill operations as well as time spent to handle faults. Tables G-11 and G-12 summarize time spend for these events.

**Table G-11.** INSPIRE's duration for a single-charge drilling and recharging.

Drilling Information	Duration	Recharge Time
Single charge drilling	7 hrs	22 hrs

**Table G-12.** INSPIRE's fault recovery durations for the route.

Fault Statistics	Every	Ave. Recovery Duration	#	w comm constraints	Total Hours
Minor faults	6 km	3 hrs	153	11 hrs	1,679
Major faults	16 km	7 hrs	57	15 hrs	858
Total fault recovery					2,537

Table G-13 summarizes the time spent in the surface mission for day driving, night driving, science operations, in communication, for charging, and for handling contingencies. Accounting for all these, the total mission duration is two years. Given the uncertainties of operations in PSRs, the plan for the mission is to allocate 3 years, which would offer an unallocated margin of 50%.

**Table G-13.** INSPIRE's total durations for the route.

Description	Duration (hours)	Comments
<b>Drive: total day hours</b>	1,602	Incl. localization, imaging, GIL assistance for route and mapping
<b>Drive: total night hours</b>	4,820	
<b>Science: total day hours</b>	400	
<b>Science: total night hours</b>	1,192	
<b>Recovery: total day hours</b>	742	Mobility errors for minor and major faults (incl comm constraints)
<b>Recovery: total night hours</b>	1,796	
<b>Recovery: total day hours</b>	163	Drilling errors 10% time penalty
<b>Recovery: total night hours</b>	486	includes extra charging needed
Communication/charging	5,964	Day/night: main time charging
Commissioning	336	
<b>Subtotal</b>	17,501	Day+Night hours
	6,225	Day hours operations
	11,276	Night/PSR hours operations
<b>Margin</b>	50%	One year for 3 years
Total lunar day/night cycle	24.72	Max of 1/2 total hours or lunar days
	2.0	Years (w/o margin)
	3.0	Years (w margin)

Table G-14 shows the average day/night traverse rate that accounts for time spent handling contingencies. On average the average traverse rate would be at 0.13 km/hour. Table G-15 compares key



parameters and durations from three lunar mission studies: INSPIRE, Endurance, and Intrepid. Given INSPIRE's total estimated path length of 1,140 km, with driving 70% of that distance at the night in the dark at the slower traverse rate, and accounting for contingencies, the unmarginated mission duration would be two years assuming the aforementioned level of performance for the day/night traverses.

**Table G-14.** INSPIRE's average speed for the route.

Summary	Value	Comments
Average speed	0.13 km/hr	Includes fault recovery

**Table G-15.** Comparison of INSPIRE, Endurance, and Intrepid mission durations.

Description	Units	INSPIRE	Endurance	Intrepid	Comments
Total drive distance	km	1,140	2,052	1,768	Incl. tortuosity and mapping
Total drive time	hours	6,423	6,521	5,234	
Ave lunar day drive time	%	32%	30%	60%	Incl. only short (eng.) stop and excludes everything else
Ave lunar night drive time	%	39%	48%	11%	Incl. only short (eng.) stop and excludes everything else
Average speed	km/hr	0.178	0.315	0.338	Excl. science stops and faults
Average speed w/ faults	km/hr	0.127	0.168	0.257	Excl. science stops
Average distance between eng. stops	km	2.5	2.0	1.35	Incl. faults
Total eng. stops	#	729	1,026	1,173	24-hr cycle (4 hr comm)
Mission duration	years	2.0	2.6	3.0	
Margin	%	50%	55%	33%	
Duration w/ margin	years	3.0	4.0	4.0	

---

## H DRILL

### H.1 LUNAR POLAR VOLATILE ROVER (LPVR) DRILLING SYSTEM



Study Results Report

Prepared for Jet Propulsion Laboratory by Honeybee Robotics, Ltd

Contract 1660888

15 April 2021

NASA TO: John Elliott  
john.o.elliott@jpl.nasa.gov

Honeybee Co- Investigator: Kris Zacny  
zacny@honeybeerobotics.com  
646-421-7902

Honeybee Mechanical Engineer: Isabel King  
irking@honeybeerobotics.com

## H.2 INTRODUCTION & HONEYBEE HERITAGE

The LPVR drill system is based on Honeybee Robotics' Regolith and Ice Drill for Exploration of New Terrains (TRIDENT) currently under development for Volatiles Investigating Polar Exploration Rover (VIPER) – see Figure H-1, and PRIME1 (Polar Resources Ice Mining Experiment) – see Figure H-2 [62-65]. PRIME1 is scheduled to fly to the Moon in 2022 while VIPER is targeting a 2023 launch year. Both missions are targeting South Pole's volatile rich deposits. The only difference between the LPVR drill and TRIDENT is the drilling depth: the LPVR drill is designed for a 2 m depth while TRIDENT has been designed for 1 m depth. As a result of greater drilling depth, the LPVR drill has additional support structure, but otherwise all other subsystems and drilling protocols are the same.

The primary goal of TRIDENT is to deliver volatile-rich samples from 1 m depth to the lunar surface. Once on the surface, the material would be analyzed by Mass Spectrometer Observing Lunar Operations (MSolo) and the Near InfraRed Volatiles Spectrometer System (NIRVSS) to determine volatile composition and mineralogy. MSolo will fly on both missions while NIRVSS will fly only on VIPER.

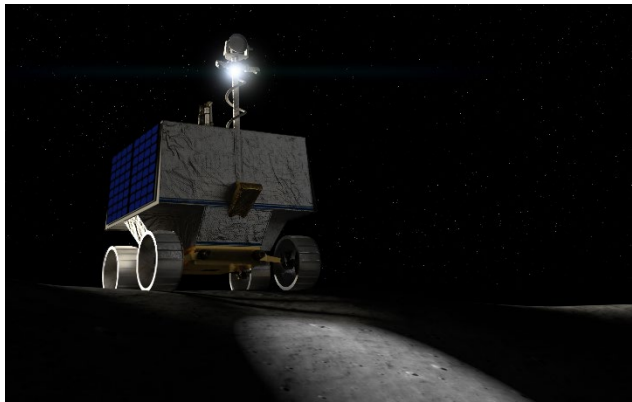


**Figure H-1.** VIPER mission. TRIDENT is placed in a vertical position in the middle of the rover.



**Figure H-2.** PRIME1 mission. TRIDENT is vertically mounted on the right hand side of the Intuitive Machines (IM) lander.

### H.2.1 LPVR DRILL

LPVR has two 2 m TRIDENT drills for redundancy and to address mission lifetime. The drills are mounted in such a way as to produce the pile of cuttings for MSolo and NIRVSS in the same location. If either of the drills get stuck, they can be detached from the lander via hold-release mechanisms.

TRIDENT is a rotary-percussive drill which enables it to cut into icy material that could be as hard as rock. The drill consists of several major subsystems: a rotary-percussive drill head for providing percussion and rotation to the drill string, a deployment stage for deploying the drill to the ground, a feed stage for advancing the drill string up to 2 m into subsurface, a drill string for drilling and sampling, and a brushing station for passively depositing material onto the surface

Percussive energy is set to  $\sim 2.5$  J/blow and the maximum frequency is  $\sim 1000$  blows per minute. The rotation speed is 120 revolutions per minute and the stall torque is 16 Nm. The mass of the 2 m TRIDENT drill is 25 kg, not including the harness and the mass of avionics at 7 kg. The same avionics box runs both drills (a similar setup is being implemented on the Dragonfly mission which has one avionics box to run two drills). The stowed drill packaging dimensions are 270.5 cm x 21.5 cm x 31.3 cm.

To reduce thermal risks, risk of getting stuck, reduce drilling power, and provide stratigraphic information, the drill will capture samples in so-called 10 cm “bites” (Figure H-4). That is, it will drill 10 cm at a time and bring up 10 cm worth of material to the surface. For this reason, the auger is split into two sections (Figure H-3 and Figure H-4). The lower section has flutes designed for sample retention: the flutes are deep and have low pitch. The upper section is designed for efficient conveyance of material to the surface: the flutes are shallow, and the pitch is steep. This combination allows efficient sampling but inefficient conveyance – the drill should not be used to drill to 2 m depth in a single run as this will lead to increase in drilling power and ultimately heat input into formation.

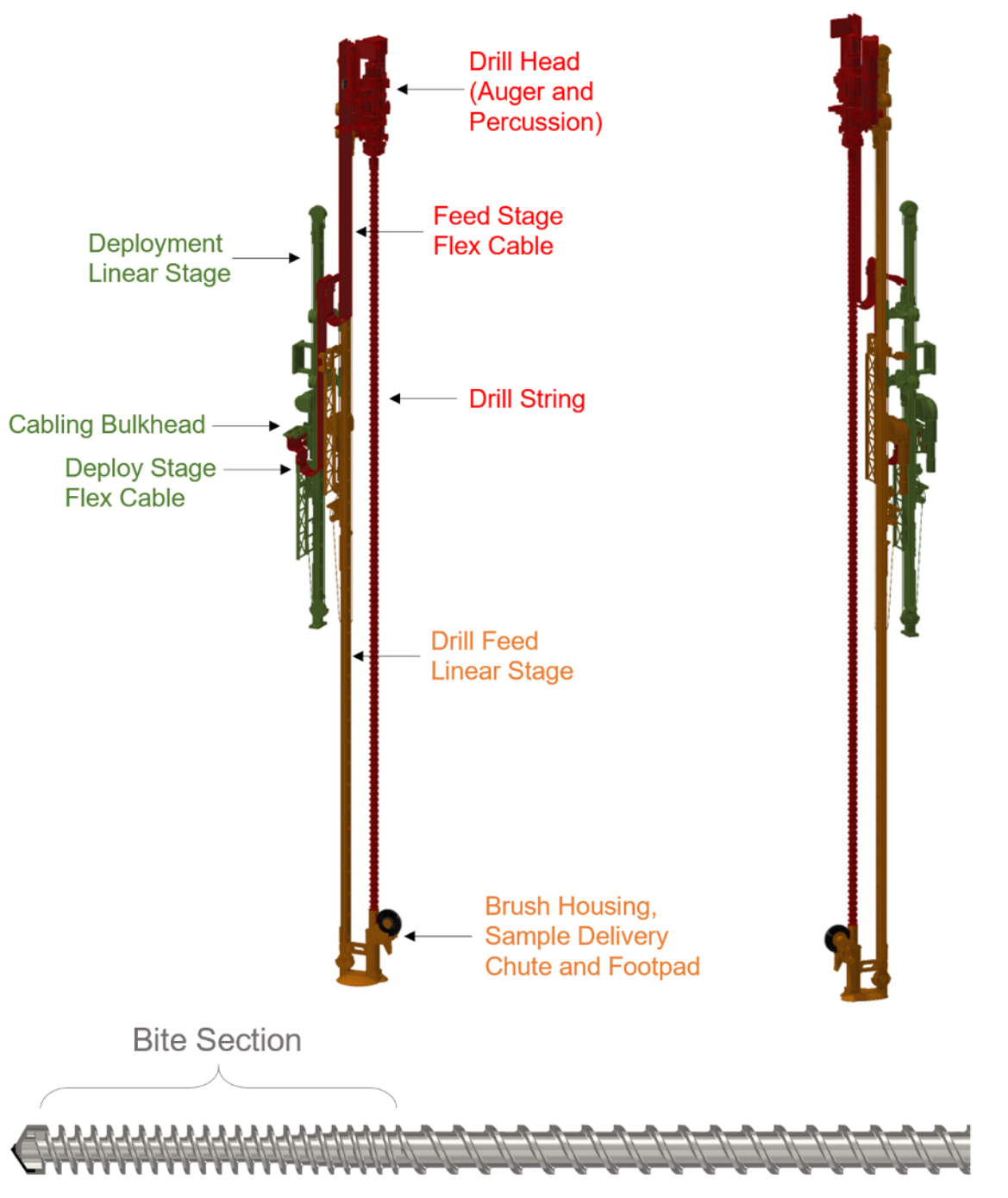


**Figure H-3.** TRIDENT subsystems. The sampling auger is pictured at the bottom.



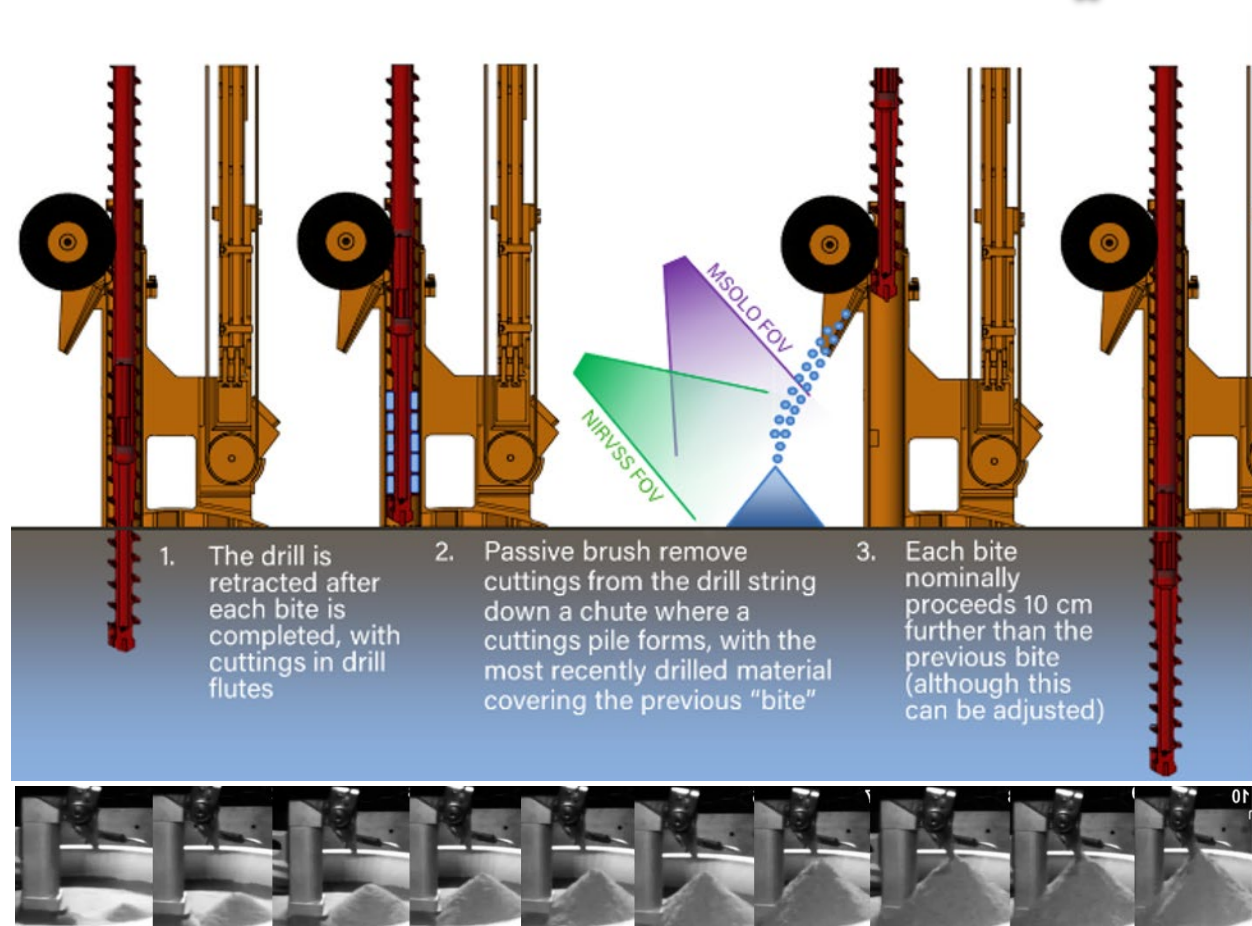


Figure H-4. Bite sampling approach. Shown below are cuttings cones every 10 cm bite.

## H.2.2 INSTRUMENTATION

In addition to serving as a sampling tool, TRIDENT is also an instrument. TRIDENT drilling power and penetration rate is used to determine regolith strength. Measuring the strength in combination with input from MSolo, NIRVSS and Neutron Spectrometer System (NSS), will enable determination of the physical state of ice – whether it’s mixed with regolith or cemented with regolith grains. The former will lead to low drilling power and the latter to high drilling power – while the water-ice concentration could be the same.

TRIDENT’s integrated 40 Watt heater and RTD temperature sensors will measure downhole temperature and can provide thermal conductivity. These two measurements, temperature and thermal conductivity, are needed to determine heat flow properties of the Moon. The first RTD is located in the drill bit and the second RTD is co-located with the heater, some 20 cm above the bit.

TRIDENT will also be able to provide bearing capacity of the top lunar surface from measuring of the sinkage of its footpad into the surface, as well as angle of repose from measuring the angle of the cuttings pile.

It needs to be emphasized that drilling in 10 cm bites enables more accurate measurement of subsurface temperature and material strength. Every time the drill is lowered into the borehole, it will be pre-loaded onto the bottom of the borehole and cold soaked without drilling (i.e. no heat input). This cold soaking will be used to extrapolate the subsurface temperature. In addition, when the drilling starts, the drilling power will be initially attributed to penetrating/breaking the icy-formation. As the drill continues drilling deeper, the power starts increasing due to the cuttings removal (i.e. auger) contribution to the total power budget (the drill can only measure the total drilling power – contribution

of drilling and cuttings removal). As such knowing the initial drilling power and the power once the drill penetrated 10 cm will allow determination of the auger-contribution to the total power budget.

TRIDENT has undergone several end to end tests at NASA Glenn Research Center (Figure H-5). These tests were conducted with NIRVSS and MSolo instruments and in the NU-LHT-3M lunar soil simulant doped with various water-ice concentrations. In all cases, the vacuum was maintained in the  $10^{-5}$  torr range (or lower) while the temperature of the chamber and the sample was maintained at around 100K or higher.

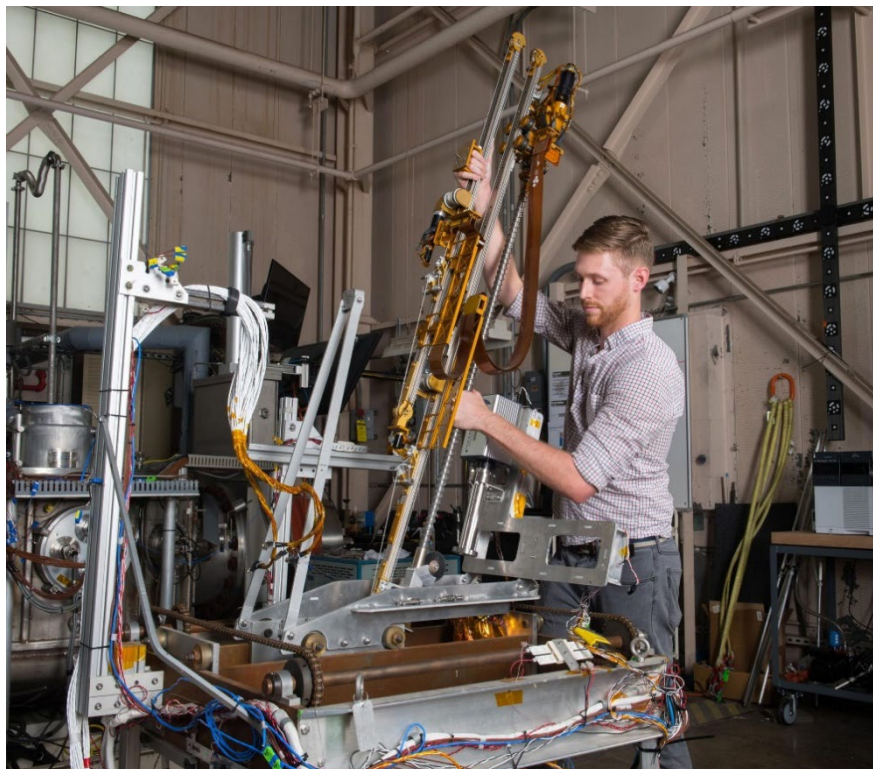


Figure H-5. TRIDENT drill undergoing TVAC tests at NASA GRC.

# I TELECOMMUNICATIONS

This appendix addresses the communication needs of the INSPIRE rover. The objective is to design a telecommunication system that meets the science requirements of the mission. The rover will operate mostly in the permanently shadowed regions of the South Pole of the Moon and will traverse hundreds of kilometers. The area that the rover will operate, South Pole permanently shadowed, does not have a clear view of the Earth most of the time, and when Earth is in view, path elevation angle is too low to provide for a reliable communication link. Hence the rover has to communicate through a relay satellite. The likely schedule of the rover is 2030 and beyond with approximately three years of mission duration.

In this appendix, we establish a baseline communications system for INSPIRE with the understanding that, by the time of the launch of the mission, a more capable communications system is likely to be available. This understanding is critical because the baseline relay, as will be discussed later, is a single satellite network, and, thus, does not provide redundancy. However, there are strong indications that by 2030 there will be multiple relay networks in the cislunar region providing more than one relay satellite option to connect with INSPIRE [33]. The landscape around 2030 seems promising for easily meeting mission data communication requirements in a reliable and robust fashion.

## I.1 LUNAR RELAY SERVICES FOR THE 2030S TIME PERIOD

The next decade is expected to see a big increase in lunar exploration [33]. These ventures will include robotic and human activities with both science and commercial flavors. NASA and other space agencies have plans to explore the Moon with emphasis given to the poles and the far side. It is safe to assume that the majority of lunar hot spots will be located in areas that direct communications with earth will be difficult or will not be possible. NASA has proposed a communication and navigation infrastructure to lower the barriers to entry for new missions and capabilities and support expanding robotic and human activities at the Moon with emphasis on commercialization [66]. Therefore, it is very likely that several relay providers will offer service in the lunar theater for the time frame of interest to us. Currently, there are several lunar relay systems that are being planned or discussed. Among the potential future relay systems, only one has reached the implementation phase: a relay system called Lunar Communications Pathfinder is being developed by SSTL, a UK commercial company, to be launched in late 2023, see Table I-1 below. This table illustrates the capabilities of three lunar relay systems planned to be launched in the next decade.

**Table I-1.** Examples of lunar relay orbiters to be launched during 2021-2030 period.

Relay Orbiter	Lunar Gateway	Lunar Communications Pathfinder (single satellite)	Andromeda (multiple satellites)
Launch Year	After 2024	Late 2023	After 2024
Agency	NASA	Goonhilly/SSTL/ESA	Argotec
Earth Station	DSN, NEN, ESTRACK	Goonhilly, ESTRACK	DSN, Commercial
Orbit Type	Near-Rectilinear Halo Orbit (NRHO)	12-hour Frozen Orbit	12-hour Frozen Orbit
Orbital Parameters	Max range from S. Pole: 71,000 km	Max range from S. Pole: ~8,400 km	Max range from S. Pole: ~8,400 km
Coverage Performance	Orbital period ~6.56 days. Continuous coverage of S. Pole for 144.6 hours with a gap 5.4 hours.	Orbital period 12 hours. Single satellite with continuous coverage of S. Pole for 9.13 hours with a gap of 2.87 hours.	Orbital period 12 hours. Multiple satellite with zero coverage gap at S. Pole.
Frequencies and Max Data Rates	Earth to Relay	X-band: 10 Msps; K-band: at least 10 Mbps (may be 30 Mbps)	X-band: 30 Kbps K-band: 16 Mbps
	Relay to Earth	X-band: 4 Msps; K-band: at least 100 Mbps (may be 300 Mbps)	X-band: 5 Mbps K-band: 100 Mbps
	Relay to Lunar surface or orbital user	S-band: 10 Msps; K-band: 10 Mbps; Optical: TBD	S-band and UHF: 128 Kbps S-band and K-band Max: 16 Mbps
	Lunar surface or orbital user to Relay	S-band: 4 Msps; K-band: 100 Mbps; Optical: TBD	S-band and UHF: 2 Mbps S-band and K-band Max: 100 Mbps
Relay Services	Store-&-forward and bent pipe, in situ tracking service, in situ navigation service (TBC)	Store-&-forward communications (Phase I); bent pipe and navigation services will be added in Phase II	Store-&-forward and bent pipe services, navigation services

No relay system will provide 100% coverage of all the lunar surface. Considering the size of the Moon, a relay network providing 100% coverage will be very costly. However, it is possible to provide great coverage to certain parts of the Moon, such as the South Pole region, with reasonable cost. While the first two relays in the above table are single satellite systems, the third one, Andromeda, will have multiple satellites, hence providing better coverage than the other two. The first two relay systems provide good coverage near the Lunar South Pole. Andromeda, on the other hand, will provide 100% coverage of the areas near the South Pole and good coverage for the rest of the Moon. As mentioned above, Pathfinder is currently under development, whereas Andromeda is in the study phase. Pathfinder is scheduled to be launched in late 2023 with a lifetime of 8 years. The service provider, SSTL, is also planning to expand its service in the future by launching additional satellites, assuming their lunar commercial investment will prove profitable. Therefore, we have selected the Pathfinder as the baseline relay service for INSPIRE because this relay system is highly likely to be available for the time frame of interest to us.

The majority of the relays being planned assume a risk posture of Class D. Therefore, although we are baselining the Pathfinder network, we realize that a Class B mission, such as INSPIRE, will need to have access to two relay satellites in order to meet its risk requirements. It is our belief that more relay satellites will be available during INSPIRE operational life time to fulfil redundancy requirements of INSPIRE.

The European Space Agency (ESA) has invested in the Pathfinder lunar relay and has a close relationship with SSTL. The plan is for NASA to launch the spacecraft in late 2023. Moreover, NASA intends to use the relay for CLPS landers, and is about to sign a MOU with ESA to have access to Pathfinder network [67]. The MOU will address the near-term needs of NASA beginning in 2024 and will not explicitly address INSPIRE.

SSTL has secured a suitable ground station (Goonhilly, UK) for its relay operation. At the start of operations in 2024, the ground antenna will be available 8-hours a day, hence, not able to provide near-real-time communications for most of a 24-hour period. SSTL claims an average data delivery latency of 24 hours [68] during the first phase of its service. However, during the 8-hours-per-day that the ground antenna is available, near-real-time communication may be possible. Moreover, SSTL intends to expand its network and improve network functionality over time (Phase 2 of the relay service), examples of which are launching additional orbiters, acquiring additional ground antennas, and improving the overall performance of the network. At the beginning, the service will be limited to communications only; the expended capability will also offer navigation services [69]. The improvements planned for Phase 2 provide multiple advantages that include relay redundancy, shortened data delivery period for better near-real-time service, and increased relay coverage and availability. Moreover, additional ground stations will be added to increase relay-Earth contact time. Another possibility regarding ground stations is NASA's Deep Space Network (DSN). Fortunately, Pathfinder has been designed to be compatible with the DSN; therefore, it will be possible to use the DSN when Pathfinder is serving INSPIRE. Although not a requirement, the use of the DSN can shorten data delivery latency, hence improving on near-real-time operations. In this report, we are assuming that, by the time of the launch of INSPIRE, near-real-time operation will be possible for close to 24 hours a day whenever rover-to-relay link is available.

The Pathfinder relay uses an orbit known as the 12-hour frozen orbit<sup>2</sup> that favors lunar southern hemisphere [69]. It covers the far side of the Moon and benefits from long access times to Earth for relaying back customer data. Since the orbit is frozen, the Moon turns slowly under the orbit making one complete cycle in about 28 days. Therefore, the coverage scenario repeats itself every 28 days. Figure I-1 shows Pathfinder's orbit.

---

<sup>2</sup> Original plan was for Pathfinder to use the 12-hour frozen orbit; however, the latest plan is to use a slightly shorter orbital period of about 11 hours. However, all the analyses in this report are done for the 12-hour orbit.



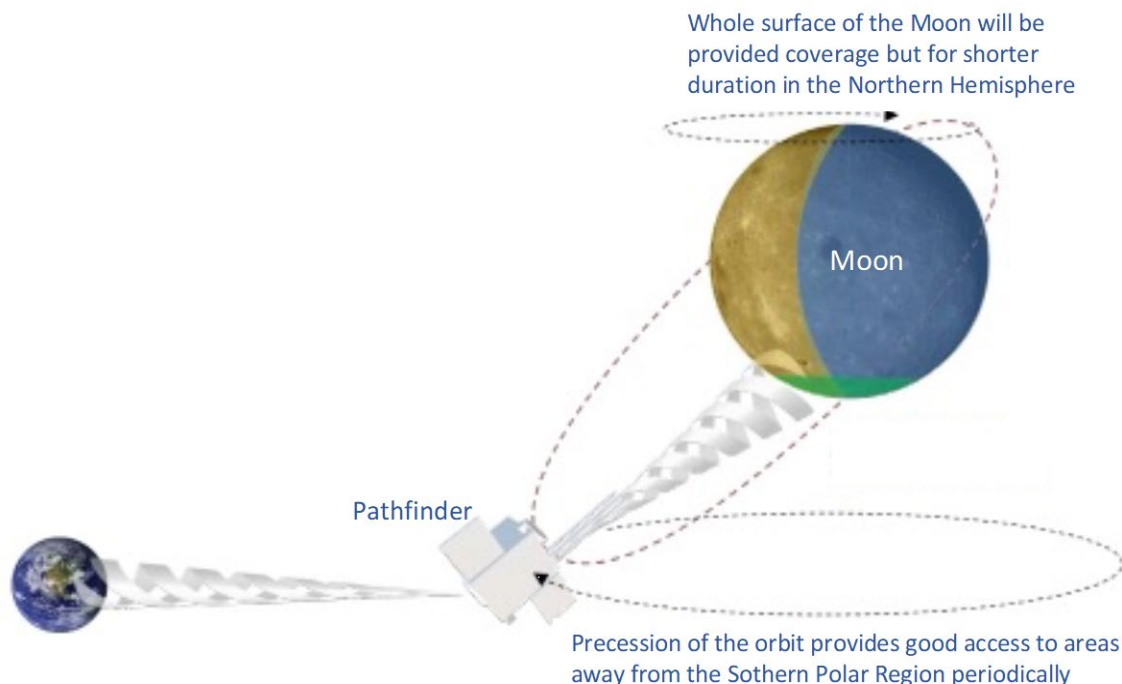


Figure I-1. Lunar Pathfinder Orbit (from SSTL User Guide).

## I.2 COVERAGE

This section provides an assessment of relay coverage of the lunar surface traversed by INSPIRE. Lunar Pathfinder orbit was selected to favor coverage for the southern hemisphere of the Moon, particularly the polar region. Depending on the location of the rover, the coverage by Lunar Pathfinder will vary. Figure I-2 shows the average contact time as a function of lunar latitude, and Figure I-3 shows the maximum gap as a function of Lunar latitude. The range of traverse for the rover is the South Pole region. Per Figure I-2, average contact time for INSPIRE is about 9 hours in a 12-hour period. The maximum gap will be about 2.9 hours for a location at the South Pole, Figure I-3.

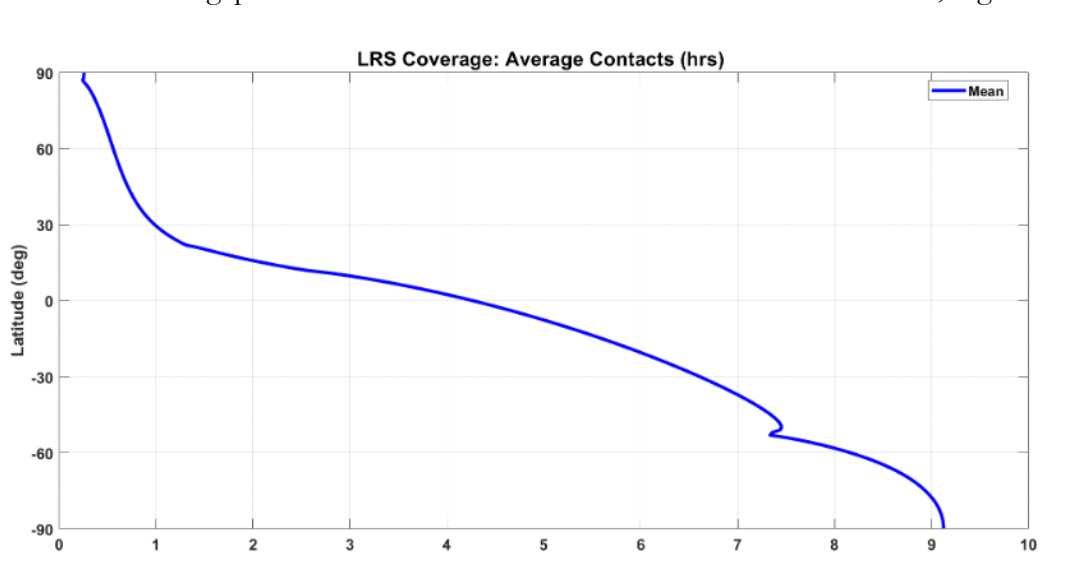
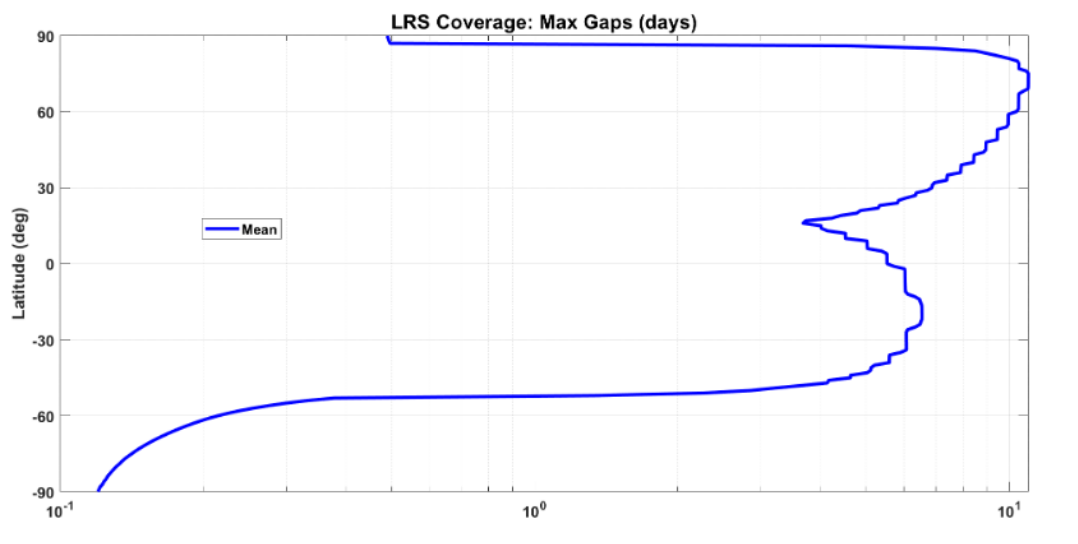


Figure I-2. Lunar Communications Pathfinder Relay Satellite Average Contact Time per 12-Hour Orbit. (Credit: C. Lee)





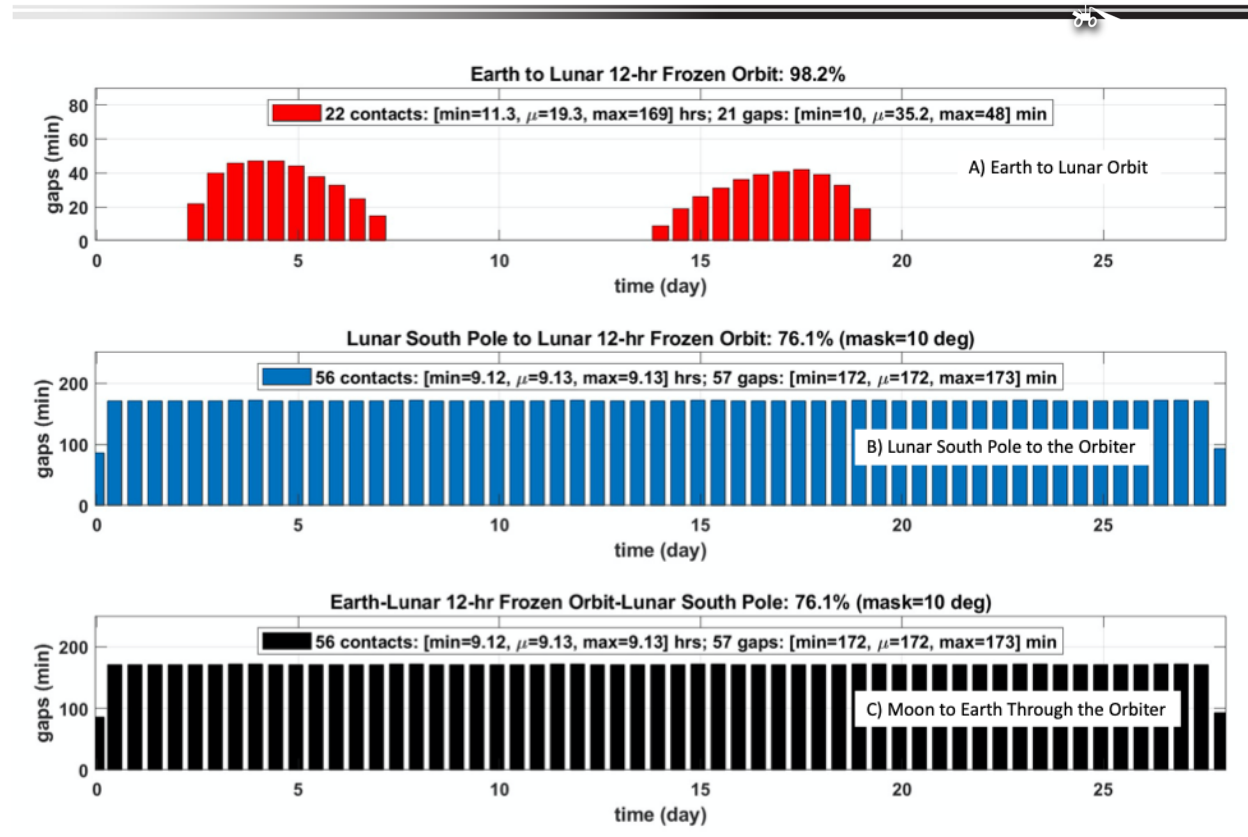
**Figure I-3.** Lunar Communications Pathfinder Relay Satellite Maximum Contact Gap Duration per 12-Hour Orbit.  
(Credit: C. Lee)

For a user on the surface of the Moon, the contact time between the user and Earth is an important figure of merit for a relay system because near-real-time communications is possible only when Earth is visible. This figure can be acquired from the cross section of two time periods, the contact time between the user and the relay and the contact time between the relay and Earth. Figure I-4-A shows Earth-to-Lunar-frozen-Orbiter contact time. It is clear that the relay orbit has a favorable view of the Earth. Indeed, 98.2% of the time there is a line of sight from the orbiter to Earth. It should be noted that the gap in contact between the orbiter and Earth occurs mostly when the orbiter is in the Moon's Northern hemisphere. Therefore, for assets, such as INSPIRE rover which is traversing the southern hemisphere near the pole, this gap has no effect.

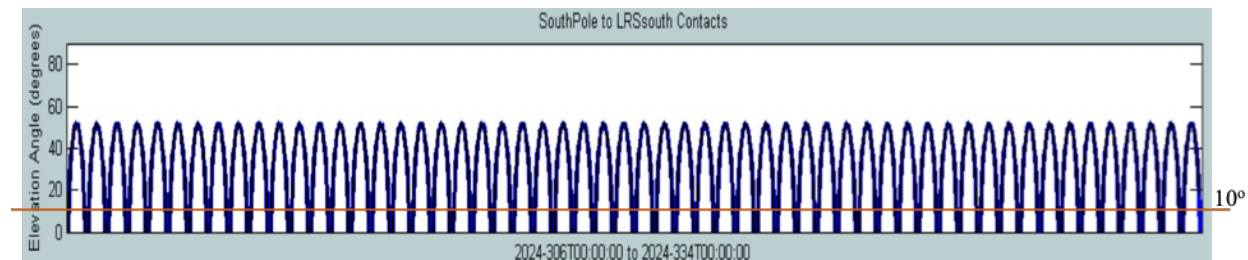
Figure I-4-B shows rover to relay orbiter gap times for a 28-day period, assuming rover at or near the South pole. All gaps are of approximate duration of 2.9 hours which occur in 12-hour periods.

Figure I-4-C is obtained from merging I-4-A with I-4-B. It provides the end-to-end gap profile for a location at or near the South Pole. Figures I-4-B and I-4-C look similar because the relay has a clear view of Earth while serving the location of interest.

Figure I-5 illustrates the path (rover-to-relay) elevation angle for a 28-day period. Coverage gaps occur when elevation angle goes below  $10^\circ$ . Note that the  $10^\circ$  is the threshold where below it the relay is assumed not visible to the rover.



**Figure I-4.** A) Earth-to-Lunar-Orbiter Contact Gap Profile; B) Lunar 90° South to the Orbiter Contact Gap Profile; C) Lunar 90° South to the Orbiter Contact Gap Profile. (Credit: C. Lee)



**Figure I-5.** Orbiter elevation angle views from the South Pole of the Moon (Credit: C. Lee)

Figure I-6 shows the average relay coverage in percentage as a function of latitude. For INSPIRE, this coverage is 76%.

There are a few noteworthy points regarding relay coverage:

- Earth visibility to the relay orbiter is very high
- Maximum Earth visibility gap period is 48 minutes
- Lunar South Pole to the relay visibility is 76% with a mask of 10 degrees (path elevation angle minimum is assumed 10°)
- Bent-pipe visibility from Lunar South Pole (to allow near real time operation) is also 76%
- Assuming ground station availability, operation can be bent-pipe rather than store-and-forward

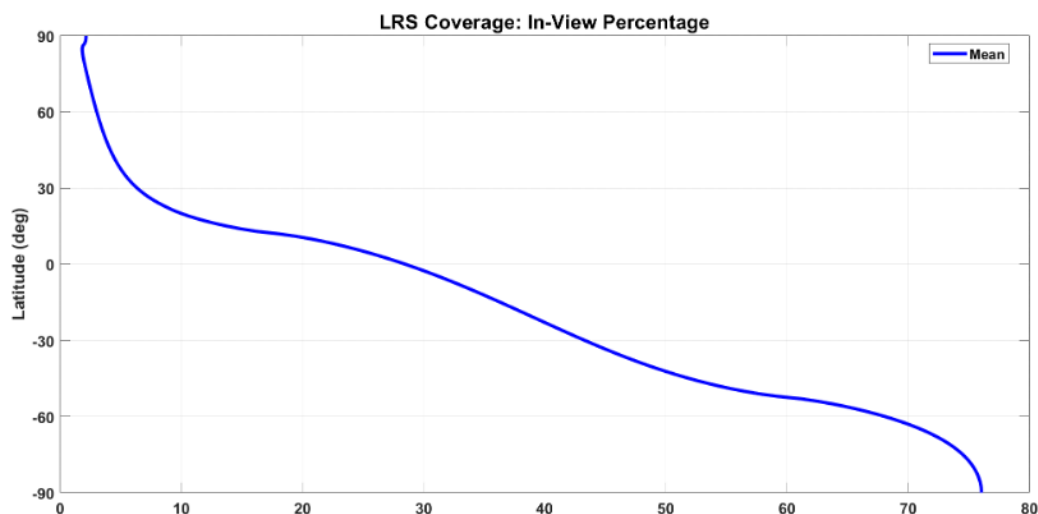


Figure I-6. Average relay coverage as a function of latitude. (Credit: C. Lee)

Figure I-7 Illustrates the maximum and minimum in-view range of the relay from lunar surface as a function of lunar latitude. Note that from the South Pole the maximum distance is about 8,400 km and the minimum distance is about 5,500 km.

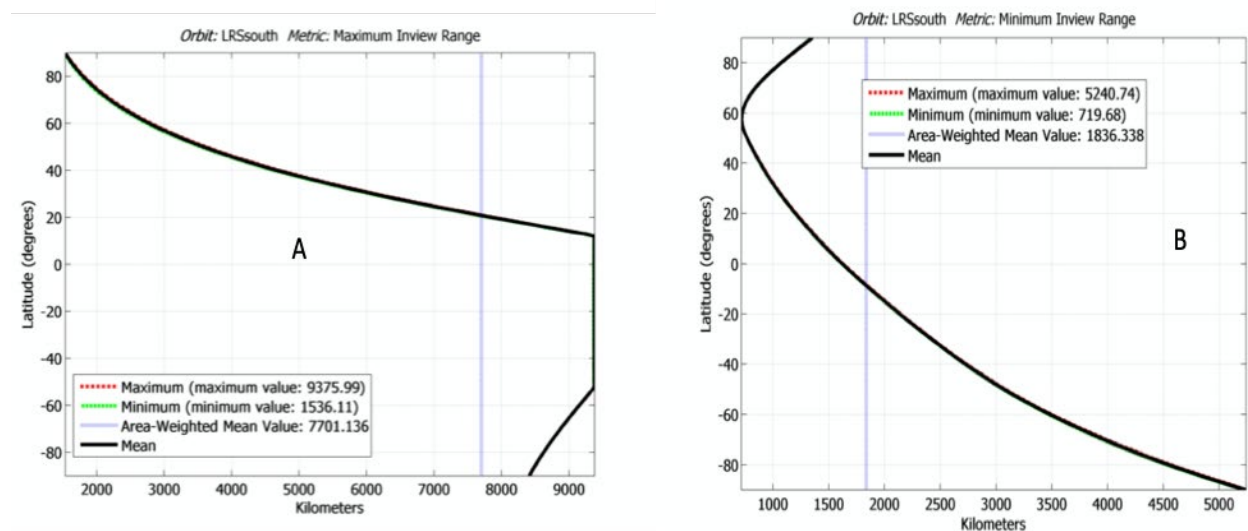


Figure I-7. Relay orbiter range from lunar surface; A) maximum distance and B) minimum distance (Credit: C. Lee)

### I.2.1 EMERGENCIES

The Relay User Manual does not address user emergencies at this time. However, the service provider will develop an emergency plan at a later date. This plan will address emergency events and how a user can contact its mission control in such events.

### I.3 COMMUNICATIONS LINK

This section provides an analysis of the link for calculating rover antenna size and amplifier power. The Pathfinder User Guide [69] provides technical data on the relay-to-rover link. The important points are summarized in Table I-2 below.

Since it is desired to operate the rover radio at the maximum transmit data rate of 2 Mbps, the rover communications system must produce an EIRP of 26.5 dBW per Table I-2. With a margin of 3 dB, the required EIRP is 29.5 dBW. This value can be obtained from the combination of a 5-W (7 dBW) power amplifier and an antenna with gain of 22.5 dBi. The size of the antenna can be obtained from Figure I-8 to be 75 cm. The antenna must track the satellite as the relay slowly moves over the sky. Satellite tracking does not have to be very precise because the antenna beam is not very narrow. Figure I-9 shows antenna gain loss as a function of tracking error. For example, a 3° tracking error will result in a small gain loss of 0.5 dB.

**Table I-2.** Important link information copied from Lunar Communications Pathfinder User Guide.

Transmit data rate (INSPIRE to relay)	≤2 Mbps
Receive data rate (relay to INSPIRE)	≤128 kbps
Required EIRP	26.5 dBW
Required G/T	-6 dB/T
Protocol	CCSDS Prox-1
Forward Frequency	2025-2110 MHz
Return Frequency	2200-2290 MHz

For rover emergencies, the high-gain antenna will not be used. In this case, a S-band low gain antenna with a gain of 3 dBi will be employed. Assuming a 5-W amplifier, the low gain antenna can support a data rate of 22.4 kbps; this figure is obtained from reducing high gain antenna data rate of 2 Mbps by 19.5 dB ( $19.5 = 22.5 - 3$ ). Similarly, the receive (commanding) rate of the low-gain antenna can be calculated. The required G/T for a receive data rate of 128 kbps, per Pathfinder User Manual,

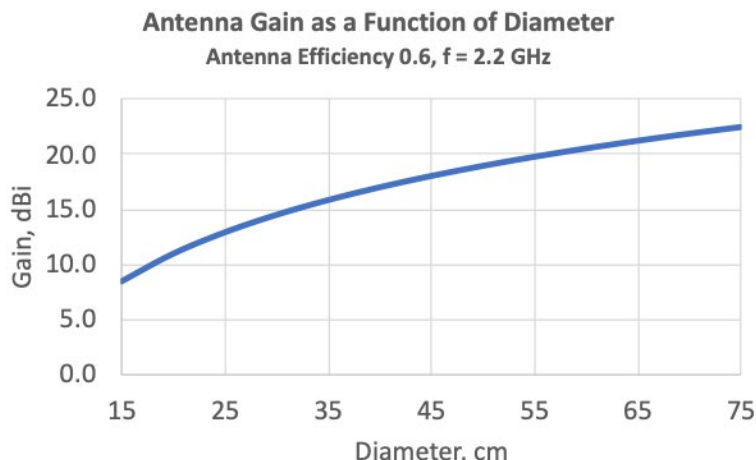


**Figure I-8.** Antenna gain as a function of diameter for a parabolic antenna.

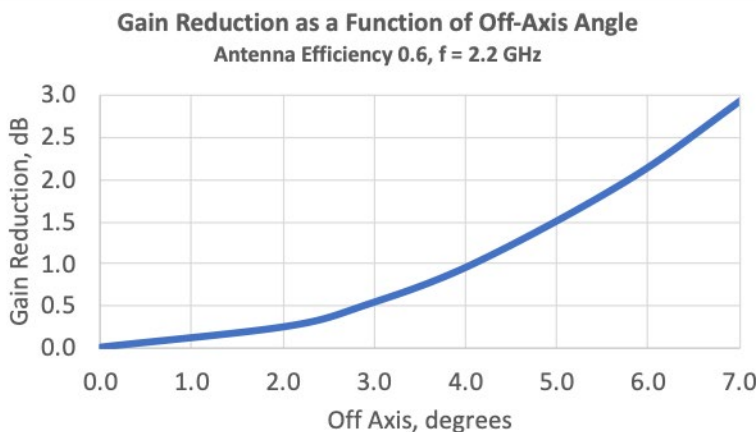


**Figure I-9.** Antenna gain loss as a function of antenna mis-pointing.



is - 6 dB/T. With a 3 dBi antenna gain and a system noise temperature of 400 K, antenna G/T becomes -23 dB/T. The difference between the low gain antenna G/T and the required G/T is 17 dB (50 decimal). Therefore supported rate is  $128/50 = 2.56$  kbps. To operate the link with a 3-dB margin, we reduce the above rate by a factor of 2 to get 1.2 kbps.

Note that in the above calculation we have used 400 K as the receiver system noise temperature which is a conservative assumption. This noise temperature does account for day time operation when sun is present. The overall effect of the sun on the noise temperature is about or less than 10 K [70].

### I.4 THE RADIO

The rover needs a radio with certain features. These features include the Proximity-1 standard, transmission rates up to 2 Mbps, and a risk posture of Class B. We identified three radio products for INSPIRE that can provide the above features. Although, these radios range in their maturity, capability, and cost, all three can meet INSPIRE's communication requirements. Table I-3 shows these options.

The UST-Lite transponder is a JPL design based on the UST radio (power amplifier is not included with the radio). One version of UST, a Ka-band modulator called KaM [71], is slated to fly on the NISAR Earth Orbiting mission in 2022. KaM flight units are being integrated into the spacecraft now. UST-Lite is currently under development at JPL; it has a mass of 1 kg and uses only 14 Watts when engaged in simultaneous reception and transmission. The Frontier-Lite radio is designed by the Applied Physics Lab (APL) based on their TRL-9 Frontier radio. It offers the lowest mass and power among the three options. Frontier radio (not Frontier-Lite) has flown before on multiple missions. The L3Harris transponder has the highest mass and power, however, it is very mature at TRL 9, and it comes with its own 8-W SSPA. This radio requires the lowest lead time among the options. Not any of the above radios is equipped with Proximity-1 protocol at the present time, but this option can be added to them. In this study, we are using UST-Lite as the baseline with the understanding that any of the above radios can be used.

Proximity-1 is a CCSDS hardware and link layer protocol for proximity links [72-74], and it is anticipated to be used widely in the future. Furthermore, it is expected that, by the time of the launch of INSPIRE, additional lunar relay satellites will be available providing backup to Pathfinder. The use of Proximity-1 will provide a standard interface for using other relay satellites. It should be noted that, although Proximity-1 is a well-defined CCSDS standard at UHF frequencies, the physical-layer part

**Table I-3. S-band radio options.**



	UST-L Transponder	Frontier Lite S-Band Transponder	L3Harris KG-150 (CXS-2000/C) Transponder
<b>Mass</b>	1 kg	0.5 kg (not incl SSPA)	5 kg max, with triplexer (includes 8W SSPA)
<b>Volume</b>	16x10x9 cm <sup>3</sup>	15.2 x 9.7 x 2.2 cm <sup>3</sup>	22.5x17.4x14.3 (cm <sup>3</sup> )
<b>Power</b>	14 W (PA not included), 10W for receive only	4.5 W	63 W
<b>RF Power</b>	SSPA not included	0.7 W	8 W
<b>TX rate</b>	10bps-1Gbps	100sps - 10Msps	8 Mbps
<b>RX rate</b>	7.8 bps-1Gbps	100sps - 1Msps	2 Mbps
<b>S/C interface</b>	RS-422 & Spacewire	Spacewire,	RS-422
<b>Encryption</b>	AES256	No, likely can add	External, Can support AES256 or Suite-A solutions
<b>Protocol</b>	Prox-1/USLP	AOS, Prox-1 can be added	Prox-1 can be added
<b>Lead time</b>	30 months	28 months	18 months nominal, can be improved with advance notice
<b>Price</b>	\$5M for the first unit, \$2M per additional unit, Class B	\$450K, quantity of 10, Class D; Class B and C are possible	Varies based on Qty, notionally \$1.5M, Class B

of the standard is not defined for S-band frequencies yet. For this reason, JPL has begun an effort to standardize the physical layer for S-band frequencies in collaboration with international space agencies, SSTL, radio manufacturers, and other interested parties.

Although the Proximity-1 standard allows for the relay as well as the rover to initiate communications through the hailing channel, however, the plan is for the relay (Pathfinder) alone to initiate communication sessions. We believe this limitation is likely to be removed by the time INSPIRE becomes operational, hence, also allowing for the rover to initiate contacts.

### I.5 THE ANTENNA

The high-gain antenna will consist of a dish and a gimbal with azimuth and elevation rotation. One of Mars antennas could be modified for this application, or a new design can be used.

### I.6 FUNCTIONAL BLOCK DIAGRAM OF THE COMMUNICATIONS SYSTEM

The functional block diagram of the communications system is provided in Figure I-10. Because the rover is a Class B asset, there are two radios and two power amplifiers for redundancy. Switches are provided to allow for switching between the radios. Each power amplifier is associated with only one of the radios. Table I-4 shows parts count of the telecom subsystem. It is recommended that the radio, SSPA, and antennas be configured in close proximity of each other to reduce coax losses, and the antennas should not be blocked by the body of the rover to prevent loss of data. Furthermore, science payloads, rover power system, etc., should not cause harmful interference to the communication system.

**Table I-4. Rover Communications Subsystem Parts Count.**

Item	Number
Radio	2
SSPA	2
Antenna	1 HGA and 1 LGA
Switch	2
Coax Cable	12
Diplexer	2

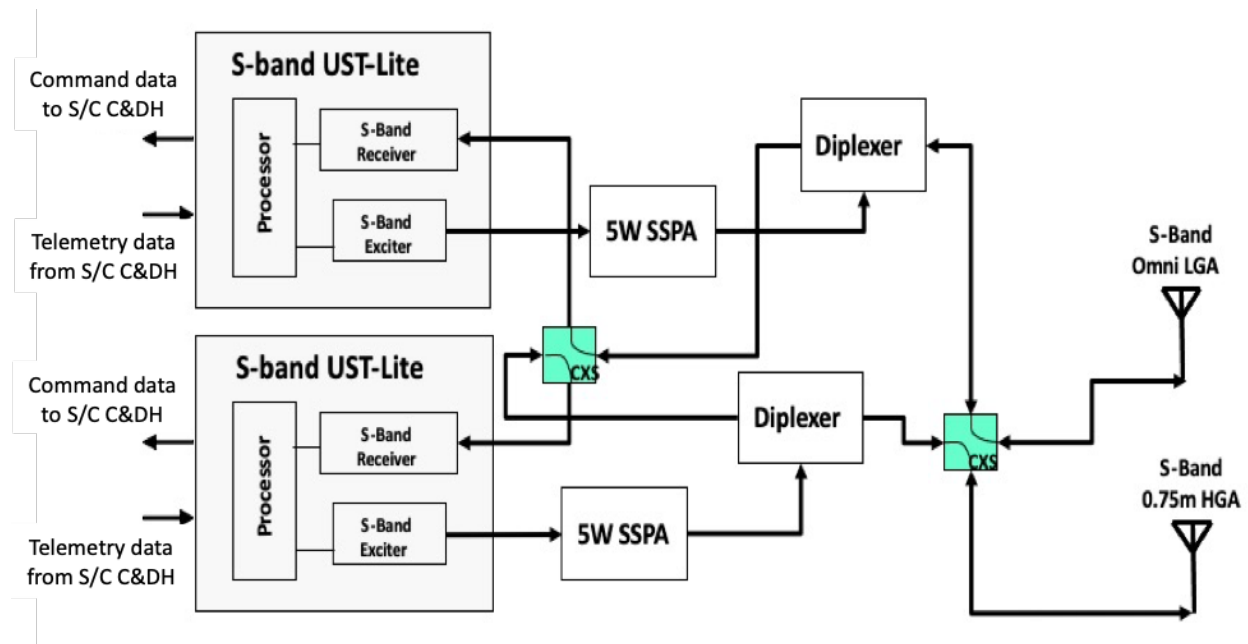


**Figure I-10.** The functional block diagram of INSPIRE communications System consisting of two redundant radio, two redundant power amplifiers, two switches, two diplexers, one tracking high-gain antenna, one low gain antenna, and coax cables. (Credit: T. Voss)

## J THERMAL DESIGN

As described above, the INSPIRE thermal design is driven by two primary requirements: 1) high degree of operability while in PSRs and also while exposed to the Sun at latitudes as low as 85° with rover tilts up to 15°; and 2) limit imposed lunar surface heat fluxes to < 6 W/m<sup>2</sup> while in PSRs to preclude volatile sublimation in the sample area. Note that a high degree of operability is defined as minimal flight rules that would otherwise restrict rover orientations and drive paths due to thermal considerations as well as minimal warm-up delays for actuator turn-on, both of which consume considerable time and/or energy that adversely impacts overall science data gathering capability. The surface heat flux limit is significant to the thermal control of the GPHS-RTG, which outputs up to 3600 W<sub>th</sub> of waste heat. The required shielding around the RTG works against the need to maintain the RTG fin root temperature to below its maximum allowable of 260 °C. The allowable temperature limits for other hardware that must be maintained are given in Table J-1.

To satisfy these requirements, INSPIRE employs a “hot-blooded” rover design where a pumped fluid loop is able to exploit the abundance of waste heat from the RTG to maintain a hot-biased thermal design that is relatively insensitive to warm electronics box (WEB) heat leaks, maintains actuators at minimum turn-on temperatures, and actively removes heat from the RTG to allow adequate shielding to meet the surface heat flux requirement that would otherwise cause too much radiative blockage to maintain fin root temperatures.

A two-phase pumped fluid loop is utilized with water as the working fluid. Saturation temperatures are set at 100 °C which limits system pressures to about 1 atm. The general architecture of the loop is shown in Figure J-1 below.

The saturation temperature is set by a cold-biased accumulator where a small heater within it is used to regulate that system pressure. Waste heat from a payload, in this case the RTG, is absorbed in the evaporator where the amount of fluid needed is passively regulated through a capillary structure. No flow boiling occurs, which allows the system to reduce the amount of pumping power required while also maintaining single-phase flows (i.e., transport lines either carry all vapor or all liquid) for greater stability. The amount of heat lifted from the RTG is based on the surface area of evaporator tubing in contact with the RTG fin roots. A conservative estimate for the heat transfer coefficient indicates that up to 700 W of waste heat may be lifted assuming four parallel evaporator tubes along the entire length of the RTG. However, analysis predictions indicated that

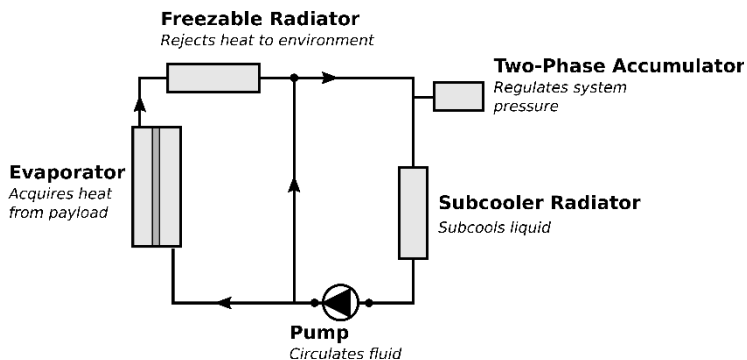


**Figure J-1.** Two-phase, mechanically pumped, fluid loop architecture.

**Table J-1.** INSPIRE Temperature Limits.

Intrepid Hardware	Allowable Flight				Protoflight or Qual			
	Operational		Nonoperational		Operational		Nonoperational	
	min	max	min	max	min	max	min	max
Sabertooth Board	-20	50	-30	50	-35	70	-45	70
Motor Controller Board	-40	50	-40	50	-55	70	-55	70
Power Board	-40	50	-40	50	-55	70	-55	70
Telecom and MUX Board	-20	50	-30	50	-35	70	-45	70
IMU	-39	51	-47	65	-54	71	-62	85
Li-Ion Battery	-20	50	NA	NA	-30	70	NA	NA
Motor Winding	-70	135	-100	135	-85	155	-120	155
Gearbox	-55	135	-131	91	-70	135	-146	111
Engineering Camera Detector	-20	40	-40	70	-35	60	-55	90
Engineering Camera Electronics	-45	55	-40	70	-60	75	-55	90
EECAM (CMOS, Optics, Elec)	-55	50	-120	50	-70	70	-135	70

only about 400 W is required to be removed to remain below the maximum RTG temperature of 260 °C, so the entire length of tubing would not be required. The subcooler is simply an additional area for the condensed liquid to subcool below the saturation temperature of 100 °C to ensure net positive suction head to the centrifugal pump to guard against cavitation. The rover block diagram with the fluid loop is shown in in Figure J-2.

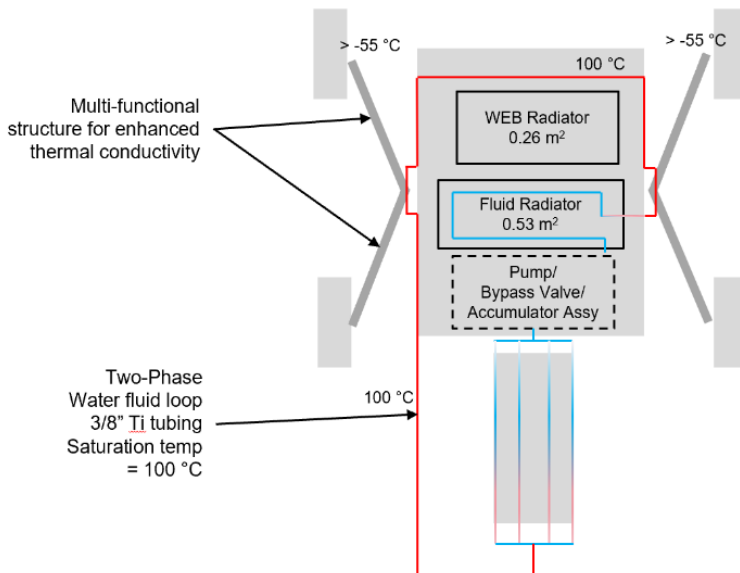


**Figure J-2.** Fluid is evaporated off of the RTG and condensed at the Rocker hub, WEB internals, and Fluid Radiator.

The high latent heat capacity of water allows flow rates as low as 20 mL/min (< 1 W pumping power assuming 2% mechanical efficiency and where the pump is digitally controlled by the flight computer) while reclaiming about 400 W<sub>th</sub> off of the RTG under worst case hot conditions, which is for operation in Sun with the rover tilted up to 17° such that the RTG is exposed to the incoming solar flux, as shown in Figure J-3.

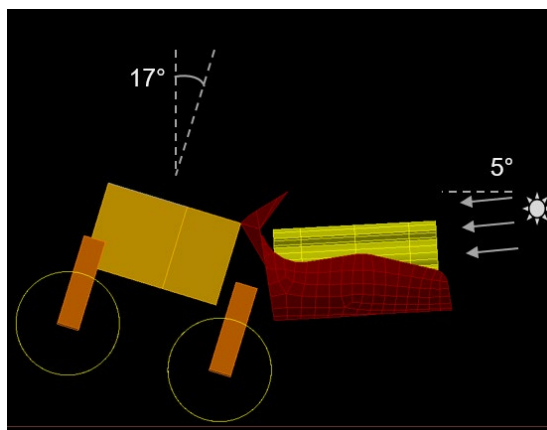


**Figure J-3.** The worst-case hot RTG condition is at 85° latitude, in sun, with a 17° tilt exposing the RTG to direct solar flux.

Note that in this specific configuration, the predicted RTG temperatures are slightly exceeding the 260 °C fin root temperature limit with 400 W lifted by the loop. But adjustments can be made to optimize the shield around the RTG to block some of the incoming solar flux or to lift additional heat beyond the 400 W via the two-phase loop. Figure J-4 shows the predicted rover and RTG temperatures for this worst-case hot scenario.

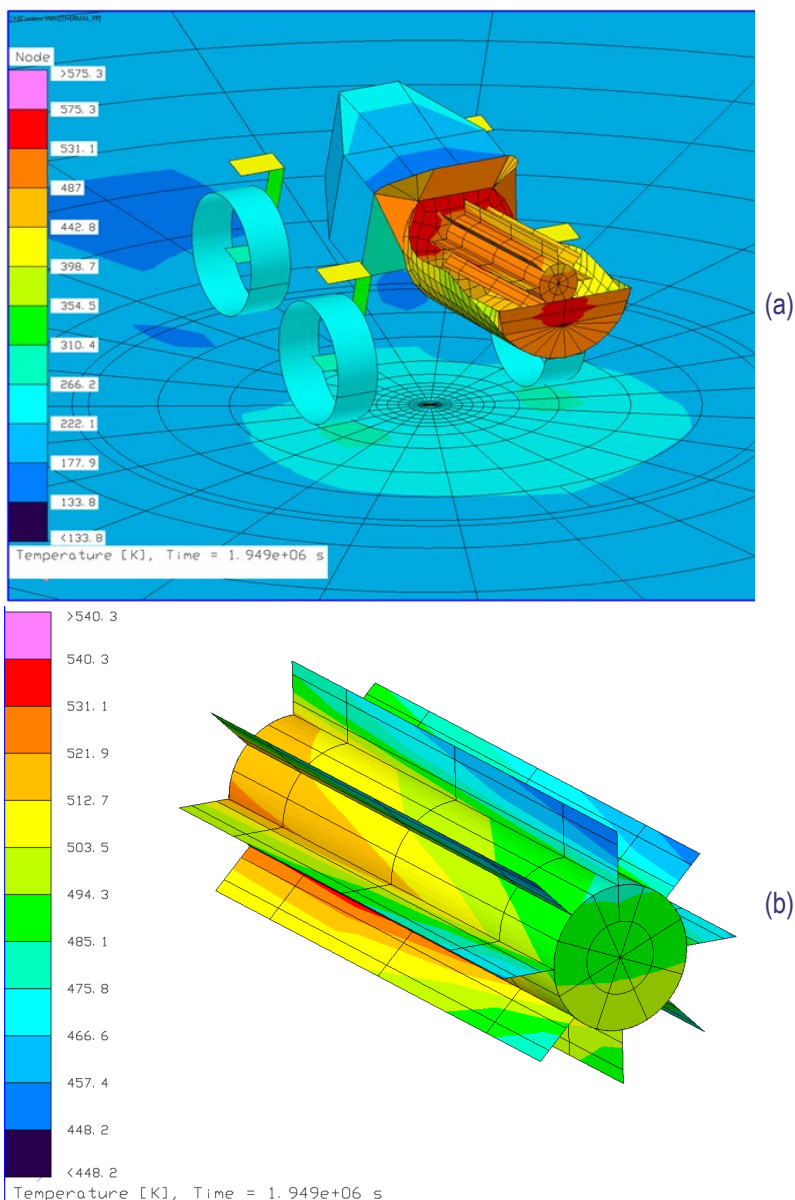


**Figure J-4.** (a) Predicted rover and regolith temperatures and (b) RTG temperatures for the worst-case hot scenario of the rover at 85° latitude and a 17° tilt allowing direct solar flux into the RTG shield.

The high quality heat at 100 °C enables passive heat conduction across joints to maintain minimum actuator temperatures of > -55 °C without the need for fluid slip rings. The fluid loop can be run by the rocker hub, maintaining its temperature at 100 °C as vapor is condensed over an interface plate attached to it. Although there are thermal interface resistances between the rocker hub, rocker arm, actuator arm, and actuator, a moderately high thermal conductivity material, such as aluminum for the rocker and actuator arms will allow sufficient heat conduction. That is, the high quality heat from the fluid loop at 100 °C enables us to tolerate the high thermal resistances across joints while maintaining actuators above -55 °C at all times. This frees us from the “heat-to-use” paradigm that has been part of the Mars heritage designs that can consume significant energy and time (up to 7 Earth hours of heating is predicted for the lunar environment) and that significantly hinders science data gathering volume over the course of the INSPIRE campaign. Figure J-5 shows the predicted temperatures of



the mobility actuators while in a shadowed region. A conservative bearing conductance of 0.2 W/K was assumed across rotating elements [75].

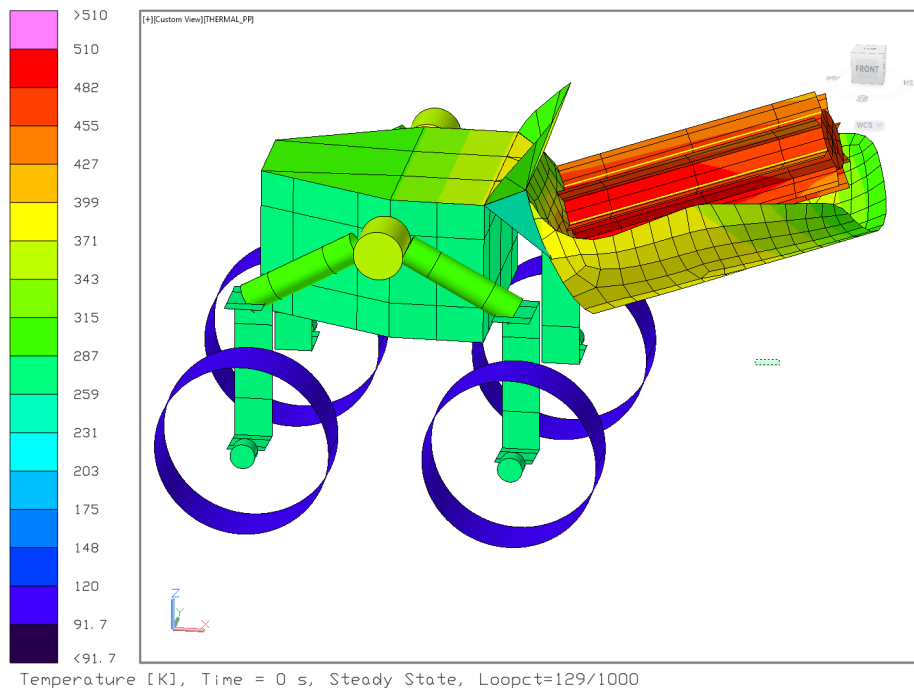


**Figure J-5.** With an interface plate to the rocker hub maintained at 100 °C, the mobility actuators run no colder than -14 °C (259 K) as shown in the above analysis prediction while in a shadowed region with no internal actuator dissipations.

A mass and volume saving opportunity exists if additive manufacturing is leveraged for the rocker arms. A multi-functional (thermal/structural) monolithic build has been demonstrated where an oscillating heat pipe (OHP) is integrated within an aluminum or titanium structure. OHPs is a specific type of a passive heat pipe that does not require a wick structure and has shown effective thermal conductivities that are 1 to 1.5 orders of magnitude beyond aluminum. Figure J-6 depicts one such configuration.

The warm-blooded rover thermal design also maintains the warm electronic box (WEB) temperatures above minimum allowable avionics temperatures with minimal resources. Similar to the rocker hub, tubing is run within the WEB as needed to maintain temperatures with very minimal fluid tubing.

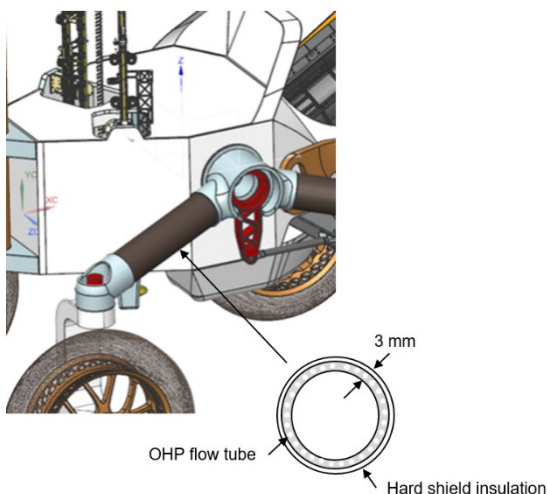


**Figure J-6.** Oscillating heat pipe technology that is monolithically built via additive manufacturing presents a mass and volume saving opportunity compared to an aluminum rocker arm built with sufficient thermal conductance.

For example a single pass of 3/8” diameter fluid tubing run along a subset of walls can maintain an entire volume well above avionics minimum temperatures of -20 °C, as shown in Figure J-7. Specific tube routing can be done as required for a given compartment configuration of the rover.

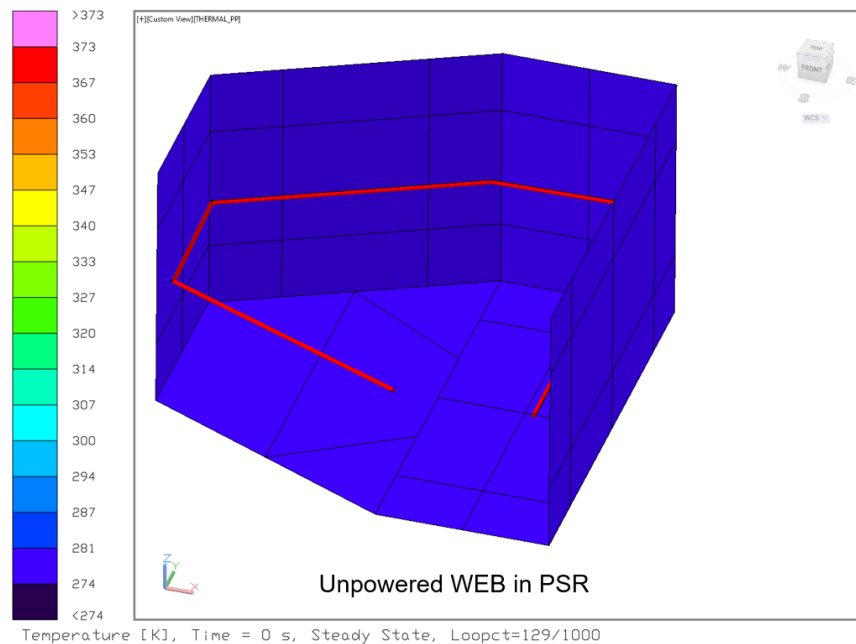


**Figure J-7.** The internal WEB temperatures are maintained with minimal fluid tube exposure within it for adequate warming via radiation.

WEB temperatures are regulated by a passive system using heat switches attached to the radiator via flexible thermal straps as shown in Figure J-8. Note that the fluid loop radiator, which runs at approximately 100 °C, is placed near the radiator shield as it is more forgiving of a hindered view to space.

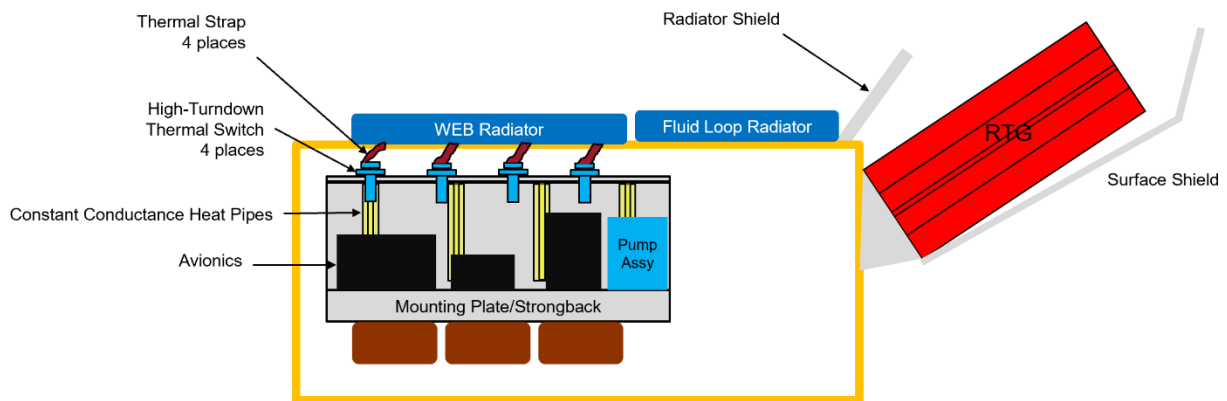


**Figure J-8.** A passive thermal control system regulates internal WEB temperatures through a set of parallel heat switches mounted to a zenith-facing radiator using flexible thermal straps.

The passive heat switches provide a variable conduction path between the components internal to the WEB and radiators and are passively actuated based entirely on differences in coefficients of thermal expansion of its selected materials (Figure J-9). The on/off conductance ratio is 5 to 0.002 W/K through a given switch, which is a 20X better than the switches flown on the Mars Exploration Rovers. The passive heat switches are developed by JPL and are currently at TRL 7, having completed flight

qualification and life testing. The flexible straps accommodate the CTE-based actuation movement of the switches.

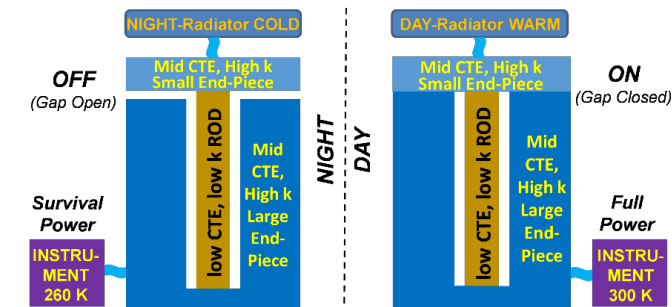


Figure J-9. Heat switch design.

External instrument temperatures are maintained with a locally placed RHU. Operation in the presence of sun exposure is accommodated by having zenith-facing surfaces reject excess dissipations.

The RTG heating is, by far, the largest threat to the science-driven requirement that imposed heat fluxes to the lunar surface remain minimal to preclude volatile sublimation while in shadowed regions. The thermal design employs shields around the RTG to limit Lunar surface heat fluxes to  $< 6 \text{ W/m}^2$  in the vicinity of the sampling location. This is contradiction to the need to maintain RTG temperatures below the maximum fin root temperature of  $260 \text{ }^\circ\text{C}$ . In order to satisfy both requirements, the shield is used in conjunction with the pumped fluid loop that removes RTG waste heat from its body for re-use elsewhere. Figures J-10 through J-12 show the analysis results that predict both requirements to be satisfied. Note that imposed heat fluxes exceed the  $6 \text{ W/m}^2$  limit in areas directly below the rover, but are below this value in area where samples are to be taken.

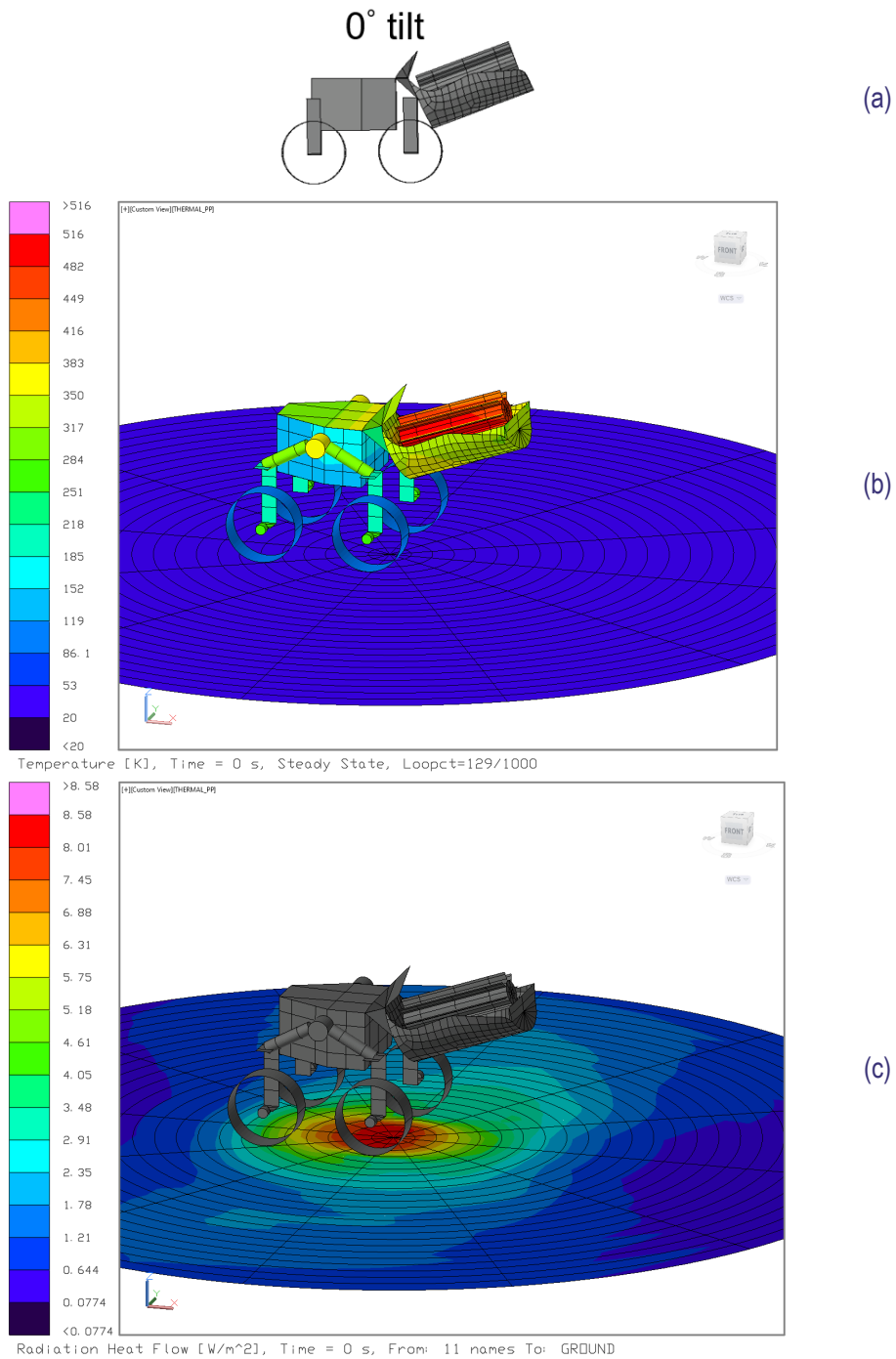
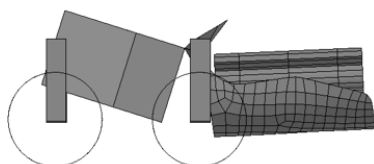
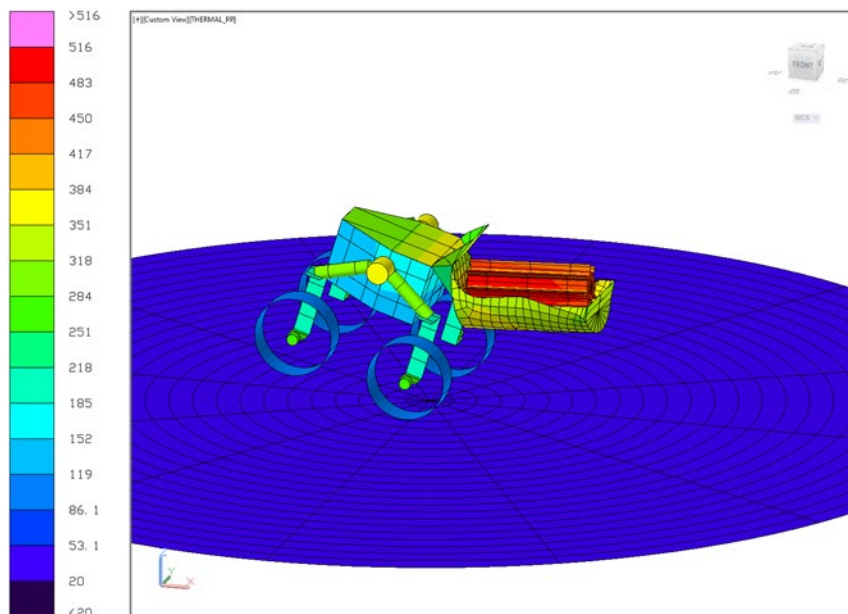


Figure J-10. RTG temperatures and imposed lunar surface heat fluxes for a 0° rover tilt

17° aft tilt

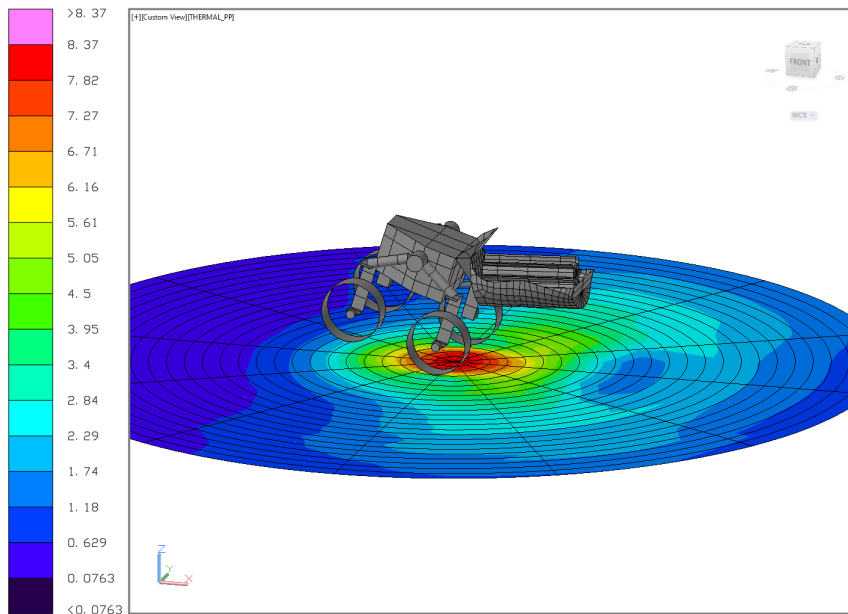


(a)



(b)

Temperature [K], Time = 0 s, Steady State, Loopct=129/1000



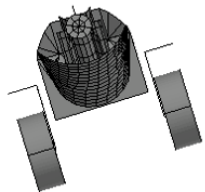
(c)

Radiation Heat Flow [W/m^2], Time = 0 s, From: 11 names To: GROUND

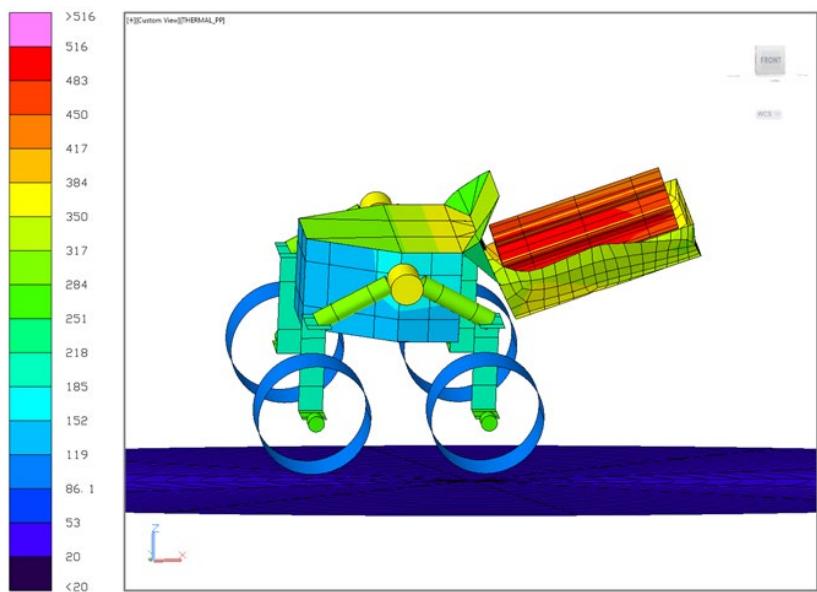
Figure J-11. RTG temperatures and imposed lunar surface heat fluxes for a 17° rover pitch



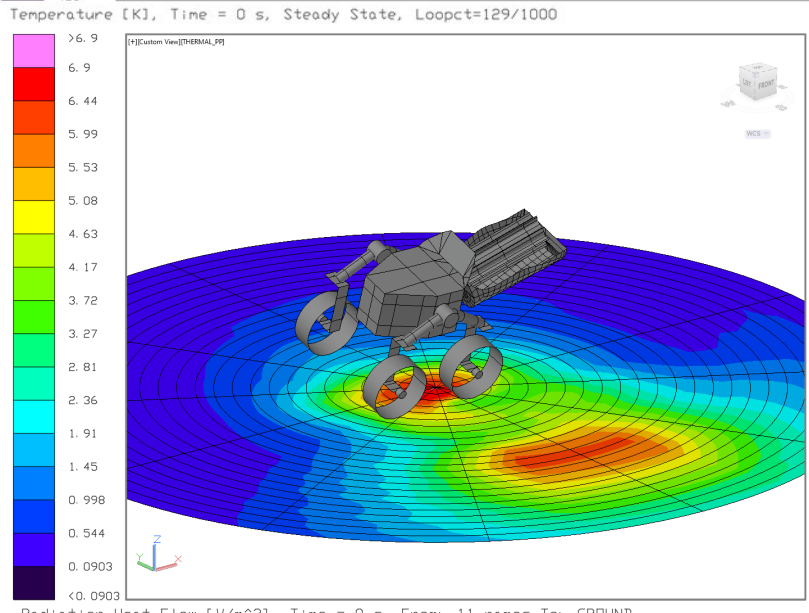
17° roll



(a)



(b)



(c)

Figure J-12. RTG temperatures and imposed lunar surface heat fluxes for a 17° rover roll

## K TRAVERSE PLANNING

### Path Planning

The INSPIRE path planning was an iterative process, starting with the identification of several Science Stations that could meet the INSPIRE science criteria (Table B-1), and continuing with the finding of topographic datasets that were available for path-planning analysis within and between these regional (300 x 300 m) sites. Notional paths between the regions were mapped. Higher resolution datasets which covered these regions were identified and used to support detailed path planning. Specifically, 5-m and a 10-m LRO Lunar Orbiter Laser Altimeter (LOLA) datasets and a Chang'E-2 20-m dataset were selected to be used for path planning (Figs. K-8a, K-8b). Additionally, some LRO NAC images were processed through a stereo pipeline to construct localized NAC-resolution (<2 mpp) DEMs (Figs. K-9–K-14).

Following preliminary discussions with the mobility team, a matrix of rover speed as a function of slope was constructed for both illuminated and dark (permanently shadowed or nighttime) regions. As the set of Science Stations was refined, a Version 1 of the path was baselined. As the list of Science Stations and the slope matrix were iterated, a Version 2 of the path was baselined. A final Version 3 was then constructed that allowed for all of the science objectives to be met (Table B-1), the traverse path to be optimized, and the mission duration to be estimated.

As discussed in Section 1.5 and Appendix B, the Science Stations include sites in five major PSRs: Cabeus, Haworth, an unnamed PSR adjacent to the Haworth crater, Shoemaker, and Faustini (Fig. 1-4). Individual path segments were constructed between each major PSR (Fig. K-3) and then inter-region traverses were constructed to connect all the Science Stations (Figs. K-2, K-4, K-5, K-6, K-7) and generate a complete mission path (Figs. K-1a–K-1e, K-15–21).

The traverse path was generated using ArcGIS's least cost path analysis. The least cost path algorithm works to determine the most cost-effective route between a user-defined source and destination point based on the eight neighboring pixels of the cost dataset. The eight neighboring pixels are iteratively evaluated to determine the smallest accumulated cost value, thus determining the path direction. The resulting path is based on the smallest sum of pixel values between the two points. The cost value used for this analysis is based on the maximum degree of slope that can be traversed by the Rover. Initially the slope constraint used to generate the paths was set to 15°; however, increments and decrements to this constraint were also analyzed to observe alternate routes and to analyze sensitivity to traverse distances on slope constraint. The slope constraint was increased to 17° and the cost dataset used for the least cost analysis was processed accordingly.

Path generation from Science Station to Science Station was conducted individually and outputted as polyline segments. All path segments were merged together so that the final version of this path represents a single integrated polyline feature (Fig. K-1a). Slope values were then extracted to obtain what percentage of the path is within a certain slope range, using 5-m and 10-m DEMs (Tables K-7, K-8).

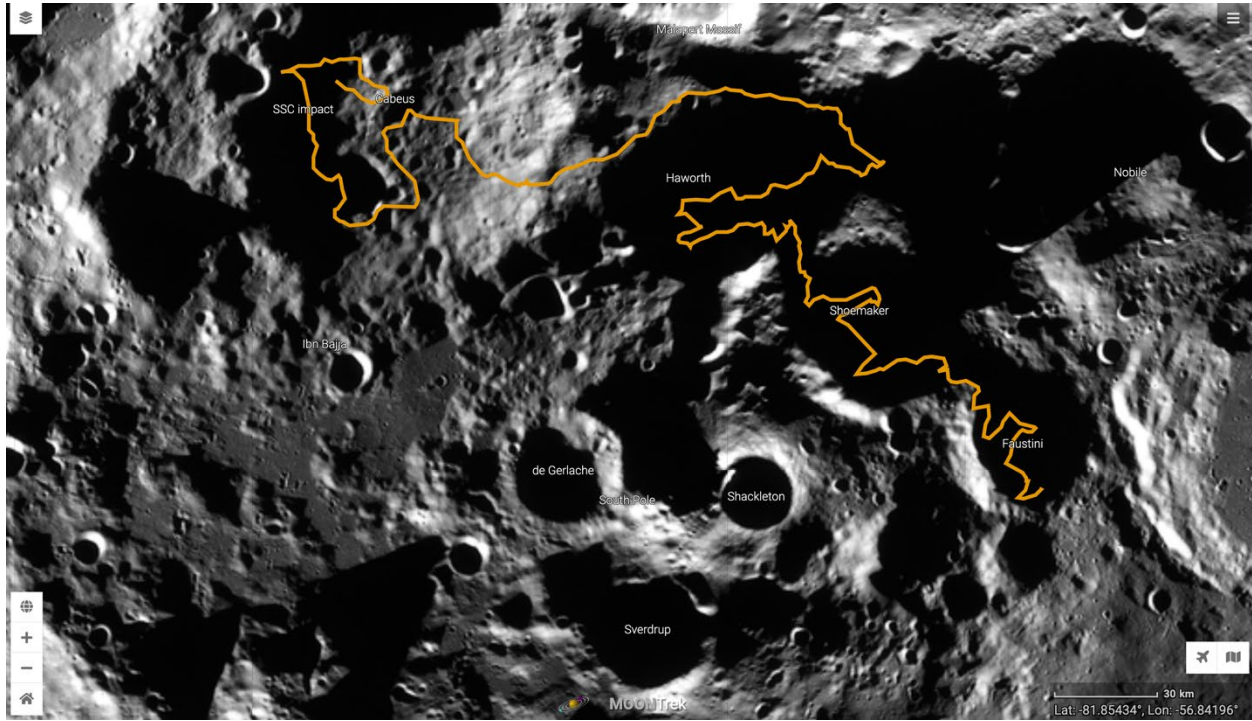


Figure K-1a. INSPIRE Traverse Path.

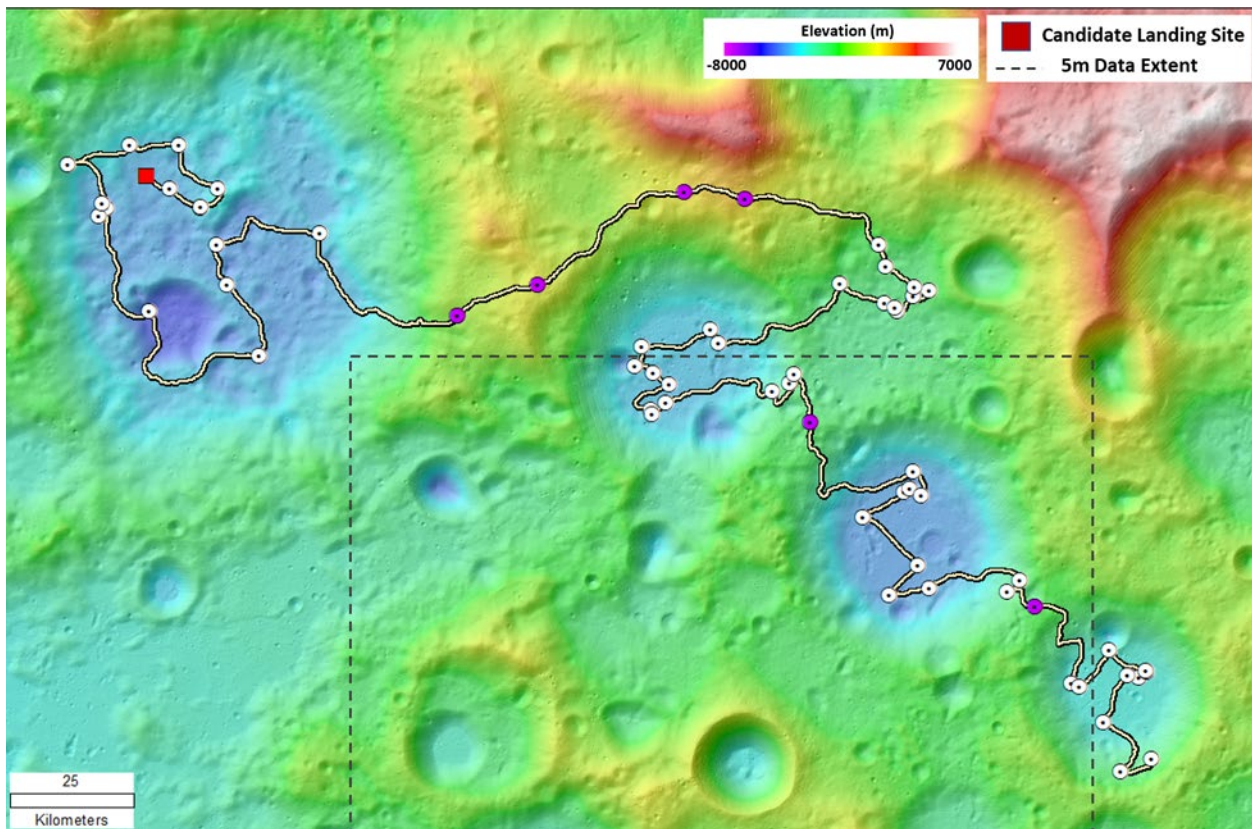


Figure K-1b. Full extent of INSPIRE version 3 path.



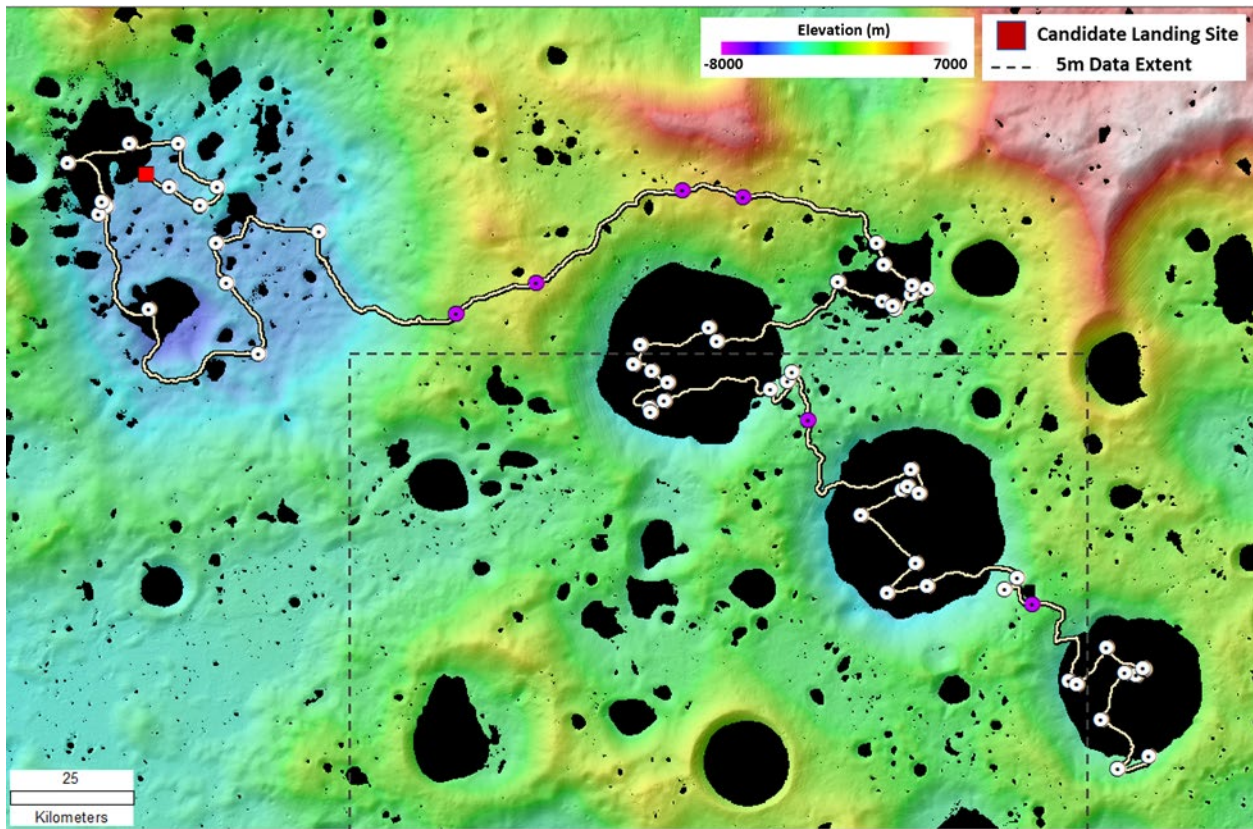


Figure K-1c. Full extent of INSPIRE version 3 path with PSR data.

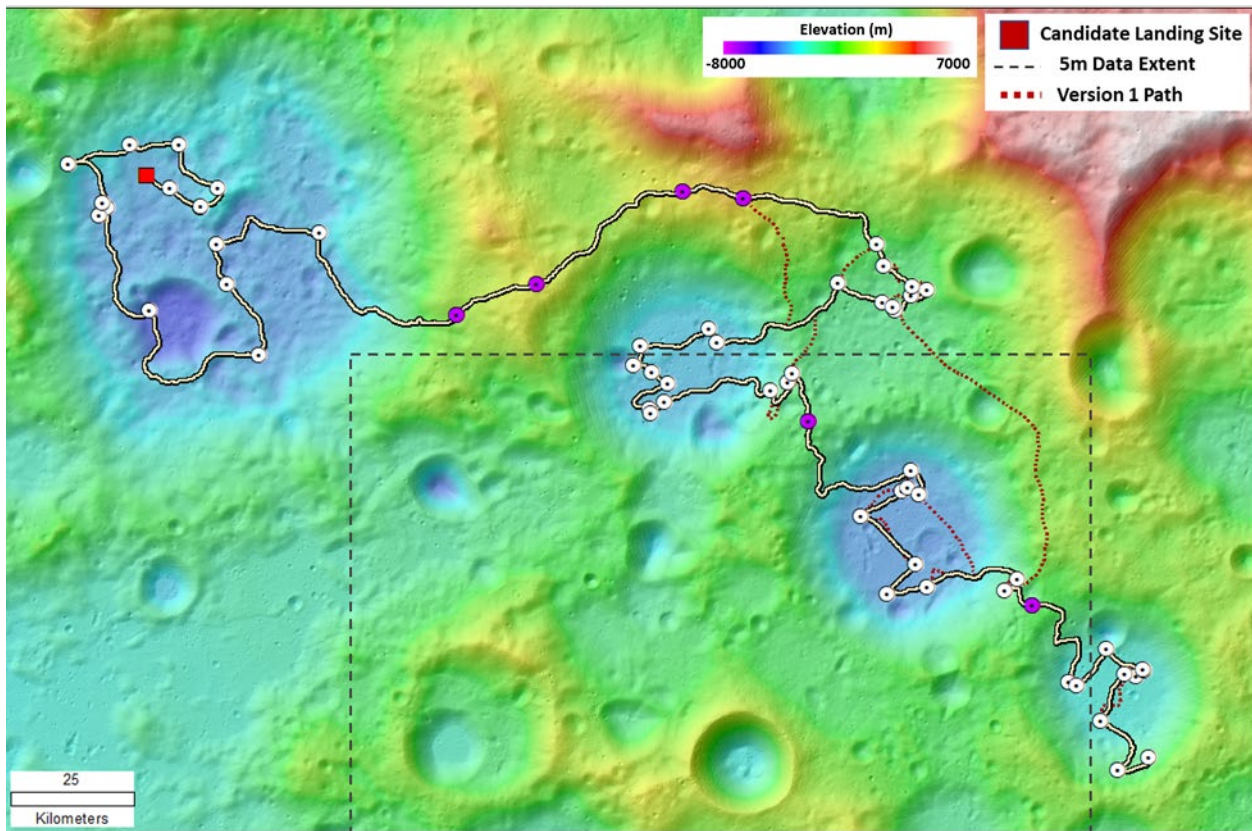


Figure K-1d. Full extent of INSPIRE version 3 path. Version 1 path depicted.



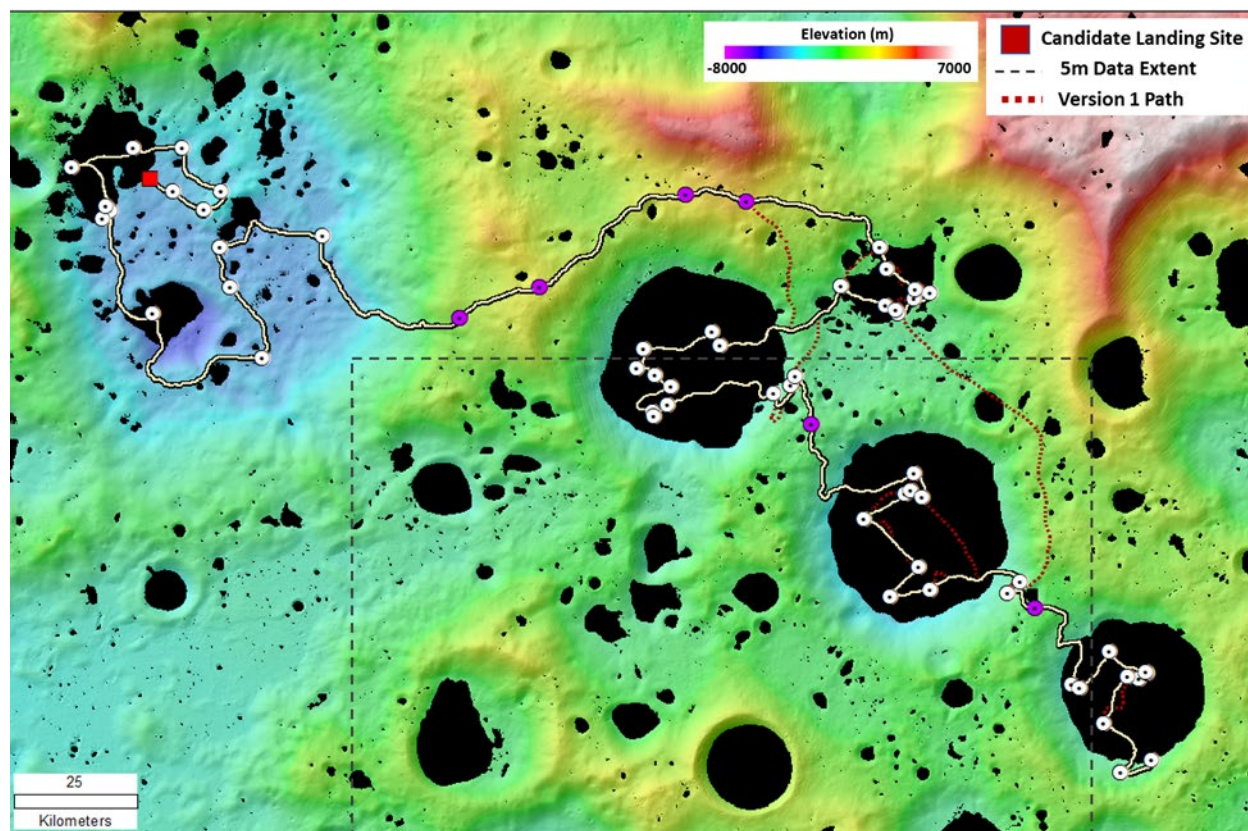
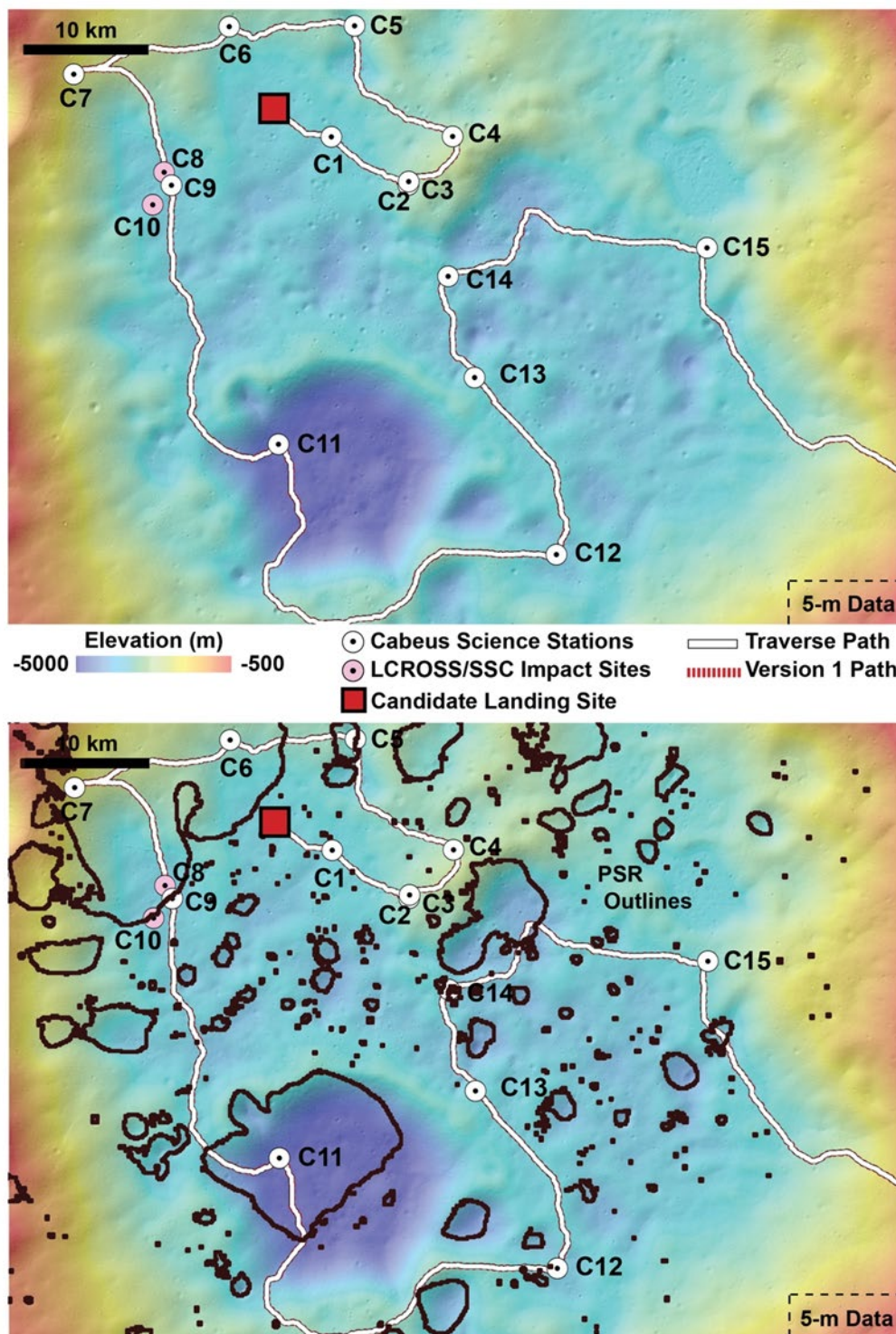


Figure K-1e. Full extent of INSPIRE version 3 path with PSR data. Version 1 path depicted.



**Figure K-2.** INSPIRE Traverse Path within Cabeus crater compared with Version 1 Path. PSRs are outlined in black in bottom figure. The majority of the region is within 10-m DEM extent, and 5-m DEM extent is denoted with black dashed lines.

**Table K-1.** Science Station traverse order within Cabeus.

Traverse Figure Labels	Location (°S, °E)	Cold-Trapping Thermal Environments				Evolution of Ice-Stability Environments					Ground-Truthing		
		Surface T			SSR	Present-day surface ice stable	Paleo surface ice stable	Present-day subsurface ice stable	Paleo subsurface ice stable	LAMP ice detection	M <sup>3</sup> ice detection	LCROSS impact	Radar anomalous
		<50 K	50-100 K	>100 K									
C-1	84.94, -44.57		X					X	X				
C-2	85.17, -43.91			X				X	X				
C-3	85.17, -43.83				X			X	X				X
C-4	85.16, -41.86			X			X	X		X			
C-5	84.77, -41.85	X				X	X						
C-6	84.54, -44.45		X			X			X		X		
C-7	84.33, -48.30		X			X			X	X			
C-8	84.68, -48.71 (x2 drill sites)			X		X			X			X	
C-9	84.72, -48.82	X				X	X			X			
C-10	84.72, -49.61 (x2 drill sites)		X			X	X					X	
C-11	85.37, -52.91	X				X	X				X		
C-12	86.13, -49.80	X					X	X					X
C-13	85.66, -46.91				X		X	X					X
C-14	85.42, -45.07		X					X	X	X	X		X
C-15	85.82, -37.70				X			X	X				



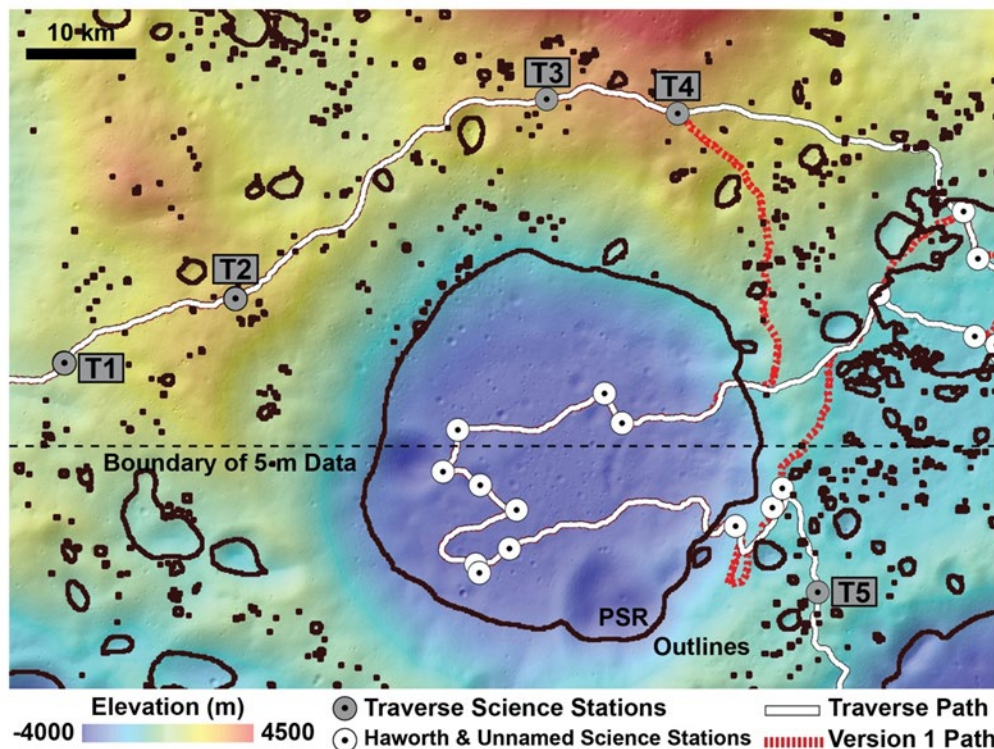


**Figure K-3.** INSPIRE Traverse Path between Cabeus (Fig. K-2), the Unnamed PSR (Fig. K-4), Haworth (Fig. K-5), and leading to Shoemaker (Fig. K-6) compared with Version 1 Path. Traverse Path Science Stations 1–5 are shown. Traverse Path Science Station 6 is located between Shoemaker and Faustini (Figs. K-6, K-7). PSRs are outlined in black.

**Table K-2.** Science Station traverse order along traverse.

Traverse Figure Labels	Location (°S, °E)	Cold-Trapping Thermal Environments				Evolution of Ice-Stability Environments					Ground-Truthing		
		Surface T			SSR	Present-day surface ice stable	Paleo surface ice stable	Present-day subsurface ice stable	Paleo subsurface ice stable	LAMP ice detection	M <sup>3</sup> ice detection	LCROSS impact	Radar anomalous
		<50 K	50-100 K	>100 K									
T-1	86.78, 30.67			X				X	X				
T-2	86.83, -20.46				X	X			X				
T-3	86.41, -2.22				X			X	X				
T-4	86.45, 4.36			X				X	X				
T-5	87.83, 18.96				X			X	X				
T-6	87.66, 69.34				X			X	X				



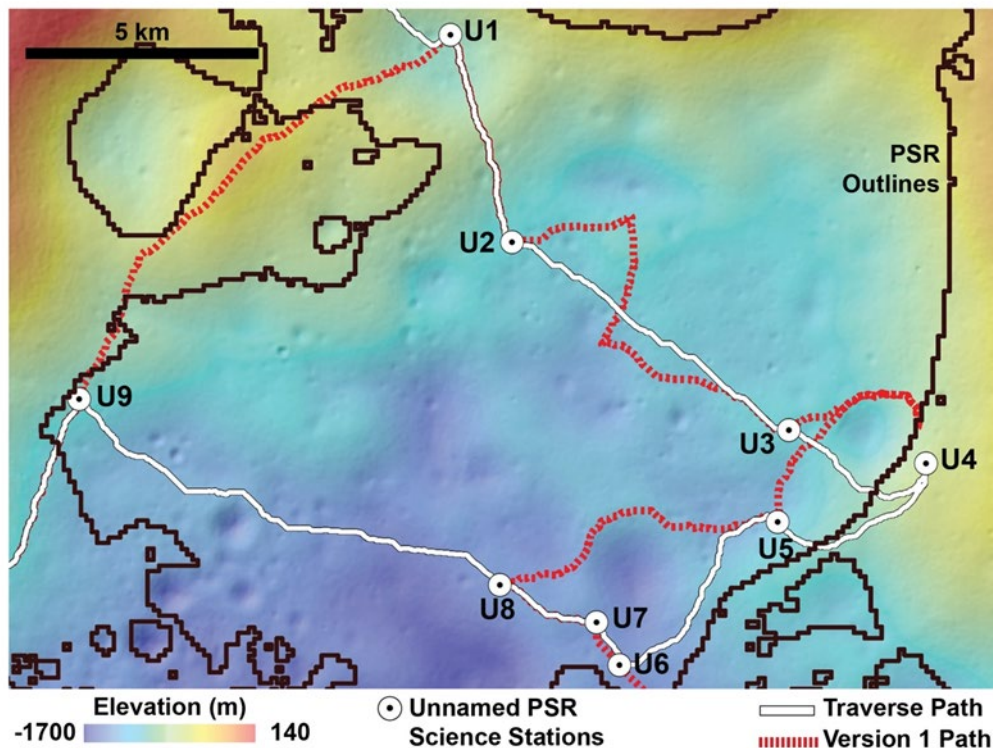


**Figure K-4.** INSPIRE Traverse Path within Unnamed PSR compared with Version 1 Path. PSRs are outlined in black. Entire region is within 10-m DEM extent.

**Table K-3.** Science Station traverse order within Unnamed PSR.

Traverse Figure Labels	Location (°S, °E)	Cold-Trapping Thermal Environments				Evolution of Ice-Stability Environments					Ground-Truthing		
		Surface T			SSR	Present-day surface ice stable	Paleo surface ice stable	Present-day subsurface ice stable	Paleo subsurface ice stable	LAMP ice detection	M <sup>3</sup> ice detection	LCROSS impact	Radar anomalous
		<50 K	50-100 K	>100 K									
U-1	86.56, 19.71	X				X			X				
U-2	86.67, 21.01	X				X			X	X			
U-3	86.69, 21.27		X			X			X				
U-4	86.73, 25.31	X				X			X	X	X		
U-5	86.71, 27.01	X					X	X					
U-6	86.93, 24.61		X			X			X		X		
U-7	86.91, 24.11		X			X			X	X			
U-8	86.91, 22.75	X				X			X		X		
U-9	86.89, 16.76		X			X			X	X	X		

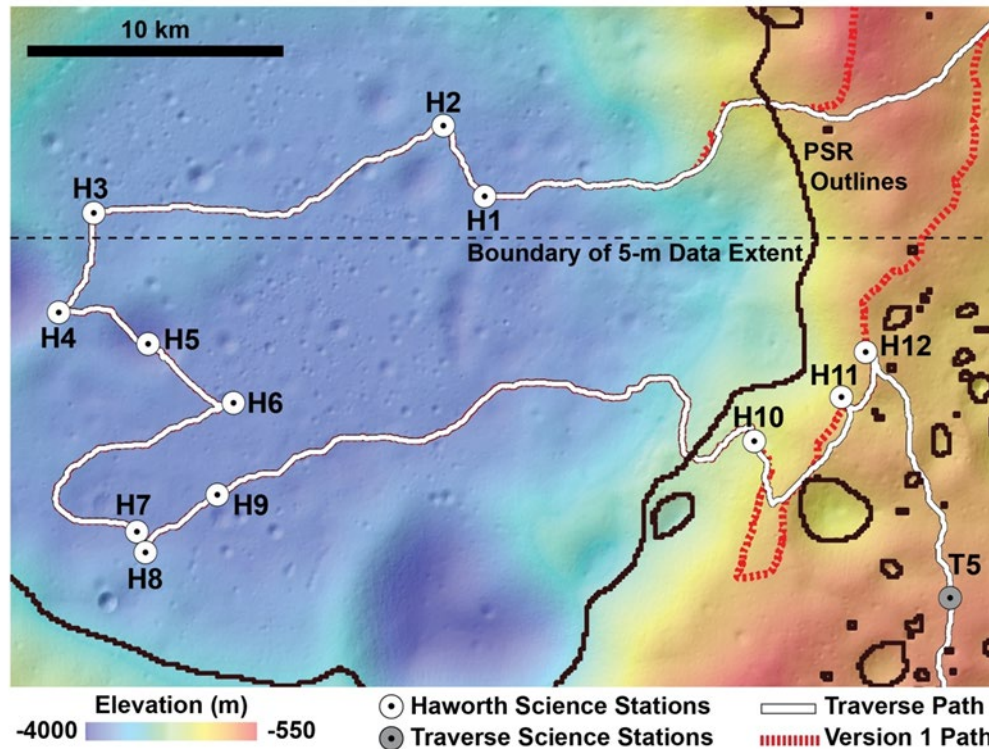
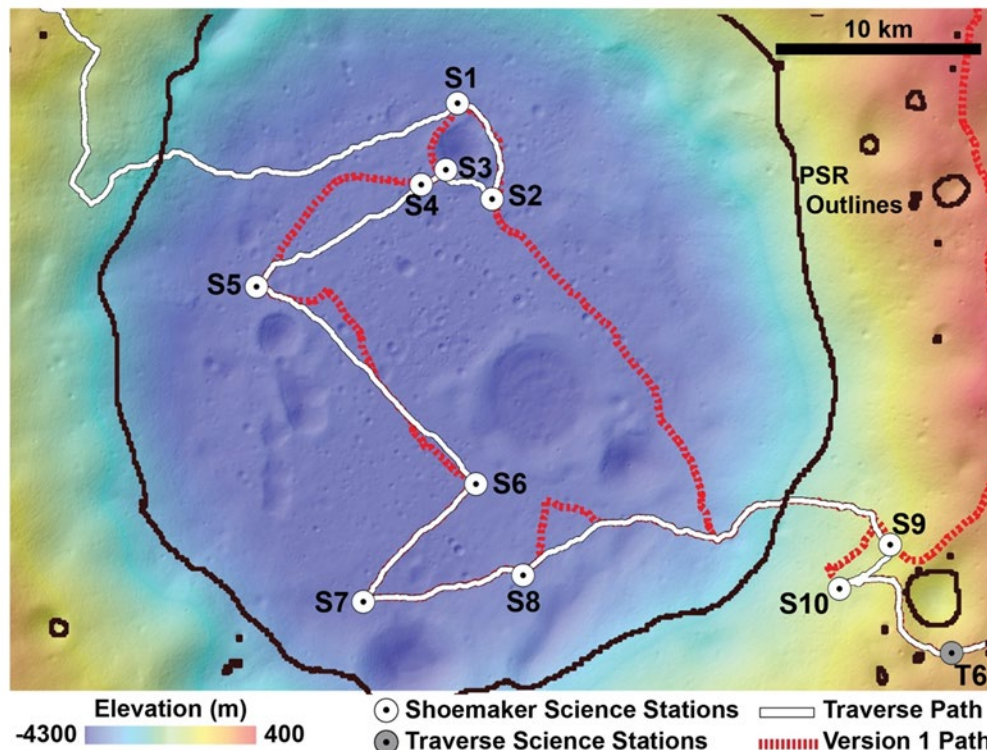


Figure K-5. INSPIRE Traverse Path within Haworth compared with Version 1 Path. PSRs are outlined in black.

Table K-4. Science Station traverse order within Haworth.

Traverse Figure Labels	Location (°S, °E)	Cold-Trapping Thermal Environments				Evolution of Ice-Stability Environments					Ground-Truthing		
		Surface T			SSR	Present-day surface ice stable	Paleo surface ice stable	Present-day subsurface ice stable	Paleo subsurface ice stable	LAMP ice detection	M <sup>3</sup> ice detection	LCROSS impact	Radar anomalous
		<50 K	50-100 K	>100 K									
H-1	87.42, 2.14	X				X	X			X	X		
H-2	87.33, 0.91	X				X			X		X		
H-3	87.41, -9.23	X				X			X	X			
H-4	87.53, -10.77	X				X	X						X
H-5	87.60, -8.23	X				X	X						
H-6	87.68, -5.75		X			X			X	X			
H-7	87.83, -9.53		X			X			X	X	X		
H-8	87.86, -9.34		X			X			X		X		
H-9	87.80, -6.61		X			X			X				
H-10	87.70, 11.25		X				X		X				
H-11	87.62, 13.67		X					X	X				
H-12	87.55, 14.07		X					X					



**Figure K-6** INSPIRE Traverse Path within Shoemaker compared with Version 1 Path. PSRs are outlined in black. Entire region is within 5-m DEM extent.

**Table K-5.** Science Station traverse order within Shoemaker.

Traverse Figure Labels	Location (°S, °E)	Cold-Trapping Thermal Environments				Evolution of Ice-Stability Environments					Ground-Truthing		
		Surface T			SSR	Present-day surface ice stable	Paleo surface ice stable	Present-day subsurface ice stable	Paleo subsurface ice stable	LAMP ice detection	M <sup>3</sup> ice detection	LCROSS impact	Radar anomalous
		<50 K	50-100 K	>100 K									
S-1	87.79, 38.76	X				X			X				
S-2	87.87, 42.56	X				X			X	X			
S-3	87.88, 40.18	X				X		X					X
S-4	87.93, 39.75	X				X			X		X		
S-5	88.23, 36.51		X			X			X		X		
S-6	88.21, 52.07		X			X			X				
S-7	88.47, 53.49		X			X			X	X			
S-8	88.23, 57.39		X			X	X			X	X		
S-9	87.68, 64.37		X					X	X				
S-10	87.79, 65.13		X				X	X					



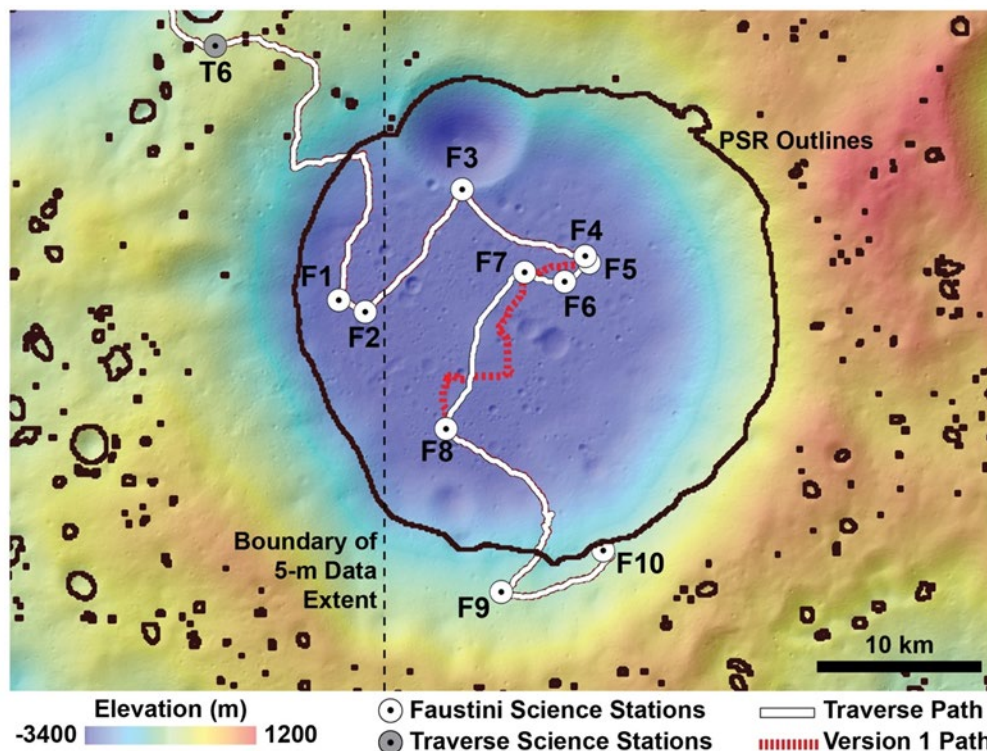
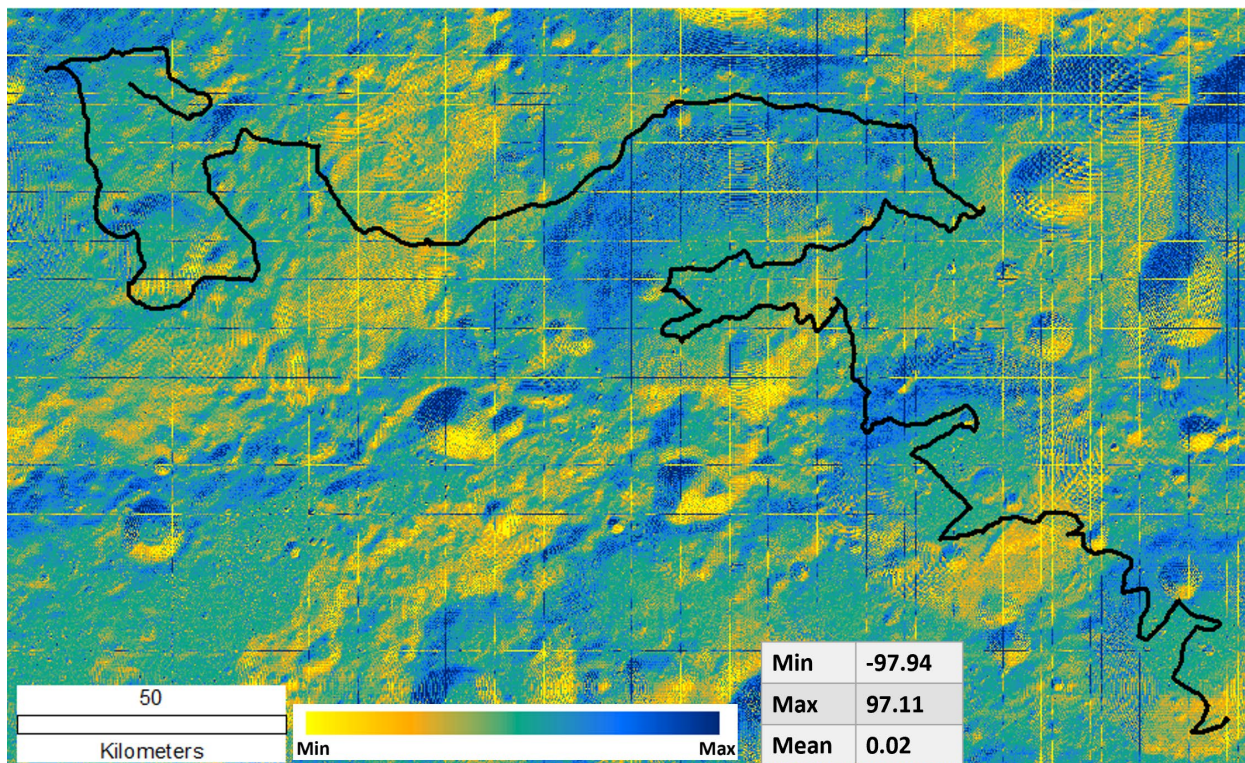


Figure K-7. INSPIRE Traverse Path within Faustini compared with Version 1 Path. PSRs are outlined in black.

Table K-6. Science Station traverse order within Faustini.

Traverse Figure Labels	Location (°S, °E)	Cold-Trapping Thermal Environments				Evolution of Ice-Stability Environments					Ground-Truthing		
		Surface T			SSR	Present-day surface ice stable	Paleo surface ice stable	Present-day subsurface ice stable	Paleo subsurface ice stable	LAMP ice detection	M <sup>3</sup> ice detection	LCROSS impact	Radar anomalous
		<50 K	50-100 K	>100 K									
F-1	87.54, 82.53		X			X			X	X	X		
F-2	87.49, 83.23		X			X			X	X			
F-3	87.26, 78.62	X				X			X				X
F-4	87.04, 82.09	X				X	X			X			
F-5	87.03, 82.37	X				X	X				X		
F-6	87.09, 82.99	X				X	X						
F-7	87.16, 82.39		X			X			X		X		
F-8	87.35, 88.64		X			X			X				
F-9	87.03, 94.13		X					X	X				
F-10	87.03, 93.47		X				X	X					





**Figure K-8a.** Elevation difference map among Chang'E-2 20m/px and LOLA 10m/px DEM. INSPIRE Traverse outlined in black.

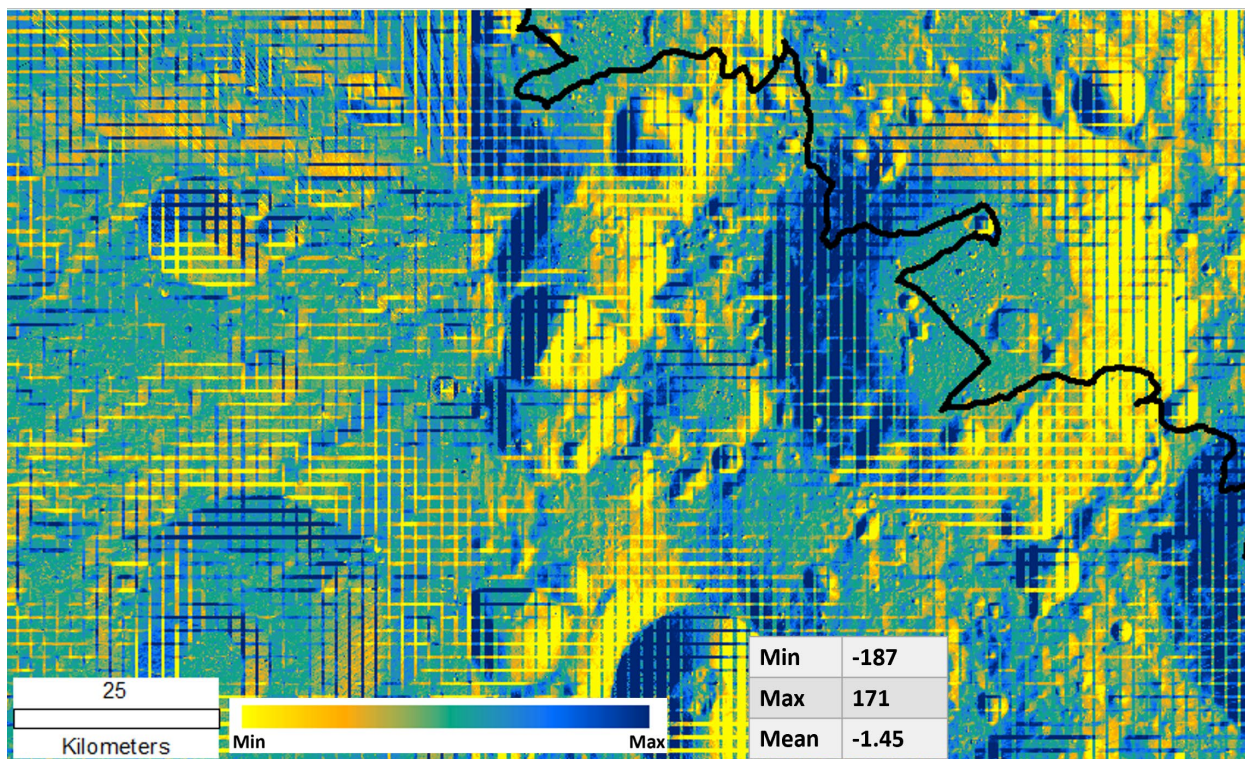


**Figure K-8b.** Elevation difference map among LOLA 10m/px and LOLA 5m/px DEM. INSPIRE Traverse outlined in black.



**Table K-7.** Slope statistics for portion of the version 3 path fully contained within the 5m DEM data extent.

Slope (deg)	Percent
0 - 5	55.76
5 - 10	25.03
10 - 15	17.06
15 - 16	1.52
16 - 17	0.62

**Table K-8.** Slope statistics for portion of the version 3 path on the 10m DEM where 5m DEM data is unavailable.

Slope (deg)	Percent
0 - 5	59.06
5 - 10	26.59
10 - 15	12.71
15 - 16	1.24
16 - 17	0.39

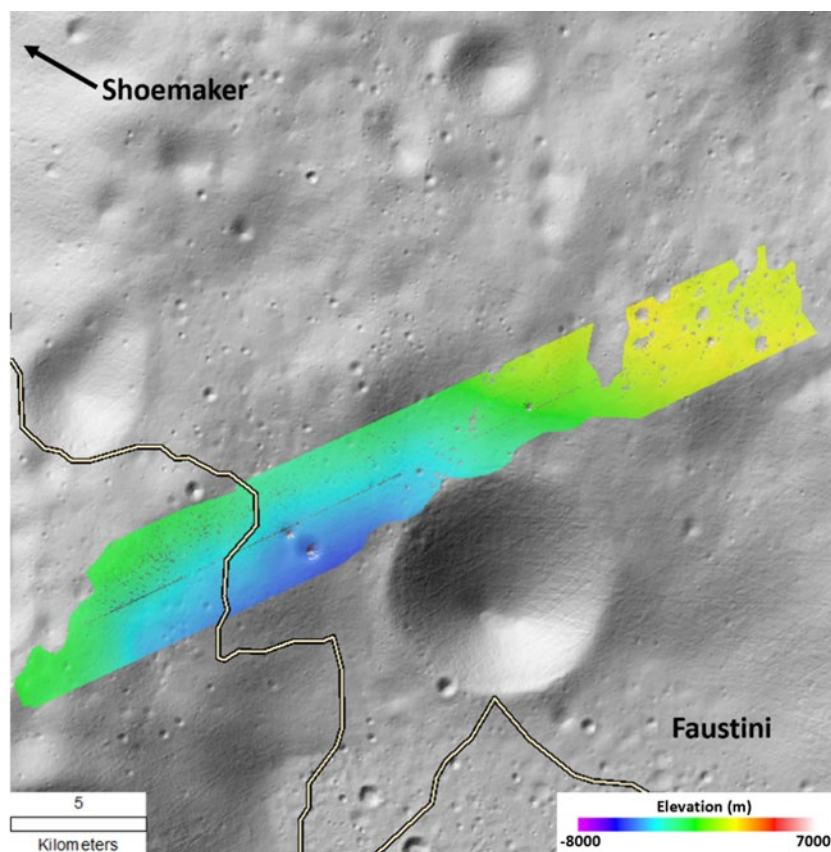


**Figure K-9.** Narrow Angle Camera (NAC) DEM generated from image pairs: M113522946 and M113529746. NAC ortho resolution is 1.25 m/px and DEM resolution is 4 m/px. Version 3 path depicted.

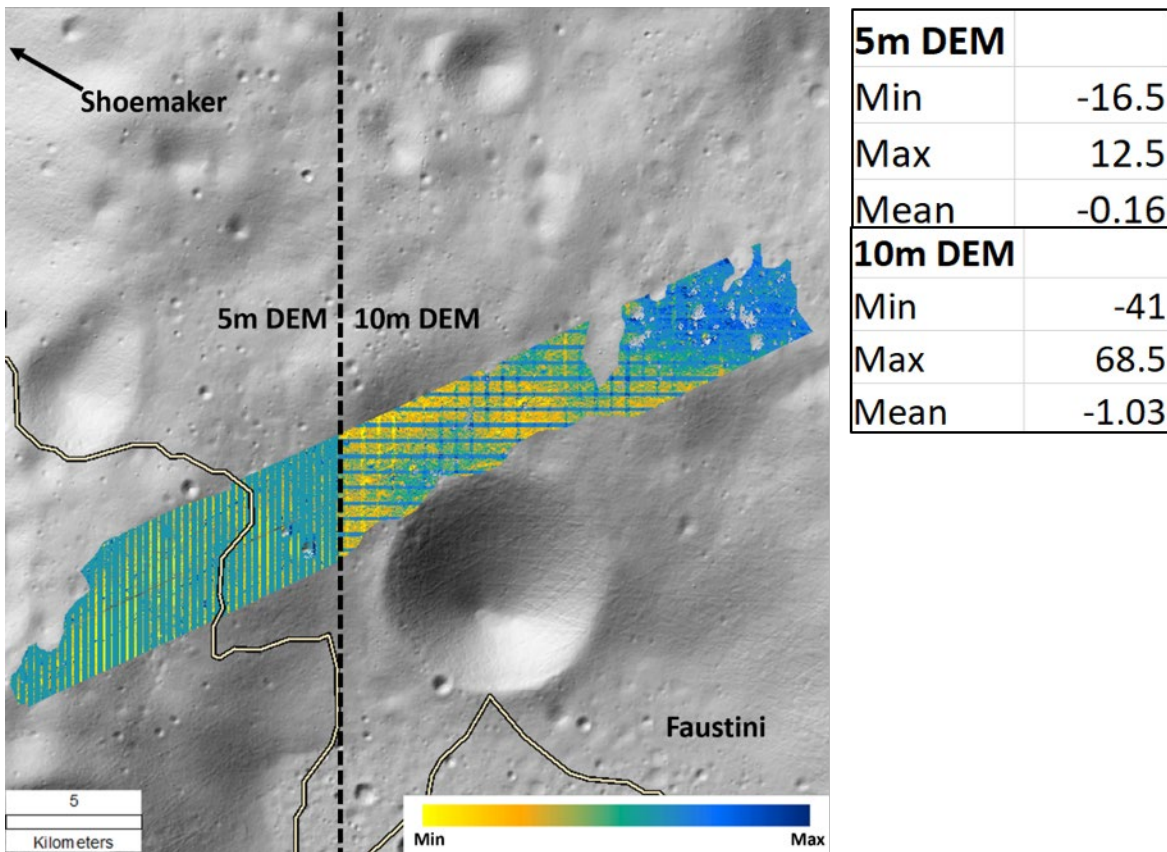


**Figure K-10.** DEM generated from image pairs: M113522946 and M113529746 Elevation Difference Map. Difference is calculated using the LOLA 5m DEM (left) and the LOLA 10m DEM (right). Version 3 path depicted.

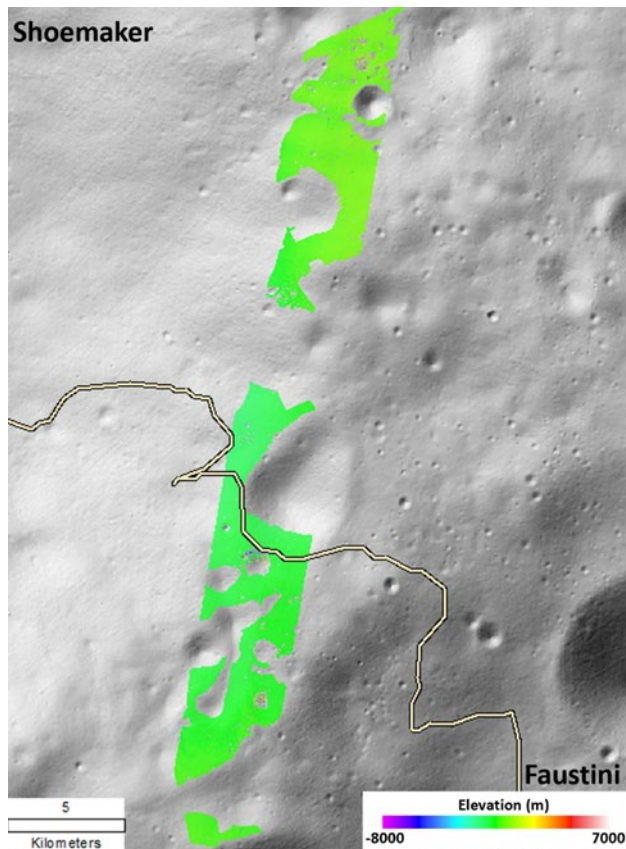


**Figure K-11.** Narrow Angle Camera (NAC) DEM generated from image pairs: M1160043430 and M1162399793. NAC ortho resolution is 1.01 m/px and DEM resolution is 3 m/px. Version 3 path depicted.



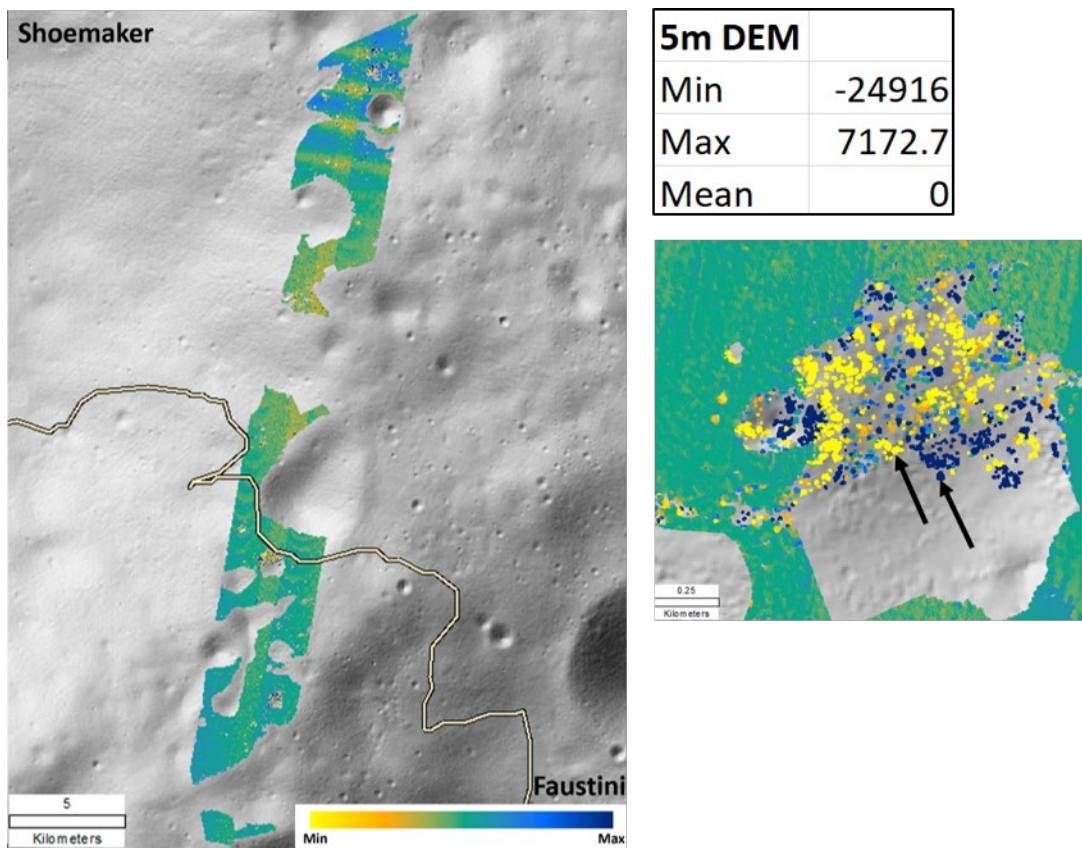


**Figure K-12.** DEM generated from image pairs: M113522946 and M113529746 Elevation Difference Map. Difference is calculated using the LOLA 5m DEM. Version 3 path depicted. Extreme outlier pixels can cause heavily skewed statistics.

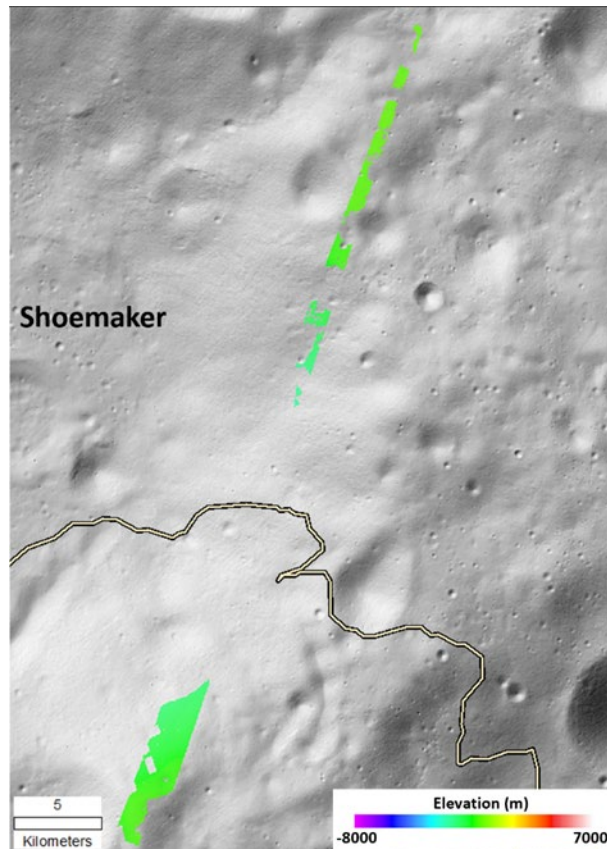


**Figure K-13.** Narrow Angle Camera (NAC) DEM generated from image pairs: M1129356077 and M1129370299. NAC ortho resolution is 0.86 m/px and DEM resolution is 2.5 m/px. Version 3 path depicted.

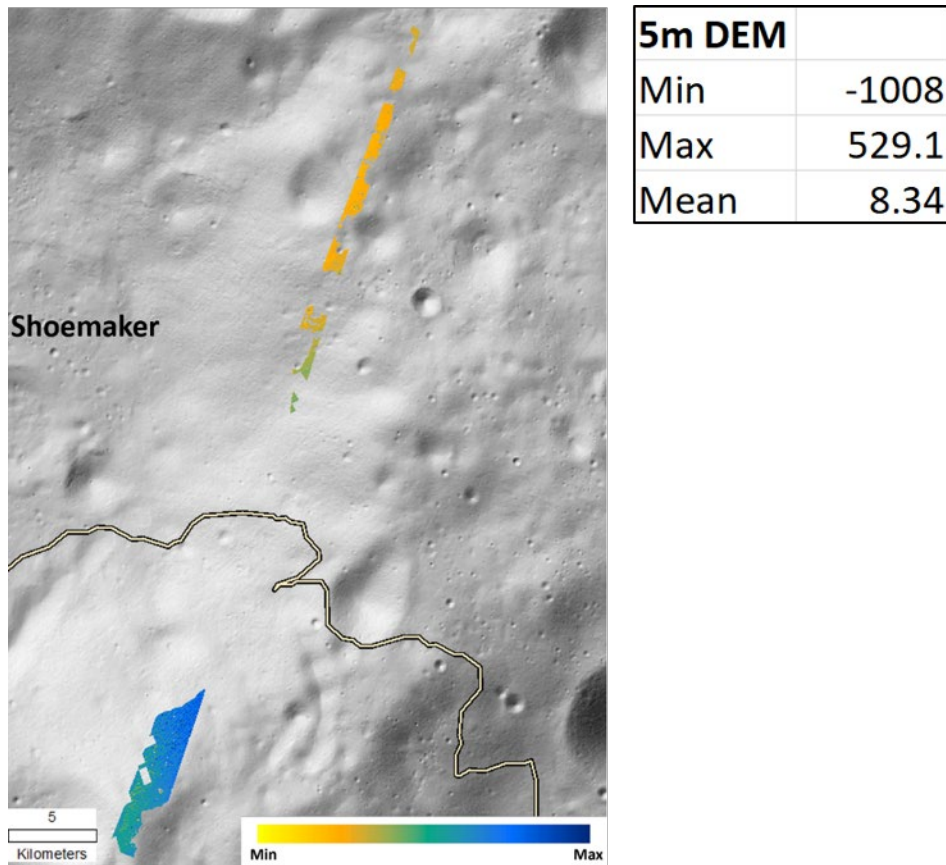


**Figure K-14.** DEM generated from image pairs: M1129356077 and M1129370299 Elevation Difference Map. Difference is calculated using the LOLA 5m DEM. Version 3 path depicted.

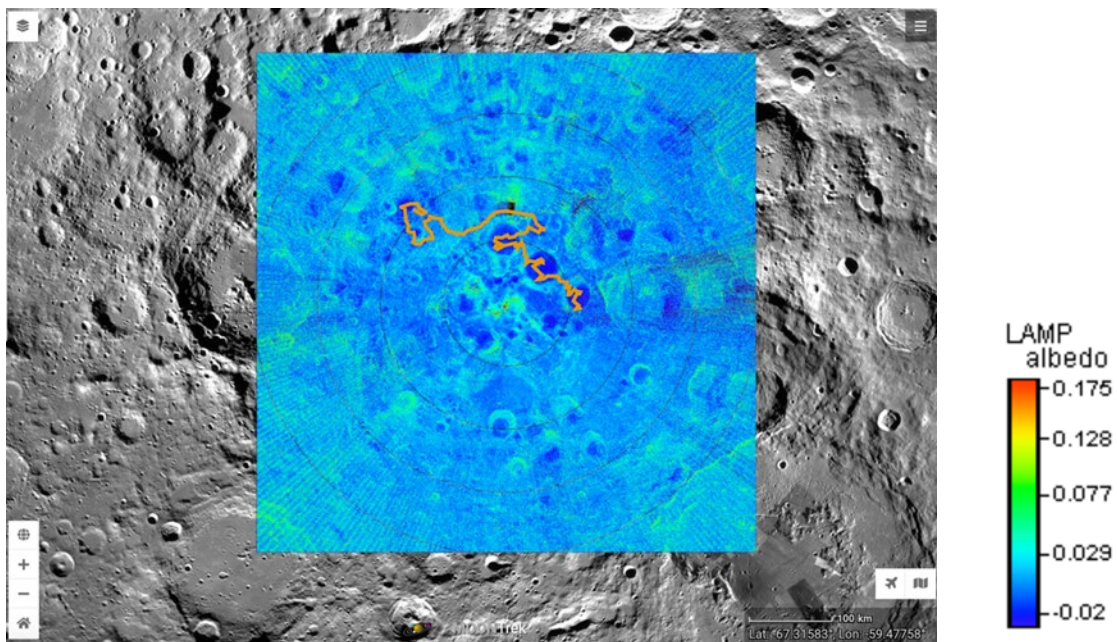
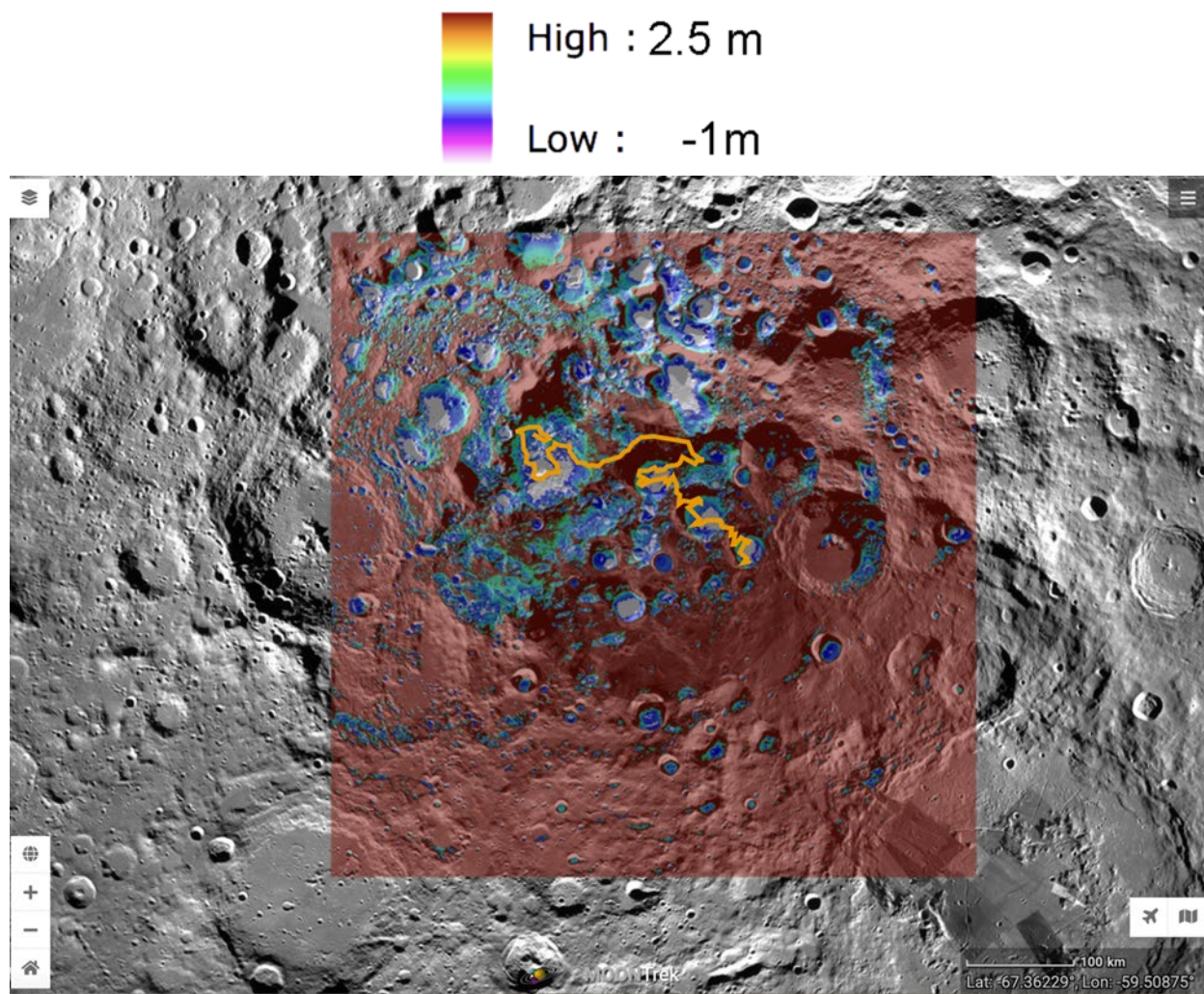
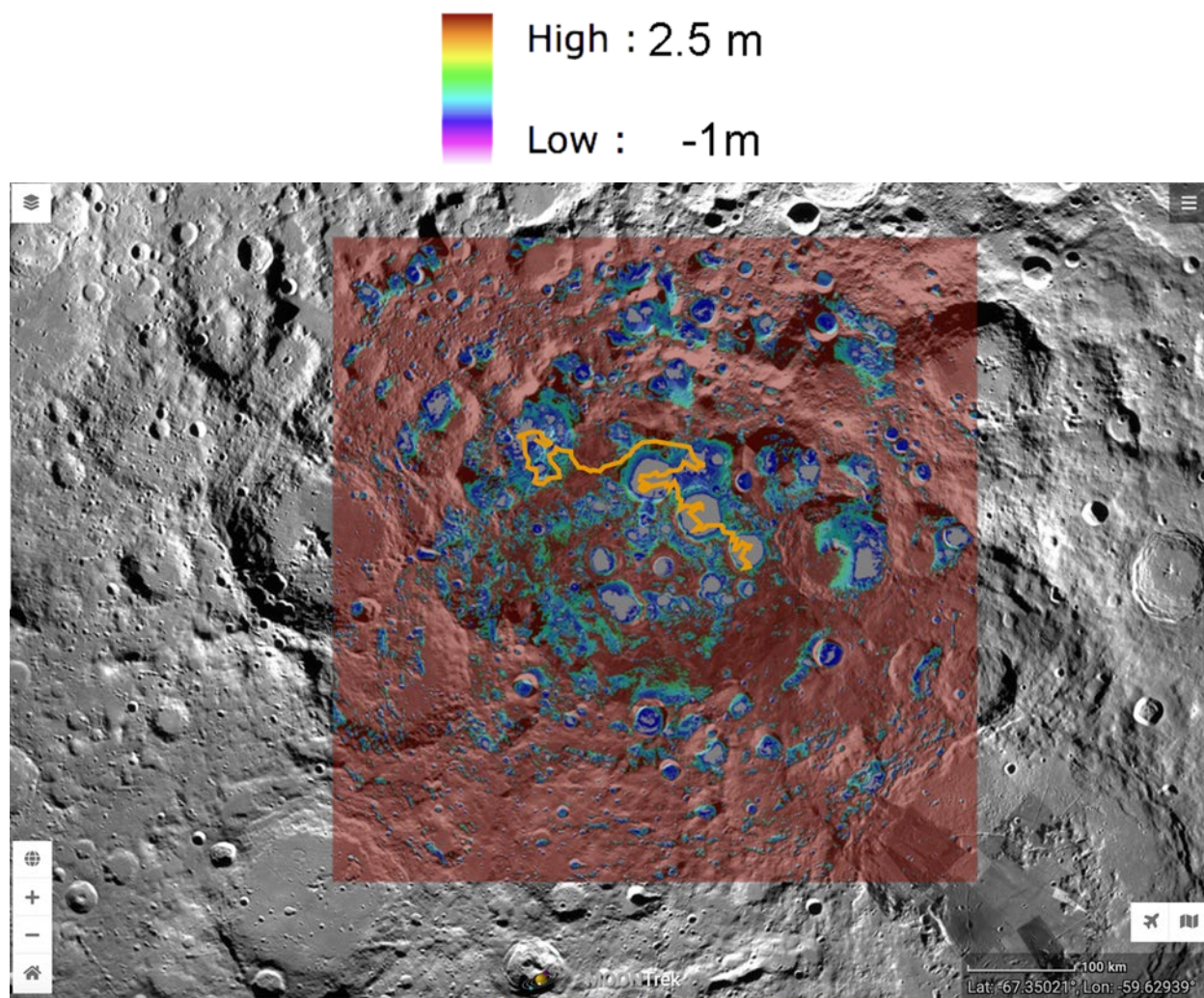


Figure K-15. Inspire Traverse Path in orange displayed overlaying LAMP Albedo.





**Figure K-16.** INSPIRE Traverse Path (orange) displayed overlying predicted paleo ice stability depths (negative numbers indicate surface stability;[14].



**Figure K-17.** INSPIRE Traverse Path (orange) displayed overlying the modeled ice stability depth (negative numbers indicate surface stability; [14].



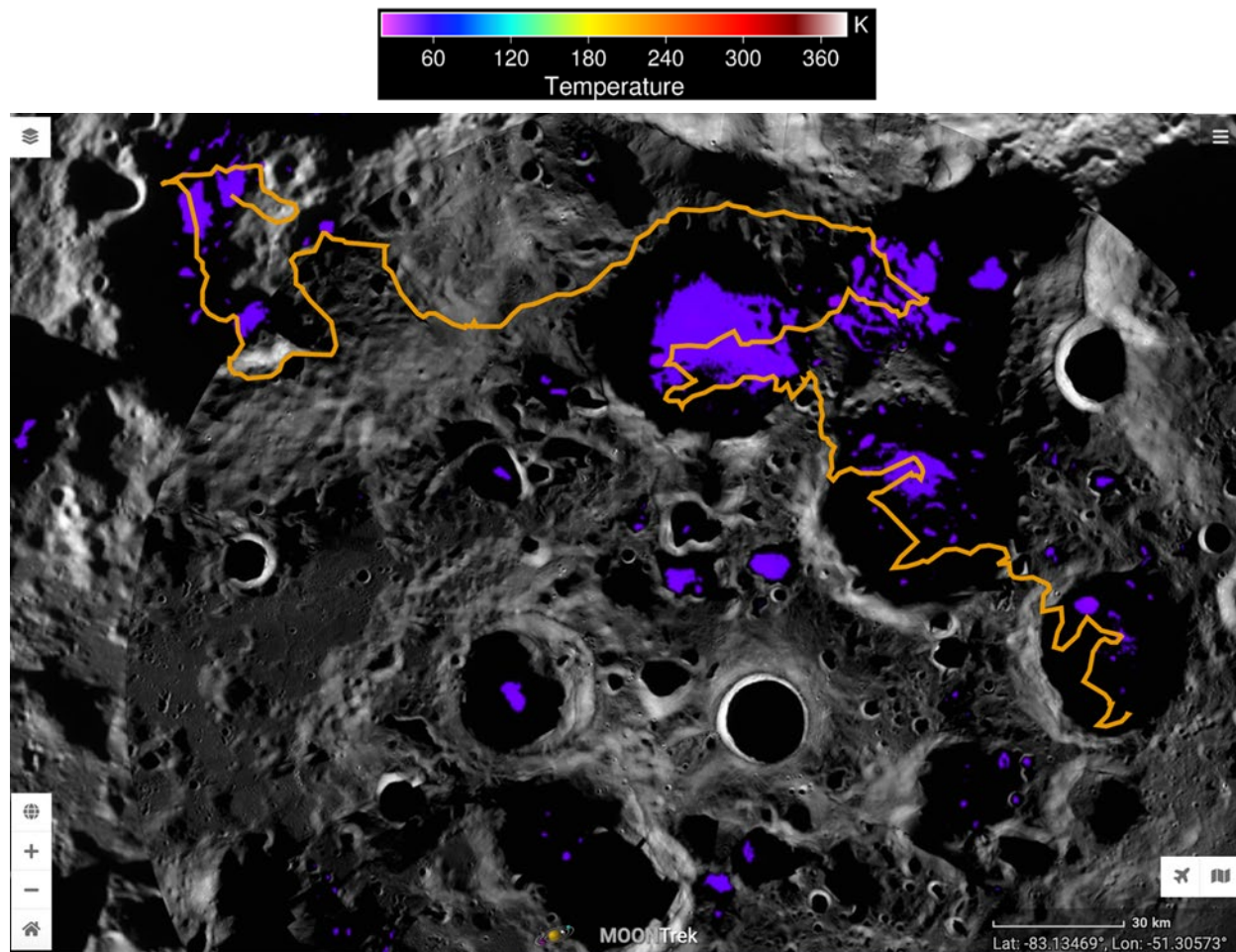


**Figure K-18.** INSPIRE Traverse Path (orange) displayed. Regions where the summer average temperature is < 50 K are highlighted in purple.

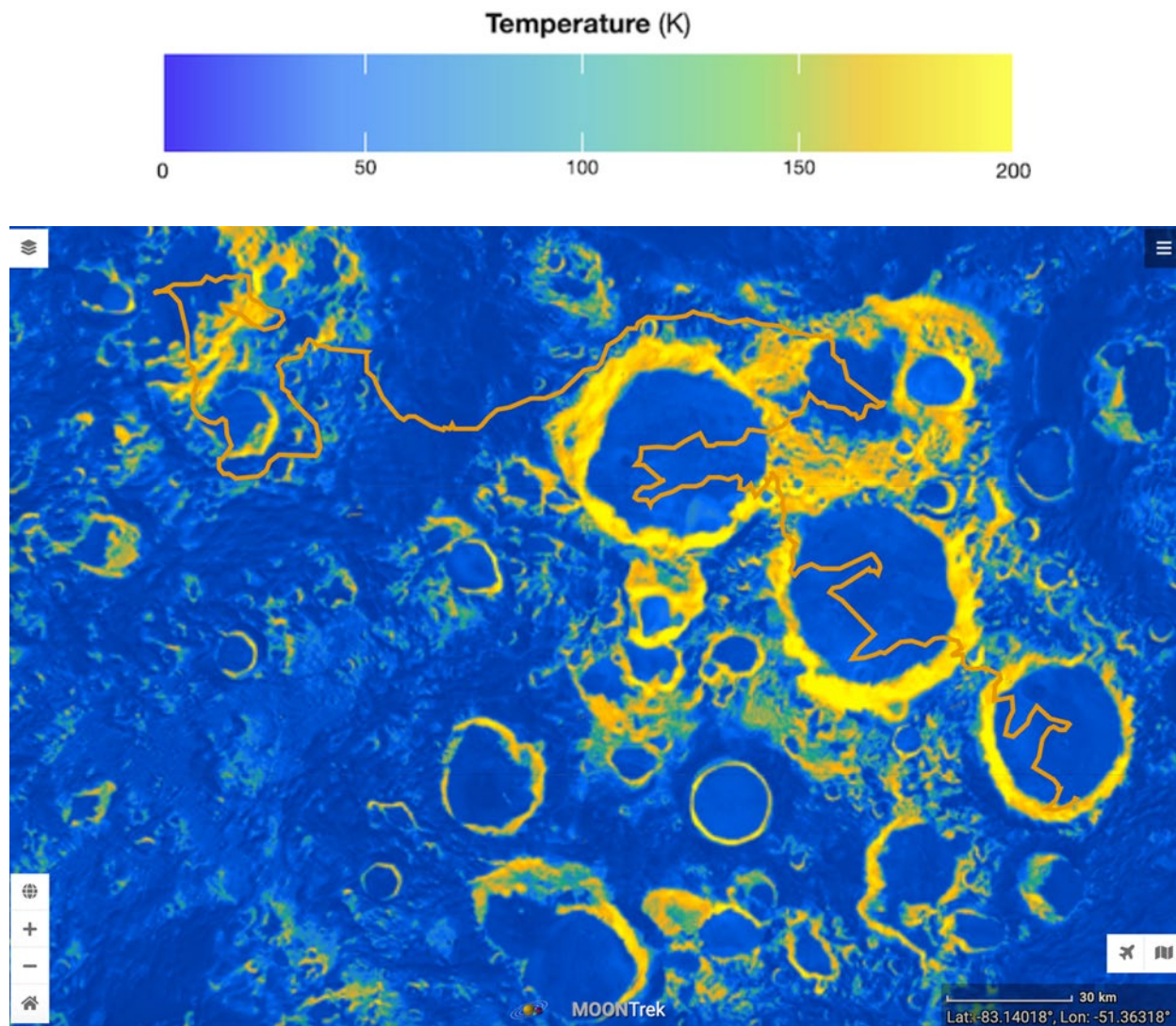


**Figure K-19.** INSPIRE Traverse Path (orange) displayed overlying the seasonal difference in maximum surface temperatures [22].



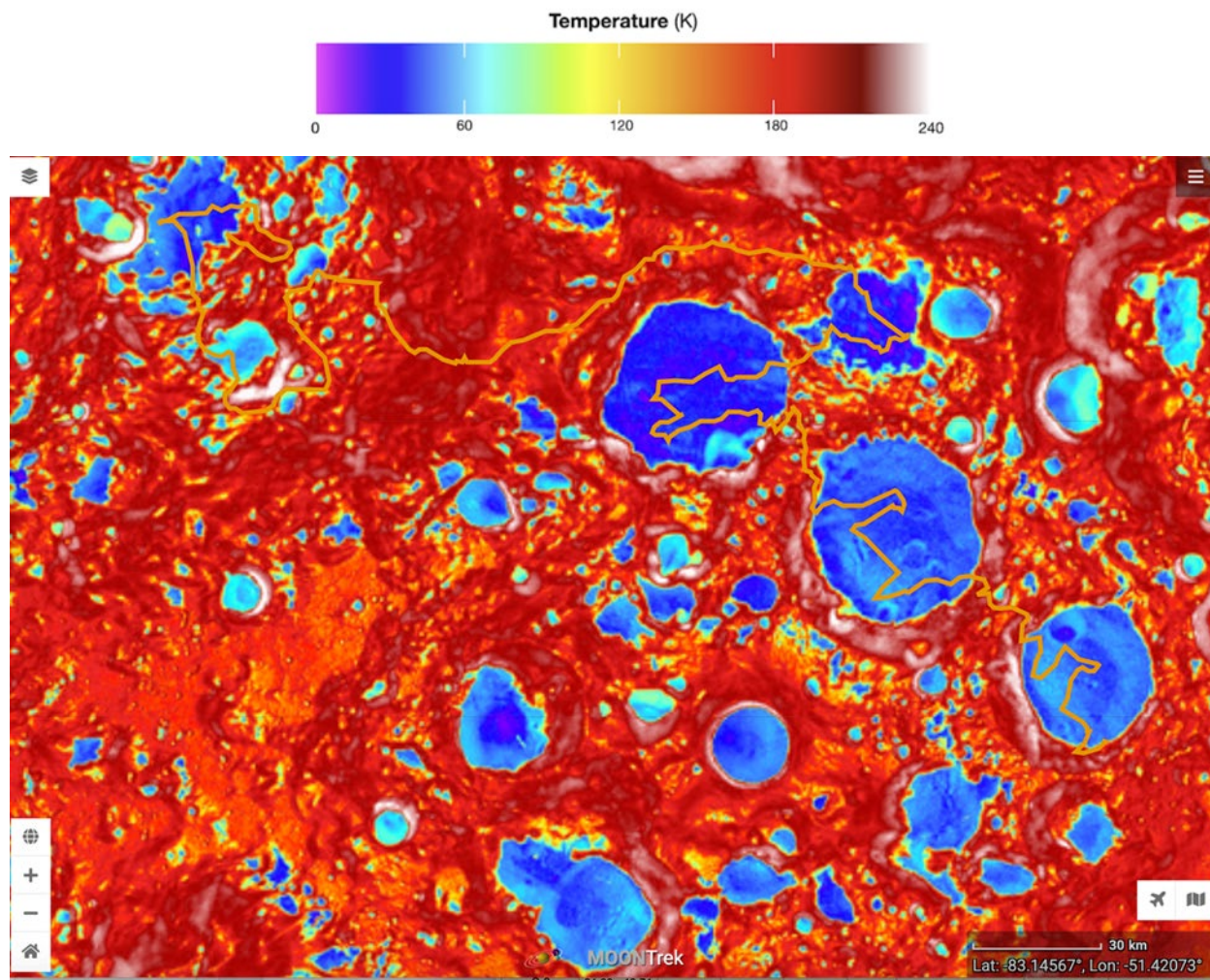


**Figure K-20.** INSPIRE Traverse Path (orange) displayed overlaying the amplitude of summer surface temperatures [22].

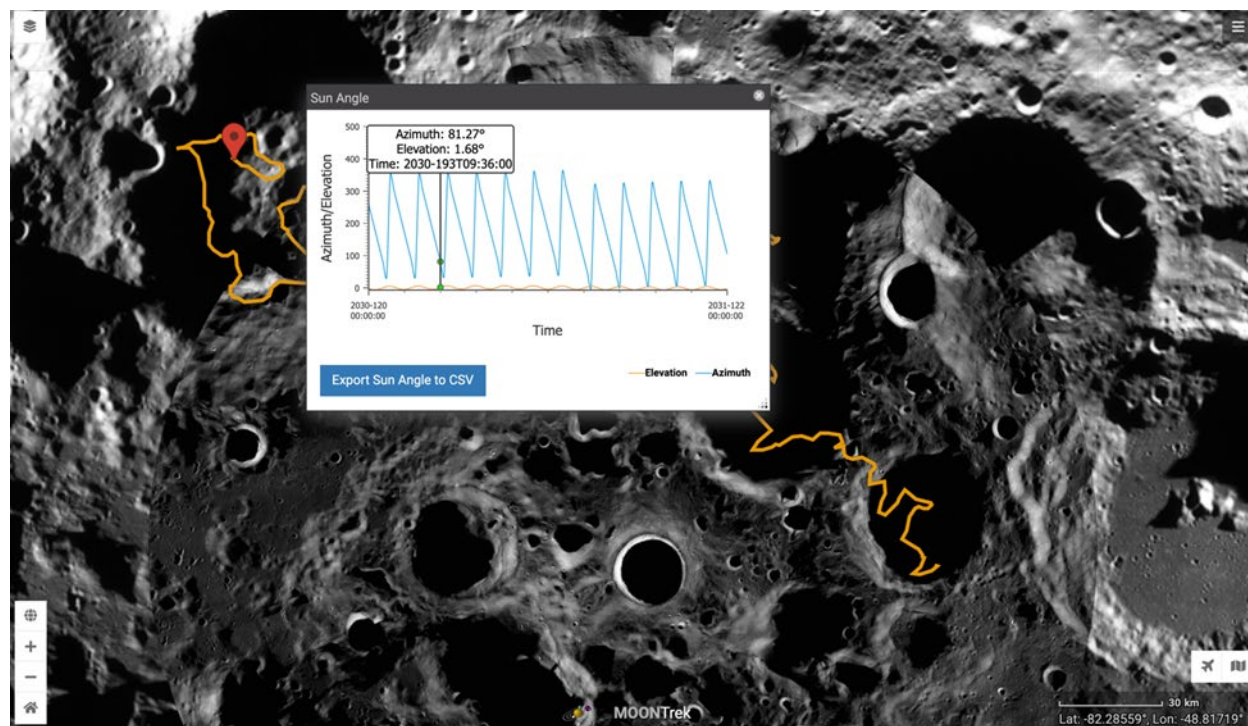


Figure K-21. INSPIRE Traverse Path in orange. Solar Illumination Azimuth and Elevation for 1 year period 2030 – 2031.

The 3D rendering of the Inspire traverse has been generated and is available here: [https://www.youtube.com/watch?v=3XfKy\\_AxW1E](https://www.youtube.com/watch?v=3XfKy_AxW1E).

---

## L CONFIGURATION

### L.1 BLOCK DIAGRAM

A high-level block diagram for the INSPIRE rover is presented in Figure L-1.

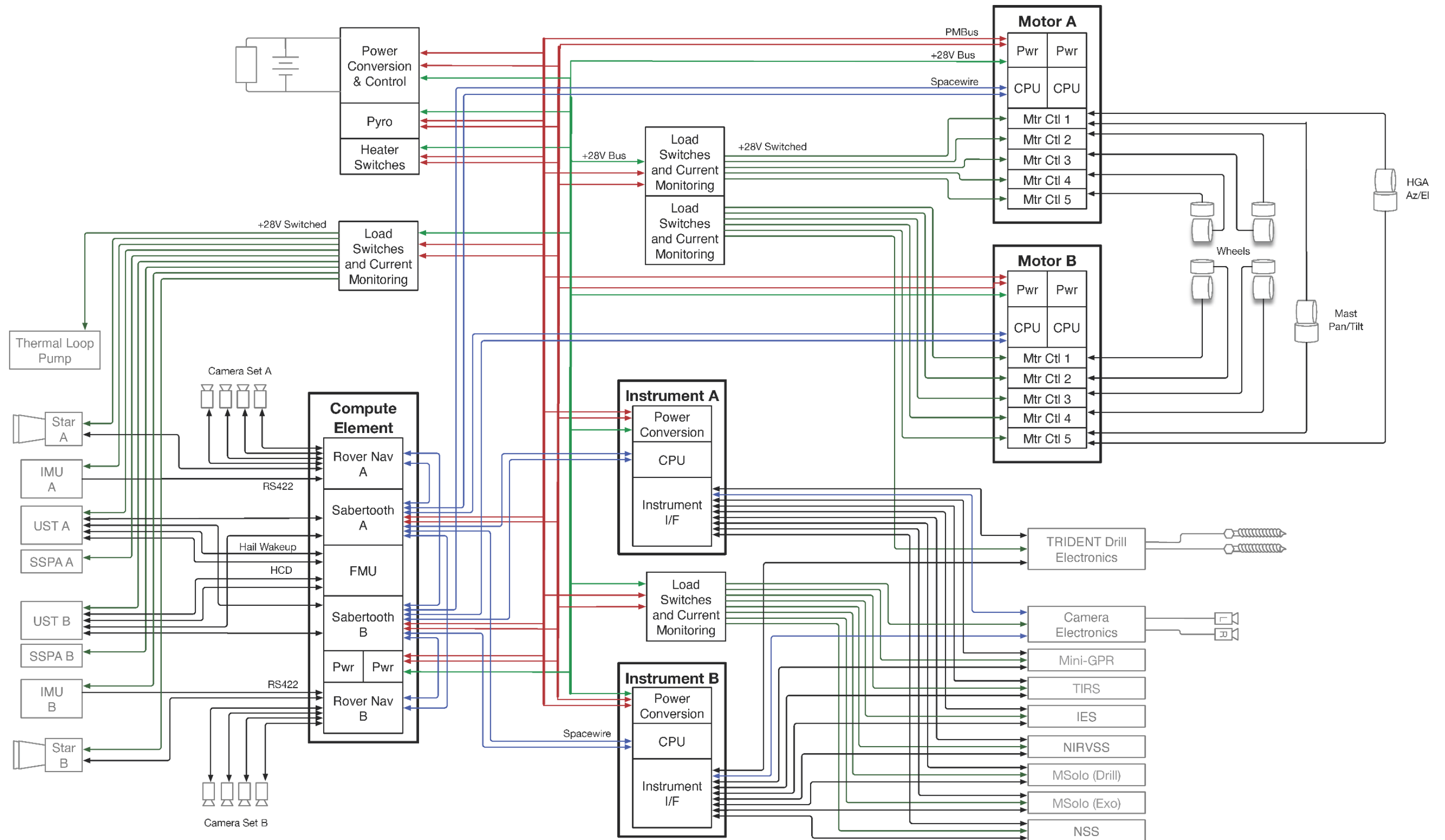


Figure L-1. INSPIRE Block Diagram.



## L.2 CONFIGURATION

The INSPIRE rover has an architecture based around a central warm electronics box (WEB) chassis which carries most of the avionics and payload electronics and is connected to the wheels via a rocker and a differential.

The rover is supported on four 80-cm compliant mesh wheels, and each is connected via its structure to a steering actuator as well as a drive actuator. The rover belly has clearance of about 60 cm on flat terrain, and the rocker provides stability over uneven terrain.

The WEB is a composite structure that is mostly hollow and has the internal payload and avionics on the underside. The RTG is attached to the back, and there is a central structural “spine” from the RTG to the front of the rover to provide additional support.

Because the RTG can provide power at all times, there is no need for a large number of batteries, and thermal isolation is less of a concern because systems remain powered and heaters can be used during the night. The internal avionics on the bottom of the WEB is shielded with a lightweight bottom cover.

The back of the rover also supports a thermal shield for the RTG, reducing radiation to the surrounding regolith to  $<6 \text{ W/m}^2$ .

Some components that require height and a zenith facing field of view, such as the star trackers, are mounted on a lightweight aluminum structure on the back of the rover which also provides thermal shielding of the deck mounted radiator from the RTG. The rear navigation cameras, along with their illuminators, are mounted on a separate aluminum structure on the back of the rover, below the RTG to ensure clear visibility.

The two TRIDENT drills are mounted to two forward body panels on either side of the rover. Each drill and body panel can be released from the rover in the event of a drill becoming irretrievably stuck, as depicted in Figures L-8 and L-9.

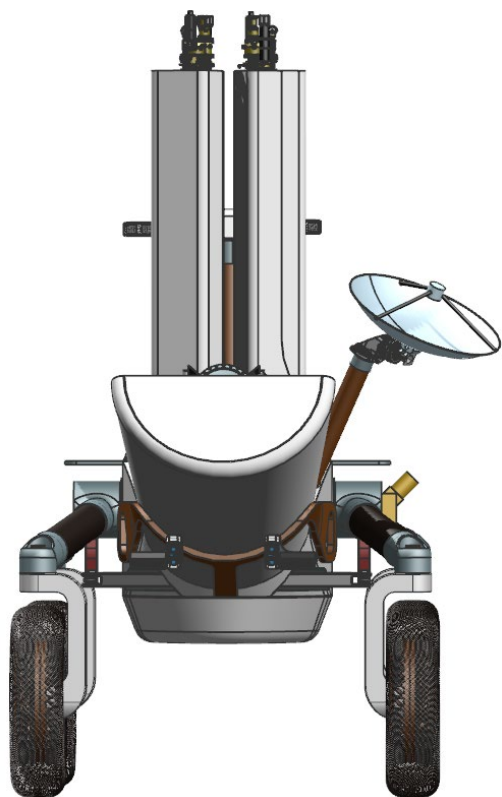


**Figure L-2.** Rear view of the rover showing RTG (w/shield), HGA, Magnetometer, Illuminators, and rear navigation cameras.

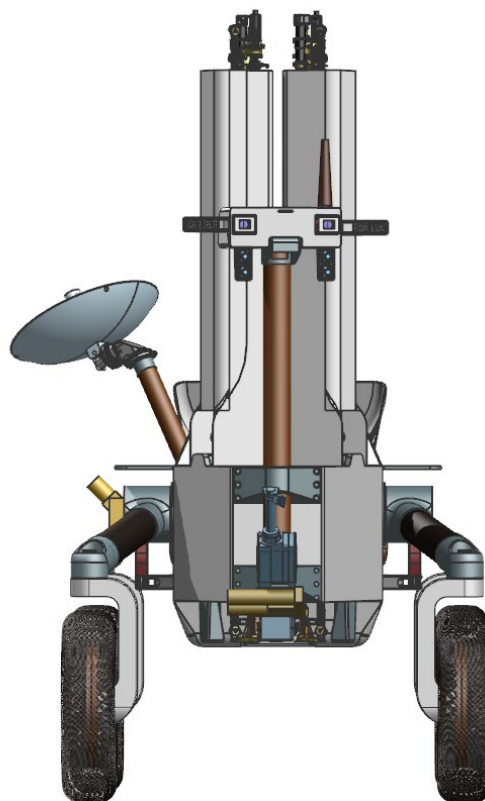


**Figure L-3.** Front view of the rover with the camera head, drills (w/shield), Magnetometer, MSolo-exosphere, NSS, and IES.

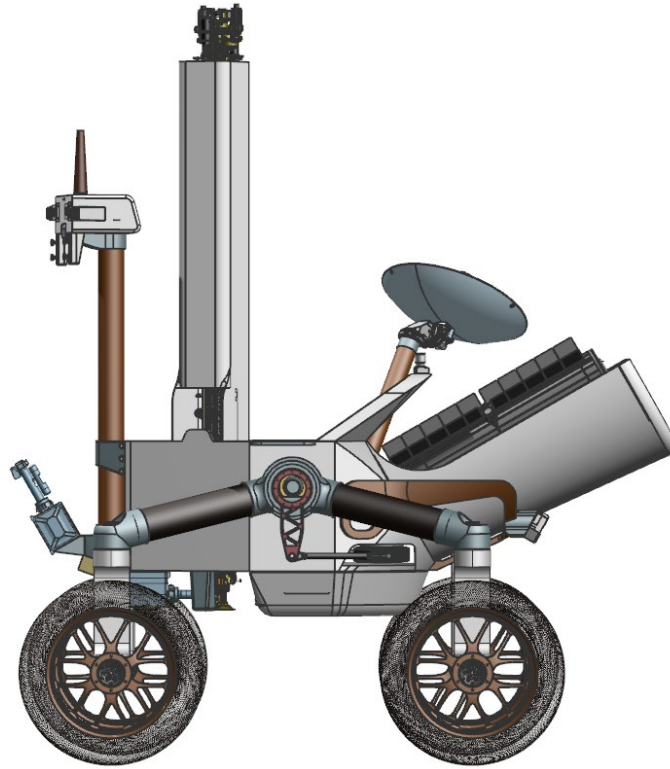


Figure L-4. Left view of the rover.

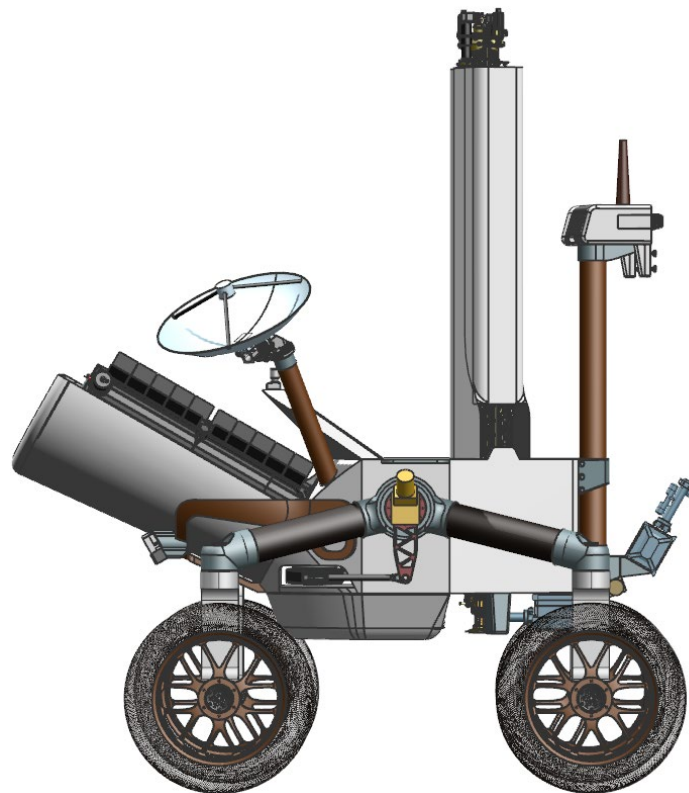


Figure L-5. Right view of the rover.

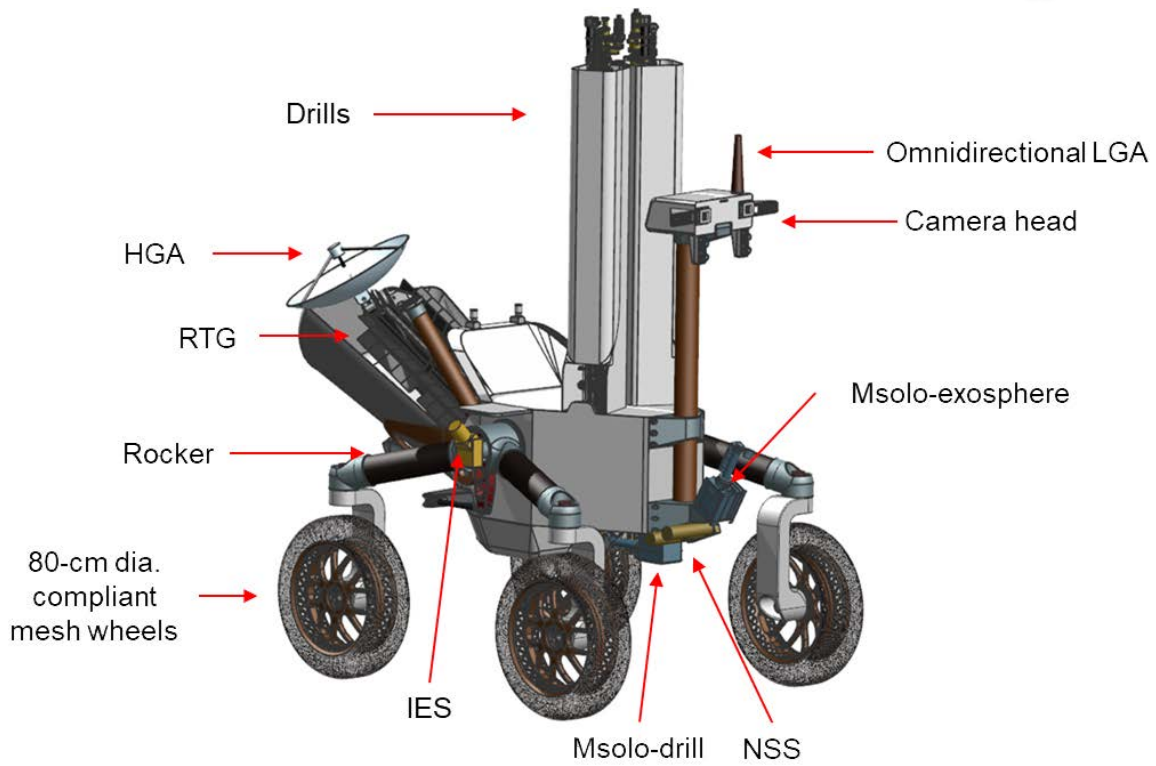


Figure L-6. Isometric view of the rover.

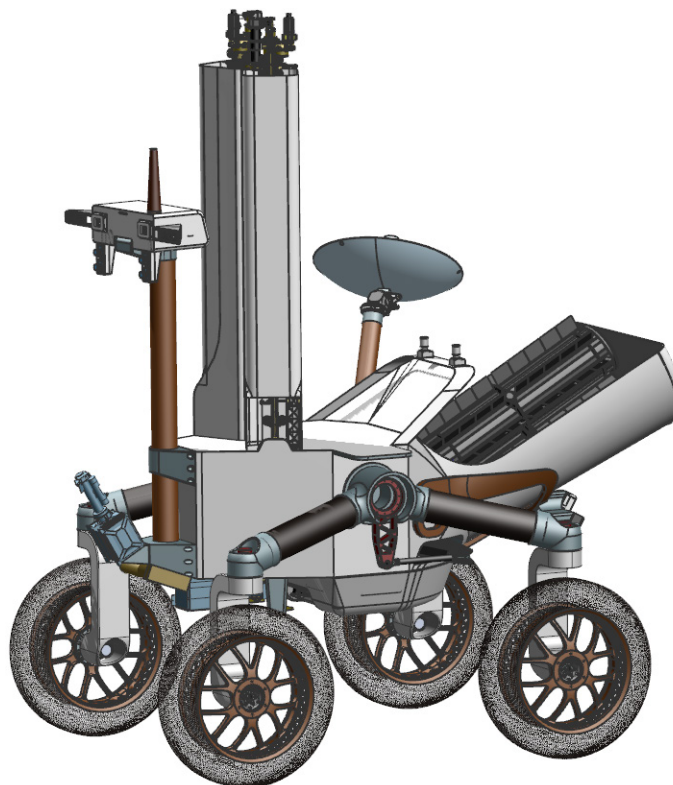
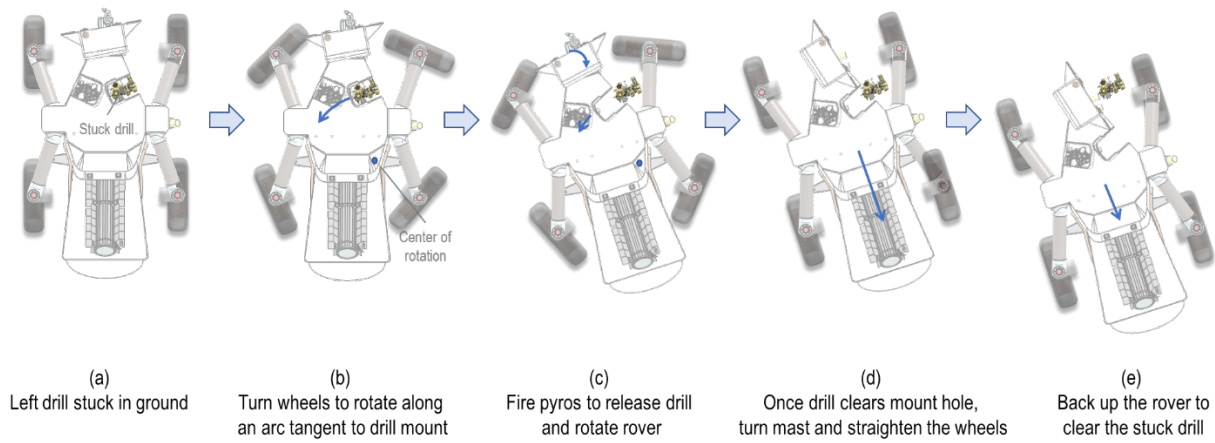


Figure L-7. Isometric view of the rover.





**Figure L-8.** In the event of an irretrievably stuck drill stem, the rover can jettison the drill and back away to separate.



**Figure L-9.** Rover showing separated right side drill.

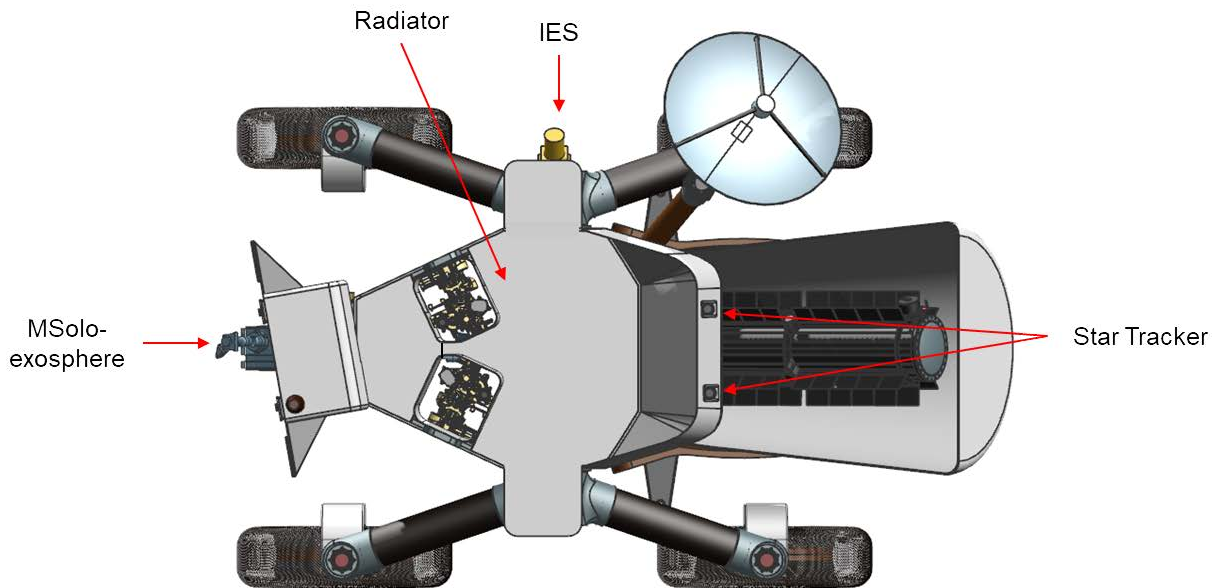


Figure L-10. Top view of the rover.

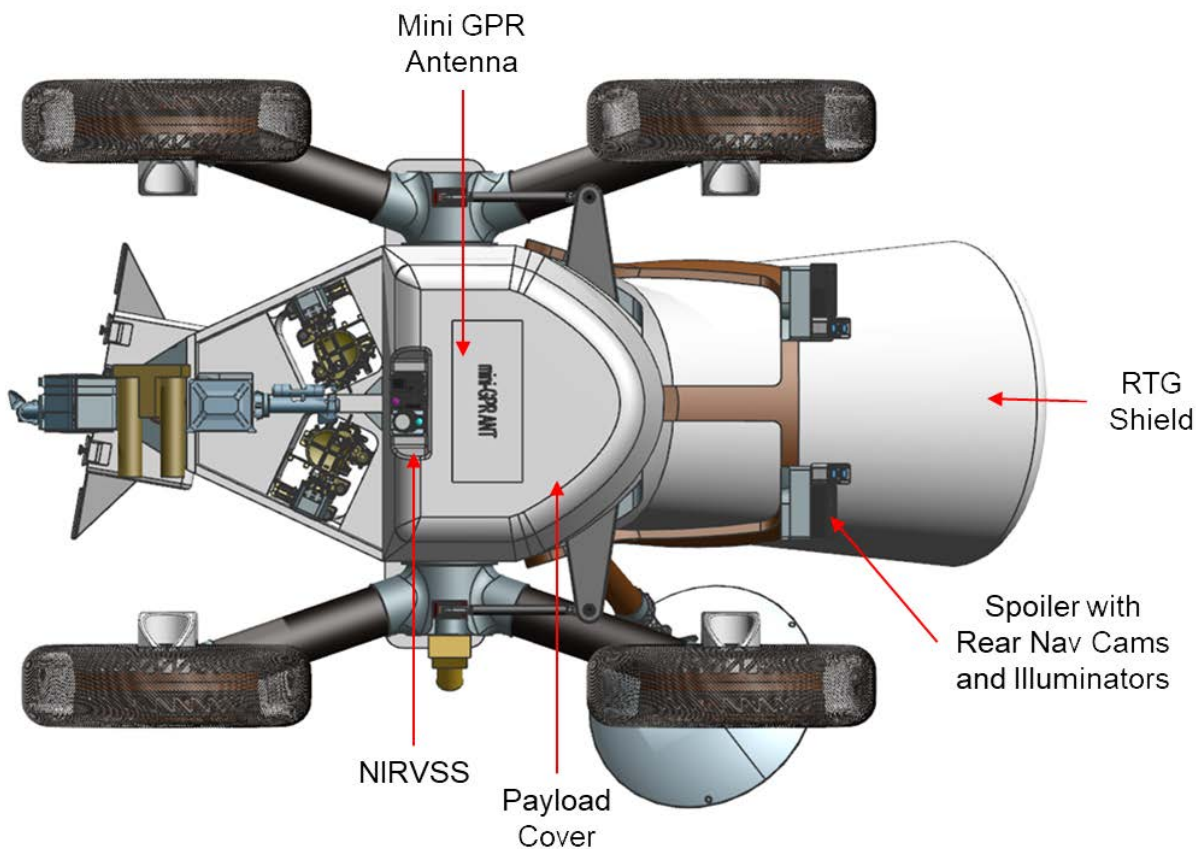


Figure L-11. Bottom view of the rover.

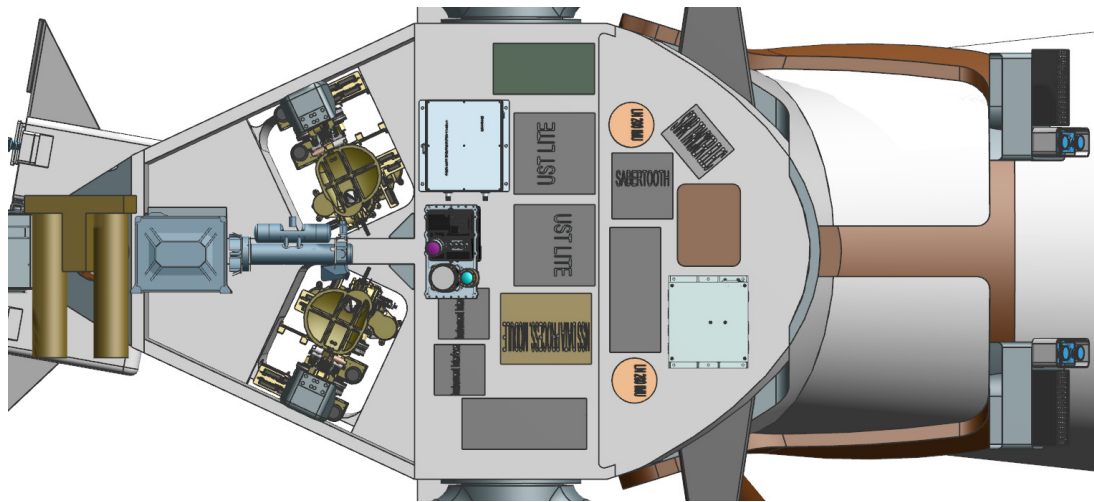


Figure L-12. Bottom view of the rover with the avionics shown.

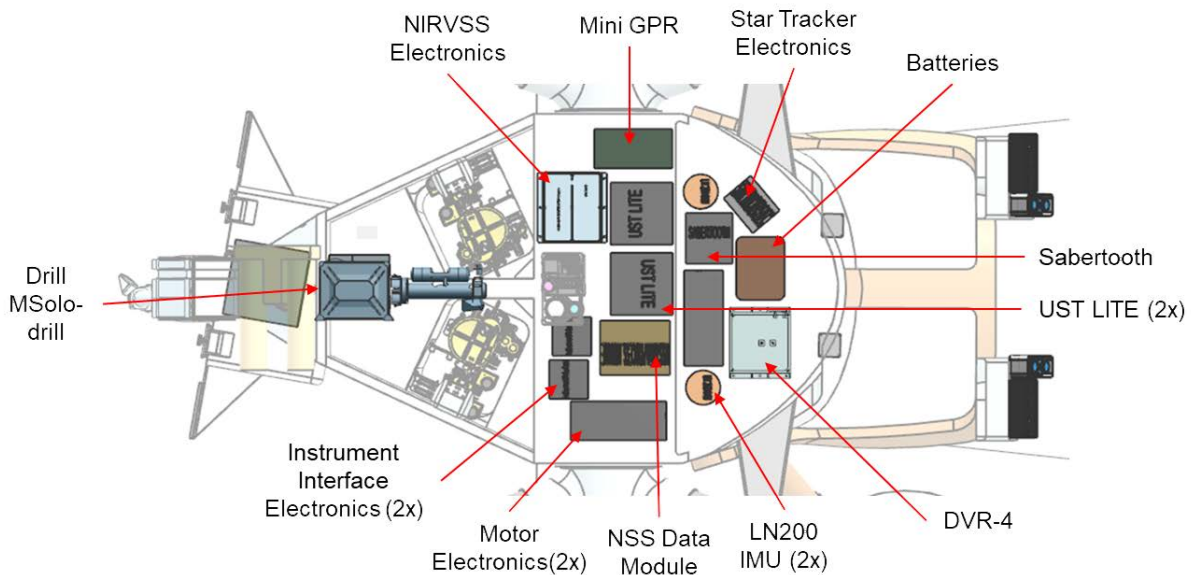
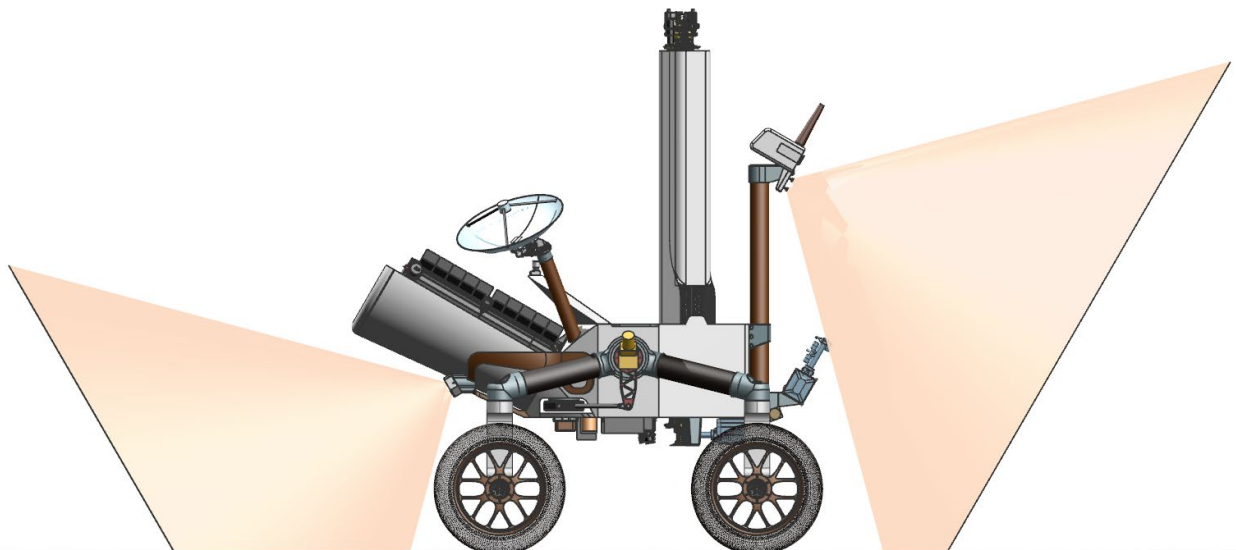
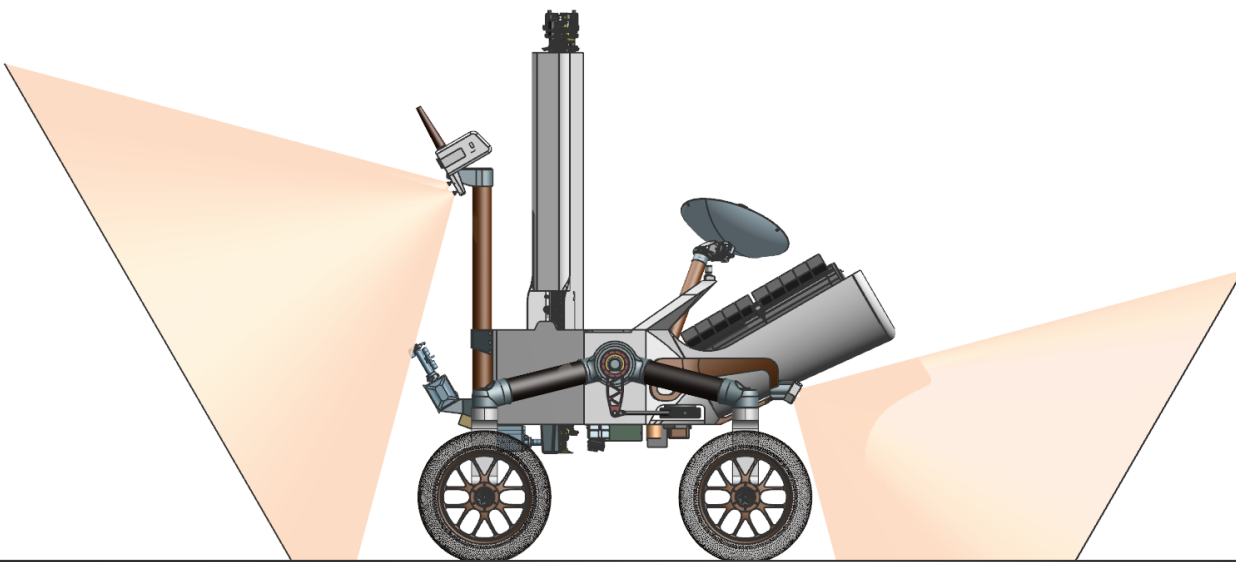


Figure L-13. Bottom view showing component layout in the WEB.



**Figure L-14.** Right side view of rover with the navigation camera FOVs shown (front and rear).



**Figure L-15.** Left side view of rover with the navigation camera FOVs shown (front and rear).



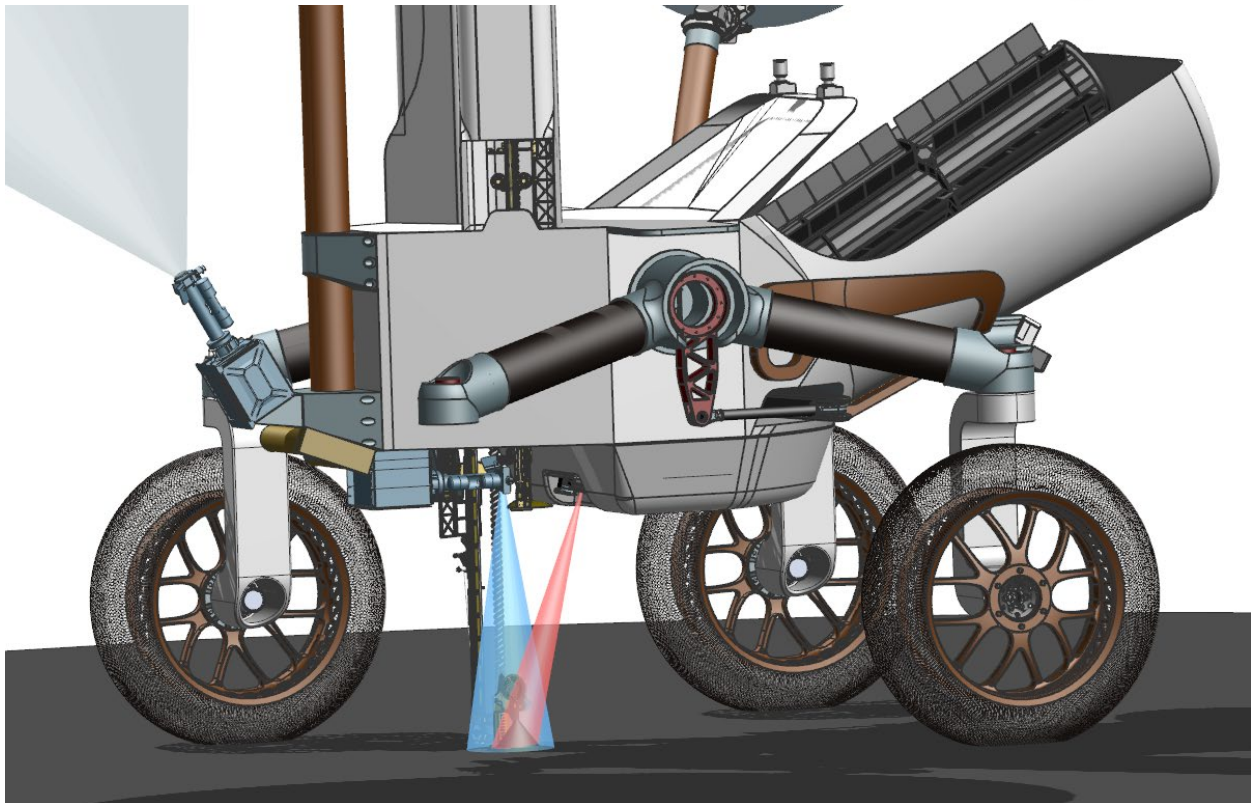


**Figure L-16** Isometric View of drill lowered with FOVs for MSolo-exosphere (gray), MSolo-drill (blue), and NIRVSS Spectrometer (red) shown.

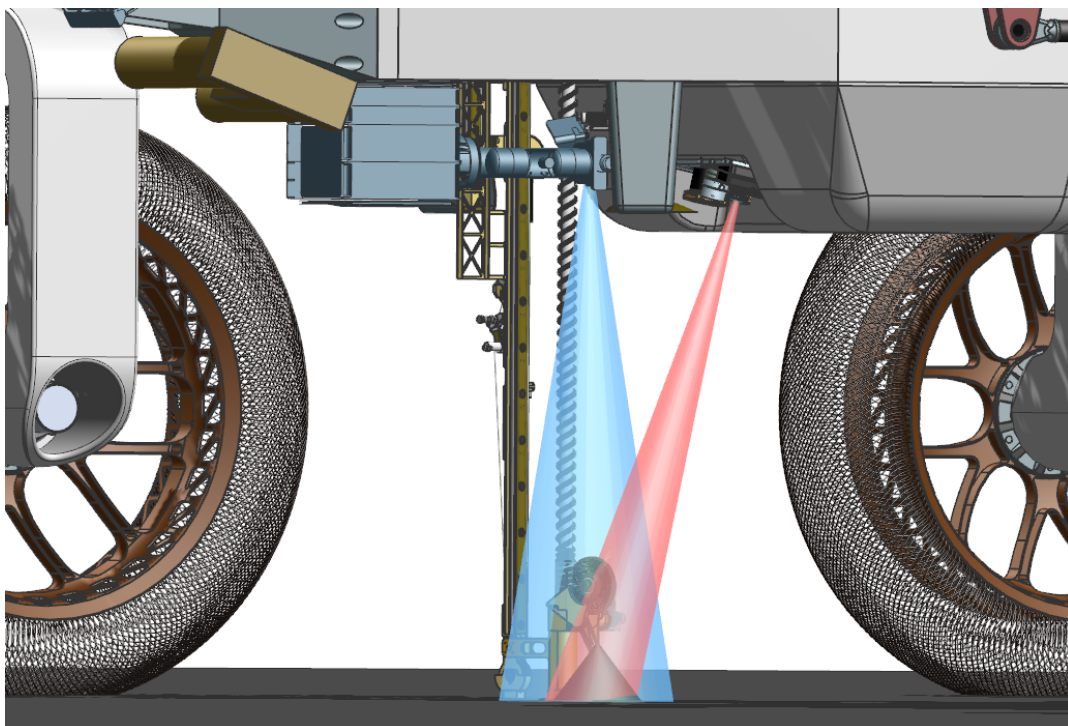


**Figure L-17.** Close-up of NIRVSS Spectrometer (red) and MSolo-drill (blue) FOVs shown, along with cuttings pile from Drill.

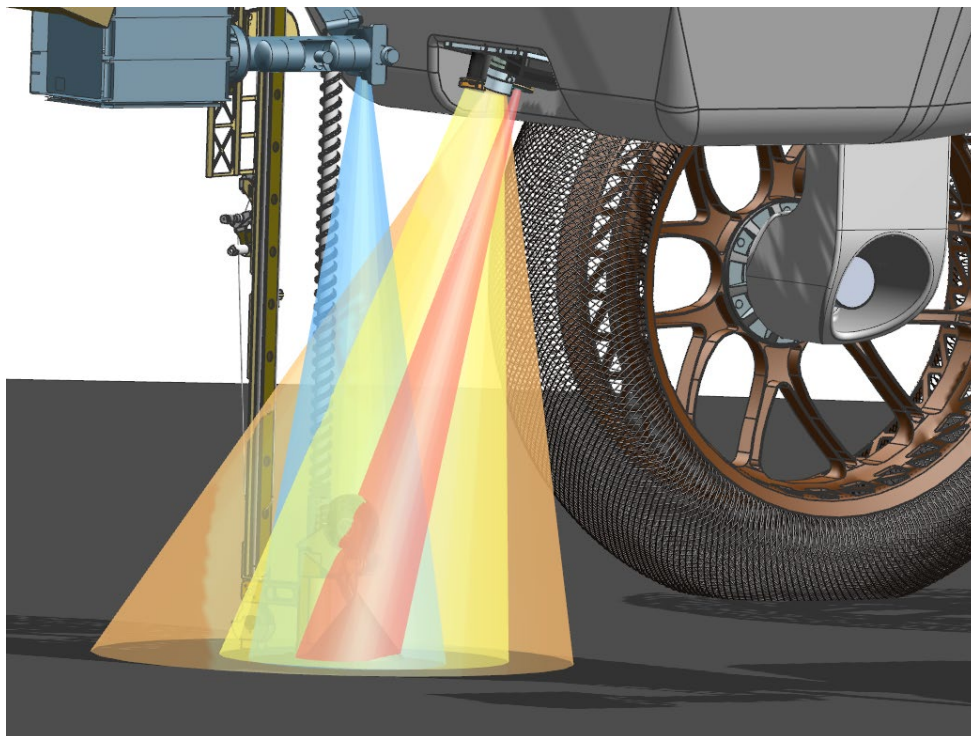


**Figure L-18.** Close-up of NIRVSS Instrument FOVs including spectrometer (red), camera (yellow), and illuminator (orange) and MSolo-drill FOV (blue), along with Regolith from Drill.

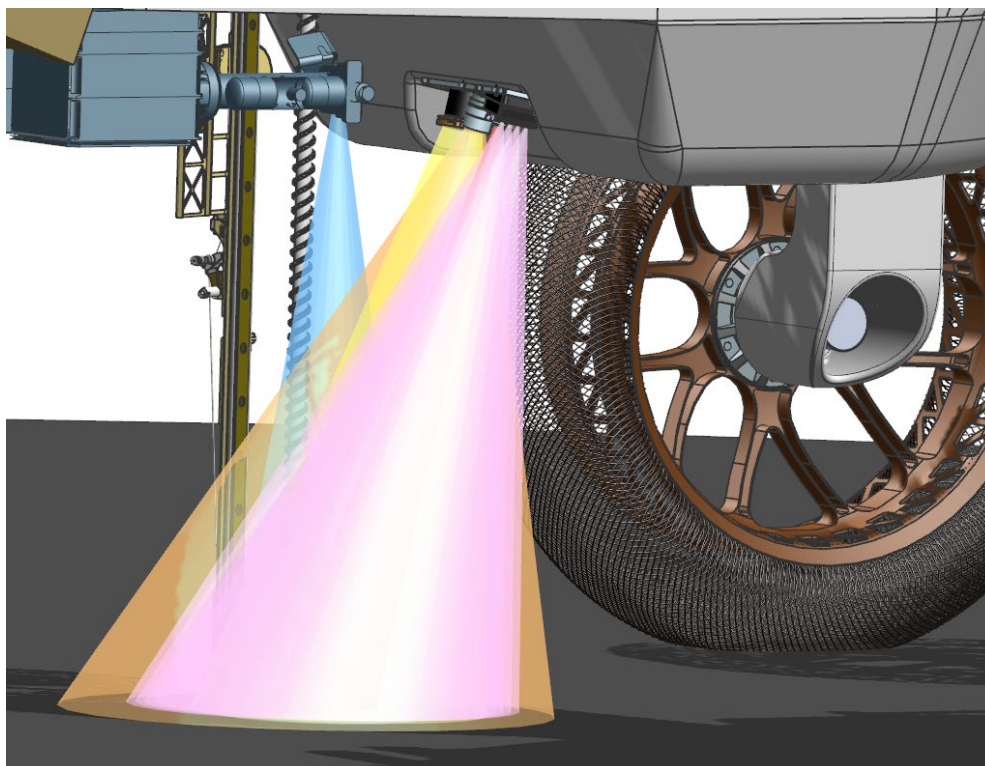


**Figure L-19.** Close-up of NIRVSS Instrument FOVs including Longwave Calibration Sensors (pink).

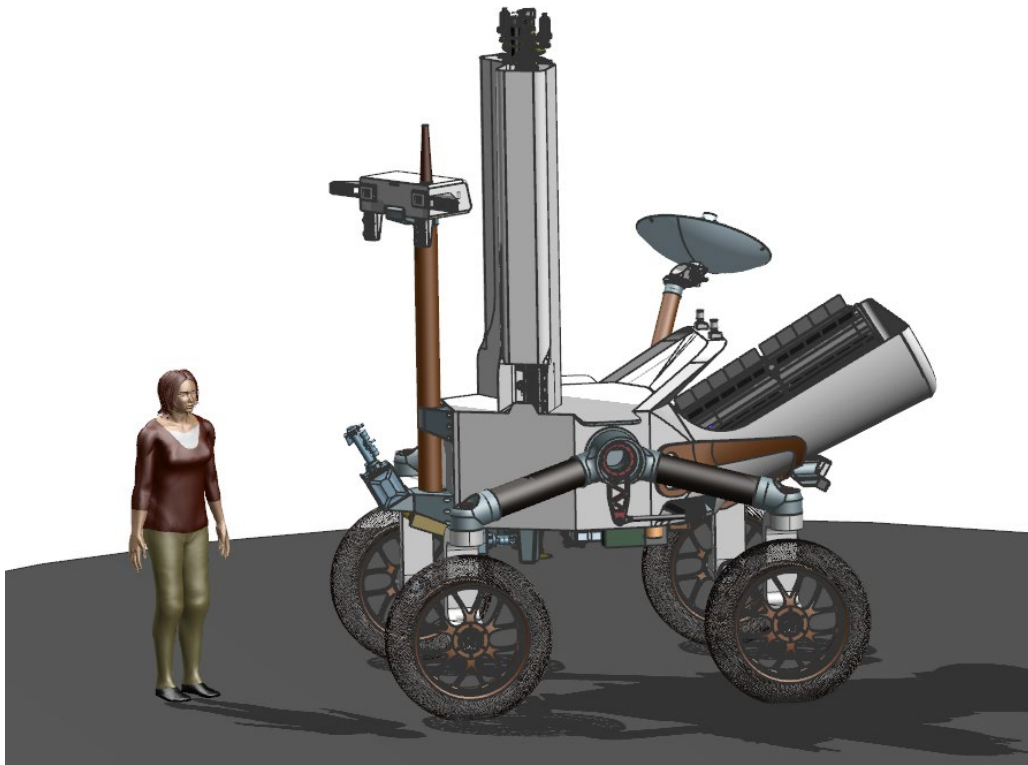


Figure L-20. Isometric view of the rover with a human shown for scale.

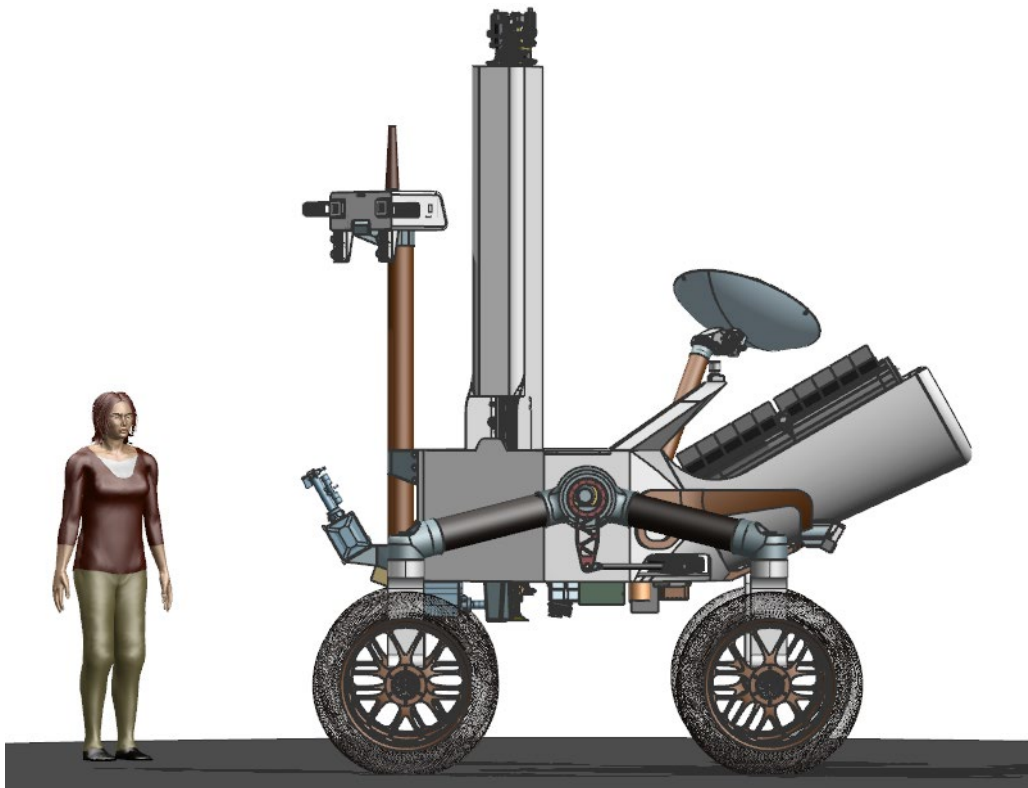


Figure L-21. Left side view of the rover with a human shown for scale.



## INSPIRE Thermal System

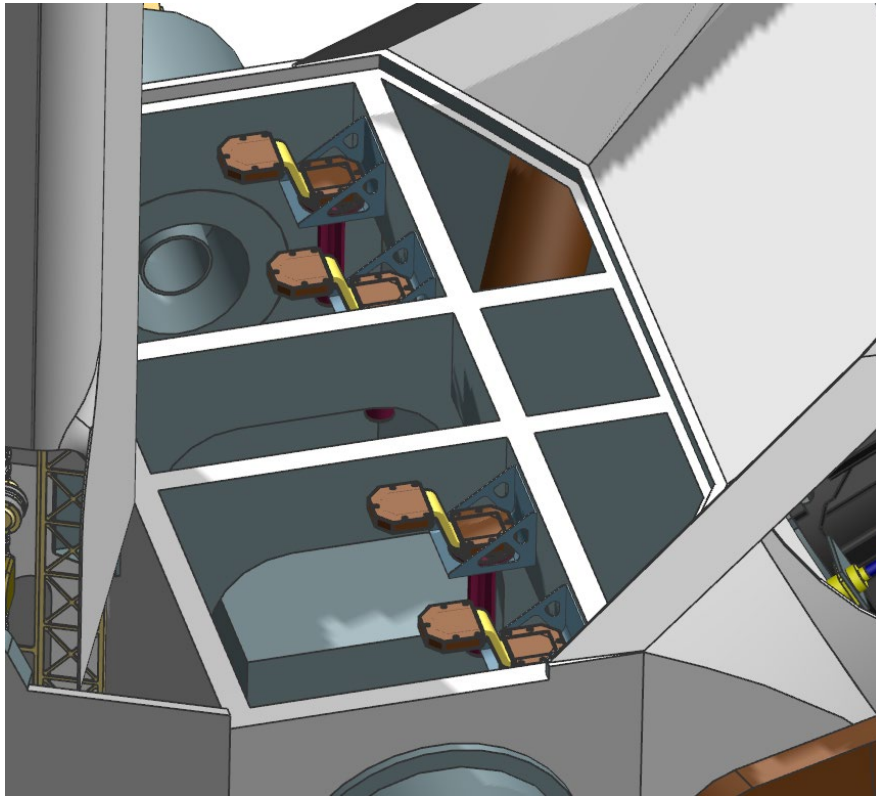


Figure L-22. Isometric view of thermal system without radiator.

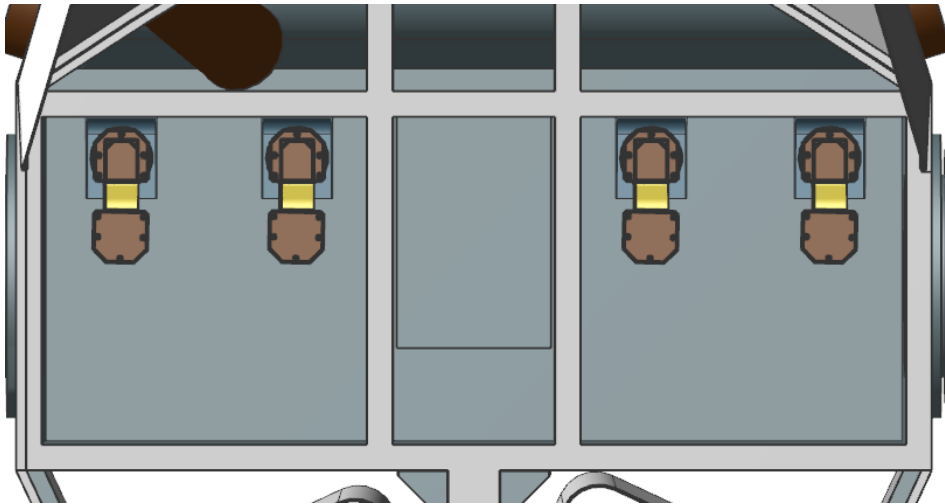
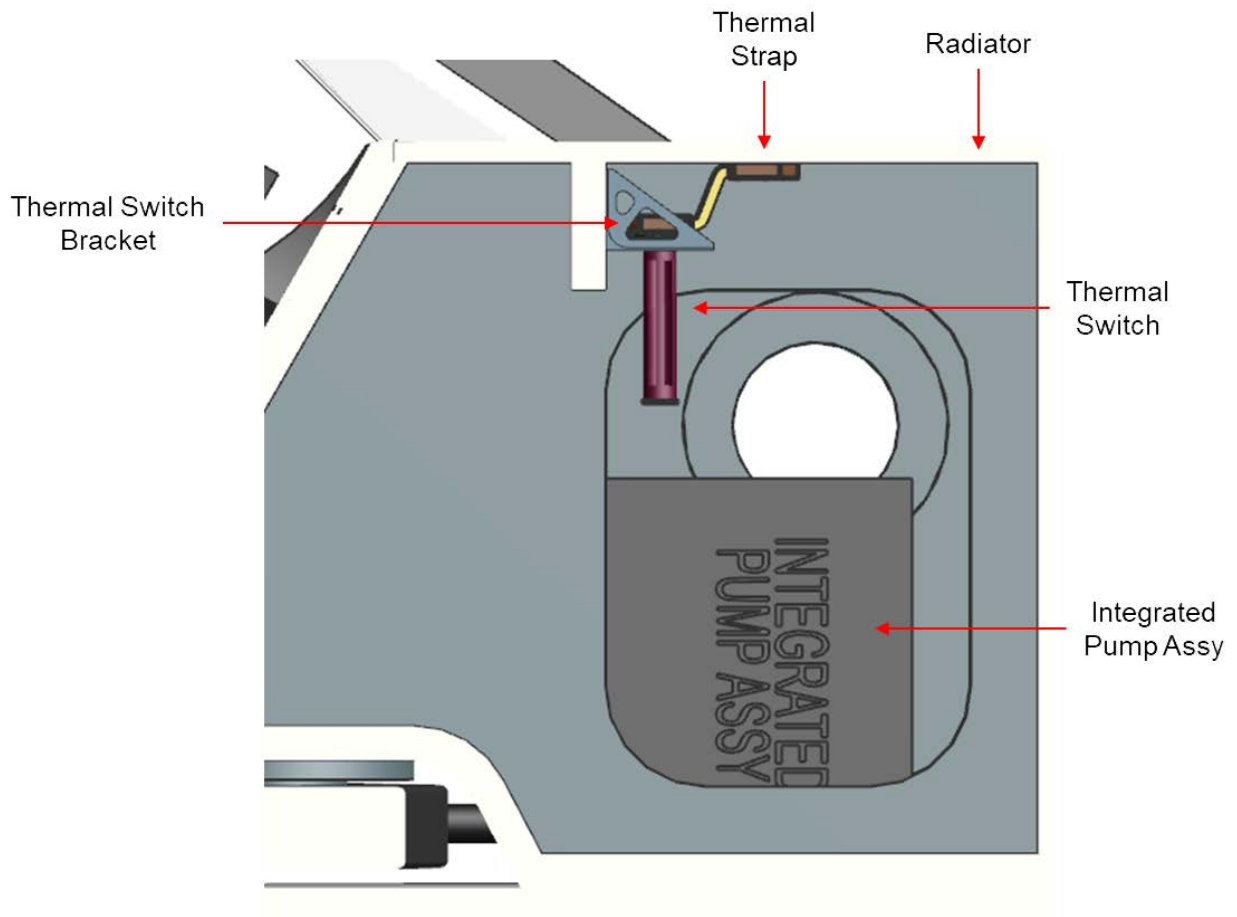


Figure L-23. Top view of thermal system without radiator.





**Figure L-24.** Cross-sectional view of thermal system with radiator.

## INSPIRE Masthead

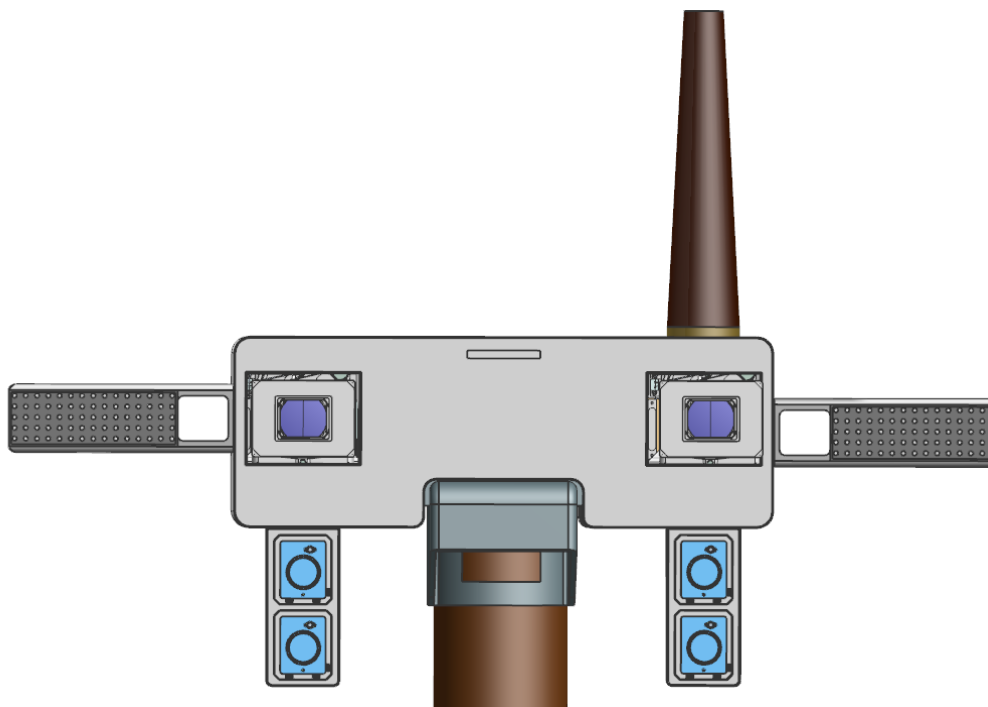


**Figure L-25.** Front view of the rover camera head, including the front navigation cameras and science cameras.

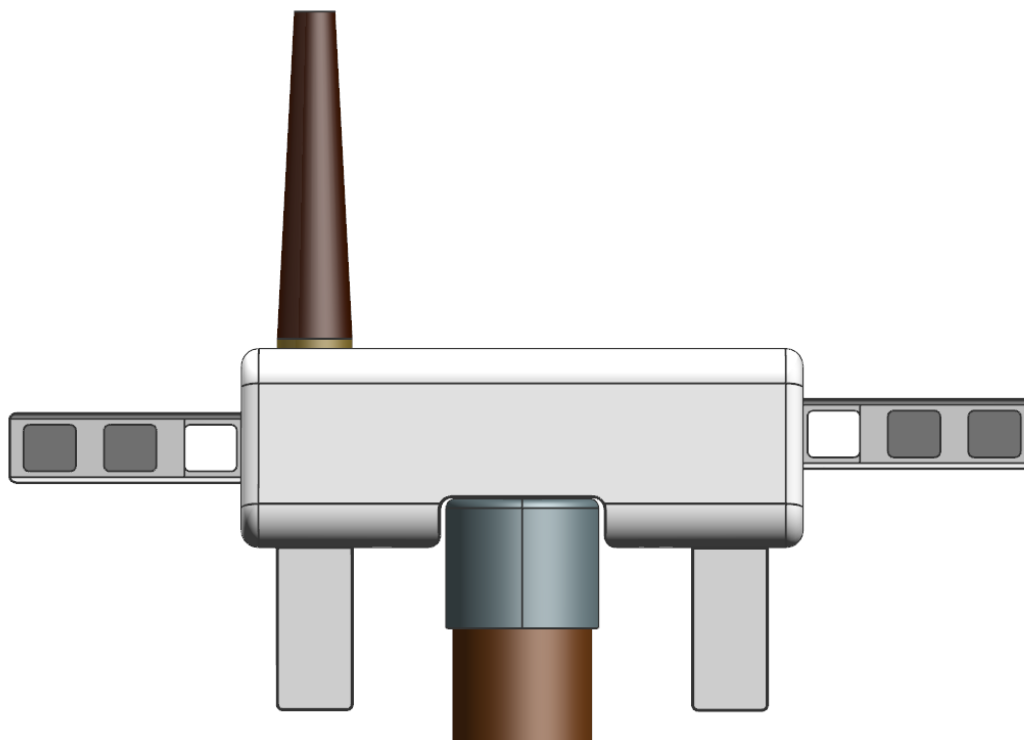


**Figure L-26.** Rear view of the rover camera head.

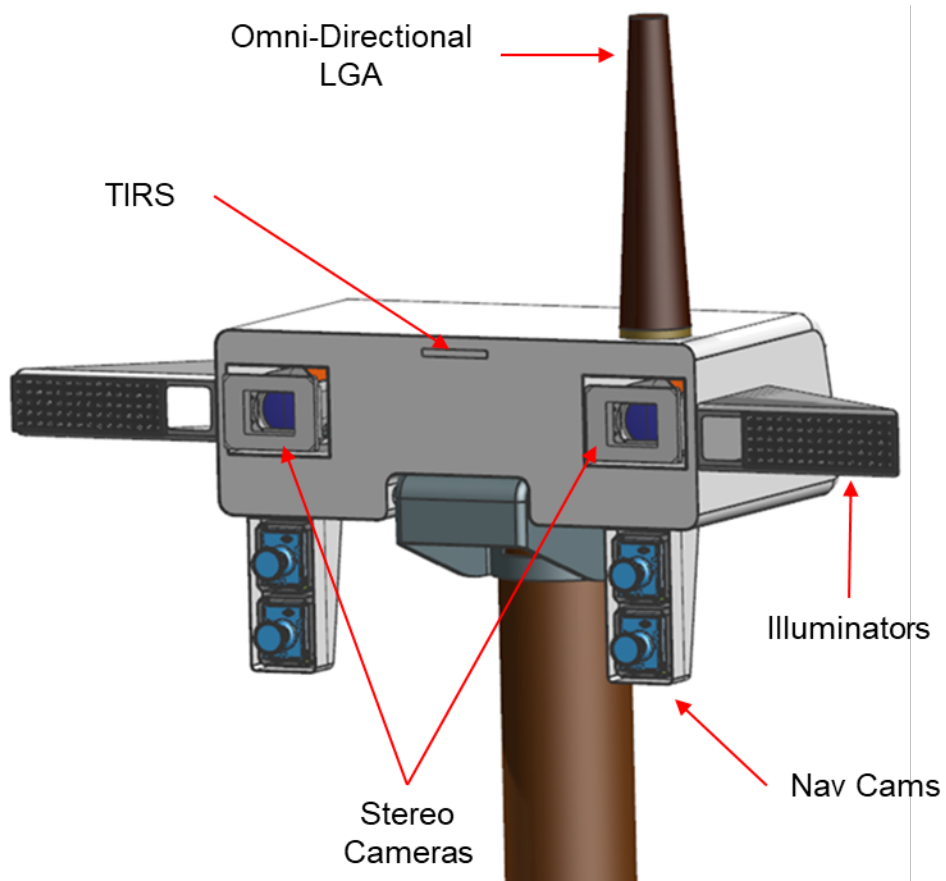


**Figure L-27.** Isometric view of the camera head, including the front navigation cameras and science cameras.

## M ADDITIONAL COST MODELING INFORMATION

JPL’s business organization performed an additional assessment of the INSPIRE costs using the following methodologies.

- Historical wrap factors for science, mission operations system, and ground data system during the development phase that are level-of-effort.
- SEER and TruePlanning for the payload and lander systems.
- Space Operations Cost Model (SOCM) for Phases E-F mission operations and data analysis costs.

The cost results from these parametric estimates are summarized in Table M-1. The reserves are 50% for Phase A–D (excluding LV and the RTG) and 25% for Phase E/F (excluding tracking costs) as called for in the Decadal study ground rules.

In addition to the parametric model validations, a top-level crosscheck of the lunar rover (WBS 06) plus system I&T (WBS 10) was performed by looking as cost versus mass. Figure M-1 plots \$/kg for the Mars rover missions (Pathfinder, MER, MSL, and Mars 2020) and the INSPIRE Team X estimate. A trendline through the Mars missions shows the INSPIRE cost above the trendline indicating that the cost is reasonable.

Phase A costs were added to the cost model estimates. As a gauge for the amount to apply, the pre-release draft of the NF 5 AO was used as the basis. New Frontiers 5 specifies a value of \$5M RY for Phase A.

**Table M-1.** Cost model results for INSPIRE (FY25\$M). Highlighted cells represent Wraps and SOCM

WBS Element	Team X	SEER	TruePlanning (MSL Calibrated)	TruePlanning (Space Msn Catalog)	Model Average	Model Avg – Team X Delta (\$)	Delta (%)
Phase A Concept Study	Incl. below	5.0	5.0	5.0	5.0	-	-
01 Project Management	24.7	46.0	25.7	30.6	91.8	2.4	3%
02 Project System Engineering	32.8	63.0	18.4	25.4			
03 Safety & Msn Assurance	31.9	Incl. above	24.5	41.9			
04 Science	37.9	21.7	24.4	10.8	19.0	-18.9	-50%
05 Payload	84.3	86.1	100.5	98.1	94.9	10.6	13%
06 Flight System	475.9	436.1	442.9	448.2	442.4	-33.5	-7%
07 Mission Ops	32.6	27.5	30.9	20.3	26.2	-6.3	-20%
09 Ground Data System	33.4	25.5	28.7	28.1	27.4	-6.0	-18%
10 Project System I&T	41.3	32.9	80.7	64.2	59.3	18.0	44%
<b>Total Dev. w/o Reserves</b>	<b>794.7</b>	<b>743.8</b>	<b>781.8</b>	<b>772.4</b>	<b>766.0</b>	<b>-28.7</b>	<b>-4%</b>
Development Reserves (50%)	362.4	336.9	355.9	351.2	348.0	-14.4	-4%
<b>Total A-D Development Cost</b>	<b>1,157.1</b>	<b>1,080.7</b>	<b>1,137.7</b>	<b>1,123.6</b>	<b>1,114.0</b>	<b>-43.1</b>	<b>-4%</b>
01/02 PM/PSE	5.3	1.8	1.8	1.8	1.8	-3.5	-66%
04 Science	63.3	67.3	67.3	67.3	67.3	4.0	6%
07 Mission Operations System	53.3	55.3	55.3	55.3	55.3	2.0	4%
09 Ground Data System	27.3	22.7	22.7	22.7	22.7	-4.6	-17%
<b>Total Ops w/o Reserves</b>	<b>149.1</b>	<b>147.1</b>	<b>147.1</b>	<b>147.1</b>	<b>147.1</b>	<b>-2.0</b>	<b>-1%</b>
Operations Reserves (25%)	35.6	35.1	35.1	35.1	35.1	-0.5	-1%
<b>Total E-F Operations Cost</b>	<b>184.8</b>	<b>182.2</b>	<b>182.2</b>	<b>182.2</b>	<b>182.2</b>	<b>-2.5</b>	<b>-1%</b>
08 Launch System	200.0	200.0	200.0	200.0	200.0	0.0	0%
<b>Total Cost</b>	<b>1,541.9</b>	<b>1,462.9</b>	<b>1,519.9</b>	<b>1,505.9</b>	<b>1,496.2</b>	<b>-45.6</b>	<b>-3%</b>



## M.1 WRAP FACTORS

Wrap factors were developed from historical costs of selected JPL missions. The mission set includes:

- Mars Pathfinder, MER, and MSL – Rover missions developed in-house at JPL
- Stardust, Genesis, Deep Impact, Dawn, GRAIL, Phoenix, Insight – Discovery class missions managed by JPL
- Juno – New Frontiers class mission managed by JPL

Historical cost data comes from the NASA Cost Analysis Data Requirement (CADRe) for Launch or End of Mission. Wrap factors for WBS 04, 07, and 09 are computed as a percentage of total Phase B/C/D cost without LV or Reserves. Figure M-2 shows the calculated historical wrap factor for each WBS that was applied to the SEER and TruePlanning models which do not estimate these costs.

## M.2 SEER

SEER (version 7.4.13) is a component level cost tool that is recognized for its built-in Knowledge Bases (KBases) that pre-populate most inputs with appropriate industry values and optional calibration adjustments. In particular, the Application and Acquisition Category KBases are important for defining the hardware component, the level of maturity, and how it will be acquired. As an additional aid for using the tool, a companion document, SEER-H Space Guidance (Rev 3.1), is available to the user. It presents a standardize approach for setting up an estimate and provides recommended setting for important inputs.

Table M-3 lists the Application and Acquisition Category KBase selections for each hardware component in the rover MEL. Table M-4 lists user-entered data that overrode the KBase default values. Software costs were added using a wrap factor of 10% on the hardware cost, which is based on historical data.

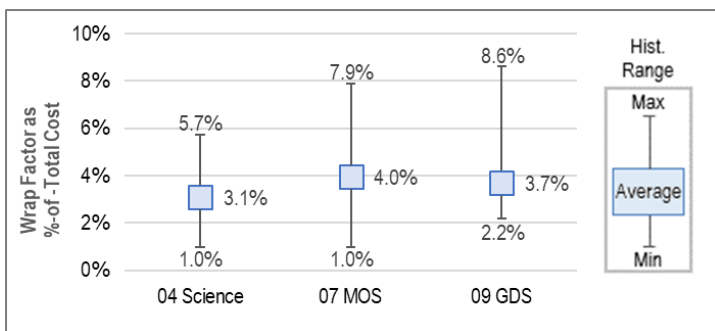


Figure M-2. Historical wrap factors for WBS 04, 07, and 09.

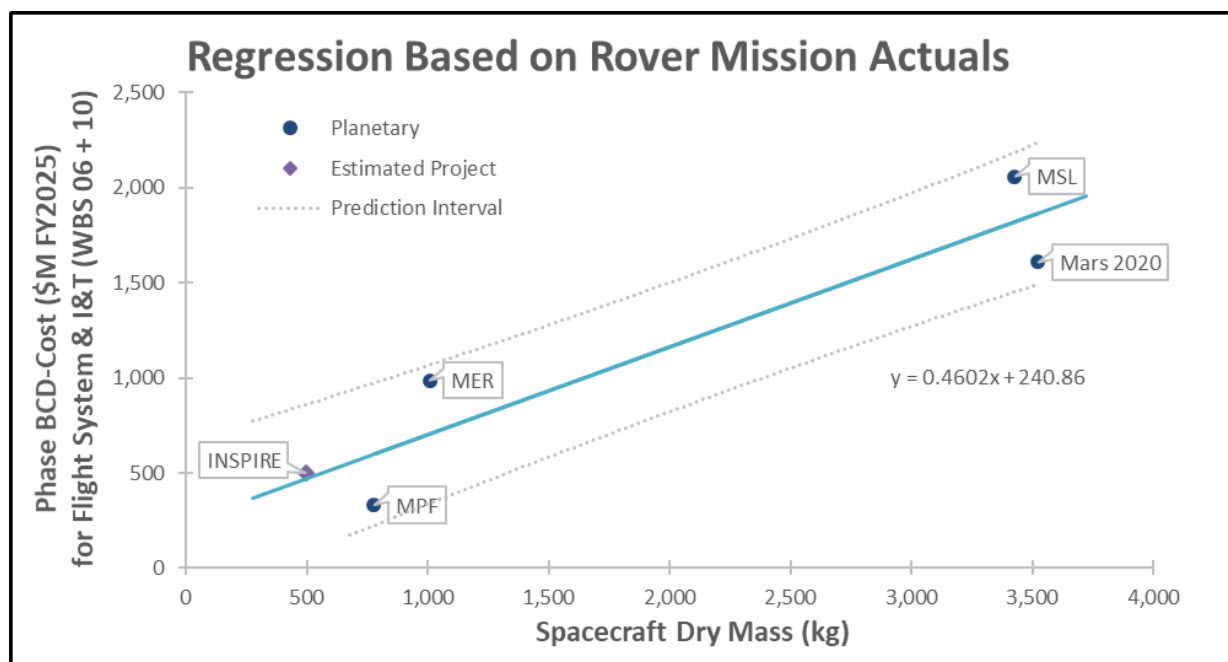


Figure M-1. \$/Kg Comparison of INSPIRE to Mars Rover Missions for WBS 06 and 10.

**Table M-3. Application and Acquisition Category KBase Settings for Rover System.**

Hardware Element	Application	Acquisition Category
Science Payload	Space System - Payload/Instrument, Science	
NIRVSS	Photon Detector - Space	Buy and Integrate
NSS	Field Sensor - Space	Buy and Integrate
Msolo	Photon Detector - Space	Buy and Integrate
IES	Field Sensor - Space	Buy and Integrate
RIMFAX	Antenna	Buy and Integrate
TIRS	Electro-Optical Sensor	Buy and Integrate
Science Camera	Electro-Optical Sensor	Buy and Integrate
Camera DVR (for thermal imager and science cameras)	Memory	Buy and Integrate
Flight System	Spacecraft Bus	
Lunar Rover	Spacecraft Bus	
C&DH Subsystem		
Sabertooth based Compute Element	Processor - Central Processing Unit	Modification - Major
Instrument Interface	Interconnect - Data Bus	Modification - Major
Motor Control	Controller - Electro-Mechanical Control	Modification - Major
Telecom Subsystem		
UST-Lite	Transponder - S-Band, Deep Space	Modification - Average
5-W SSPA	Power Amplifier - Solid State (SSPA)	Modification - Average
Coax Transfer Switches	RF Components - Space	Make
S-band Diplexer	RF Components - Space	Make
S-band Omnidirectional LGA	Antenna - Conical/Horn, Space	Modification - Major
S-band HGA & Feed (0.75m diameter)	Antenna - Dish, Space	Modification - Major
S-band HGA Gimbal	Gimbal Mechanism	Modification - Major
Coax Cabling	Cabling	Make
GN&C Subsystem		
LN 200 IMU	Inertial Measurement Unit - Space	Space Procure To Print
Front Nav Cameras (EECAM)		
Detector	Area Si CCD	Modification - Minor
Optics	!~Optical General	Modification - Minor
Back Nav Cameras (EECAM)		
Detector	Area Si CCD	Modification - Minor
Optics	!~Optical General	Modification - Minor
Star Trackers Optical Head	Star Tracker - Standard, Space	Space Procure To Print
Star Tracker Electronics	Navigation - Comm, Navigation and Identification (CNI)	Modification - Major
Illuminators	!~Optical General	Modification - Major
Power Subsystem		
RTG	Auxiliary Power Unit	Buy and Integrate
Small battery 8s6p	Battery - Lithium, Space	Modification - Major
SBIS/ PBC - Shunt & Battery I/F / Power Bus Controller	Power Supply	Modification - Major
Load and Heater Switching	Controller - Process Control	Modification - Major
Placeholder Pyro Drivers	Controller - Electro-Mechanical Control	Modification - Major
Thermal Control Subsystem		
Avionics radiator	Radiator/Heat Pipe - Space	Make
Two-phase pumped loop + tubing	Thermal Control - Passive	Make
Thermal switch	Thermal Control - Active	Make
Thermal strap	Thermal Control - Passive	Make
MLI	Thermal Control - MLI/Paint/Coating	Make
CCHPs	Radiator/Heat Pipe - Space	Make
PRT temperature sensors	Thermal Control - Active	Make

**Table M-3. Application and Acquisition Category KBase Settings for Rover System.**

Hardware Element	Application	Acquisition Category
Mechanical thermostats	Thermal Control - Active	Make
RHUs	Thermal Control - Passive	Make
RTG Bathtub	Thermal Control - Passive	Make
Structures & Mechanisms Subsystem		
Structures		
Web Chassis	Spacecraft Structure	Make
Chassis Bottom Platform	Spacecraft Structure	Make
Chassis Bottom Cover	Spacecraft Structure	Make
Camera Mast Bracket	Spacecraft Structure	Make
Drill Side Panels	Spacecraft Structure	Make
Drill Side Brackets	Spacecraft Structure	Make
Radiator Shield	Thermal Control - MLI/Paint/Coating	Make
Msolo Bracket	Spacecraft Structure	Make
Antenna Mast	Spacecraft Structure	Make
Spoiler	Spacecraft Structure	Make
Spoiler Brackets	Spacecraft Structure	Make
Rover Launch Restraint	Separation Mechanism	Make
Fasteners	!~Structural General	Make
Mobility		
Drive Actuators	Precision Mechanism	Make
Steer Actuators	Precision Mechanism	Make
Drive Actuator housing	Spacecraft Structure	Make
Steer Actuators Housing	Spacecraft Structure	Make
Wheels (+ Tires)	Spacecraft Structure	Make
Wheel Structure	Spacecraft Structure	Make
Rocker Booms	Spacecraft Structure	Make
Rocker Articulation Wheel	Spacecraft Structure	Make
Rocker Articulation Boom Fitting	Spacecraft Structure	Make
Rocker Lever	Spacecraft Structure	Make
Rocker Hub	Spacecraft Structure	Make
Dif Rotator	Spacecraft Structure	Make
Dif Lever	Spacecraft Structure	Make
Launch Locks / wheel-steer restraints / rocker restraints	Separation Mechanism	Make
Mast		
Camera Mast	Spacecraft Structure	Make
Camera Head Bracket	Spacecraft Structure	Make
Camera Mast Head	Spacecraft Structure	Make
Camera Mast Illuminator Bracket	Spacecraft Structure	Make
Drill		
TRIDENT 2m Drill	Precision Mechanism	Make
TRIDENT Drill Avionics	Processor - Central Processing Unit	Modification - Major
Drill Heater & RTD	Thermal Control - Active	Make
Harnesses		
Harnessing	Harness - Space	Make

**Table M-4.** User-specified inputs for SEER.

Input Parameter	Least	Likely	Most	Notes
<i>Global Settings applied across the entire SEER Estimate</i>				
Weight (kg)	CBE	CBE + contingency	1.3 * (CBE + Contingency)	SEER-H Space Guidance applied to all Mechanical elements.
Prototype Quantity		0.65 per unit		SEER Rule of Thumb for an EM. It was assumed all subsystems would build an EM.
Certification Level	Hi	Hi	Hi+	SEER-H Space Guidance for a Class B mission applied to all elements.
Reliability Standard	Hi+	VHi-	VHi-	SEER-H Space Guidance for a Class B mission applied to all EOS elements.
<i>Rover Specific Hardware Settings</i>				
<i>Sabertooth based Compute Element - Total PCBs</i>	5	6	7	Assume ~1 kg per board
<i>Motor Control in C&amp;DH Subsystem - Total PCBs</i>	7	7	7	1 power conversion board, 5 motor controllers and Sphinx per box
<i>Camera Detectors - Array Size Rows</i>	5,120	5,120	5,120	Based on EECAM for Mars2020.
<i>Camera Detectors - Array Size Columns</i>	3,840	3,840	3,840	Based on EECAM for Mars2020.
<i>Camera Detectors - Pitch</i>	6	6	6	Based on EECAM for Mars2020.
<i>Hardware Elements using the "Spacecraft Structure" Application KBase - Complexity of Form</i>	VHi	VHi	VHi+	SEER-H Space Guidance for 8 instruments.

### M.3 TRUEPLANNING

TruePlanning (version 16.1 SR1) was used two ways to develop an estimate. One method was at the subsystem level using MSL as an analogy to calibrate the model and the other was at the component level using the Space Missions catalog.

For the calibrated estimate, the MSL Launch CADRe was the source for the cost and mass data. A subsystem level estimate is developed with the mass information. Then the built-in calibration tool is used to solve for the value of Manufacturing Complexity for Structure and Manufacturing Complexity for Electronics with the known cost as the target. With the calibrated complexity factors in hand, these settings can now be applied to INSPIRE by simply replacing and entering the mission’s subsystem mass.

For the second estimate, INSPIRE was modeled using the Space Missions Model with the Component Type Calculator. Inputs for the Component Type Calculator include Subsystem Type, Component Type, Platform, Parts Class, Unit Mass, Quantities, Heritage for Structure and Electronics, Advanced Technology Development, and a few other element unique parameters. The calculator uses these inputs to define values for Operating Specification, Weight of Structure, Weight of Electronics, Volume, Manufacturing Complexity for Structure, Manufacturing Complexity for Electronics, Percent New for Structure and Electronics, and Engineering Complexity. Software costs are included as part of the hardware estimate, so it does not need to be modeled. The model inputs used for each component in the MEL is provided in Table M-5. For Platform and Parts Type, the same setting of “Planetary” and “S1” was used for all elements.

For the Payload System cost object, data was entered for the following inputs.

- Number of Production Units – set to 1
- Number of Prototypes – set to 1 for the assumption that there will at least one EM or prototype built for every instrument.
- Payload – set to Yes
- Mission Class – set to Class A/B



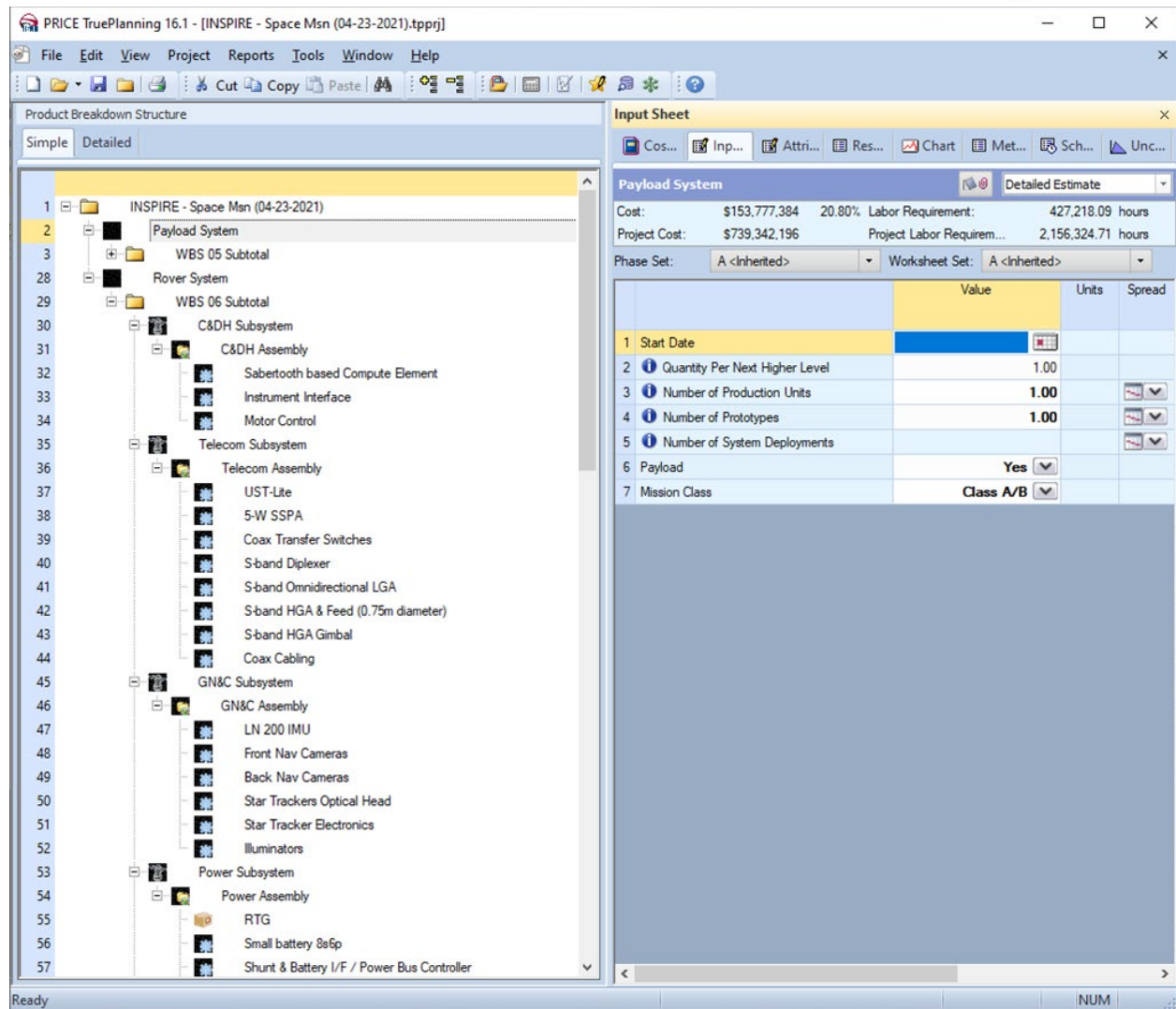


Figure M-3. TruePlanning Structure for Space Missions Model.

Table M-5. Inputs for Space Missions Model Component Type Calculator.

Hardware Element	Subsystem Type	Component Type	Unit Mass (kg)	Heritage	Additional Input
Science Payload					Payload set to Yes; Mission Class set to A/B
NIRVSS	Sensor Systems	Sensors/Detectors	3.927	Minimal Mod	Type set to Nominal
NSS	Sensor Systems	Neutron Sensor	2.09	Minimal Mod	Type set to Standard
Msolo	Sensor Systems	Ion Source	6.6	Minimal Mod	Type set to Standard
IES	Sensor Systems	Ion Source	1.144	Minimal Mod	Type set to Standard
RIMFAX	N/A	N/A	4.5	Major Mod	Used the Space Radar Altimeter cost object
TIRS	Sensor Systems	Sensors/Detectors	3.9	Minimal Mod	Type set to Simple
Science Camera	Sensor Systems	Charge Coupled Device Detectors	0.3861	Minimal Mod	Type set to Silicon-based Charge Coupled Device

**Table M-5.** Inputs for Space Missions Model Component Type Calculator.

Hardware Element	Subsystem Type	Component Type	Unit Mass (kg)	Heritage	Additional Input
Camera DVR (for thermal imager and science cameras)	Command and Data Handling	Solid State Memory	1.221	Minimal Mod	Type set to Nominal Space-based Solid State
Lunar Rover					Payload set to No; Mission Class set to A/B
C&DH Subsystem	Command and Data Handling				
Sabertooth based Compute Element	Command and Data Handling	Command/Data Processing	7.2	New	Type set to Most Microprocessors, RAD6000
Instrument Interface	Command and Data Handling	Command/Data Processing	2.5	New	Type set to Simple or non-Programmable
Motor Control	Command and Data Handling	Command/Data Processing	3.75	Major Mod	Type set to Advanced Devices
Telecom Subsystem	Communications				
UST-Lite	Communications	Transponder	1.5	Minimal Mod	Frequency Band set to S - band
5-W SSPA	Communications	Amplifier	0.5	Major Mod	Frequency Band set to Most S and X- Band Solid State Power Amplifiers
Coax Transfer Switches	Communications	Miscellaneous RF Electronics	0.125	Major Mod	Frequency Band set to S - band
S-band Diplexer	Communications	Miscellaneous RF Electronics	0.375	Major Mod	Frequency Band set to S - band
S-band Omnidirectional LGA	Communications	Medium Gain Antenna/Low Gain Antenna	0.375	Major Mod	Frequency Band set to S - band; Antenna set to Array
S-band HGA & Feed (0.75m diameter)	Communications	High Gain Antenna	7.5	Major Mod	Frequency Band set to S - band
S-band HGA Gimbal	Guidance, Navigation and Control	Gimbals	12.5	Major Mod	Material set to Composite
Coax Cabling	Communications	Waveguides - Comm Cabling	0.0625	New	Frequency Band set to S - band
GN&C Subsystem	Guidance, Navigation and Control				
LN 200 IMU	Guidance, Navigation and Control	IMU-Gyro	0.814	Minimal Mod	
Front Nav Cameras (EECAM)	Sensor Systems	Charge Coupled Device Detectors	0.6325	Minimal Mod	Type set to Advanced Visible Detector or UV/IR Detector
Back Nav Cameras (EECAM)	Sensor Systems	Charge Coupled Device Detectors	0.6325	Minimal Mod	Type set to Advanced Visible Detector or UV/IR Detector
Star Trackers Optical Head	Guidance, Navigation and Control	Star Tracker	0.22	Minimal Mod	Type set to Standard
Star Tracker Electronics	Guidance, Navigation and Control	Star Tracker	0.33	Minimal Mod	Type set to Standard
Illuminators	Sensor Systems	Photodiode	0.12	Major Mod	Type set to Advanced
Power Subsystem	Power				
RTG	N/A	N/A	72.8	N/A	Used the Purchased Good cost object; Unit Cost set to \$70,000,000; Component Type set to Hardware; Component Integration Size set to Midsize Components or Assemblies; Component Complexity set to High; External Integration Complexity set to 4.00

**Table M-5.** Inputs for Space Missions Model Component Type Calculator.

Hardware Element	Subsystem Type	Component Type	Unit Mass (kg)	Heritage	Additional Input
Small battery 8s6p	Power	Batteries	3.8125	Major Mod	Chemistry set to Li-ion
Shunt & Battery I/F / Power Bus Controller	Power	Power Management and Distribution	1.35	Major Mod	Type set to Nominal Space based Device
Load and Heater Switching	Power	Power Management and Distribution	2.6325	Major Mod	Type set to Complex Device with Advanced Switching
Placeholder Pyro Drivers	Power	Pyrotechnics	1.35	Major Mod	Type set to Standard
Thermal Control Subsystem	Thermal Control				
Avionics radiator	Thermal Control	Radiators/Louvers	3.25	New	Material set to Aluminum
Two-phase pumped loop + tubing	Thermal Control	Heat Pipes	19.5	New	Material set to Composite
Thermal switch	Thermal Control	Heaters, RHUs, Thermostats	0.192	New	Material set to Composite
Thermal strap	Thermal Control	Heaters, RHUs, Thermostats	0.12	New	Material set to Composite
MLI	Thermal Control	MLI, Paints, Coatings	5.85	New	
CCHPs	Thermal Control	Heat Pipes	0.13	New	Material set to Aluminum
PRT temperature sensors	Thermal Control	Heaters, RHUs, Thermostats	0.0013	New	Material set to Stainless Steel
Mechanical thermostats	Thermal Control	Heaters, RHUs, Thermostats	0.0325	New	Material set to Stainless Steel
Heaters	Thermal Control	Heaters, RHUs, Thermostats	0.078	New	Material set to Stainless Steel
RTG Bathhtub	Thermal Control	Heaters, RHUs, Thermostats	5.2	New	Material set to Composite
Structures & Mechanisms Subsystem	Structure and Mechanisms				
Structures					
Web Chassis	Structure and Mechanisms	Primary Structure	42.0	New	Material set to Aluminum; Advanced Technology Development set to New
Chassis Bottom Platform	Structure and Mechanisms	Primary Structure	2.4	New	Material set to Aluminum; Advanced Technology Development set to New
Chassis Bottom Cover	Structure and Mechanisms	Primary Structure	2.4	New	Material set to Aluminum; Advanced Technology Development set to New
Camera Mast Bracket	Structure and Mechanisms	Secondary Structure	0.0	New	Material set to Aluminum
Drill Side Panels	Structure and Mechanisms	Primary Structure	4.2	New	Material set to Aluminum; Advanced Technology Development set to New
Drill Side Brackets	Structure and Mechanisms	Secondary Structure	1.2	New	Material set to Aluminum
Radiator Shield	Structure and Mechanisms	Shielding	1.08	New	Material set to Aluminum
Msolo Bracket	Structure and Mechanisms	Secondary Structure	0.0	New	Material set to Aluminum
Antenna Mast	Structure and Mechanisms	Primary Structure	0.6	New	Material set to Aluminum; Advanced Technology Development set to New
Spoiler	Structure and Mechanisms	Primary Structure	3.48	New	Material set to Aluminum; Advanced Technology Development set to New
Spoiler Brackets	Structure and Mechanisms	Secondary Structure	0.12	New	Material set to Aluminum
Rover Launch Restraint	Structure and Mechanisms	Mechanism	3.6	New	Type set to Standard
Fasteners	Structure and Mechanisms	Secondary Structure	4.0884	New	Material set to Aluminum

**Table M-5.** Inputs for Space Missions Model Component Type Calculator.

Hardware Element	Subsystem Type	Component Type	Unit Mass (kg)	Heritage	Additional Input
<b>Mobility</b>					
Drive Actuators	Structure and Mechanisms	Motor-Actuator	3.3125	New	Type set to Advanced; Advanced Technology Development set to New
Steer Actuators	Structure and Mechanisms	Motor-Actuator	3.3125	New	Type set to Advanced; Advanced Technology Development set to New
Drive Actuator housing	Structure and Mechanisms	Primary Structure	1.8	New	Material set to Aluminum; Advanced Technology Development set to New
Steer Actuators Housing	Structure and Mechanisms	Primary Structure	1.8	New	Material set to Aluminum; Advanced Technology Development set to New
Wheels (+ Tires)	Structure and Mechanisms	Mechanisms	6.84	New	Type set to Very Advanced; Advanced Technology Development set to New
Wheel Structure	Structure and Mechanisms	Primary Structure	3.0	New	Material set to Aluminum; Advanced Technology Development set to New
Rocker Booms	Structure and Mechanisms	Primary Structure	1.2	New	Material set to Aluminum; Advanced Technology Development set to New
Rocker Articulation Wheel	Structure and Mechanisms	Primary Structure	8.4	New	Material set to Aluminum; Advanced Technology Development set to New
Rocker Articulation Boom Fitting	Structure and Mechanisms	Secondary Structure	3.0	New	Material set to Aluminum; Advanced Technology Development set to New
Rocker Lever	Structure and Mechanisms	Primary Structure	2.04	New	Material set to Aluminum; Advanced Technology Development set to New
Rocker Hub	Structure and Mechanisms	Primary Structure	4.8	New	Material set to Aluminum; Advanced Technology Development set to New
Dif Rotator	Structure and Mechanisms	Mechanisms	2.916	New	Type set to Advanced; Advanced Technology Development set to New
Dif Lever	Structure and Mechanisms	Mechanisms	0.312	New	Type set to Advanced; Advanced Technology Development set to New
Launch Locks / wheel-steer restraints / rocker restraints	Structure and Mechanisms	Mechanisms	0.6	New	Type set to Standard; Advanced Technology Development set to New
<b>Mast</b>					
Camera Mast	Structure and Mechanisms	Primary Structure	0.3	New	Material set to Composite; Advanced Technology Development set to New
Camera Head Bracket	Structure and Mechanisms	Secondary Structure	1.68	New	Material set to Aluminum
Camera Mast Head	Structure and Mechanisms	Primary Structure	4.2	New	Material set to Aluminum; Advanced Technology Development set to New
Camera Mast Illuminator Bracket	Structure and Mechanisms	Secondary Structure	0.504	New	Material set to Aluminum
<b>Drill</b>					
TRIDENT 2m Drill	Structure and Mechanisms	Mechanisms	30.0	New	Type set to Very Advanced; Advanced Technology Development set to New
TRIDENT Drill Avionics	Command and Data Handling	Command/Data Processing	8.4	New	Type set to Advanced Devices; Advanced Technology Development set to New
Drill Heater & RTD	Thermal Control	Heaters, RHUs, Thermostats	0.6	New	Material set to Stainless Steel
<b>Harness Subsystem</b>					
Harnessing	Power	Power Harness/Cabling	28.47	New	



## M.4 SOCM

The Space Operations Cost Model (SOCM) was used for the validation of Phase E/F. SOCM estimates the costs and staffing for space operations projects using high-level project characteristics that are typically known at the early stages of a project’s lifecycle. Running the cost model at Level 1 generates an estimate with an accuracy of  $\pm 30\%$ . The Level 1 Earth Orbiting inputs selected to reflect the INSPIRE mission are identified in Figure M-4. The INSPIRE rover will be an augmented hybrid development where a significant portion is done in-house and some hardware is contracted out.

The Level 2 Earth Orbiting inputs may also be adjusted to refine the estimate and improve the accuracy. Figure M-5 provides the Level 2 settings.

The Space Operations Cost Model (SOCM) estimates all Phase E/F costs, with the exception of ground station tracking (WBS 07.03). Therefore, the Team X estimates for tracking (\$6.58M) was used as a pass-through and added to the SOCM results. The final outputs from SOCM are provided in Figure M-6.

EARTH ORBITING - LEVEL 1 INPUTS							
	Value ->	1	2	3	4	5	6
<b>MISSION CHARACTERIZATION</b>							
Mission Type	4	Survey - Earth Science	Survey - Space Science	Targeted - Earth Science	Targeted - Space Science		
Tracking Network	3	Ground	TDRSS	DSN			
Orbit	4	LEO, circular	L1, halo	Highly Elliptical	Non-Standard/"Evolving"		
# of Identical Flight Systems	1	1	2	3	4	5	6
Nominal Mission Duration (mo)	38						
Extended Mission Duration (mo)	0						
Post-Flight Data Analysis Duration (mo)	6						
<b>PROGRAMMATICS CHARACTERIZATION</b>							
Mission Risk Class	4	Technology Demo (tech > sci)	SMEX	MIDEX/ESSP	Explorers	Great Observatories	
Development Schedule	3	Fast (< 2.5 yrs)	Moderate (2.5-4 yrs)	Long (> 4 yrs)			
Management Mode	1	PI	NASA				
Contract Type	2	In-House	Augmented Hybrid	Hybrid	Out-of-House		
<b>GDS/MOS CHARACTERIZATION</b>							
Operations Approach	2	Dedicated MOC	Multimission MOC	Remote MOC/SOC	Contracted		
Architecture Design	2	COTS	Heritage/GOTS	New/Custom			
Science Team Role	3	Data Processing	Instrument Health	Sequence Planning			
<b>PAYLOAD CHARACTERIZATION</b>							
# of Non-Imaging Instruments	6						
# of Imaging Instruments	3						
Pointing Requirements	2	Low	Medium	High			
Conflicts Among Instruments	2	Low	Medium	High			
Scope of Guest Investigator Program	3	Small	Medium	Large			
# of Separate Science Investigations	4	1-2	3-5	6-10	11-15	> 15	
Science Team Size (not all FT)	3	Less than 10	10-20	more than 20	more than 50		
Science Team Location/Distribution	4	Colocated at 1 facility	Central SOC, 1-2 remotes	Central SOC, 3+ remotes	Central SOC, wide distr.	2 - 3 SOC locations	Multiple SOCs, wide distr
<b>S/C DESIGN CHARACTERIZATION</b>							
S/C Design Implementation	2	High Heritage	Cost-Capped	Requirements-Driven			
Design Complexity	3	Low (few flight rules)	Medium	High (unique engrng reqs)			
						Science Instrument Score	
						Score	12
						Max Score	20

Figure M-4. SOCM Level 1 Cost Inputs for INSPIRE.

EARTH ORBITING - LEVEL 2 INPUTS					
LEVEL 2 ESTIMATE		<b>Earth-Orbiting - LEVEL 2 INPUTS</b>			
INSPIRE LEVEL 2 INPUTS		Use Low or High when driver is known; Medium is default value			
Selected Cost Drivers:		units			Definitions
Mission Implementation	Low	Medium	High		
Engineering Event Complexity	<input checked="" type="radio"/> Routine, Non-hazardous events	<input type="radio"/> Repetitive/No Hazardous Events	<input type="radio"/> Risky events/Significant Real-Time Contact		Number of unique engineering command sequences
Targeted Observations	<input checked="" type="radio"/> No targeted observations or >24 hours to implement	<input type="radio"/> Targeted observations implemented in 6-24 hours	<input type="radio"/> Targeted observations implemented in less than 6 hours		High level characterization of operation concept
Science Event Complexity	<input type="radio"/> Survey	<input type="radio"/> Few constraints	<input checked="" type="radio"/> Constrained, Multiple observation modes		Number of unique science instrument command sequences
Programmatic Implementation	Low	Medium	High		
Staff Experience	<input type="radio"/> More than 2 similar missions	<input checked="" type="radio"/> 1 or 2 similar missions	<input type="radio"/> New OPS team		Experience of ops staff with similar systems
Risk Plan - S/C	<input type="radio"/> Small S/C, No redundancy, Tech demo mission	<input type="radio"/> Class C, \$100M fit system development	<input checked="" type="radio"/> Redundant S/C, several \$100M development		Measure of the S/C operational risk based on design implementation
Risk Plan - Instruments/Payload	<input type="radio"/> Simple payload, No redundancy	<input checked="" type="radio"/> Few hazardous OPS, Limited redundancy	<input type="radio"/> Complex, redundant S/C		Measure of the instrument/payload operational risk based on design implementation
Risk Plan - GDS/MOS	<input type="radio"/> Accept min risk to msn safety, and mod data loss	<input checked="" type="radio"/> Accept mod risk to efficiency and data loss < 5%	<input type="radio"/> Accept min risk to efficiency and data loss < 1%		Measure of the GDS/MOS operational risk based on design implementation
Crosstraining/Staffing Overlaps	<input type="radio"/> Fully crosstrained	<input checked="" type="radio"/> Crosstrained within functions	<input type="radio"/> Limited crosstraining		Number of staff assigned/trained to perform same function
H/W Redundancy	<input type="radio"/> Limited or no redundancy	<input checked="" type="radio"/> Selected redundancy	<input type="radio"/> Full redundancy with rapid switchover		GDS/MOS system redundancy
Spacecraft Design Impl.	Low	Medium	High		
S/C Autonomy	<input type="radio"/> Proven sophisticated autonomy	<input checked="" type="radio"/> Simple robust safe mode; Onboard telemetry monitor	<input type="radio"/> Complex safe modes or experimental approach		Ability of the s/c to operate without ground control
Maneuver Frequency	<input type="radio"/> Once per year or less	<input type="radio"/> Couple of times per year	<input checked="" type="radio"/> Once a month or more		Frequency of S/C maneuvers over nominal operations period
Data Return Margin	<input type="radio"/> > 2	<input checked="" type="radio"/> 1.1 - 2	<input type="radio"/> < 1.1		Ratio of max amount of data that can be downlinked to the average amount required per downlink
Power Margin	<input checked="" type="radio"/> > 1.2	<input type="radio"/> 1 - 1.2	<input type="radio"/> < 1		Ratio of max avail power to peak power demand
Memory Margin	<input checked="" type="radio"/> > 2	<input type="radio"/> 1.5 - 2	<input type="radio"/> < 1.2		Ratio of on-board storage capacity to max quantity of data to be downlinked in a single pass

Figure M-5. SOCM Level 2 Cost Inputs.

GDS/MOS Implementation		Low	Medium	High		
Command Frequency - Sequences	<input checked="" type="radio"/>	Loaded less than once per day	<input type="radio"/> Daily	<input type="radio"/> Loaded more than once per day		Frequency of developing sequences for uplink
Data Processing - Data Completeness	<input type="radio"/>	< 95%	<input checked="" type="radio"/> 95-98%	<input type="radio"/> > 98%	%	Measure of data return requirement vs. minimal acceptable data return
Data Processing - Data Delivery Time	<input type="radio"/>	More than 24 hours	<input checked="" type="radio"/> 6 to 24 hours	<input type="radio"/> Less than 6 hours	hrs	Time allowed to deliver data products after raw data is downlinked
Data Processing - Autonomy	<input type="radio"/>	Extensive	<input checked="" type="radio"/> Nominal	<input type="radio"/> Minimal		Measure of the degree of autonomy in ground data handling system
Data Processing - Heritage/Reuse	<input type="radio"/>	More than 85%	<input checked="" type="radio"/> 75%	<input type="radio"/> Less than 60%	%	% of ground data processing system based on existing designs
Command Frequency - Generation Time	<input checked="" type="radio"/>	More than one day before upload	<input type="radio"/> One day before upload	<input type="radio"/> Less than one day before upload		Time allowed to generate commands to modify/affect mission ops
Command Frequency - Real-Time Commands	<input type="radio"/>	No commands on some passes	<input checked="" type="radio"/> Routine commands on most passes	<input type="radio"/> Special commands on some passes		Frequency of real-time commands for uplink
Data Processing - Max. Downlink Rate	<input type="radio"/>	less than 1	<input checked="" type="radio"/> 1 to 2	<input type="radio"/> 10s to 100s	Mbps	Maximum downlink data rate accommodated
Data Processing - Max. Bits/Day	<input type="radio"/>	< 10	<input checked="" type="radio"/> 10-100	<input type="radio"/> > 100	Gb	Maximum # of bits downlinked per day
Data Processing - On-Line Storage	<input type="radio"/>	> 20	<input checked="" type="radio"/> 2 - 20	<input type="radio"/> < 2	GB	Size/capacity of onboard data storage system
Data Processing - Storage/Playback Frequency	<input type="radio"/>	Once per day or less	<input checked="" type="radio"/> Several times per day	<input type="radio"/> Once per orbit		Number of days that data can be stored without downlink
Payload Implementation		Low	Medium	High		
Instrument Support Complexity	<input type="radio"/>	Simple instrument with few operations	<input checked="" type="radio"/> Routine calibrations, few sched constraints	<input type="radio"/> Constrained operation, Complex instr interactions		Relates to # of instruments, conflicts, flight rules for instr operation
Payload Flight Heritage	<input type="radio"/>	Most instruments have flown together; No advanced technology	<input checked="" type="radio"/> Most instruments have flight heritage	<input type="radio"/> New instruments; Payload includes advanced technology		Measure of individual instruments and total payload package flight experience
Instrument/Payload Operating Modes	<input type="radio"/>	2-3 operating modes per instrument; One observing mode for all instruments	<input checked="" type="radio"/> Less than 3 operating modes per instrument; 2-3 observing modes	<input type="radio"/> Several instruments with multiple operating modes; 3+ observing modes		Number of operating modes for each instrument and observing modes for total payload; Modes include calibration

Figure M-5 (continued). SOCM Level 2 Cost Inputs.

LEVEL 2 MISSION OPERATIONS COST INSPIRE	ESTIMATE				Phase E Total	JPL WBS	
	Phase E Nominal	Phase E Extended	2025 constant FY \$K			Mapping	Cost
1.0 MISSION PLANNING & INTEGRATION	3252.9	0.0			3252.9	MOS	7 MOS 48,746.9
2.0 COMMAND/UPLINK MANAGEMENT	7738.1	0.0			7738.1	MOS	
3.0 MISSION CONTROL & OPS	9029.0	0.0			9029.0	MOS	9 GDS 22,681.0
4.0 DATA CAPTURE	8737.5	0.0			8737.5	GDS	
5.0 POS/LOC PLANNING & ANALYSIS	439.4	0.0			439.4	MOS	
6.0 S/C PLANNING & ANALYSIS	1532.2	0.0			1532.2	MOS	
7.0 SCI PLANNING & ANALYSIS	26755.3	0.0			26755.3	MOS	
8.0 SCIENCE DATA PROCESSING	33078.1	0.0	5222.9		38301.0	Science	4 Science 67,307.8
9.0 LONG-TERM ARCHIVES	16951.4	0.0	2676.5		19627.9	Science	
10.0 SYSTEM ENGINEERING, INTEG, & TEST	9071.7	0.0			9071.7	GDS	
11.0 COMPUTER & COMM SUPPORT	4207.5	0.0	664.3		4871.9	GDS	
12.0 SCIENCE INVESTIGATIONS	8100.0	0.0	1279.0		9379.0	Science	
13.0 MANAGEMENT	1790.9	0.0			1790.9	Mgmt	1 Mgmt 1,790.9
<b>Project Direct Total</b>	<b>130,684.0</b>	<b>0.0</b>	<b>9,842.7</b>		<b>140,526.7</b>		

Tracking costs from Team X 6,580.0

Figure M-6. SOCM Level 2 Cost Results for INSPIRE.

### M.5 POTENTIAL COST SAVINGS

In addition to developing a cost estimate for the INSPIRE concept, Team X also provided feedback on potential cost savings. Team X findings include:

- If instruments can be made as build to print of reference instruments, savings can be up to 50%.
- Reduce redundancy of drill and implement more system level testing to raise drill reliability.
- Perform a deeper examination of the mobility system’s design. A soft touchdown and lower loads would indicate a simpler system.
- EE cameras have become a common component. The cost will continue to go down as the number of units built increases.
- Battery cost is heuristic based on \$/wh or \$/ah. Need to contact a vendor for pricing and alternative cost options.

Table M-6. JPL Team X estimates for alternative scenarios (FY25\$M).

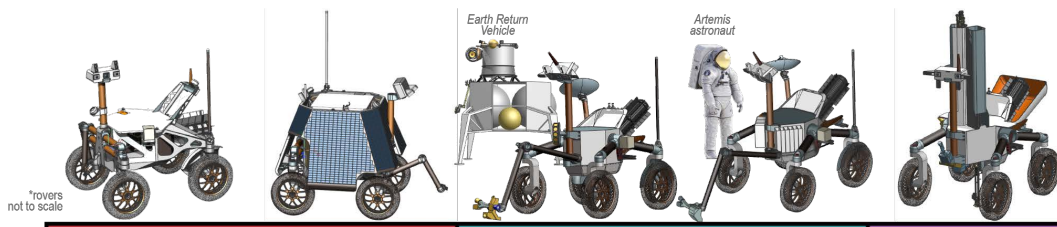
WBS Element	5 Year Phase E	4 Year Phase E
Phase A Concept Study	Incl. below	Incl. below
01/02/03 PM/PSE/SMA	89.4	89.4
04 Science	37.9	37.9
05 Payload	84.3	84.3
06 Flight System	475.9	475.9
07 Mission Ops System	32.6	32.6
09 Ground Data System	33.4	33.4
10 Project System I&T	41.3	41.3
<b>Total Dev. w/o Reserves</b>	<b>794.7</b>	<b>794.7</b>
Development Reserves (50%)	362.4	362.4
<b>Total A-D Development Cost</b>	<b>1,157.1</b>	<b>1,157.1</b>
01/02 PM/PSE	8.2	6.7
04 Science	98.2	80.8
07 Mission Ops System	86.6	70.0
09 Ground Data System	44.2	35.7
<b>Total Ops w/o Reserves</b>	<b>237.2</b>	<b>193.2</b>
Operations Reserves (25%)	56.6	46.1
<b>Total E-F Operations Cost</b>	<b>293.8</b>	<b>239.3</b>
08 Launch System	200.0	200.0
<b>Total Cost</b>	<b>1,650.9</b>	<b>1,596.4</b>

### M.6 COSTS FOR ALTERNATIVE MISSION SCENARIOS

Team X originally costed a mission concept that was baselined with a 5 year Phase E. They were also asked for the cost if the lunar operations could be completed in 4 years. For these two scenarios, the development costs were unchanged by the mission duration and only the operations cost were affected. The cost for these two scenarios is provided in Table M-6.



**N SUMMARY OF LONG-RANGE LUNAR ROVER CONCEPTS FOR THE DECADAL SURVEY**



**LONG-RANGE LUNAR ROVER MISSION CONCEPTS**

five rovers with a common design lineage  
2023–2032 Planetary Science and Astrobiology Decadal Survey

Intrepid		Endurance		INSPIRE
Intrepid (RTG) (baseline Intrepid)	Intrepid (Solar)	Endurance-R (R = robotic sample return)	Endurance-A (A = astronaut sample return)	(In Situ Solar System Polar Ice Roving Explorer)
Pre-Decadal Planetary Mission Concept Study (PMCS)		Decadal Survey Mission Concept Study		
PI: Mark Robinson (ASU)		Science Champion: James Tuttle Keane (JPL) Deputy Science Champion: Sonia Tikoo (Stanford)		Science Champion: Jennifer Heldmann (NASA Ames)
Study Lead: John Elliott (JPL)				

Notes:

CONCEPT SUMMARY:	Description:	Long-range lunar rover for exploring, collecting, and returning samples and the largest and oldest impact basin on the Moon, South Pole-Aitken (SPA) basin, in order to answer critical questions about Solar System chronology and planetary evolution.	Long-range lunar rover for exploring the Moon's permanently shadowed regions (PSRs) to determine the origin, age, and evolution of lunar volatiles.	
	Landing Site:	Lunar nearside, Oceanus Procellarum (6.5°N, -58.9°E)	Lunar farside, Poincaré basin (57.2°S, 163.0°E)	Lunar farside, central South Pole-Aitken basin (57.9°S, -161.7°E)
	Lunar Delivery:	Rover delivered by a CLPS lander (for comparison, VIPER a ~500-kg rover will be delivered by CLPS to the lunar south pole in 2022)		
	Nominal Launch Date:	2030 (set by RTG availability for most options; launch dates for the Moon are extremely flexible)		
	Nominal Traverse Distance:	1,800 km	1,750 km	2,000 km
	Mission Duration:	4 years (including 1 year of margin)	7 years (including 1 year of margin)	4 years (including 1.1 years of margin)

Intrepid, Endurance, and INSPIRE all address different priority planetary science questions—as detailed in their respective reports.

COST:	Total A-D Development Costs (with 50% reserves):	\$1,049M	\$997M	\$1,778M	\$1,105M	\$1,157M
	Total E-F Operations Cost (with 25% reserves):	\$242M	\$350M	\$252M	\$233M	\$184M
	Launch and Commercial Lunar Payload Service:	\$220M	\$200M	\$400M	\$200M	\$200M
	Total Project Cost:	\$1,511M	\$1,547M	\$2,430M	\$1,538M	\$1,541M
	Mission Class:	New Frontiers	New Frontiers	Flagship	New Frontiers	New Frontiers

Team-X costs reported, following Decadal Survey concept study guidelines.  
Endurance-R has higher costs (Flagship class) because it includes the development and operations of a separate Earth Return Vehicle. The cost of just the Endurance-R rover would be very nearly identical to the costs for Endurance-A.  
Intrepid (Solar) has a higher operations cost than Intrepid (RTG) because the solar-powered version requires a longer mission duration (since it cannot do substantial operations at night).  
Intrepid (RTG)'s launch service costs included an extra \$20M for RTG special services. For Endurance and INSPIRE, all RTG costs are carried in A-D costs.

SCIENCE INSTRUMENTS	Instruments:	Stereo cameras Long-range camera (FarCam) Visible/Near-IR point spectrometer Hand lens imager (HLI) Alpha-particle X-ray spectrometer (APXS) Magnetometer Gamma-ray and neutron spectrometer (GRNS) Radiation monitor (ARMAS) Electrostatic analyzer (ESA) Laser retro-reflector (LRR)	Near-IR spectrometer (NIRVSS) Neutron spectrometer Mass spectrometer (MSolo) Ion and electron detector (IES) Thermal-IR spectrometer (TIRS) Mini Ground Penetrating Radar (Mini-GPR)	
	Arm:	1-m long arm (0.5-m links)	2-m long arm (1-m links)	No arm
	Drill:	No drill		2-m TRIDENT drill
	Sample Collection:	No sample collection	Combined scoop and rake Sample container, capable of storing 2.2-kg (total) of lunar regolith and rocks in 12 individually sealed chambers Rover delivers samples to robotic Earth Return Vehicle	Scoop Sample boxes, capable of storing 100-kg (total) of lunar regolith and rocks in 12 open-air boxes No sample collection Rover delivers samples to Artemis astronauts at the lunar south pole

Intrepid, Endurance-R, and Endurance-A have identical instrument suites. INSPIRE's instrument suite is largely distinct.  
Endurance's arm is identical to Intrepid's arm, but with longer links to extend the workspace for sampling and, for Endurance-R, to facilitate transfer of the sample canister to the Earth Return Vehicle.  
Endurance-R's combined scoop and rake separates out regolith fines (<0.5 cm diameter) and rocklets (0.5–2 cm diameter). Endurance-A's simple scoop is just that—a scoop. Both are designed off of successful Apollo sampling equipment.  
Both Endurance sample systems are substantially simpler than the Perseverance (Mars 2020) sample collection and caching system.

ROVER DESIGN AND SUBSYSTEMS:	Rover Mass:	500 kg	500 kg	570 kg	570 kg	655 kg
	Rover Size:	width: 1.8-m length: 2.7-m height: 3.0-m	width: 2.4-m length: 2.4-m height: 3.0-m	width: 2.1-m length: 2.7-m height: 2.8-m	width: 2.1-m length: 2.7-m height: 2.8-m	width: 2.1-m length: 3.0-m height: 3.4-m
	Mobility:	Four-wheel, all-wheel drive steering 0.8-m diameter mesh compliant wheels				Dual side-rocker and differential
	Autonomy:	Preplanned traverse with onboard decide autonomy for traverse and science operations				
	Communications:	Direct-to-Earth communications via Deep Space Network (DSN)		Communications to Earth via lunar relay orbiter (Lunar Pathfinder baselined)		
	Power:	12-GPHS NextGen RTG (beginning of life power: 300-W)	Fixed, wrap-around triple junction solar arrays (6.3 m <sup>2</sup> total, 1.3 m <sup>2</sup> illuminated at any time; beginning of life power: 317-W)	Mod-1 NextGen RTG (beginning of life power: 245-W)		Secondary Li-Ion battery (100 amp-hr)
		Secondary Li-Ion battery (20 amp-hr)	Secondary Li-Ion battery (612 amp-hr)	Secondary Li-Ion battery (20 amp-hr)		Secondary Li-Ion battery (100 amp-hr)
	Attitude Control System (ACS):	Cameras Inertial Measurement Units (IMUs) Sun sensors Star trackers Headlights (for night driving)				
	Thermal:	Radiator, thermal switch, electronics placed in central Warm Electronics Box (WEB)				Two-phase pumped loop system to distribute RTG heat
	Command and Data Handling (C&DH):	Dual-string Sabretooth				

Masses are fully margined.  
Endurance is heavier than Intrepid (RTG) largely due to the addition of the high-gain antenna, heavier RTG, and dual-rocker mobility system.  
INSPIRE is heavier than Intrepid for the same reasons as Endurance, and INSPIRE is heavier than Endurance largely due to the addition of a larger battery and the drill system.  
INSPIRE is taller because of the drill.  
Endurance and INSPIRE opted for a dual side-rocker mobility system to enable traversing steeper slopes (<20°) than Intrepid (<15°).  
Intrepid, Endurance, and INSPIRE all take a common approach to traverse operations, including substantial pre-planning, autonomy, and prioritizing traverse speed and accomplishing science objectives.  
Endurance-R and Endurance-A operate on the lunar farside, and INSPIRE operates at the south pole, frequently out of view of the Earth, so these concepts require orbital communications relays. There are several relays planned in the next decade, including Lunar Gateway, Lunar Communications Pathfinder, and Andromeda. Lunar Pathfinder was baselined.  
Endurance-R, Endurance-A, and INSPIRE were required to use different RPS, due to changes in the NextGen RTG program.  
Intrepid (Solar) has a large battery for night survival, and INSPIRE has a large battery for drill operations.  
Intrepid did not require headlights, since it could utilize Earthshine for night driving. Endurance and INSPIRE are designed for substantial operations at lunar night or in permanent shadow.  
INSPIRE required additional thermal capabilities to survive in cold permanently shadowed regions.

JPL can provide a complete Master Equipment Lists (MEL) for each rover concept.

Pre-decisional Information. For Planning and Discussion Purposes Only.

---

**O REFERENCES****O.1 SECTIONS 1-5**

- [1] E. Mazarico, G. Neumann, D. Smith, M. Zuber, and M. Torrence, "Illumination conditions of the lunar polar regions using LOLA topography," *Icarus*, vol. 211, no. 2, pp. 1066-1081, 2011.
- [2] D. A. Paige *et al.*, "Diviner lunar radiometer observations of cold traps in the Moon's south polar region," *science*, vol. 330, no. 6003, pp. 479-482, 2010.
- [3] A. R. Vasavada, D. A. Paige, and S. E. Wood, "Near-surface temperatures on Mercury and the Moon and the stability of polar ice deposits," *Icarus*, vol. 141, no. 2, pp. 179-193, 1999.
- [4] J. P. Williams *et al.*, "Seasonal polar temperatures on the Moon," *Journal of Geophysical Research: Planets*, vol. 124, no. 10, pp. 2505-2521, 2019.
- [5] J. Mitchell, "The curation of cryogenic samples," in *Decadal Survey in Planetary Science and Astrobiology 2023-2032, Committee on Mercury and the Moon, 2021*, 2021.
- [6] N. L. Chabot, E. E. Shread, and J. K. Harmon, "Investigating Mercury's south polar deposits: Arecibo radar observations and high-resolution determination of illumination conditions," *Journal of Geophysical Research: Planets*, vol. 123, no. 2, pp. 666-681, 2018.
- [7] A. N. Deutsch *et al.*, "Comparison of areas in shadow from imaging and altimetry in the north polar region of Mercury and implications for polar ice deposits," *Icarus*, vol. 280, pp. 158-171, 2016.
- [8] D. A. Paige *et al.*, "Thermal stability of volatiles in the north polar region of Mercury," *Science*, vol. 339, no. 6117, pp. 300-303, 2013.
- [9] N. Schorghofer *et al.*, "The permanently shadowed regions of dwarf planet Ceres," *Geophysical Research Letters*, vol. 43, no. 13, pp. 6783-6789, 2016.
- [10] G. Black, D. Campbell, and J. Harmon, "Radar measurements of Mercury's north pole at 70 cm wavelength," *Icarus*, vol. 209, no. 1, pp. 224-229, 2010.
- [11] J. K. Harmon, "Radar Imaging of Mercury," *Space Science Reviews*, vol. 132, no. 2-4, pp. 307-349, 2007.
- [12] B. J. Butler, D. O. Muhleman, and M. A. Slade, "Mercury: Full-disk radar images and the detection and stability of ice at the north pole," *Journal of Geophysical Research: Planets*, vol. 98, no. E8, pp. 15003-15023, 1993.
- [13] D. J. Lawrence *et al.*, "Evidence for water ice near Mercury's north pole from MESSENGER Neutron Spectrometer measurements," *Science*, vol. 339, no. 6117, pp. 292-296, 2013.
- [14] N. L. Chabot *et al.*, "Images of surface volatiles in Mercury's polar craters acquired by the MESSENGER spacecraft," *Geology*, vol. 42, no. 12, pp. 1051-1054, 2014.
- [15] A. N. Deutsch, G. A. Neumann, and J. W. Head, "New evidence for surface water ice in small-scale cold traps and in three large craters at the north polar region of Mercury from the Mercury Laser Altimeter," *Geophysical Research Letters*, vol. 44, no. 18, pp. 9233-9241, 2017.
- [16] G. A. Neumann *et al.*, "Bright and dark polar deposits on Mercury: Evidence for surface volatiles," *Science*, vol. 339, no. 6117, pp. 296-300, 2013.
- [17] E. A. Fisher *et al.*, "Evidence for surface water ice in the lunar polar regions using reflectance measurements from the Lunar Orbiter Laser Altimeter and temperature measurements from the Diviner Lunar Radiometer Experiment," *Icarus*, vol. 292, pp. 74-85, 2017.
- [18] A. Ermakov *et al.*, "Constraints on Ceres' internal structure and evolution from its shape and gravity measured by the Dawn spacecraft," *Journal of Geophysical Research: Planets*, vol. 122, no. 11, pp. 2267-2293, 2017.

- 
- [19] T. Platz *et al.*, "Surface water-ice deposits in the northern shadowed regions of Ceres," *Nature Astronomy*, vol. 1, no. 1, pp. 1-6, 2016.
- [20] S. Li *et al.*, "Direct evidence of surface exposed water ice in the lunar polar regions," *Proceedings of the National Academy of Sciences*, vol. 115, no. 36, pp. 8907-8912, 2018.
- [21] A. Raponi *et al.*, "Variations in the amount of water ice on Ceres' surface suggest a seasonal water cycle," *Science advances*, vol. 4, no. 3, p. eaa03757, 2018.
- [22] J. L. Kloos, J. E. Moores, J. Sangha, T. G. Nguyen, and N. Schorghofer, "The temporal and geographic extent of seasonal cold trapping on the Moon," *Journal of Geophysical Research: Planets*, vol. 124, no. 7, pp. 1935-1944, 2019.
- [23] M. Siegler *et al.*, "Lunar true polar wander inferred from polar hydrogen," *Nature*, vol. 531, no. 7595, pp. 480-484, 2016.
- [24] M. A. Siegler, B. G. Bills, and D. A. Paige, "Effects of orbital evolution on lunar ice stability," *Journal of Geophysical Research: Planets*, vol. 116, no. E3, 2011.
- [25] E. Costello, R. Ghent, M. Hirabayashi, and P. Lucey, "Impact Gardening as a Constraint on the Age, Source, and Evolution of Ice on Mercury and the Moon," *Journal of Geophysical Research: Planets*, vol. 125, no. 3, p. e2019JE006172, 2020.
- [26] E. Costello, R. Ghent, and P. Lucey, "Impact Gardening on Ceres," *Geophysical Research Letters*, p. e2021GL092960, 2021.
- [27] A. N. Deutsch, J. W. Head III, and G. A. Neumann, "Age constraints of Mercury's polar deposits suggest recent delivery of ice," *Earth and planetary science letters*, vol. 520, pp. 26-33, 2019.
- [28] D. J. Lawrence, "A tale of two poles: Toward understanding the presence, distribution, and origin of volatiles at the polar regions of the Moon and Mercury," *Journal of Geophysical Research: Planets*, vol. 122, no. 1, pp. 21-52, 2017.
- [29] L. Rubanenko, J. Venkatraman, and D. A. Paige, "Thick ice deposits in shallow simple craters on the Moon and Mercury," *Nature Geoscience*, vol. 12, no. 8, pp. 597-601, 2019.
- [30] P. Prem *et al.*, "Lunar Volatiles and Solar System Science," *arXiv preprint arXiv:2012.06317*, 2020.
- [31] W. Farrell, E. Beltran, P. Prem, M. Poston, A. Deutsch, and D. Hurley, "Lunar polar volatile resources: Obtaining their origins prior to extraction," presented at the Decadal Survey on Planetary Science and Astrobiology, 2020.
- [32] K. M. Cannon, A. N. Deutsch, J. W. Head, and D. T. Britt, "Stratigraphy of ice and ejecta deposits at the lunar poles," *Geophysical Research Letters*, vol. 47, no. 21, p. e2020GL088920, 2020.
- [33] D. M. Hurley, D. J. Lawrence, D. B. J. Bussey, R. R. Vondrak, R. C. Elphic, and G. R. Gladstone, "Two-dimensional distribution of volatiles in the lunar regolith from space weathering simulations," *Geophysical Research Letters*, vol. 39, no. 9, 2012.
- [34] V. Eke, L. Teodoro, and R. Elphic, "The spatial distribution of polar hydrogen deposits on the Moon," *Icarus*, vol. 200, no. 1, pp. 12-18, 2009.
- [35] W. Feldman *et al.*, "Polar hydrogen deposits on the Moon," *Journal of Geophysical Research: Planets*, vol. 105, no. E2, pp. 4175-4195, 2000.
- [36] W. C. Feldman, S. Maurice, D. J. Lawrence, B. L. Barraclough, R. C. Elphic, and A. B. Binder, "Deposits of Hydrogen on the Moon," in *New Views of the Moon: Integrated Remotely Sensed, Geophysical, and Sample Datasets*, January 1 1998, p. 29. [Online]. Available: <https://ui.adsabs.harvard.edu/abs/1998nvmi.conf...29F>. [Online]. Available: <https://ui.adsabs.harvard.edu/abs/1998nvmi.conf...29F>
-



- [37] W. C. Feldman *et al.*, "Evidence for water ice near the lunar poles," *Journal of Geophysical Research: Planets*, vol. 106, no. E10, pp. 23231-23251, 2001.
- [38] D. J. Lawrence *et al.*, "Improved modeling of Lunar Prospector neutron spectrometer data: Implications for hydrogen deposits at the lunar poles," *Journal of Geophysical Research: Planets*, vol. 111, no. E8, 2006.
- [39] A. Sanin *et al.*, "Hydrogen distribution in the lunar polar regions," *Icarus*, vol. 283, pp. 20-30, 2017.
- [40] L. Teodoro, V. Eke, and R. Elphic, "Spatial distribution of lunar polar hydrogen deposits after KAGUYA (SELENE)," *Geophysical Research Letters*, vol. 37, no. 12, 2010.
- [41] I. Matsuyama, F. Nimmo, and J. X. Mitrovica, "Planetary reorientation," *Annual Review of Earth and Planetary Sciences*, vol. 42, pp. 605-634, 2014.
- [42] J. R. Arnold, "Ice in the lunar polar regions," *Journal of Geophysical Research: Solid Earth*, vol. 84, no. B10, pp. 5659-5668, 1979.
- [43] R. R. Vondrak and D. H. Crider, "Ice at the Lunar Poles: That the Moon harbors ice at high latitudes is well known. The source of that water, however, may come as something of a surprise," *American Scientist*, vol. 91, no. 4, pp. 322-329, 2003.
- [44] A. Colaprete *et al.*, "Detection of water in the LCROSS ejecta plume," *Science*, vol. 330, no. 6003, pp. 463-468, 2010.
- [45] G. R. Gladstone *et al.*, "LRO-LAMP observations of the LCROSS impact plume," *Science*, vol. 330, no. 6003, pp. 472-476, 2010.
- [46] P. O. Hayne *et al.*, "Evidence for exposed water ice in the Moon's south polar regions from Lunar Reconnaissance Orbiter ultraviolet albedo and temperature measurements," *Icarus*, vol. 255, pp. 58-69, 2015.
- [47] L. Qiao, Z. Ling, J. W. Head, M. A. Ivanov, and B. Liu, "Analyses of Lunar Orbiter Laser Altimeter 1,064-nm albedo in permanently shadowed regions of polar crater flat floors: Implications for surface water ice occurrence and future in situ exploration," *Earth and Space Science*, vol. 6, no. 3, pp. 467-488, 2019.
- [48] M. Benna, D. Hurley, T. Stubbs, P. Mahaffy, and R. Elphic, "Lunar soil hydration constrained by exospheric water liberated by meteoroid impacts," *Nature geoscience*, vol. 12, no. 5, pp. 333-338, 2019.
- [49] K. D. Retherford *et al.*, "LRO-Lyman Alpha Mapping Project (LAMP) Observations of the GRAIL Impact Plumes," in *AAS/Division for Planetary Sciences Meeting Abstracts# 45*, 2013, p. 107.08.
- [50] J. Carpenter, R. Fisackerly, and B. Houdou, "Establishing lunar resource viability," *Space Policy*, vol. 37, pp. 52-57, 2016.
- [51] "NASA's Lunar Exploration Program Overview," NASA, 2020. [Online]. Available: [https://www.nasa.gov/sites/default/files/atoms/files/artemis\\_plan-20200921.pdf](https://www.nasa.gov/sites/default/files/atoms/files/artemis_plan-20200921.pdf)
- [52] D. R. Andrews, A. Colaprete, J. Quinn, D. Chavers, and M. Picard, "Introducing the resource prospector (RP) mission," in *AIAA SPACE 2014 Conference and Exposition*, 2014, p. 4378.
- [53] A. Colaprete *et al.*, "The Volatiles Investigating Polar Exploration Rover (VIPER) Mission – Measurements and Constraints," presented at the Lunar and Planetary Science Conference, 2021.
- [54] G. Sanders, W. Larson, K. Sacksteder, and C. Mclemore, "NASA In-Situ Resource Utilization (ISRU) Project: Development and Implementation," in *AIAA SPACE 2008 Conference & Exposition*, 2008, p. 7853.



- [55] A. N. Deutsch, N. L. Chabot, and Coauthors, "Science opportunities offered by Mercury's ice-bearing polar deposits," presented at the Decadal Survey in Planetary Science and Astrobiology 2023-2032, Committee on Mercury and the Moon, 2020.
- [56] A. Tye *et al.*, "The age of lunar south circumpolar craters Haworth, Shoemaker, Faustini, and Shackleton: Implications for regional geology, surface processes, and volatile sequestration," *Icarus*, vol. 255, pp. 70-77, 2015.
- [57] I. Mitrofanov *et al.*, "Testing polar spots of water-rich permafrost on the Moon: LEND observations onboard LRO," *Journal of Geophysical Research: Planets*, vol. 117, no. E12, 2012.
- [58] W. Marshall *et al.*, "Locating the LCROSS impact craters," *Space science reviews*, vol. 167, no. 1-4, pp. 71-92, 2012.
- [59] G. Patterson *et al.*, "Bistatic radar observations of the Moon using Mini-RF on LRO and the Arecibo Observatory," *Icarus*, vol. 283, pp. 2-19, 2017.
- [60] P. Spudis *et al.*, "Initial results for the north pole of the Moon from Mini-SAR, Chandrayaan-1 mission," *Geophysical Research Letters*, vol. 37, no. 6, 2010.
- [61] T. L. Roush *et al.*, "Volatile monitoring of soil cuttings during drilling in cryogenic, water-doped lunar simulant," *Advances in Space Research*, vol. 62, no. 5, pp. 1025-1033, 2018.
- [62] A. P. Crotts and C. Hummels, "Lunar outgassing, transient phenomena, and the return to the Moon. II. Predictions and tests for outgassing/regolith interactions," *The Astrophysical Journal*, vol. 707, no. 2, p. 1506, 2009.
- [63] J. W. Head, L. Wilson, A. N. Deutsch, M. J. Rutherford, and A. E. Saal, "Volcanically Induced Transient Atmospheres on the Moon: Assessment of Duration, Significance, and Contributions to Polar Volatile Traps," *Geophysical Research Letters*, vol. 47, no. 18, p. e2020GL089509, 2020.
- [64] D. H. Needham and D. A. Kring, "Lunar volcanism produced a transient atmosphere around the ancient Moon," *Earth and Planetary Science Letters*, vol. 478, pp. 175-178, 2017.
- [65] K. Watson, B. Murray, and H. Brown, "On the possible presence of ice on the Moon," *Journal of Geophysical Research*, vol. 66, no. 5, pp. 1598-1600, 1961.
- [66] S. Li and R. E. Milliken, "Water on the surface of the Moon as seen by the Moon Mineralogy Mapper: Distribution, abundance, and origins," *Science Advances*, vol. 3, no. 9, p. e1701471, 2017.
- [67] E. H. Hauri, T. Weinreich, A. E. Saal, M. C. Rutherford, and J. A. Van Orman, "High pre-eruptive water contents preserved in lunar melt inclusions," *Science*, vol. 333, no. 6039, pp. 213-215, 2011.
- [68] A. E. Saal, E. H. Hauri, M. L. Cascio, J. A. Van Orman, M. C. Rutherford, and R. F. Cooper, "Volatile content of lunar volcanic glasses and the presence of water in the Moon's interior," *Nature*, vol. 454, no. 7201, pp. 192-195, 2008.
- [69] A. E. Saal, E. H. Hauri, J. A. Van Orman, and M. J. Rutherford, "Hydrogen isotopes in lunar volcanic glasses and melt inclusions reveal a carbonaceous chondrite heritage," *Science*, vol. 340, no. 6138, pp. 1317-1320, 2013.
- [70] D. T. Wetzell, E. H. Hauri, A. E. Saal, and M. J. Rutherford, "Carbon content and degassing history of the lunar volcanic glasses," *Nature Geoscience*, vol. 8, no. 10, pp. 755-758, 2015.
- [71] H. Hiesinger, J. Head, U. Wolf, R. Jaumann, and G. Neukum, "Ages and stratigraphy of lunar mare basalts: A synthesis," *Recent advances and current research issues in lunar stratigraphy*, vol. 477, pp. 1-51, 2011.

- [72] J. P. Greenwood, S. Itoh, N. Sakamoto, P. Warren, L. Taylor, and H. Yurimoto, "Hydrogen isotope ratios in lunar rocks indicate delivery of cometary water to the Moon," *Nature Geoscience*, vol. 4, no. 2, pp. 79-82, 2011.
- [73] R. T. Daly and P. H. Schultz, "The delivery of water by impacts from planetary accretion to present," *Science advances*, vol. 4, no. 4, p. eaar2632, 2018.
- [74] L. Ong, E. I. Asphaug, D. Korycansky, and R. F. Coker, "Volatile retention from cometary impacts on the Moon," *Icarus*, vol. 207, no. 2, pp. 578-589, 2010.
- [75] R. N. Clayton and T. K. Mayeda, "Oxygen isotope studies of carbonaceous chondrites," *Geochimica et Cosmochimica Acta*, vol. 63, no. 13-14, pp. 2089-2104, 1999.
- [76] W. Fujiya, "Oxygen isotopic ratios of primordial water in carbonaceous chondrites," *Earth and Planetary Science Letters*, vol. 481, pp. 264-272, 2018.
- [77] N. Sakamoto *et al.*, "Remnants of the early solar system water enriched in heavy oxygen isotopes," *Science*, vol. 317, no. 5835, pp. 231-233, 2007.
- [78] C. O. D. Alexander, R. Bowden, M. Fogel, K. Howard, C. Herd, and L. Nittler, "The provenances of asteroids, and their contributions to the volatile inventories of the terrestrial planets," *Science*, vol. 337, no. 6095, pp. 721-723, 2012.
- [79] H. Cottin, M. Gazeau, and F. Raulin, "Cometary organic chemistry: a review from observations, numerical and experimental simulations," *Planetary and Space Science*, vol. 47, no. 8-9, pp. 1141-1162, 1999.
- [80] P. Ehrenfreund and S. B. Charnley, "Organic molecules in the interstellar medium, comets, and meteorites: a voyage from dark clouds to the early Earth," *Annual Review of Astronomy and Astrophysics*, vol. 38, no. 1, pp. 427-483, 2000.
- [81] P. Prem, N. Artemieva, D. Goldstein, P. Varghese, and L. Trafton, "Transport of water in a transient impact-generated lunar atmosphere," *Icarus*, vol. 255, pp. 148-158, 2015.
- [82] B. D. Stewart, E. Pierazzo, D. B. Goldstein, P. L. Varghese, and L. M. Trafton, "Simulations of a comet impact on the Moon and associated ice deposition in polar cold traps," *Icarus*, vol. 215, no. 1, pp. 1-16, 2011.
- [83] V. Svetsov and V. Shuvalov, "Water delivery to the Moon by asteroidal and cometary impacts," *Planetary and Space Science*, vol. 117, pp. 444-452, 2015.
- [84] C. M. Ernst, N. L. Chabot, and O. S. Barnouin, "Examining the potential contribution of the Hokusai impact to water ice on Mercury," *Journal of Geophysical Research: Planets*, vol. 123, no. 10, pp. 2628-2646, 2018.
- [85] J. P. Greenwood, S.-i. Karato, K. E. Vander Kaaden, K. Pahlevan, and T. Usui, "Water and volatile inventories of Mercury, Venus, the Moon, and Mars," *Space Science Reviews*, vol. 214, no. 5, pp. 1-39, 2018.
- [86] L. Starukhina, "Water detection on atmosphereless celestial bodies: Alternative explanations of the observations," *Journal of Geophysical Research: Planets*, vol. 106, no. E7, pp. 14701-14710, 2001.
- [87] J. Roth, "Chemical sputtering," *Sputtering by particle bombardment II*, pp. 91-146, 1983.
- [88] M. Dyar, C. Hibbitts, and T. Orlando, "Mechanisms for incorporation of hydrogen in and on terrestrial planetary surfaces," *Icarus*, vol. 208, no. 1, pp. 425-437, 2010.
- [89] Y. Liu, Y. Guan, Y. Zhang, G. R. Rossman, J. M. Eiler, and L. A. Taylor, "Direct measurement of hydroxyl in the lunar regolith and the origin of lunar surface water," *Nature Geoscience*, vol. 5, no. 11, pp. 779-782, 2012.
- [90] D. H. Crider and R. R. Vondrak, "The solar wind as a possible source of lunar polar hydrogen deposits," *Journal of Geophysical Research: Planets*, vol. 105, no. E11, pp. 26773-26782, 2000.

- 
- [91] T. McCord *et al.*, "Sources and physical processes responsible for OH/H<sub>2</sub>O in the lunar soil as revealed by the Moon Mineralogy Mapper (M3)," *Journal of Geophysical Research: Planets*, vol. 116, no. E6, 2011.
- [92] C. M. Pieters *et al.*, "Character and spatial distribution of OH/H<sub>2</sub>O on the surface of the Moon seen by M3 on Chandrayaan-1," *science*, vol. 326, no. 5952, pp. 568-572, 2009.
- [93] J. M. Sunshine *et al.*, "Temporal and spatial variability of lunar hydration as observed by the Deep Impact spacecraft," *Science*, vol. 326, no. 5952, pp. 565-568, 2009.
- [94] M. J. Cintala, "Impact-induced thermal effects in the lunar and Mercurian regoliths," *Journal of Geophysical Research: Planets*, vol. 97, no. E1, pp. 947-973, 1992.
- [95] E. S. Costello, R. R. Ghent, and P. G. Lucey, "The mixing of lunar regolith: Vital updates to a canonical model," *Icarus*, vol. 314, pp. 327-344, 2018.
- [96] W. Farrell, D. Hurley, M. Poston, P. Hayne, J. Szalay, and J. McLain, "The young age of the LAMP-observed frost in lunar polar cold traps," *Geophysical Research Letters*, vol. 46, no. 15, pp. 8680-8688, 2019.
- [97] S. Marchi, A. Morbidelli, and G. Cremonese, "Flux of meteoroid impacts on Mercury," *Astronomy & Astrophysics*, vol. 431, no. 3, pp. 1123-1127, 2005.
- [98] S. Crites, P. Lucey, and D. Lawrence, "Proton flux and radiation dose from galactic cosmic rays in the lunar regolith and implications for organic synthesis at the poles of the Moon and Mercury," *Icarus*, vol. 226, no. 2, pp. 1192-1200, 2013.
- [99] N. Schorghofer and O. Aharonson, "The lunar thermal ice pump," *The Astrophysical Journal*, vol. 788, no. 2, p. 169, 2014.
- [100] T. L. Jackson, W. M. Farrell, and M. I. Zimmerman, "Rover wheel charging on the lunar surface," *Advances in Space Research*, vol. 55, no. 6, pp. 1710-1720, 2015.
- [101] M. Maimone, J. Biesiadecki, E. Tunstel, Y. Cheng, and C. Leger, "Surface navigation and mobility intelligence on the Mars Exploration Rovers," *Intelligence for Space Robotics*, pp. 45-69, 2006.
- [102] M. McHenry *et al.*, "Mars 2020 Autonomous Rover Navigation," *American Astronomical Society*, 2020.
- [103] I. A. Nesnas, M. W. Maimone, and H. Das, "Rover Maneuvering for Autonomous Vision-Based Dexterous Manipulation," in *IEEE International Conference on Robotics and Automation*, San Francisco, CA, April 24-28 2000: IEEE, in ICRA 2000 Proceedings, pp. 2296-2301, doi: 10.1109/ROBOT.2000.846369.
- [104] V. Asnani, D. Delap, and C. Creager, "The development of wheels for the Lunar Roving Vehicle," *Journal of Terramechanics*, vol. 46, no. 3, pp. 89-103, 2009, doi: 10.1016/j.jterra.2009.02.005.
- [105] T. Roush *et al.*, "The Volatiles Investigating Polar Exploration Rover (VIPER) Near Infrared Volatile Spectrometer System (NIRVSS)," in *Lunar and Planetary Science Conference*, 2021, no. 2548, p. 1678.
- [106] T. L. Roush *et al.*, "In Situ Resource Utilization (ISRU) field expedition 2012: Near-Infrared Volatile Spectrometer System (NIRVSS) science measurements compared to site knowledge," *Advances in Space Research*, vol. 55, no. 10, pp. 2451-2456, 2015.
- [107] K. Ennico-Smith, A. Colaprete, R. Elphic, J. Quinn, and K. Zachny, "The Volatiles Investigating Polar Exploration Rover Payload," in *Lunar and Planetary Science Conference*, 2020, no. 2326, p. 2898.

- [108] D. Needham and B. Bailey, "Explore Moon to Mars: Volatiles Science Objectives Addressed by CLPS Deliveries," in *Decadal Survey on Planetary Science and Astrobiology: Panel on Mercury and the Moon*, 2020.
- [109] S. Clarke, "Explore Science: Lunar Discovery and Exploration Program Status," in *Planetary Science Advisory Committee Meeting*, 2019.
- [110] J. Burch *et al.*, "RPC-IES: the ion and electron sensor of the Rosetta Plasma Consortium," *Space Science Reviews*, vol. 128, no. 1, pp. 697-712, 2007.
- [111] R. Goldstein *et al.*, "The Rosetta Ion and Electron Sensor (IES) measurement of the development of pickup ions from comet 67P/Churyumov-Gerasimenko," *Geophysical Research Letters*, vol. 42, no. 9, pp. 3093-3099, 2015.
- [112] E. Peral *et al.*, "RainCube, a Ka-band Precipitation Radar in a 6U CubeSat," presented at the 31st Annual AIAA/USU Conference on Small Satellites, 2017.
- [113] E. Peral *et al.*, "The Radar-in-a-Cubesat (RAINCUBE) and measurement results," in *IGARSS 2018-2018 IEEE International Geoscience and Remote Sensing Symposium*, 2018: IEEE, pp. 6297-6300.
- [114] D. Bekker, P. Pingree, T. Werne, T. Wilson, and B. Franklin, "The COVE payload—a reconfigurable FPGA-Based processor for CubeSats," 2011.
- [115] S. Padmanabhan *et al.*, "The Polar Radiant Energy in the Far InfraRed Experiment (PREFIRE)," in *IGARSS 2019: 2019 IEEE International Geoscience and Remote Sensing Symposium*, 2019, pp. 8834-8836.
- [116] T. S. L'Ecuyer *et al.*, "The Polar Radiant Energy in the Far InfraRed Experiment: A New Perspective on Polar Longwave Energy Exchanges," (in English), *Bulletin of the American Meteorological Society*, pp. 1-46, 07 Apr. 2021 2021, doi: 10.1175/bams-d-20-0155.1.
- [117] B. Bos *et al.*, "Touch And Go Camera System (TAGCAMS) for the OSIRIS-REx asteroid sample return mission," *Space Science Reviews*, vol. 214, no. 1, pp. 1-23, 2018.
- [118] C. Nuttall Jr., "A dimensionless consolidation of WES data on the performance of sand under tire loads," U.S. Army Engineer Waterways Experiment Station, 1965.
- [119] M. Sutoh, K. Nagaoka, K. Nagatani, and K. Yoshida, "Evaluation of Influence of Wheel Surface Shapes on Tractive Efficiencies of Planetary Rovers in Various Soil Environments," in *International Symposium on Artificial Intelligence, Robotics and Automation in Space (i-SAIRAS)*, 2012, vol. Proceedings of the International Symposium on Artificial Intelligence, Robotics and Automation in Space.
- [120] A. Colaprete, R. C. Elphic, and M. Shirley, "Characterizing Lunar Polar Volatiles at the Working Scale: Going from Exploration Goals to Mission Requirements," in *50th Lunar and Planetary Science Conference (LPSC)*, 2019: The Woodlands, TEXAS.
- [121] J. Yoshida, "Full AV Stacks: Who, What, Where, etc.," *EE|Times*. [Online]. Available: <https://www.eetimes.com/full-av-stacks-who-what-where-etc/#>



## O.2 APPENDICES

- [1] E. A. Fisher *et al.*, "Evidence for surface water ice in the lunar polar regions using reflectance measurements from the Lunar Orbiter Laser Altimeter and temperature measurements from the Diviner Lunar Radiometer Experiment," *Icarus*, vol. 292, pp. 74-85, 2017.
- [2] P. O. Hayne *et al.*, "Evidence for exposed water ice in the Moon's south polar regions from Lunar Reconnaissance Orbiter ultraviolet albedo and temperature measurements," *Icarus*, vol. 255, pp. 58-69, 2015.
- [3] S. Li *et al.*, "Direct evidence of surface exposed water ice in the lunar polar regions," *Proceedings of the National Academy of Sciences*, vol. 115, no. 36, pp. 8907-8912, 2018.
- [4] V. Eke, L. Teodoro, and R. Elphic, "The spatial distribution of polar hydrogen deposits on the Moon," *Icarus*, vol. 200, no. 1, pp. 12-18, 2009.
- [5] W. Feldman *et al.*, "Polar hydrogen deposits on the Moon," *Journal of Geophysical Research: Planets*, vol. 105, no. E2, pp. 4175-4195, 2000.
- [6] W. C. Feldman, S. Maurice, D. J. Lawrence, B. L. Barraclough, R. C. Elphic, and A. B. Binder, "Deposits of Hydrogen on the Moon," in *New Views of the Moon: Integrated Remotely Sensed, Geophysical, and Sample Datasets*, January 1 1998, p. 29. [Online]. Available: <https://ui.adsabs.harvard.edu/abs/1998nvmi.conf...29F>. [Online]. Available: <https://ui.adsabs.harvard.edu/abs/1998nvmi.conf...29F>
- [7] W. C. Feldman *et al.*, "Evidence for water ice near the lunar poles," *Journal of Geophysical Research: Planets*, vol. 106, no. E10, pp. 23231-23251, 2001.
- [8] D. J. Lawrence *et al.*, "Improved modeling of Lunar Prospector neutron spectrometer data: Implications for hydrogen deposits at the lunar poles," *Journal of Geophysical Research: Planets*, vol. 111, no. E8, 2006.
- [9] A. Sanin *et al.*, "Hydrogen distribution in the lunar polar regions," *Icarus*, vol. 283, pp. 20-30, 2017.
- [10] L. Teodoro, V. Eke, and R. Elphic, "Spatial distribution of lunar polar hydrogen deposits after KAGUYA (SELENE)," *Geophysical Research Letters*, vol. 37, no. 12, 2010.
- [11] K. M. Cannon, A. N. Deutsch, J. W. Head, and D. T. Britt, "Stratigraphy of ice and ejecta deposits at the lunar poles," *Geophysical Research Letters*, vol. 47, no. 21, p. e2020GL088920, 2020.
- [12] A. N. Deutsch, N. L. Chabot, and Coauthors, "Science opportunities offered by Mercury's ice-bearing polar deposits," presented at the Decadal Survey in Planetary Science and Astrobiology 2023-2032, Committee on Mercury and the Moon, 2020.
- [13] A. Tye *et al.*, "The age of lunar south circumpolar craters Haworth, Shoemaker, Faustini, and Shackleton: Implications for regional geology, surface processes, and volatile sequestration," *Icarus*, vol. 255, pp. 70-77, 2015.
- [14] M. Siegler *et al.*, "Lunar true polar wander inferred from polar hydrogen," *Nature*, vol. 531, no. 7595, pp. 480-484, 2016.
- [15] D. H. Crider and R. Vondrak, "Hydrogen migration to the lunar poles by solar wind bombardment of the Moon," *Advances in Space Research*, vol. 30, no. 8, pp. 1869-1874, 2002.
- [16] D. H. Crider and R. R. Vondrak, "The solar wind as a possible source of lunar polar hydrogen deposits," *Journal of Geophysical Research: Planets*, vol. 105, no. E11, pp. 26773-26782, 2000.
- [17] W. Farrell, D. Hurley, M. Poston, P. Hayne, J. Szalay, and J. McLain, "The young age of the LAMP-observed frost in lunar polar cold traps," *Geophysical Research Letters*, vol. 46, no. 15, pp. 8680-8688, 2019.

- [18] D. M. Hurley and M. Benna, "Simulations of lunar exospheric water events from meteoroid impacts," *Planetary and Space Science*, vol. 162, pp. 148-156, 2018.
- [19] C. M. Pieters *et al.*, "Character and spatial distribution of OH/H<sub>2</sub>O on the surface of the Moon seen by M3 on Chandrayaan-1," *science*, vol. 326, no. 5952, pp. 568-572, 2009.
- [20] J. M. Sunshine *et al.*, "Temporal and spatial variability of lunar hydration as observed by the Deep Impact spacecraft," *Science*, vol. 326, no. 5952, pp. 565-568, 2009.
- [21] J. L. Kloos, J. E. Moores, J. Sangha, T. G. Nguyen, and N. Schorghofer, "The temporal and geographic extent of seasonal cold trapping on the Moon," *Journal of Geophysical Research: Planets*, vol. 124, no. 7, pp. 1935-1944, 2019.
- [22] J. P. Williams *et al.*, "Seasonal polar temperatures on the Moon," *Journal of Geophysical Research: Planets*, vol. 124, no. 10, pp. 2505-2521, 2019.
- [23] P. Prem *et al.*, "Lunar Volatiles and Solar System Science," *arXiv preprint arXiv:2012.06317*, 2020.
- [24] D. A. Paige *et al.*, "Diviner lunar radiometer observations of cold traps in the Moon's south polar region," *science*, vol. 330, no. 6003, pp. 479-482, 2010.
- [25] A. R. Vasavada, D. A. Paige, and S. E. Wood, "Near-surface temperatures on Mercury and the Moon and the stability of polar ice deposits," *Icarus*, vol. 141, no. 2, pp. 179-193, 1999.
- [26] P. Hayne, M. Siegler, D. Paige, P. Lucey, and E. Fisher, "Carbon dioxide frost at the poles of the Moon: Thermal stability and observational evidence from the Lunar Reconnaissance Orbiter," in *Lunar and Planetary Science Conference*, 2019, no. 2132, p. 2628.
- [27] C. Hibbitts *et al.*, "Thermal stability of water and hydroxyl on the surface of the Moon from temperature-programmed desorption measurements of lunar analog materials," *Icarus*, vol. 213, no. 1, pp. 64-72, 2011.
- [28] N. Schorghofer and O. Aharonson, "The lunar thermal ice pump," *The Astrophysical Journal*, vol. 788, no. 2, p. 169, 2014.
- [29] A. Colaprete *et al.*, "Detection of water in the LCROSS ejecta plume," *Science*, vol. 330, no. 6003, pp. 463-468, 2010.
- [30] G. Patterson *et al.*, "Bistatic radar observations of the Moon using Mini-RF on LRO and the Arecibo Observatory," *Icarus*, vol. 283, pp. 2-19, 2017.
- [31] P. D. Spudis *et al.*, "Initial results for the north pole of the Moon from Mini-SAR, Chandrayaan-1 mission," *Geophysical Research Letters*, vol. 37, no. 6, 2010, doi: 10.1029/2009GL042259.
- [32] "Report of the Interagency Operations Advisory Group (IOAG)," 2019. [Online]. Available: <https://www.ioag.org/layouts/15/WopiFrame.aspx?sourcedoc={168928FC-BF71-4DB0-B69B-36C9DC614A1E}&file=Lunar%20communications%20architecture%20study%20report%20Final%20v1.1%2010-10-2019.docx&action=default>
- [33] D. M. Hurley, D. J. Lawrence, D. B. J. Bussey, R. R. Vondrak, R. C. Elphic, and G. R. Gladstone, "Two-dimensional distribution of volatiles in the lunar regolith from space weathering simulations," *Geophysical Research Letters*, vol. 39, no. 9, 2012.
- [34] D. H. Needham and D. A. Kring, "Lunar volcanism produced a transient atmosphere around the ancient Moon," *Earth and Planetary Science Letters*, vol. 478, pp. 175-178, 2017.
- [35] E. Costello, R. Ghent, M. Hirabayashi, and P. Lucey, "Impact Gardening as a Constraint on the Age, Source, and Evolution of Ice on Mercury and the Moon," *Journal of Geophysical Research: Planets*, vol. 125, no. 3, p. e2019JE006172, 2020.

- [36] A. N. Deutsch, J. W. Head III, and G. A. Neumann, "Age constraints of Mercury's polar deposits suggest recent delivery of ice," *Earth and planetary science letters*, vol. 520, pp. 26-33, 2019.
- [37] L. Rubanenko, J. Venkatraman, and D. A. Paige, "Thick ice deposits in shallow simple craters on the Moon and Mercury," *Nature Geoscience*, vol. 12, no. 8, pp. 597-601, 2019.
- [38] J. W. Boyce *et al.*, "Lunar apatite with terrestrial volatile abundances," *Nature*, vol. 466, no. 7305, pp. 466-469, 2010.
- [39] Y. Chen, Y. Zhang, Y. Liu, Y. Guan, J. Eiler, and E. M. Stolper, "Water, fluorine, and sulfur concentrations in the lunar mantle," *Earth and Planetary Science Letters*, vol. 427, pp. 37-46, 2015.
- [40] J. P. Greenwood, S. Itoh, N. Sakamoto, P. Warren, L. Taylor, and H. Yurimoto, "Hydrogen isotope ratios in lunar rocks indicate delivery of cometary water to the Moon," *Nature Geoscience*, vol. 4, no. 2, pp. 79-82, 2011.
- [41] E. H. Hauri, A. E. Saal, M. J. Rutherford, and J. A. Van Orman, "Water in the Moon's interior: Truth and consequences," *Earth and Planetary Science Letters*, vol. 409, pp. 252-264, 2015.
- [42] E. H. Hauri, T. Weinreich, A. E. Saal, M. C. Rutherford, and J. A. Van Orman, "High pre-eruptive water contents preserved in lunar melt inclusions," *Science*, vol. 333, no. 6039, pp. 213-215, 2011.
- [43] F. M. McCubbin, A. Steele, E. H. Hauri, H. Nekvasil, S. Yamashita, and R. J. Hemley, "Nominally hydrous magmatism on the Moon," *Proceedings of the National Academy of Sciences*, vol. 107, no. 25, pp. 11223-11228, 2010.
- [44] A. E. Saal, E. H. Hauri, M. L. Cascio, J. A. Van Orman, M. C. Rutherford, and R. F. Cooper, "Volatile content of lunar volcanic glasses and the presence of water in the Moon's interior," *Nature*, vol. 454, no. 7201, pp. 192-195, 2008.
- [45] S. Madzunkov, LCMS PI, private communication.
- [46] P. Clark *et al.*, "Preparing for delivery of the Lunar Ice Cube compact IR spectrometer payload," in *SPIE Optical Engineering + Applications*, 2020, vol. 11505: SPIE, doi: 10.1117/12.2568027.
- [47] (1970). *Performance evaluation of wheels for lunar vehicles*.
- [48] I. A. Nesnas, M. W. Maimone, and H. Das, "Rover Maneuvering for Autonomous Vision-Based Dexterous Manipulation," in *IEEE International Conference on Robotics and Automation*, San Francisco, CA, April 24-28 2000: IEEE, in ICRA 2000 Proceedings, pp. 2296–2301, doi: 10.1109/ROBOT.2000.846369.
- [49] V. Asnani, D. Delap, and C. Creager, "The development of wheels for the Lunar Roving Vehicle," *Journal of Terramechanics*, vol. 46, no. 3, pp. 89–103, 2009, doi: 10.1016/j.jterra.2009.02.005.
- [50] M. G. Bekker, "The Development of a Moon Rover," *Journal of the British Interplanetary Society*, vol. 38, p. 537, 1985.
- [51] C. Nuttall Jr., "A dimensionless consolidation of WES data on the performance of sand under tire loads," U.S. Army Engineer Waterways Experiment Station, 1965.
- [52] M. Sutoh, K. Nagaoka, K. Nagatani, and K. Yoshida, "Evaluation of Influence of Wheel Surface Shapes on Tractive Efficiencies of Planetary Rovers in Various Soil Environments," in *International Symposium on Artificial Intelligence, Robotics and Automation in Space (i-SAIRAS)*, 2012, vol. Proceedings of the International Symposium on Artificial Intelligence, Robotics and Automation in Space.
- [53] J. Y. C. Chen, E. C. Haas, and M. J. Barnes, "Human Performance Issues and User Interface Design for Teleoperated Robots," *IEEE Transactions on Systems, Man, and Cybernetics, Part C*

- (*Applications and Reviews*), vol. 37, no. 6, pp. 1231-1245, 2007, doi: 10.1109/TSMCC.2007.905819.
- [54] M. Maimone, J. Biesiadecki, E. Tunstel, Y. Cheng, and C. Leger, "Surface navigation and mobility intelligence on the Mars Exploration Rovers," *Intelligence for Space Robotics*, pp. 45–69, 2006.
- [55] M. Buehler, K. Iagnemma, and S. Singh, *The DARPA urban challenge: autonomous vehicles in city traffic*. Springer Tracts in Advanced Robotics: Springer, 2009.
- [56] K. Iagnemma and M. Buehler, "Editorial for Journal of Field Robotics—Special Issue on the DARPA Grand Challenge," *Journal of Field Robotics*, vol. 23, no. 9, pp. 655–656, 2006, doi: 10.1002/rob.20154.
- [57] M. Heverly *et al.*, "Traverse Performance Characterization for the Mars Science Laboratory Rover," *Journal of Field Robotics*, vol. 30, no. 6, pp. 835-846, 2013, doi: 10.1002/rob.21481.
- [58] H. Kanamori, S. Udagawa, T. Yoshida, S. Matsumoto, and K. Takagi, "Properties of Lunar Soil Simulant Manufactured in Japan," in *Sixth ASCE Specialty Conference and Exposition on Engineering, Construction, and Operations in Space*, 1998, pp. 462-468, doi: 10.1061/40339(206)53. [Online]. Available: <https://ascelibrary.org/doi/abs/10.1061/40339%28206%2953>
- [59] G. H. Heiken, D. T. Vaniman, and B. M. French, *Lunar Sourcebook, A User's Guide to the Moon*. Cambridge University Press, 1991.
- [60] L. Ding, H. Gao, Z. Deng, J. Guo, and G. Liu, "Longitudinal slip versus skid of planetary rovers' wheels traversing on deformable slopes," in *2013 IEEE/RSJ International Conference on Intelligent Robots and Systems*, 3-7 Nov. 2013, pp. 2842-2848, doi: 10.1109/IROS.2013.6696758.
- [61] G. Paulsen *et al.*, "The Regolith and Ice Drill for Exploration of New Terrains (TRIDENT); a One-Meter Drill for the Lunar Resource Prospector Mission," in *44th Aerospace Mechanisms Symposium*, 2018, p. 13.
- [62] G. Paulsen *et al.*, "Development and Testing of the Lunar Resource Prospector Drill (RPD)," presented at the Earth and Space 2016, 2016. [Online]. Available: <https://ascelibrary.org/doi/abs/10.1061/9780784479971.031>.
- [63] K. Zacny *et al.*, "Development of the Lunar Drill for the Resource Prospector Mission," presented at the IEEE Aerospace Conference, 2016.
- [64] K. Zacny *et al.*, "Resource prospector drill performance during the integrated payload tests," presented at the 2016 IEEE Aerospace Conference, 2016.
- [65] G. W. Heckler and A. Petro, "Commercialization of Communications and Navigation Services for the Earth and the Moon," in *The Space Economy*, ed, 2021.
- [66] A. Patro, private communication.
- [67] J. Friend, private communication.
- [68] "Lunar Pathfinder Service User Guide," 2020. [Online]. Available: <https://irp-cdn.multiscreensite.com/19e31c60/files/uploaded/LunarPathfinder-UserManual-WebSite-v002-2.pdf>
- [69] C. Ho, S. Slobin, A. Kantak, and S. Asmar, "Solar Brightness Temperature and Corresponding Antenna Noise Temperature at Microwave Frequencies," IPN Progress Report 42-175, 2008. [Online]. Available: [https://ipnpr.jpl.nasa.gov/progress\\_report/42-175/175E.pdf](https://ipnpr.jpl.nasa.gov/progress_report/42-175/175E.pdf)
- [70] M. Pugh, I. Kuperman, M. Kobayashi, F. Aguirre, M. Kilzer, and C. Spurgers, "High-rate Ka-band modulator for the NISAR mission," in *2018 IEEE Aerospace Conference*, March 3-10 2018, pp. 1-13, doi: 10.1109/AERO.2018.8396451.
- [71] (2003). *CCSDS 211.2-B-1, PROXIMITY-1 SPACE LINK PROTOCOL—CODING AND SYNCHRONIZATION SUBLAYER BLUE BOOK*.



- 
- [72] (2004). *CCSDS 211.1-B-2, PROXIMITY-1 SPACE LINK PROTOCOL—PHYSICAL LAYER BLUE BOOK*.
- [73] (2004). *CCSDS 211.0-B-3, PROXIMITY-1 SPACE LINK PROTOCOL—DATA LINK LAYER BLUE BOOK*.
- [74] M. Redmond, K. Novak, and V. Mireles, "Static Ball Bearing Thermal Conductance in Air and Vacuum: Review and Correlation," *Journal of Thermophysics and Heat Transfer*, vol. 31, no. 4, pp. 841-846, 2017, doi: 10.2514/1.T5071.